# CONVEYING AIR REQUIREMENTS FOR A DENSE PHASE FLY ASH PNEUMATIC CONVEYING SYSTEM

Rofhiwa Nemutandani

A research report submitted to the Faculty of Engineering and the Built Environment, University of the Witwatersrand, in partial fulfilment of the requirements for the degree of Master of Science in Engineering.

Johannesburg, 2020

# DECLARATION

I declare that this research report is my own unaided work. It is being submitted for the Degree of Master of Science in Mechanical Engineering to the University of the Witwatersrand, Johannesburg. It has not been submitted before for any degree or examination to any other university.

Rofhiwa Nemutandani …05... day of …September…, 2020

# ABSTRACT

An investigation was undertaken into the air usage for a dense-phase pneumatic conveying system that removes fly ash from coal-fired power station generating 800 MW each per each Unit. The objective of the research was to establish the air flowrate required to convey fly ash in dense phase and also determine if the installed compressors will be sufficient to supply the required air flow and pressure. Based on the experimental findings, theoretical models were to be developed that could be used to predict performance of similar systems operating in dense-phase. Three Units in commercial operation (out of six eventually) were used as test facilities for the research with conveying distances of 402 m, 516 m and 628 m respectively for Units 1, 2 and 3. The conveying pipelines used in the research all had a pipe diameter of 265 mm. All the equipment and facilities had been installed prior to the research. Tests were conducted to determine the air flow rate, solids flow rate and pressure drop during conveying cycles for the three Units. These tests were performed as part of normal plant operations without any modifications. Of the three Units, Unit 2 displayed results close to predictions for a dense phase system with an air flow rate of 1.86 kg/s and solids loading ratios averaging 19. Unit 1 and Unit 3 results indicated the need for further optimization with average air flow rates and solids loading ratios of 2.8 kg/s and 10 respectively. The pneumatic conveying characteristics observed during the experimentation allowed for estimation of the solids friction factors for the horizontal conveying sections using the back-calculation method. This experimental friction factors were then compared with expected results from literature-proposed models such as the Jones and Williams (2003) and Behera *et al* (2015) models. These models gave over predictions when compared with the experimental results, with the Jones and Williams' model predicting values averaging 72% higher than expected, and the Behera model with an average 60% over prediction across all Units. Applying the same approach as adopted by Behera *et al* to develop their model and using the experimental results from this research; new models were developed for predicting the solids friction factors for each of the Unit under investigation. Although these new models provided better estimation when compared with the Jones and Williams and the Behera *et al* models, they were also prone to over prediction. The model developed from Unit 3 results proved to be the best Equation from all the models considered with an overall over prediction of 48% across all Units. This model was also used to estimate performance of the last Unit and predicted a conveying pressure drop of 270 kPa which is realistic considering the performance of Units 1, 2 and 3. As such, although there are ranges of models available in literature that are useful to estimate the conveying pressure drop, these must be applied with considerable caution if experimental performance data are not available. The research

revealed that plant modifications are necessary to improve the current performance for Unit 1 and Unit 3. These modifications will also assist in verifying available models used to predict solids friction factors inclusive of the models proposed in this research.

***“Let him who boasts, boast in the Lord.”***

***1 Corinthians 1:31***

Soli Deo Gloria

*I dedicate this research to the memories of my good friend, the late Dr. Avhasei Mudau and my beloved uncle, the late Justice Azwinndini Ramunasi.*

# ACKNOWLEDGMENTS

The author would like to acknowledge and deeply appreciate the following individuals and organizations for their contribution to this work:

- My wife Ridovhusanae and daughters, Ulangazwothe and Ulondavhawe. Without your many sacrifices this research would not have been a success.
- My brother Tshifhiwa Nemutandani for the warm hospitality and support on the many study days away from home.
- My Supervisors; Professors John Sheer and Walter Schmitz, thank you for your patience, understanding and guidance. I have learned so much from you.
- My industrial mentor, Mr. Henk Fourie, your contribution to my development both professionally and academically will never be forgotten.
- My managers who indeed have been pillars of support in my further my studies, Messrs., Mfundo Verby and Jacky Mathobela.
- To the rest of my family members, friends and colleagues who supported me in this research and gave encouraging words to enable me to carry on. I thank you.
- To my Employer, thank you for the financial assistance, the further study programme and the EPPEI initiative to equip Engineers.
- The original equipment manufacturer, and in particular, Mr. Jeremy Kirsch, for the advice and guidance when requested.

# CONTENTS

**PAGE**

# LIST OF FIGURES

# LIST OF TABLES

# NOMENCLATURE

| Symbol | Description | Units |
|---|---|---|
| $D$ | Diameter | m |
| $e_v$ | Voids ratio | - |
| $\rho_b$ | Bulk density | $\mathrm{kg/m^3}$ |
| $\rho_p$ | Particle density | $\mathrm{kg/m^3}$ |
| $\rho_a$ | Air density | $\mathrm{kg/m^3}$ |
| $\varepsilon$ | Voidance | - |
| $P$ | Pressure drop | kPa |
| $R_e$ | Reynolds Number | - |
| $v_a$ | Air velocity | $\mathrm{m/s}$ |
| $v_s$ | Solids velocity | $\mathrm{m/s}$ |
| $L$ | Length | m |
| g | Gravitational acceleration | $\mathrm{m/s^2}$ |
| $\mu\ (m^*)$ | Solid loading ratio | - |
| $T$ | Temperature | Kelvin |
| $m_s$ | Solids mass flow rate | tons/hour |
| $m_a$ | Air mass flow rate | $\mathrm{kg/s}$ |
| $V_f$ | Volumetric flow rate | $\mathrm{m^3/min}$ |
| $B$ | Bend factor | - |
| $\lambda_a$ | Air friction factor | - |
| $\lambda_s$ | Solids friction factor | - |

| Symbol | Description | Units |
|---|---|---|
| $Fr$ | Froude Number | - |
| $d_p$ | Particle diameter | μm |
| $D$ | Pipe diameter | m |
| $R$ | Universal gas constant | $\mathrm{kJ/(kg.K)}$ |
| $N$ | Number of bends | - |
| $P_V$ | Vertical pressure loss | kPa |
| $P_H$ | Horizontal pressure loss | kPa |
| $P_B$ | Bend pressure loss | kPa |
| $P_A$ | Acceleration pressure loss | kPa |
| $P_T$ | Total pressure drop | kPa |
| $\rho_{bl}$ | Loose poured bulk density | $\mathrm{kg/m^3}$ |
| $Fr_i$ | Inlet Froude Number | - |
| $w_{fo}$ | Terminal settling velocity | $\mathrm{m}/s$ |
| $\mathrm{Fr_{max}}$ | Maximum Froude number | - |
| $\mathrm{Fr_{min}}$ | Minimum Froude number | - |
| $\tau_1$ | Dense phase contribution in solids friction factor | - |
| $\tau_2$ | Dilute phase contribution in solids friction factor | - |

# LIST OF ABBREVIATIONS

| Abbreviation | Description |
|---|---|
| SLR | Solids loading ratio |
| VLR | Volumetric loading ratio |
| MW | Megawatt |
| PCC | Pneumatic conveying characteristics |
| PSD | Particle size distribution |

# CHAPTER 1 INTRODUCTION

This research project is concerned with the performance of an existing dense-phase pneumatic conveying system used for transporting fly ash from the six boilers of a coal-fired power station to ash storage silos, through pipelines of various lengths. There has been some uncertainty about the optimum quantity of conveying air required for these various pipelines, which led to the formulation of the project.

## 1.1 Background

Pneumatic conveying is a process of moving bulk solids using gas as the transport medium, with air as the commonly used gas. The earliest use of pneumatic conveying was in 1887 in agricultural processing (Bansal, 2012). Pneumatic conveying has since been developed and is now in use successfully around the world in other areas such as power generation, the mining industry, and paper and pulp industries (Williams, 2008). The main advantages of this conveying system compared to traditional belt conveying are that pneumatic conveying is fully enclosed, environmentally friendly and can be fully automated leading to improved efficiency (Mills, 2016).
Efficient design and operation of the pneumatic conveying system requires sufficient knowledge of the medium (air) requirements and the type of solids to be transported. Air flow rate is one of the most important parameters determining the performance of a pneumatic conveying system (Mills and Agarwal, 2015, Kalman et *al*., 2005). If the air flow rate is not high enough to keep the bulk solids in motion this may lead to pipe blockages and if a system is over-specified with a higher air flow rate this leads to increase in pipe wear and power requirements (Mills and Agarwal, 2015). The air flow rate relationship with other conveying parameters such as pressure drop per unit length and solids mass flow rate is also used to distinguish between the various pneumatic conveying modes available (Williams, 2008). Researchers currently define two modes of conveying, namely dilute phase and dense phase, although it is not unlikely to experience both of them during a conveying cycle (Mills, 2016). Dilute phase conveying is also known as suspension flow as the bulk solids are carried with the air stream. This mode of conveying has been widely researched and models are available that can be used to predict the behavior of these systems quite accurately, for known materials (Mills and Agarwal, 2015). Dense phase conveying is defined as non-suspension flow, i.e., the bulk solids are not suspended as in a fully developed dilute phase mode. Dense phase flow is not yet clearly defined but it is characterized by lower air velocities,

higher pressures, and mixtures of dilute and dense phase as well as turbulent flows (Bansal, 2016). This current research was aimed at establishing the air flow rate required for efficient conveying of fly ash in a dense phase conveying system.

The research project was based on a coal-fired power station that makes use of pneumatic conveying for transportation of fly ash from the boilers. The system was designed to transport fly ash using dense phase conveying into ash silos. These silos were located some distance away from the six Units of the power station. This power station is a dry-cooled coal-fired power station made up of six individual Units, each producing approximately 800 MW of power. Figure 1.1 shows a simplified schematic of the conveying system for all six Units, with the total conveying distances per Unit also indicated.

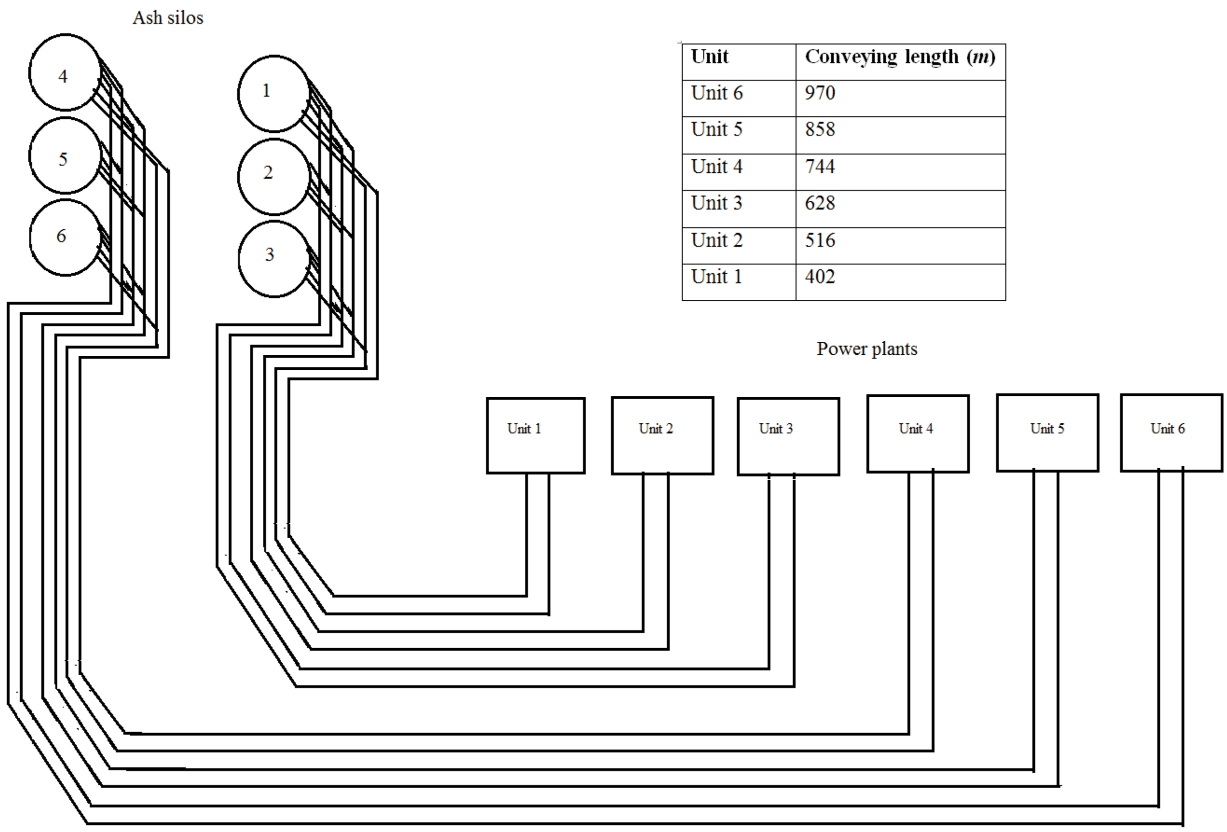


| Unit | Conveying length (*m*) |
|---|---|
| Unit 6 | 970 |
| Unit 5 | 858 |
| Unit 4 | 744 |
| Unit 3 | 628 |
| Unit 2 | 516 |
| Unit 1 | 402 |

**Figure 1.1** Simplified schematic of the pneumatic conveying system with distances indicated

At the time of writing this report, five Units were already in commercial operation with the last Unit (6) expected towards the end of 2020. Each boiler Unit consumes approximately 384 tons of coal per hour and based on 35% ash content, each Unit produces 134 tons of ash per hour during boiler combustion. The ash production is categorized in two groups, namely coarse ash and fly or fine ash (also termed dust). Based on operational experience on average, 90% of the total ash produced is fly ash (121 tons per hour) and coarse ash makes up the remaining 10%, at approximately 14 tons per hour. In order to maintain reliable power production, it is necessary to ensure an efficient ash collection and removal system. Coarse ash is conveyed mechanically in belt conveyors while the majority of the ash produced i.e., fly ash, is transported in a dense phase pneumatic conveying system. While dense phase conveying offers certain potential benefits to the power producer, there have been challenges experienced recently as pipe leaks and excessive environmental spillages occurred which necessitated an in-depth analysis of the system to the effect of resolving these challenges.

## 1.2 Motivation

Problems associated with this pneumatic conveying system were visible as early as 2015-2016 during the initial stages of commissioning the first Unit. Initially some of the problems were attributed to the varying fly ash quality as the boiler combustion processes were being optimized. This variation in fly ash has since been addressed as part and parcel of optimization during start-ups of each Unit. The fly ash being produced since then is well within the expected parameters for the life cycle of the station. As such, with the current quality of ash being conveyed it is necessary to review the system performance in order to improve the efficiency of the pneumatic conveying system. Various methods have been employed to try and improve the system, however two challenges still remain; that is increased air usage and system leaks, these are covered in sections 1.2.1 and 1.2.2.

### 1.2.1 Increased air usage

The first challenge encountered when commissioning the first Unit was regular blockages during initial conveying cycles. This was overcome by increasing the air flow rate into the system through increasing the number of orifice holes and sizes in throttles in the main air supply pipes. The increase of air flow rate into the conveying system can help in reducing the conveying pressure necessary to move the fly ash; this is because of the reduction of the solids to air ratio as the air flow is increased and this figure is directly proportional to pressure drop (Mallick, 2009). While this air flow rate increase has adequately addressed the blockage issues and these are no longer experienced, it has introduced another problem, of having a higher air flow rate and velocity in the pipelines than was initially intended. The increased air flowrate and air velocity can cause other problems such as increased pipe wear from higher air velocities. This is especially the case towards the discharge end of the conveying line due to the expansion of the air as a result of the lower pressures at the end of the conveying cycle (Wypych, 1989).

Experience suggests that a good dense phase system should have an air usage, as defined by the solids to air mass flow ratio, in excess of 20 (Mills, 2016). This means that for every 20 kg of bulk solids conveyed in a second, air mass flow rate should not be expected to exceed 1 kg per second for a system to operate in dense phase conveying. It is necessary to understand what the reliable air flow rate for this system would be and draw comparison with literature to predict whether there may be possible improvements in the current air consumption.

The increased air consumption also leads to operations of the air compressors at peak cycles and may lead to system constraint if the compressors fail to supply the air required during conveying cycles. The cost implications of increasing air usage should not be understated. An internal investigation into efficiency of pneumatic systems conducted in 2011 concluded that R3000 would be used per hour to generate compressed air for this power station during normal operation, amounting to over R26 million per year (van Deventer, 2011). This can be expected to have increased in real terms with the increased air usage.

### 1.2.2 Increased system leaks

The system has been plagued by sporadic ash leaks into the environment, this also led to measures required to minimize this impact such as increased maintenance and reduction in system performance. Whilst there could be various reasons for these environmental leaks such as incorrect pipe installation where flanges are not aligned, another reason could be the increased air flow rate and corresponding increased wear as discussed in 1.2.1 and this should be thoroughly investigated. It is expected that increase in air flow rate leads to higher velocities and the position with the highest velocities and pipe wear is at the end of the conveying pipeline due to the air expansion within the pipe (Mills, 2016). As such incorrect provision of the air required for conveying can have far reaching consequences.

### 1.2.3 Impact in plant unavailability

It is therefore important to understand the optimal operating regime for efficient performance of a dense phase system at a suitable air flow rate and supply pressure to reduce the wear on the system. The unavailability of such a conveying system in a power generation Unit leads to load losses, and at worst case to a power station shut down. These full Unit load losses have been experienced in the past when excessive environmental leaks of fly ash have forced the conveying to be stopped in order to do the necessary plant pipe changes. The system was designed with an eight hour window for repairs on the pneumatic conveying system, before the Unit has to be shut down and in the past such repairs have taken longer which necessitated a Unit shut down (Internal report, Design report: 200-215389).

## 1.3 Research Objectives

The purpose of this research is to determine air supply requirements for a dense phase system with the following sub-objectives:

(i) Determine the minimum air flow rate for reliable conveying of the fly ash on each of the Units already commissioned.

(ii) Determine if the compressors currently installed will be able to meet the air demands for reliable conveying in all six Units.

(iii) Develop a theoretical model for predicting air flow rate and pressure drop based on measurements from the operating Units.

(iv) Predict the minimum and maximum air velocity in the system for all six Units.

## 1.4 Research Overview

Understanding the air flow requirements for dense phase systems required a review of published literature and this is covered in chapter 2 of the report. The literature review was focused on air consumption in pneumatic systems as the main parameter for this investigation. The literature survey revealed considerable information available on pneumatic systems and air consumption; although there was little data on research on an industrial scale fly ash production Unit such as was considered in this research.

Information obtained from the literature review assisted in broadening the author’s understanding of the research topic as well as assisting in developing the methodology to be followed in acquiring data. A similar approach to acquire data as proposed by Williams (2008) was followed. The first three Units (Unit 1, 2 and 3) served as three experimental facilities for the research project. These were chosen for the research as they share a common pipe diameter and the various conveying lengths allow for one to study the effect of air flow over long and varying conveying lengths; this is detailed in chapters 3 and 4. The data was collected over an operating period of three years from 2017 to 2019 and system performance during this period is covered in chapter 5 under System Performance and Results. The major limitation with experimentation on an operational power plant was the inability to make modifications as the plant cannot be shut down as and when requested due to demand for power on the network. As such data collection was based on operational requirements, although this still provided sufficient data necessary to conduct the research. Data was then analyzed and discussed in chapters 6 and 7 where the air flow rate, air velocity, solids friction factor and pressure drop are calculated and results thereof discussed. Sample calculations are included in the appendices. Chapter 8 draws conclusions with suggestions for future work. One of the main recommendations for future work is removal of the limitations currently imposed on experimentation on commercial Units.

# CHAPTER 2 LITERATURE REVIEW

## 2.1 Introduction

The literature review was focused on the relationship between the air flow rate and other pneumatic conveying characteristics (PCCs) such as pressure drop and solids mass flow rate. These pneumatic conveying characteristics must be known in order to ensure a functional pneumatic conveying system (Bansal, 2012). These relationships have often been combined into what is termed phase diagrams or pneumatic conveying characteristic diagrams that illustrate the dependence of these functions one to another (Mills, 2016). Whilst there is a vast amount of literature already available with these PCCs for dense phase systems, it should be noted that "published conveying data for one material are generally not applicable to another" (Sheer, 1991). As such, it is important in determining the minimum air flow required to start by understanding the type of material to be conveyed i.e., characterization of bulk solids. Knowledge of material properties such as particle size and density assists in the selection of an appropriate conveying mode (Mills, 2016).

## 2.2 Bulk Solids Characterization

Characterization of bulk solids is a process in which solids to be conveyed such as fly ash are grouped into pneumatic conveying groups. This is achieved by observing the solids with special attention to the solids' particle size distribution, density and, more recently, taking into account particle sphericity (Anantharaman *et al.*, 2016). The seminal contribution to this field is accredited to Geldart (1973) and recent studies by Anantharaman et *al*. (2016) have proved the validity of Geldart's work. Geldart developed a fluidization chart (Figure 2.1) that can be used to classify various bulk solids based on density and particle size. Based on density and particle size, bulk solids are then grouped according to fluidization groups that indicate if bulk solids can be conveyed pneumatically or cannot be fluidized and transported using air. The fluidization charts with focus on mean particle diameter also assist in the selection of the suitable conveying mode, either dense phase or dilute phase (Deng and Bradley, 2016). Geldart was able to categorize bulk solids into four (4) groups or categories as indicated in Figure 2.1.

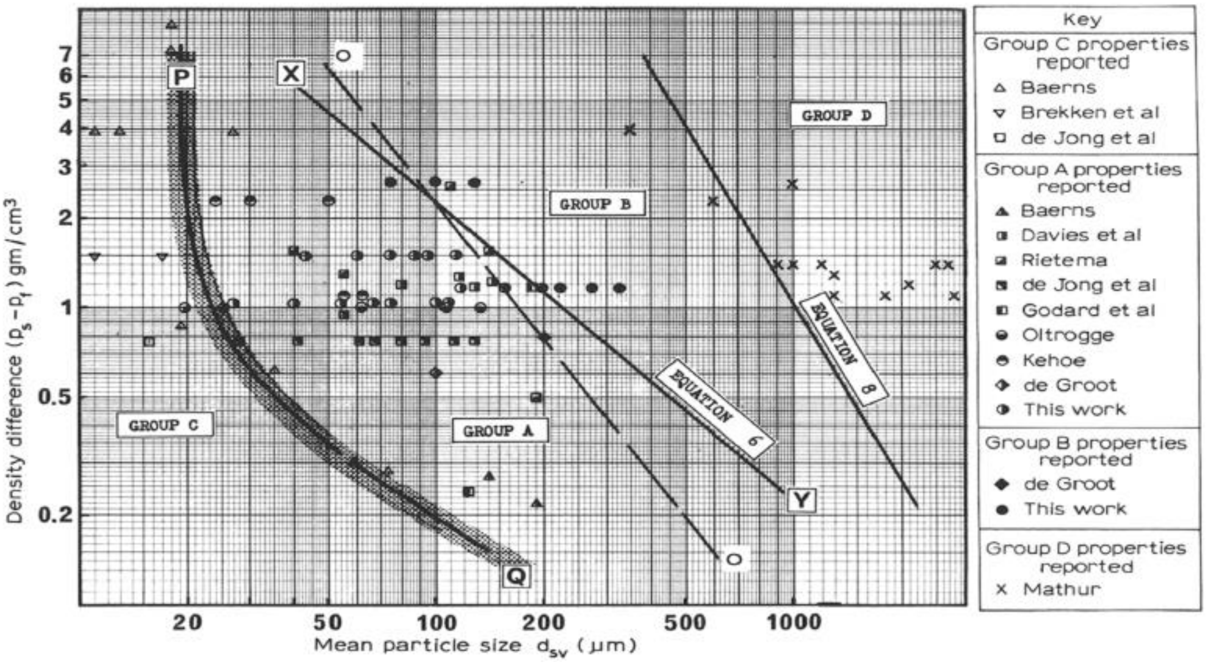


**Figure 2.1** Powder classification diagram for air (Geldart, 1973)

Based on Figure 2.1, a typical fly ash with a density difference ($\rho_S - \rho_g$) of 2200 kg/m$^3$ (2.2 g/cm$^3$) and mean particle diameter ($d_s$) of 80 microns; is well within the Group A category of materials. This agrees with work by Setia *et al* (2017) who concluded that fly ash is in general a cohesive material which can be classified under Group A on the Geldart diagram and conveyed in dense phase. Further work (Deng and Bradley, 2016) on the selection of the mode of conveying proposed the following selection criteria based on the particle size distribution of bulk solids:

(i) Material with a mean diameter (termed D50) of less than 70 microns can be conveyed in dense phase (fluidized), provided a minimum air velocity is maintained (operating at any air velocity below that can result in blockages).

(ii) Material with a narrow size range expressed as a ratio (termed D90/D10) of less than 2.5 will be conveyed in low velocity dense phase (slug flow).

(iii) Materials that cannot be grouped in any of the above will block at velocities lower than the saltation velocity and they are suggested to be conveyed in dilute phase.

The above criteria are widely accepted with authors noting that finer materials can be conveyed in either type of dense phase flow (plug or fluidised) and coarser materials are to be conveyed in dilute phase (Williams, 2008; Mills, 2016). It should however be noted that the above criteria are only a starting point and further research is required in collecting and analysing data for a number of bulk solids (Deng and Bradley, 2016).

It is also clear from Figure 2.1 and the work by Deng and Bradley (2016) that for efficient pneumatic conveying there exists a relationship between the particle size and density and the minimum air flow required to convey such solids. As such it is necessary for the design of any pneumatic conveying system that the particle diameter is known as well as its density.

### 2.2.1 Measurement of particle diameter

The particle diameter is used to classify the bulk solids as either coarse or fine. As noted by Guya (2018), the bulk solids are usually developed from a process plant such as boiler combustion for fly ash production or mineral processing in mining application, there is a wide variance of particle diameters and as such a mean value is used. The particle size distribution (PSD) defines the percentage contribution of the various particle diameters (Guya, 2018).

One of the simplest ways in which the PSD is determined is by using the sieving test which creates a restriction for a particle due to a smaller bore on the sieve than the particle diameter (Snowsill, 2010). There are other methods such as scanning electron microscopy, however sieving provides accurate results and this is accepted in this research as a preferred method to be used because of its simplicity and availability. The particle diameter is determined using sieving (dry) by taking a representative sample of solids in containers that have varying sieving holes, and depending on the amount in mass that pass the sieves, these are then divided per sieving container, Figure 2.2 (Blittersdorff and Klatt, 2017).

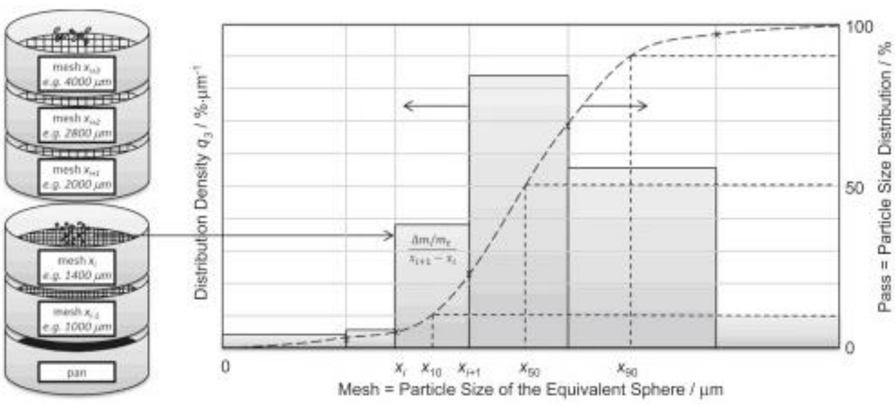


**Figure 2.2** Typical particle size distribution sieve containers and graphs (Blittersdorff and Klatt, 2017)

This test is well defined and typical results from a sieving test are in the form of Figure 2.3 which is then used to deduce the mean diameter (Li *et al.*, 2014). Refer to chapter 5 for PSD data findings specific to this research.

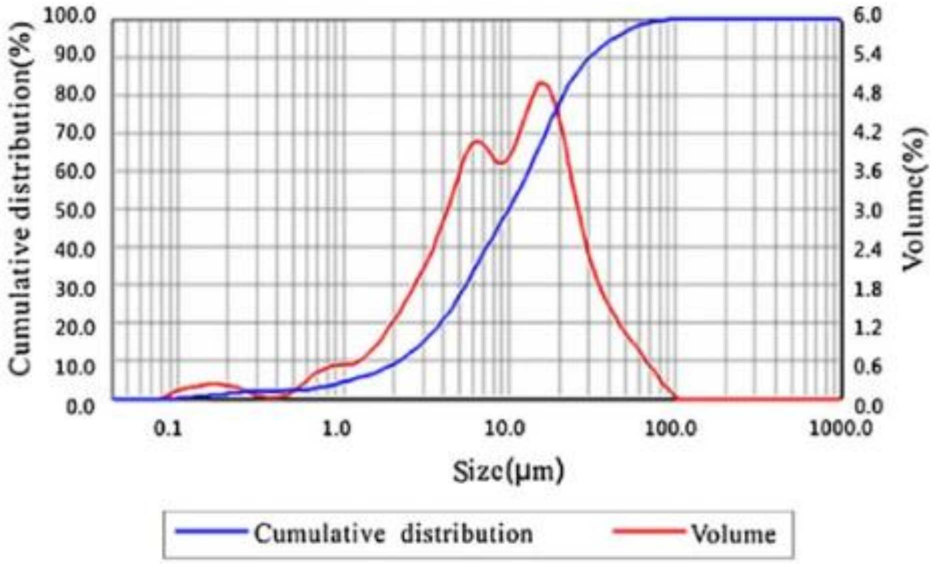


**Figure 2.3** Typical particle size distribution for fly ash produced in power generation (Li et al., 2014)

### 2.2.2 Measurement of density

In bulk materials handling and transportation, density of solids is either defined as bulk density or particle density (Guya, 2018). In this research, the bulk density is used as this represents the density when a material is mixed with a fluid medium such as air (fluidization), whilst the particle density is the "free" density of a material, and is always larger than the bulk density due to the absence of voids (Williams, 2008). As such, there exists a relationship between the bulk density and particle density together with the voids as defined in Equation 2.1 (Guya, 2018),

$$\rho_b = \frac{\rho_p}{1+e_v} \tag{2.1}$$

In Equation 2.1, $\rho_b$ represents the bulk density in $\mathrm{kg/m^3}$, $\rho_p$ represents the particle density in $\mathrm{kg/m^3}$ and $e_v$ is the dimensionless voids ratio.

A loose poured approach is used to measure the bulk density, where a known mass of bulk solids is poured into a container with a known volume and the bulk density is then determined (Guya, 2018). The consolidated (or compressed) bulk density is then determined by applying a known load onto the solids and measuring the change in density, using facilities such as Modified Jenike direct shear tester (Wits Course, Bulk Storage and Flow, Bulk Material Characterization, p34-36). As the bulk solids are compressed the voids are minimized. This process is then repeated by increasing the applied force (stress) until the bulk density reaches a steady state value and any increase in load does not result in significant bulk density changes (Gu *et al.*, 1991). Figure 2.2 shows typical results for bulk density under consolidated stress.

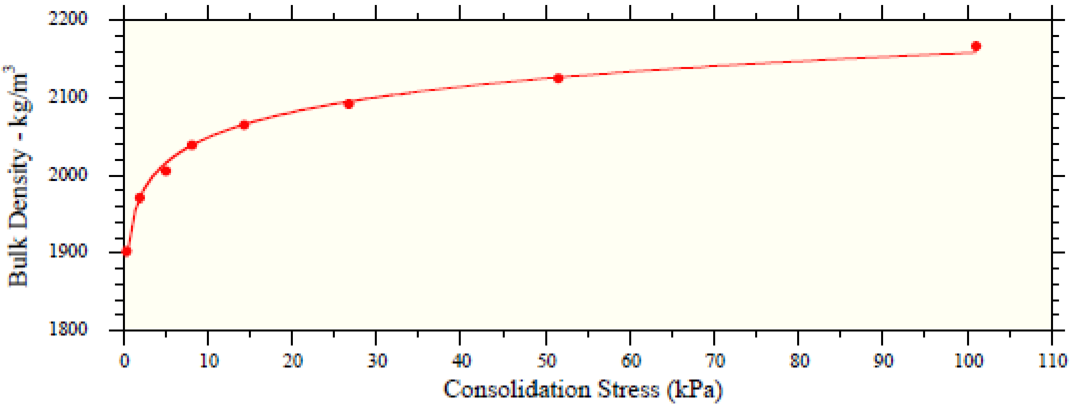


**Figure 2.4** Bulk density under compressibility test typical results (Wits Course, Bulk Storage and Flow, Bulk Material Characterization, p34-36)

After the bulk density has been determined the particle density can be computed using Equation 2.1 if the voids ratio is known. When both density (bulk or particle) and particle size distribution have been determined, one is then able to select the mode of pneumatic conveying suitable for the bulk solids to be transported (Williams, 2008).

## 2.3 Pneumatic Conveying Modes

Dense phase conveying systems are gaining wider appreciation due to their use of minimum compressed air, when compared with dilute conveying systems (Mills, 2016). While there are various descriptions with regard to dilute and dense phase, an understanding exists that these are typically differentiated by the amount of air required to either have the solids in suspension or non-suspension (Mills, 2016). A factor which is used to compare the amount of air to the amount of bulk solids in a conveying system is known as the solids loading ratio (SLR), $\mu$. The solids loading ratio (μ) is a dimensionless quantity described by the Equation 2.2:

$$\mu = \frac{m_s}{3.6 m_a} \qquad (2.2)$$

In Equation 2.2, $m_s$ is bulk solids flow rate in tonnes per hour and $m_a$ is the air mass flow rate in kg/s. Solids loading ratio can also be symbolized by ($m^*$).

The research described by Mills indicates that when the solids loading ratio is greater than 20, a dense phase flow system should be expected and at less than about 15, the system is dilute. The range in between (10-20) is termed the "transitional zone" as it is a mixed zone with unpredictable flow regimes. Figure 2.4 by Mills (2016) best illustrates the mixed zone as transitional from dilute to dense or vice versa.

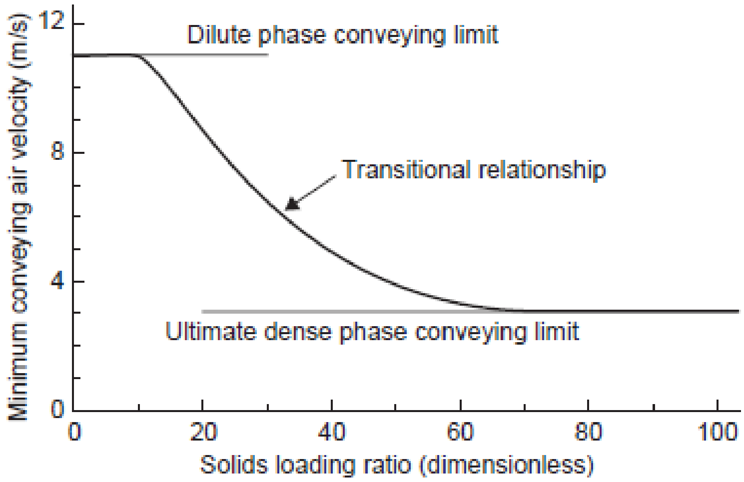


**Figure 2.5** Typical conveying limits for a fine grade of fly ash (Mills, 2016)

It should be noted that most researchers define dense and dilute phase simply based on whether the bulk solids are in suspension or not as they are being conveyed (Bansal, 2012). As such, dense phase conveying can be defined as a non-suspension flow in which the conveyed material is transported at low air velocities, below the saltation velocity (Deng and Bradley, 2016). This definition is widely accepted (Mills, 2016; Setia and Mallick, 2015). Within dense phase conveying systems, it is generally agreed that there are two distinct flow patterns visible (Williams 2008). Flow can be fluidized, which others (Mills, 2016) termed as moving bed, and this is typically observed for fine powders with good air retention properties. The second type is when flow can be viewed as slugs or plugs; this is for more coarse or granular materials and is characterized by consolidated plugs separated by air gaps (Mills 2016; Deng and Bradley, 2016). The literature review on these two forms of dense phase is based on the research conducted by Williams (2008: 4-7).

### 2.3.1 Plug flow

Williams defined plug or slug flow, "when fully developed, is characterized by distinct separated areas with large air gaps between full plugs of material" (Williams, 2008: 4). Figure 2.6 shows formation of plug flow. The size of the plugs varies based on pressure, air flow rate and bulk solids flow rate (Williams, 2008). Figure 2.6 illustrates that it is possible to destroy plugs in a conveying system and develop a dilute phase flow by increasing the air flow rate, and this is also reversible.

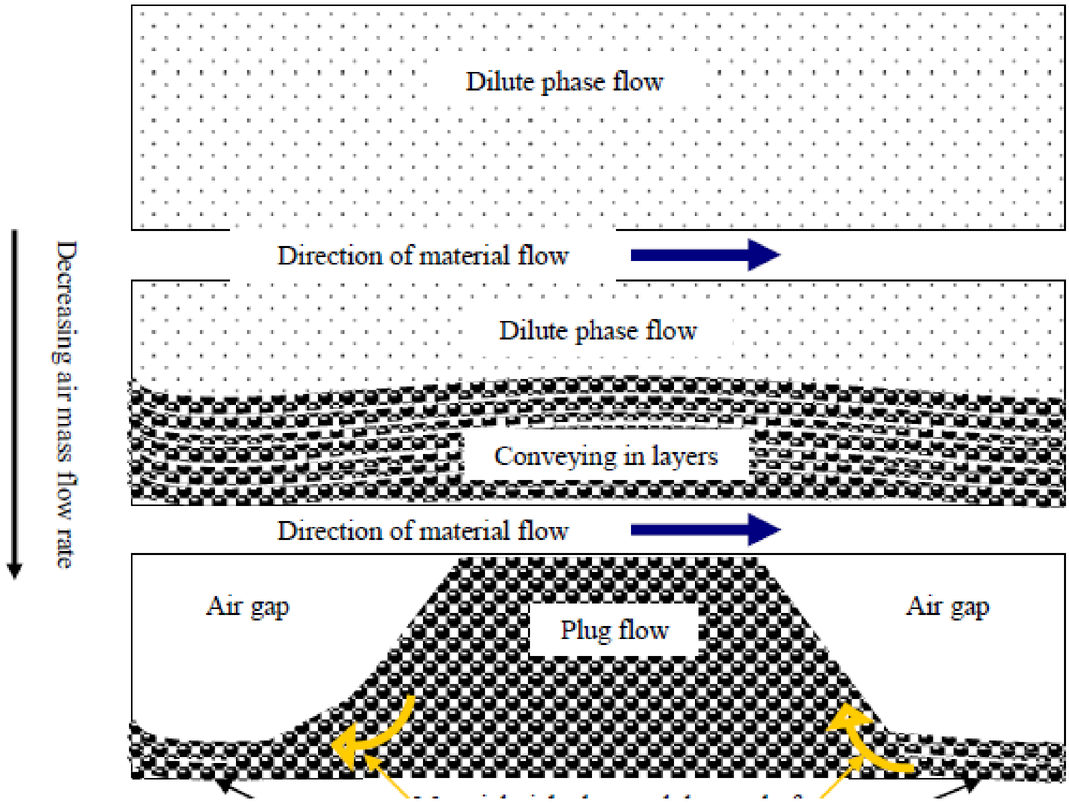


**Figure 2.6** Pneumatic conveying transitions from dilute to plug dense flow (Williams, 2008)

What is to be noted is that based on the air flow rate, there is a transition zone between the full plugs and full dilute phase as the air flow rate is increased (or reduced if flow was initially dilute phase). This transition zone as indicated in Figure 2.7 can also be termed an unstable or no-go zone for certain materials as it results in erratic flow behavior with high pressure peaks and high system vibration (Williams 2008).

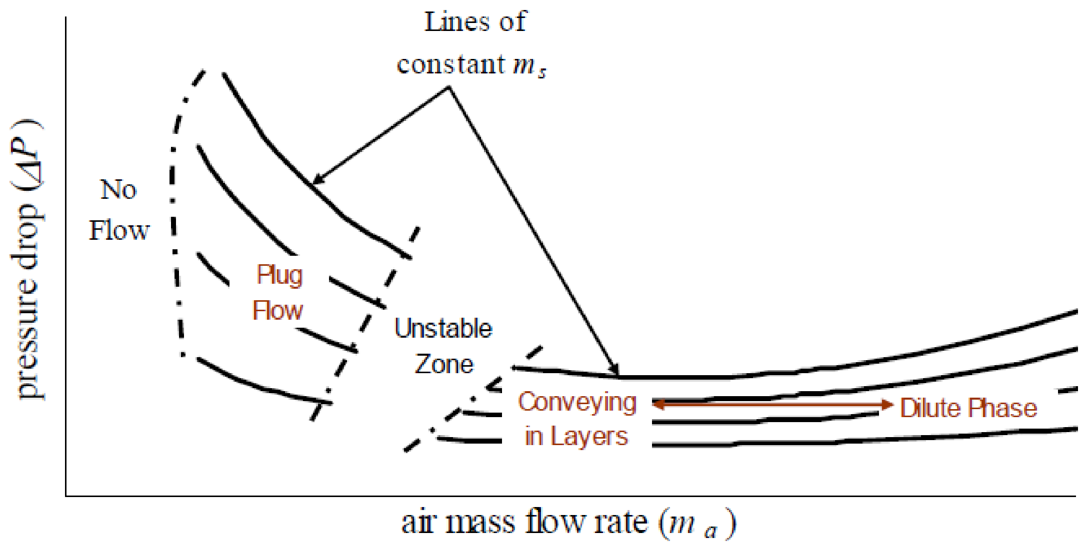


**Figure 2.7** Plug flow pneumatic conveying diagram (Williams, 2008)

Based on Figures 2.5 to 2.7 indicating a transition zone (unstable) it is important that the air mass flow rate is limited in order to avoid unnecessary transitions from a plug (dense) flow into a dilute phase as the transition zone may also be prone to blockage.

### 2.3.2 Fluidized flow

A fluidized bed flow is characterized by a dilute flow in the upper sections of the pipe, and a moving bed flow in the bottom section of the pipe as indicated in Figure 2.8. This is typical for materials with mean diameters of less than 100 microns and a large particle size distribution (Williams, 2008),

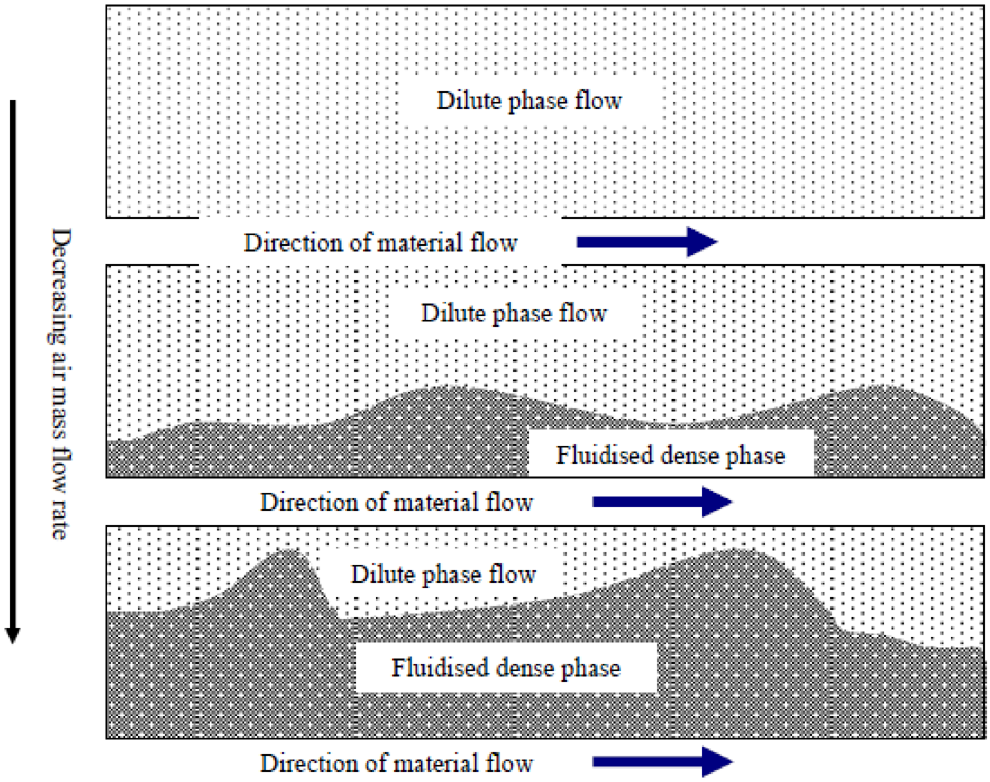


**Figure 2.8** Transition from Dilute Phase to Fluidized dense flow (Williams, 2008)

Similar transition zones are encountered for fluidized dense phase flow, as shown in Figure 2.9. As indicated in the plug flow case, it is necessary to maintain a reliable and constant low air mass flow rate to maintain a dense phase system, and any increase in air flow rate will lead to a high air flow dilute system.

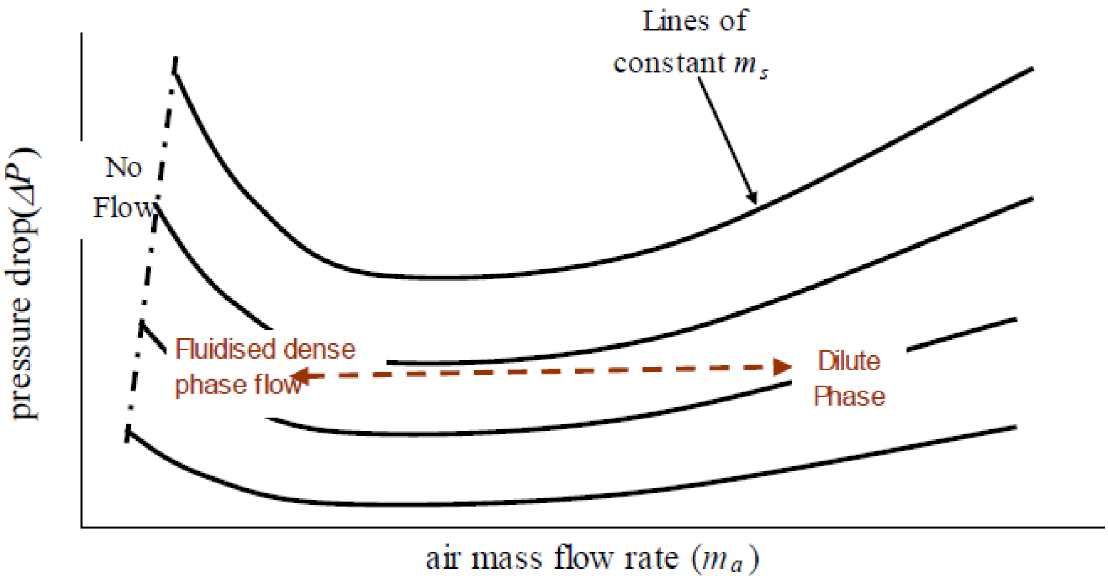


**Figure 2.9** Fluidized dense flow pneumatic conveying (Williams, 2008)

Figures 2.7 and 2.9 represent pneumatic conveying characteristics where the pressure drop is defined as a function of air flow rate. These figures indicate that for efficient conveying in a particular conveying mode, it is necessary to maintain the air flow rate. Any increase or decrease of flow rate from design value can lead to a pneumatic system that performs in an unstable flow regime that is characterized by possible blockages, sporadic pressure drops and high turbulence. It is therefore necessary for efficient operation to accurately determine the required air flow rate and then ensure that the system operates at this flow rate, taking into account air expansion along the pipeline.

## 2.4 Conveying Pressure

In order to maintain a reliable flow of bulk solids without blockages, a minimum conveying pressure is required which must be high enough to overcome the frictional effects imposed on the system (Williams, 2008). This pressure is a function of the friction dynamics that exist within a conveying pipe between the solids-air mixture and the pipe wall. This pressure must be sufficient to also overcome the resistance caused by the following: length of the conveying pipe, resistances created on flow at bends and gravitational forces acting against the flow along the vertical sections of the pipe (Mills, 2016) as well as pressure losses when the solids are introduced into the pipe, and any pressure necessary to move the solids from a rest position. This methodology of breaking up the various pressure components and consolidating at a later stage was proposed by Marcus and Chambers (Mallick, 2009). These aspects are discussed in sections 2.4.1-2.4.5, and a consolidated expression of pressure is shown in section 2.4.6.
Methods of estimating the friction factor are discussed in section 2.5.

### 2.4.1 Conveying pressure loss over a horizontal length

In long distance conveying, i.e., conveying with distances of greater than 300 m, the most dominant resistance is the length. As such, a designer must ensure that the conveying pressure is greater than the frictional losses due to the conveying distance (Bettman, 1987).

This pressure loss due to the conveying distance is described by the Equation (2.3) as first proposed by Barth as noted by Mallick (2009). Although Barth had described this equation for use in dilute phase, it has been applied for use in dense phase as well (Mallick, 2009, Sheer 1991).

$$\Delta P_H = \frac{(\lambda_a + \mu\lambda_s)\rho_a {v_a}^2 L}{2D} \qquad (2.3)$$

In Equation 2.3, $\Delta P_H$ is the pressure loss due to horizontal conveying length in kPa, $\lambda_a$ and $\lambda_s$ represent the dimensionless friction factors due to the air and bulk solids respectively whilst $\mu$ is the solids loading ratio. Air density is indicated as $\rho_a$ in kg/m$^3$, $v_a$ is the air velocity m/s, $L$ is the conveying length in m and $D$is the pipe diameter in m.

Equation 2.3 represents the pressure drop on the conveying line due to both the air and solids over a conveying distance, and the friction factors ($\lambda_a$, $\lambda_s$) and solids loading ratio relate to how much this air-solids mixture contributes to this pressure drop. This Equation is widely accepted as sufficient to express the pressure drop over a conveying distance in dense phase conveying (Bettman 1987, Setia and Mallick 2015). It is also worth noting that the air contribution to pressure drop is typically 10% of the overall pressure drop and hence the largest contribution comes from the pipe interaction of solids along the conveying distance (Williams 2008).
In most design cases, the conveying length is given, possibly due to mining process output location, or in power generation this is determined by where the ash can be dumped. As such, most designers try to minimize the pressure drop ($\Delta P$) by increasing the pipe diameter ($D$). Especially for very long conveying distances, in excess of 1000 m, one finds what is termed telescoping piping where the pipe diameters are stepped up, for example every 300 m (Bettman, 1987). Telescoping piping has been widely researched (Bettman 1987, Mills 2016) and does provide improvements in reducing pressure drop along the length of the conveying pipe.

The air density is computed from actual conditions, i.e., pressure and temperature in the conveying pipe and this varies along the length of the pipe (Mills and Agarwal, 2001) and the velocity is computed from the density and air flow rate. Equations for calculating density and velocity are shown in 2.4 and 2.5 respectively,

$$\rho = \frac{P}{RT} \tag{2.4}$$

In Equation 2.4, $\rho$ is the air density in kg/m$^3$, $P$ is the absolute pressure in kPa, $R$ is the universal constant of air as 0.287 kJ/kg K and $T$ is the temperature in Kelvin. It should be noted that the density varies along the conveying pipe as the pressure and temperature change (Mills and Agarwal, 2001).

$$v_a = \frac{4 m_a R T}{P \pi D^2} \tag{2.5}$$

In Equation 2.5, $v_a$ or simply $v$ is the air velocity in m/s, $m_a$ is the air mass flow rate in kg/s, and all other parameters are as defined under Equations 2.3 and 2.4.

Once Equations 2.4 and 2.5 have been solved with known values of flow rate and air density, the designer is able to determine the pressure drop along the length and select a suitable pipe diameter using Equation 2.3, provided the friction factors are known.

### 2.4.2 Pressure loss along a bend

Another area where there is a pressure loss that needs to be overcome by the conveying pressure is the loss as the flow comes along a bend, and this is expressed as proposed by Marcus and Chambers (Mallick, 2009) as indicated in Equation 2.6,

$$P_B = \frac{NB(1+\mu)\rho v^2}{2} \tag{2.6}$$

In Equation 2.6, $P_B$ is the bend pressure, $N$ is the number of bends, $B$ is the dimensionless bend factor and $\rho$ and $v$ are as per Equations 2.4 and 2.5 respectively.

The bend factor is based on the radius to diameter ratio of a bend, as defined in Table 2.1 (Bettman, 1987).

**Table 2.1** Bend factor Table

| Radius-diameter ratio $(R/D)$ | Bend factor $(B)$ |
|---|---|
| 2 | 1.5 |
| 4 | 0.75 |
| 5 | 0.5 |

As noted by Bettman (1987), Table 2.1 illustrates that the pressure drop along a bend will increase as the bend radius is decreased. As such, designers always try to minimize the impact of bend loss by increasing the radius around the bend.

Another form researchers use for calculation of bend pressure loss is to convert the bend radius into an equivalent length and then Equation 2.3 can used considering the bend as a straight section (Bansal, 2012).

### 2.4.3 Pressure loss at pick up of material (acceleration)

Marcus and Chambers (Mallick, 2009) presented Equation 2.7 as a form that can be used to estimate the pressure drop due to initial pick-up of solids,

$$P_A = \frac{\rho v^2 (1+2\mu \frac{v_s}{v_a})}{2} \quad (2.7)$$

In Equation 2.7, $P_A$ is the acceleration pressure drop, and $\frac{v_s}{v_a}$ represents the ratio between the solids and air velocities. Density and velocity, $\rho$ and $v$, are as per Equations 2.4 and 2.5 respectively.

The pick-up pressure loss is difficult to predict due to the interactions between the air and solids particles in highly turbulent flows at pick-up. These turbulent flows are also induced at times in order to break up consolidation of bulk solids that may lead to a blockage scenario (Mills, 2016).

### 2.4.4 Pressure loss along the vertical section of the pipe

Equation 2.8 can be used to estimate the pressure exerted by the weight of the products as they are lifted along the length of the pipe in an upward direction (Mallick, 2009).

$$P_V = \mu \rho g L_v \left(\frac{v_s}{v_a}\right) \quad (2.8)$$

In the Equation 2.8, $P_V$ is the pressure drop to overcome the vertical distance in kPa, $L_v$ is the equivalent length in m. Density and velocity, $\rho$ and $v$, are as per Equations 2.4 and 2.5 respectively. The velocity ratio in Equation 2.8 is calculated as shown in Equation 2.9 from the work of Hinkle (Rhodes, 2008).

$$\frac{v_s}{v_a} = 1 - 0.0638 d_p^{0.3} \rho_s^{0.5} \quad (2.9)$$

In Equation 2.9, $d_p$ is the particle diameter in mm, and $\rho_s$ is the solids bulk density in kg/m$^3$.

Equation 2.9 is also used to evaluate the solids velocity with Klinzing having proposed a similar model for the prediction of solids velocity, as indicated in Equation 2.10 (Sharma *et al.*, 2018).

$$v_s = (v_a - {w_{fo}}^{0.71})D^{0.019} \tag{2.10}$$

In Equation 2.10, $w_{fo}$ is the terminal velocity in m/s (described in greater detail in Equation 2.18) and $D$ is the pipe diameter in meters.

It should also be noted that the pressure prediction models presented in sections 2.4.1 to 2.4.4 use the air velocity and the velocity ratio to predict the pressure losses along the pipe. The solids velocity is not used in pressure prediction models presented thus far but Equations 2.9 and 2.10 can be used if one is interested in the solids velocity.

### 2.4.5 Total pressure loss (minimum conveying pressure)

The minimum conveying pressure required to convey the bulk solids must be able to overcome all the pressures described in sections 2.4.1-2.4.4, and this is the total pressure expressed in Equation 2.11.

$$P_T = P_H + P_B + P_A + P_V = \Delta P \tag{2.11}$$

In Equation 2.11, $\Delta P$ represents the total pressure loss in kPa.

## 2.5 Friction Factor

Pressure drop along the pipe relies on the friction factors; Equation 2.3 is made up of friction factors for the bulk solids and air. Friction pressure models are typically based on this two-phase flow approach, where the air friction factor is analyzed separately from the bulk solids friction factor, (Williams, 2008). Air-only friction and pressure models are common and some of these Equations are indicated in section 2.5.1 and the solids friction factor is discussed in section 2.5.2.

### 2.5.1 Air friction factors

Review of air-only friction models reveals that there is extensive and well documented literature on calculation of air friction factor and the Equations 2.12 and 2.13 are two of the commonly used forms (Williams, 2008).

Equation 2.12 is to calculate the pressure drop due to air only for most pipes by using average values for air velocity and density (this is the air only component of Equation 2.3),

$$\Delta P_A = \frac{4fL\rho_{ave}v_{ave}^2}{2D} \tag{2.12}$$

In Equation 2.12, $(4f)$ or $\lambda_a$ is the friction factor for air only. Whilst there are numerous methods for calculating the air only friction factor, the form preferred in this research is the one used by Williams (2008),

$$\lambda_a = \frac{1.325}{\ln\left(\frac{5.74}{{Re_a}^{0.9}}\right)^2} \tag{2.13}$$

Equations 2.12 and 2.13 have been derived from numerous researches, and these are not discussed in further detail as the air pressure drop contribution is much less at usually less than 10% compared to solids pressure drop (Williams, 2008).

### 2.5.2 Solids friction factors

The solids friction factor is a complex entity and currently there are no widely accepted theoretical models to accurately predict solids friction factors and pressure drop; however some of the generally used approaches are included here.

***Weber Equation***

One of the initial Equations (2.14) for solid friction factors is from Weber (1981),

$$\lambda_s = \frac{2.1Fr_s^{0.5}}{m^{*0.3}Fr^2}\left(\frac{D}{d_p}\right)^{0.1} \tag{2.14}$$

In Equation 2.14, $\lambda_s$ is the solid friction factor, D is the pipe diameter in $m$, $d_p$ is the particle diameter in $m$, $Fr$ is the dimensionless Froude number, $m^*$ represents the dimensionless solids loading ratio (used as $\mu$ in this research report).

This Equation was further developed by Jones and Williams (2003) with specific research on fluidized materials resulting in an improved equation for fluidized dense phase conveying (2.15):

$$\lambda_s = \frac{83}{m^{*0.9}Fr^2} \tag{2.15}$$

Jones and Williams developed Equation (2.15) for fly ash by using what is termed the power law, and this is the preferred method for most researchers in terms of developing a model to estimate solids friction factor (Jones and Williams, 2003; Williams 2008, Behera *et al*., 2015).

***The power law method***

Williams (2018) and Behera *et al*. (2015) have improved on Equations (2.14) and (2.15) by using a power law function that established the relationship between the solids friction factor, the solids loading ratio and the Froude number. This relationship is expressed in (2.16),

$$\lambda_s = C(m^*)^a (Fr_i)^b \left(\frac{\rho_s}{\rho_a}\right)^d \qquad (2.16)$$

In Equation 2.16, $Fr_i$ is the inlet gas Froude number according to Behera *et al*. (2015), however other researchers advocate for use of mean or average Froude numbers to cater for the expansion of the air (Wypych, 1989; Sheer, 1991).

Equation (2.16) is the basic form for Equations (2.14) and (2.15) expressed using dimensionless coefficients or power functions, *a*, *b* and *c*. Using experimental data, these coefficients can be determined using known values for solids loading ratio, inlet Froude numbers and solids to air density ratio. As such, a new model can be developed based on specific experimental data. This then represents an improved form of the Weber Equation, and this has been used with success (Williams, 2008). Behera *et al* used this approach to develop a model for prediction of solids friction factor, shown by Equation (2.17).

To illustrate how this is achieved, from Equation (2.15), Behera *et al* solved for the power functions such that, $C = 364.4$, $a = -1.29$, $b = -2.36$ and $c = 0.01$ for fly ash and alumina solids conveying in dense phase. Substituting in Equation (2.15), Behera *et al* developed Equation (2.17) for dense phase fly ash conveying,

$$\lambda_s = 364.4(m^*)^{-1.29} (Fr_i)^{-2.36} \left(\frac{\rho_s}{\rho_a}\right)^{0.01} \qquad (2.17)$$

As expected from results by Williams and Jones (2003), Behera *et al* also found that the density ratio $\left(\frac{\rho_s}{\rho_a}\right)$ is negligible, and hence Equation (2.17) can be simplified to be similar to the findings by Jones and Williams in Equation (2.15) as expressed below in Equation (2.18),

$$\lambda_s = \frac{364.4}{m^{*1.29} Fr^{2.36}} \tag{2.18}$$

As such, a designer is able to develop a model for calculating solids friction factor specific to a particular set of bulk solids data, giving a model similar to Equations (2.15) and (2.18).

***Volumetric loading ratio (VLR)***

In recent years researchers have suggested another method that considers the air and solids relationship separately in the flow, using a dimensionless factor called the volumetric loading ratio (VLR) and the dimensionless velocity ratio (Setia *et al*, 2015). The VLR represents the respective volumes occupied in the pipe stream by solids and air as expressed in Equation (2.19) (Setia *et al.*, 2015),

$$VLR = \left( \left(\frac{m_s}{\rho_s}\right) \Big/ \left(\frac{m_a}{\rho_a}\right) \right) \tag{2.19}$$

In Equation (2.19), $VLR$ is the volumetric loading ratio, with $m$ and $\rho$ representing the mass flow rate in kg/s and density in kg/m$^3$ for solids and air as denoted by subscripts, $s$ and $a$ respectively.

The dimensionless velocity ratio attempts to define the dense-dilute phase relationship that exists in the pipe line (Setia *et al*, 2015) and is described by an Equation of the form (2.20),

$$\text{Dimensionless velocity} = \left(\frac{w_{fo}}{v}\right) \tag{2.20}$$

In Equation (2.20), $v$ is the air velocity in m/s and $w_{fo}$ represents the terminal settling velocity of the solids, solved using Equation (2.21),

$$w_{fo} = \left[\frac{4gd(\rho_s - \rho_a)}{3C_D\rho_a}\right]^{0.5} \quad (2.21)$$

In Equation (2.21), $C_D$ is the drag coefficient in the conveying stream.

Equations (2.19) and (2.20) were used in a similar approach to the power law to solve for $a, b$ and $K$ to develop a model for the solids friction factor as shown in Equation (2.22),

$$\lambda_s = K(VLR)^a \left(\frac{w_{fo}}{v}\right)^b \quad (2.22)$$

Using data from experiments, Setia *et al* (2015) were able to develop Equation (2.23) that can be used to predict the solids friction factor for fly ash,

$$\lambda_s = 0.643\mathrm{VLR}^{0.316} \left(\frac{\mathrm{w_{fo}}}{\mathrm{v}}\right)^{0.777} \quad (2.23)$$

Setia *et al.*, (2016) further developed the volumetric loading ratio methodology into what they termed the two-layer theory, where instead of developing an Equation such as (2.23), the dilute contribution is calculated separately from the dense phase contribution.
The resulting two layered approach is expressed as shown in Equation (2.24),

$$\lambda_s = \tau_1 \left(K(VLR)^a \left(\frac{w_{fo}}{v}\right)^b\right) + \tau_2 \left(\frac{\lambda_s^* C}{V} + \frac{2\beta_0}{\left[\frac{C}{V} Fr^2\right]}\right) \quad (2.24)$$

In Equation (2.24), the first part represents the dense phase (similar to Equation 2.22), and the second part represents the dilute phase wherein $\tau_1$ and $\tau_2$ are defined as shown in Equation (2.25) and (2.26),

$$\tau_1 = \frac{1 - (\mathrm{Fr} - \mathrm{Fr_{min}})}{\mathrm{Fr_{max}} - \mathrm{Fr_{min}}} \quad (2.25)$$

$$\tau_2 = \frac{\mathrm{Fr} - \mathrm{Fr_{min}}}{\mathrm{Fr_{max}} - \mathrm{Fr_{min}}} \quad (2.26)$$

The Froude numbers are based on velocity conditions at various conveying regimes, as defined in Setia *et al* (2016).

Equations (2.14), (2.15), (2.18), (2.23) and (2.24) show that uncertainty and interest still remains to adequately develop a model that accurately predicts solids friction factor with minimum deviation to actual data. Unfortunately, a method does not currently exist that can reliably predict conveying pressure drop to accuracy of less than 10% and this is an area of continued research.

## 2.6 Air Flow Rate

Using ideal gas laws, the relationship between two positions, such as between the actual condition and the standard condition can be computed from the following Equation given by (2.27) (Mills, 2016),

$$\frac{P_1\dot{V}_1}{T_1} = \frac{P_2\dot{V}_2}{T_2} \tag{2.27}$$

Where, $P$ is the pressure in kPa, T is in Kelvin and $\dot{V}$ is the volumetric air flow rate in $m^3/s$. The air mass flow rate can be computed using Equation (7.28), as,

$$\dot{m}_a = \rho\dot{V} \tag{2.28}$$

Where, $\dot{m}_a$ is the mass air flow rate in kg/s, $\rho$ is the air density in $kg/m^3$ and $\dot{V}$ is the volumetric air flow rate in $m^3/s$.

## 2.7 Long Distance Conveying for Dense Phase Conveying in Fly Ash

It was also necessary to review the influence of conveying distance on a pneumatic system. Data from previous researchers considering dense phase conveying and specific to fly ash were also reviewed, to ascertain typical conveying characteristics for fly ash in dense phase as the conveying distance is varied. This was done by observing the pressure drop and air flow rate as the conveying distance is increased, as well as the various operating regimes that have been noted.

### 2.7.1 Conveying characteristics as the conveying distance is increased

It was necessary to review the relationship between air flows as the conveying distance is increased. This is due to the nature of this research as the three boiler Units have different conveying distances as covered in detail in Chapter 3, Table 3.2. For illustration purposes, the conveying length difference between Unit 1 and Unit 3 is 223 m in this power station and hence it was necessary to review the impact of conveying distance on pneumatic conveying variables such as air flow and pressure drop.

Review of this literature was based largely on the work by Bettman (1987), who conducted tests at various conveying distances and pipe diameters. Bettman showed that as the conveying distance is increased, more energy and air consumption is required for the same amount of material up to an optimum point, refer to Figure 2.10.

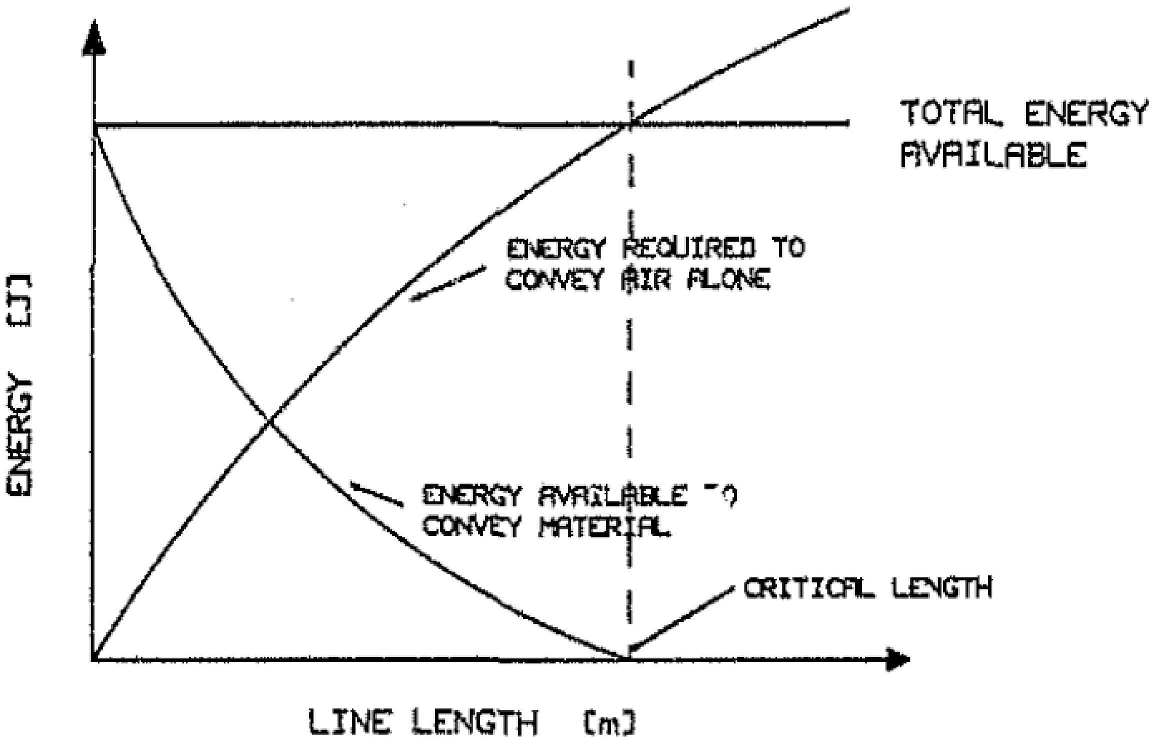


**Figure 2.10** Conveying distance impact on energy consumption (Bettman, 1987)

Experimental results obtained by Bettman (1987) are also considered of particular interest in this research as they closely resemble the present experimentation and these were reviewed to highlight what results could be expected. The main difference that must be highlighted is that Bettman's long distance conveying was made up of stepped pipe diameters and hence it is expected that at stepped positions along the pipe length there is a pressure gradient reduction and hence the overall pressure drop will not be similar for a continuous pipe length with constant diameter such as in this research.

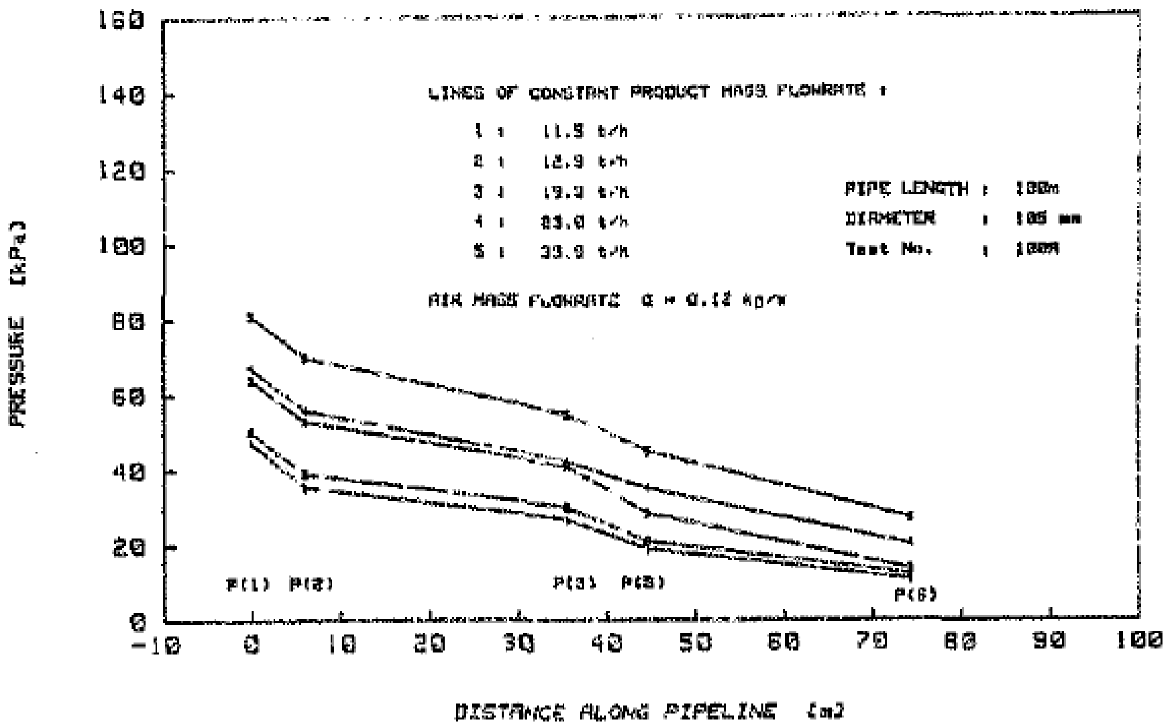


**Figure 2.11** Pressure drop per conveying distance (Bettman, 1987)

Figure 2.11 illustrates that as the conveying distance is increased, the pressure drop is also expected to increase, this is as expressed in Equation (2.3), pressure drop across a conveying distance. As such, one expects that there is a considerable pressure drop difference comparing two Units that are spaced apart by approximately 200 m length as is the case in this research.

### 2.7.2 Tandem pressure vessels and pre-pressurization

Another issue that the present author investigated was the operation of pressure vessels (blow tanks) as installed in this power station. Jardine discussed the importance of operating pressure vessels in tandem as well as pre-pressurization of these vessels (Jardine, 1986).

***Tandem pressure vessels***

Jardine (1986) observed that the efficiency of pneumatic conveying systems can be improved by operating pressure vessels in a parallel manner, instead of in series where conveying waits for one cycle to complete and then the next new cycle is initiated. This is best explained in Figure 2.12, where the dotted lines indicate performance in parallel between the conveying vessels. This is referred to as tandem vessels, where two vessels or a series of vessels are connected to a single conveying pipe. Figure 2.12 depicts this configuration,

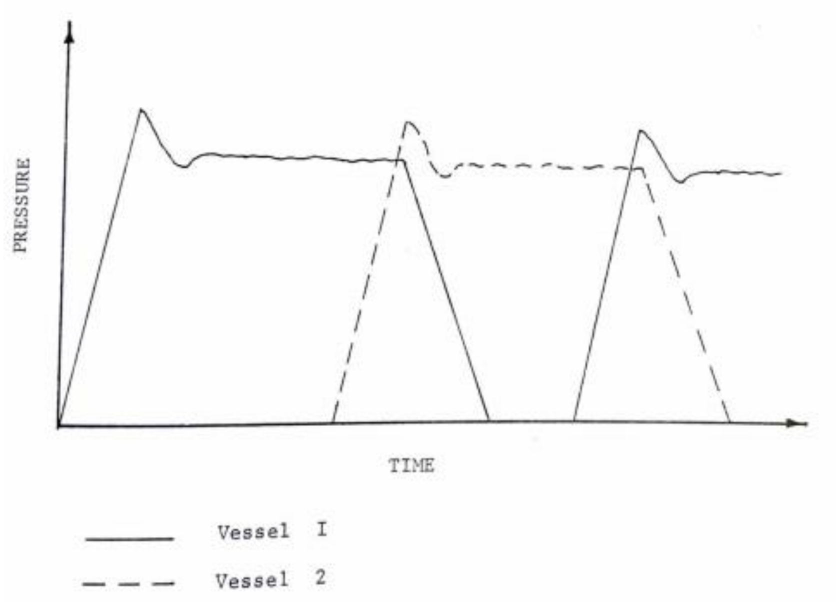


**Figure 2.12** Tandem pressure vessel configuration (Jardine, 1986)

Jardine concluded that this needs to be tested at long distance conveying to observe the impact as many researchers typically test up to 400 m, and longer distances have been found in industry (Jardine, 1986).

***Pre-pressurization of pressure vessels***

Williams (Williams, 2008) observed that as the material first comes into contact with air inside the pressure vessel or blow tank, there appears an over-pressurization above the steady state conveying pressure required. Figure 2.13 best summarizes his observation about this phenomenon and it is included here as the present author has observed in many conveying cycles that this is how ash is actually conveyed.

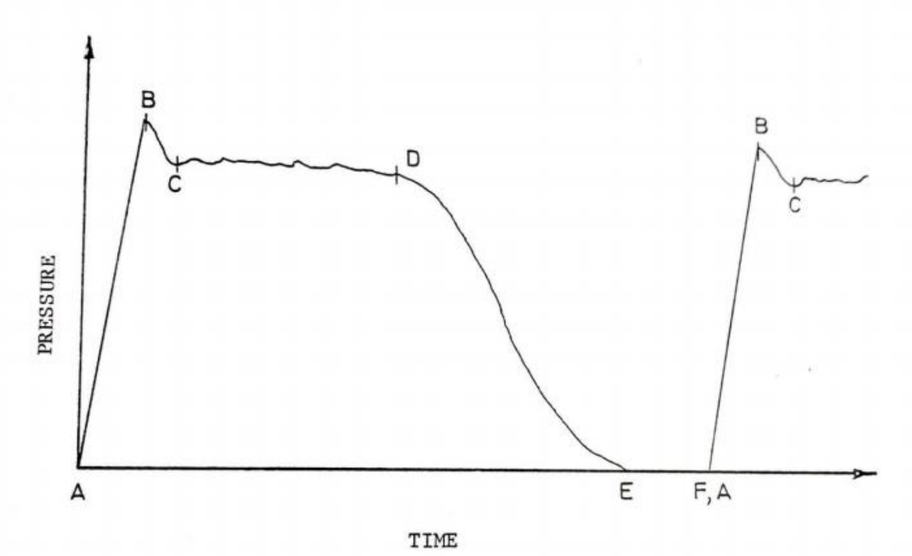


**Figure 2.13** Pre-pressurization and steady state conveying (Jardine, 1986)

In figure 2.13, the sections are defined as (Jardine, 1986):

A-B: Initial vessel pressurization
B- C: Initial transient on opening discharge valve
C-D: Average steady state conveying
D-E: Final transient as last material is conveyed
E-F: Venting and refilling

As such, a designer must ensure that over the minimum conveying pressure, one has also ensured sufficient pressure is available to overcome the initial surge of material that results in what Williams termed as “pre-pressurization” as it appears in Figure 2.13, A-B (Williams, 2008).

## 2.8 Typical Values for Dense Phase Fly Ash Conveying

This section reviews data from literature on expected values of air flow rate, pressure drop and friction factors for fly ash conveying in dense phase mode. It should be noted that there is a wide range of data available from literature, however as noted in section 2.2, each set of data should be reviewed in line with its material properties. As such, this section is limited to results for fly ash.

**Table 2.2** Pneumatic conveying characteristics for dense phase conveying of fly ash from selected previous researchers

| Test number reference | Fly ash properties | | Pipe characteristics | | Pneumatic conveying characteristics | | | | |
|---|---|---|---|---|---|---|---|---|---|
| | Particle diameter (µm) | Bulk density (kg/m$^3$) | Pipe length (m) | Pipe diameter (m) | Air flow rate (kg/s) | Solids flow rate (kg/s) | Solids loading ratio (-) | Experimental pressure drop (kPa) | % Error in predicted pressure drop (kPa) |
| A173-1 (Williams, 2008) | 19 | 810 | 173 | 53 | 0.0809 | 3.60 | 44.5 | 377 | +/- 15% |
| SI.No.1 (Behera *et al.*, 2015) | 14.91 | 724 | 221 | 63 | 0.038 | 3.9 | 103 | 180 | +/- 14.8% |
| Setia (Setia et al, 2016) | 30 | 700 | 168 | 105 | 0.15 | 6.3 | 42 | 120 | +/-4.76 |
| Jardine (Jardine, 1986) | Not indicated | Not indicated | 202 | 100 | 0.307 | 12.3 | 40 | 210 | Not indicated |

*N/A – Not available

# CHAPTER 3 DESCRIPTION OF EQUIPMENT

## 3.1 Introduction

This chapter details the facilities and equipment used in investigating the air flow in a dense phase pneumatic conveying system for fly ash. The research was performed at an operating power station that was in commercial operation. The three power station Units, named in this report as Units 1, 2 and 3 were used as test facilities for the research. The plant and all associated equipment were installed prior to the research and the systems were in production mode and supplying power to the national network. Because of the constraints on the network, it was not possible to make any modifications or changes to the operating conditions. As such, the adjustment of set points, such as reducing the air flow until a blockage occurred, was not possible. Therefore, data collection was in the form of observation of the conveying system performance at various Unit operating conditions.

Description of the main systems is included in section 3.2, however due to the sensitivity of the information it was not possible to disclose all the details of the plant, as such drawings and photographs are not included. Limitations in terms of performance are shown in section 3.3. The type of fly ash produced is investigated as well as the test facility in 3.4. The instruments used and data acquisition system are discussed in 3.5 and 3.6 respectively.

## 3.2 Description of the Main Systems and Equipment

The main equipment used in the research is discussed in detail in the following sections:

- 3.2.1 Boiler ash hoppers
- 3.2.2 Pressure vessels
- 3.2.3 Conveying pipes
- 3.2.4 Compressed air supply
- 3.2.5 Ash silo and filter system.

### 3.2.1 Ash hoppers

Ash is produced from the boiler combustion process and the fly ash is discharged into ash hoppers directly beneath the pulse jet fabric filter plant. Ash production and quantities are discussed under section 4.2 as part of the power station operating philosophy. Ash is transferred from a hopper and fed into the pressure vessel (blow tank) through a dome valve. The main purpose of the pneumatic system in this installation was to ensure that the hopper remains as empty as possible. Each Unit was provided with 28 hoppers and when the Unit is in operation, ash is continuously discharged into these hoppers and conveyed to the ash silos, refer to Figure 3.1. To this end, all ash hoppers were fitted with a level indicator (section 3.5.2) to ensure continuous ash removal if ash is detected in the hopper. The total volume for each hopper was approximately 74 $m^3$.

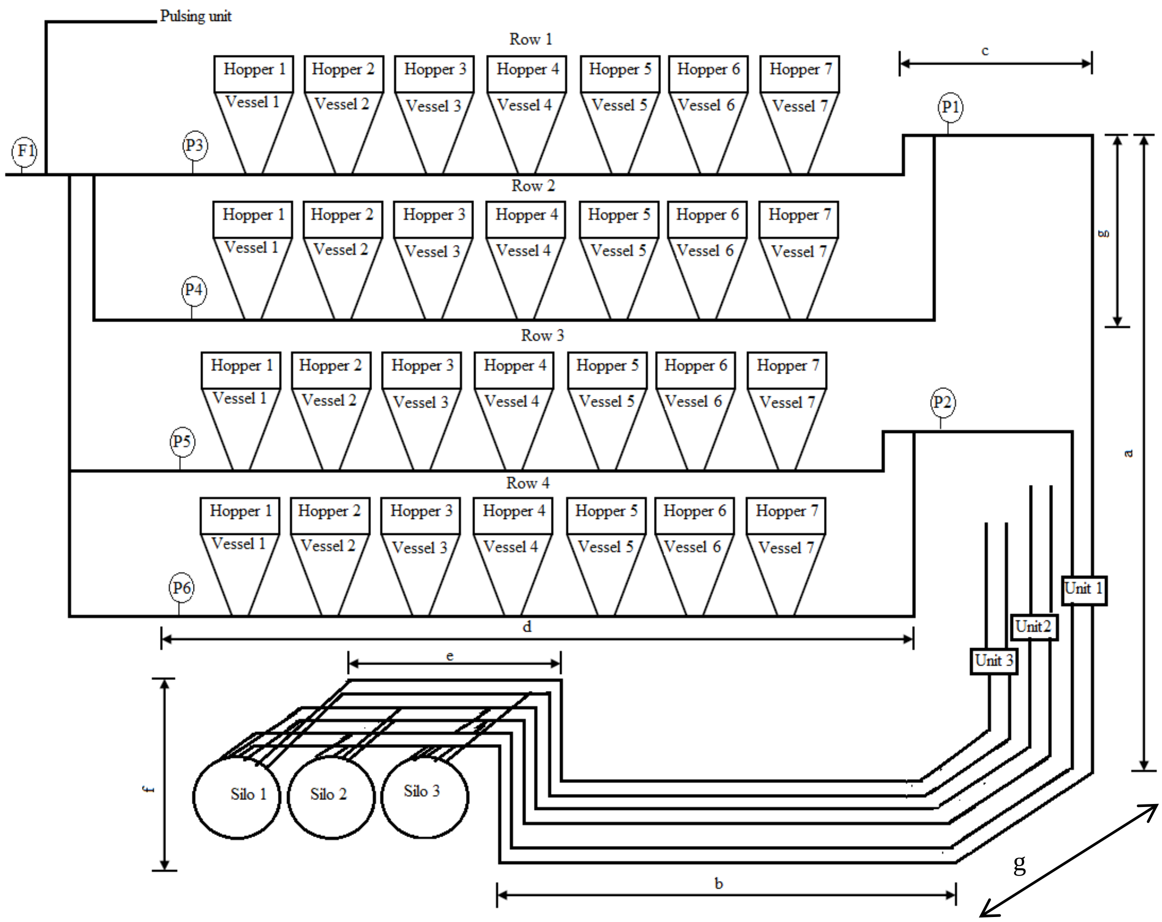


**Figure 3.1** Layout of the pneumatic conveying system

### 3.2.2 Blow tanks (pressure vessels)

Located directly underneath the ash hoppers are blow tanks are which in this report are generally referred to as pressure vessels. There is an isolation valve between each hopper and pressure vessel; these are dome valves (feeding mechanism).

During conveying cycles, the pressure vessel system witnesses initial pressurization effects and these pressures are always higher than the conveying pressures necessary for conveying (Jardine, 1986). As such, blow tanks are preferred as feeding devices as they can withstand high pressures, in excess of 350 kPa (Mi, 1994). These pressure vessels, also 28 per Unit, are smaller in size compared to the hoppers (refer to Appendix C for specification of these vessels). Each pressure vessel is 2.2 $m^3$ in volume. Figure 3.2 shows part of the pressure vessel and hopper arrangement.

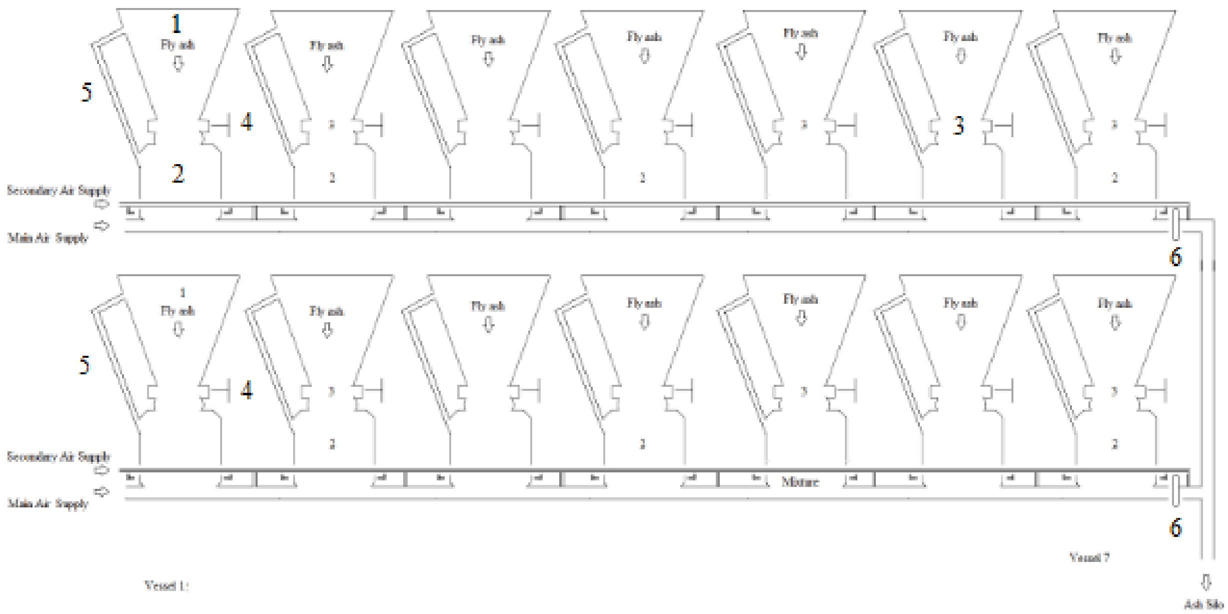


**Figure 3.2** Fly ash hoppers and pressure vessels

Description of the items 1-6 as shown on figure 3.2 is explained in Table 3.1 with their functions also noted, numbers in table 3.1 relate to numbers in figure 3.2. Vessel 1 is also termed the master vessel and vessel 7 is the outlet vessel, and the vessels in between are slaves; refer to figure 4.1 where these are explained as part of the operating philosophy.

**Table 3.1** Description of hopper and vessel arrangement

| Item | Description | Function |
|---|---|---|
| 1 | Fly ash hopper | Temporarily stores fly ash for discharge into the vessel. |
| 2 | Pressure vessel | Ash and air are mixed at high pressure in preparation for pneumatic conveying. |
| 3 | Inlet valve | Opens and closes to allow ash into the pressure vessel. |
| 4 | Knife gate | Used to isolate a specific ash hopper. |
| 5 | Vent line | Used to depressurize the vessel after conveying and when ash is transferred from hopper to vessel. |
| 6 | Outlet valve | Opens and closes to allow ash to pass into the conveying line for discharge to the ash silo. |

The secondary and main air supply is made up of numerous airlines, with orifice plates at supply points as indicated on figure 3.3 and Appendix E. Figure 3.3 is also discussed as in chapter 4, as Figure 4.1; this was necessary to explain the system operation. The list of equipment is also indicated in chapter 4 and Table 4.3 where these are discussed in terms of how the system operates.

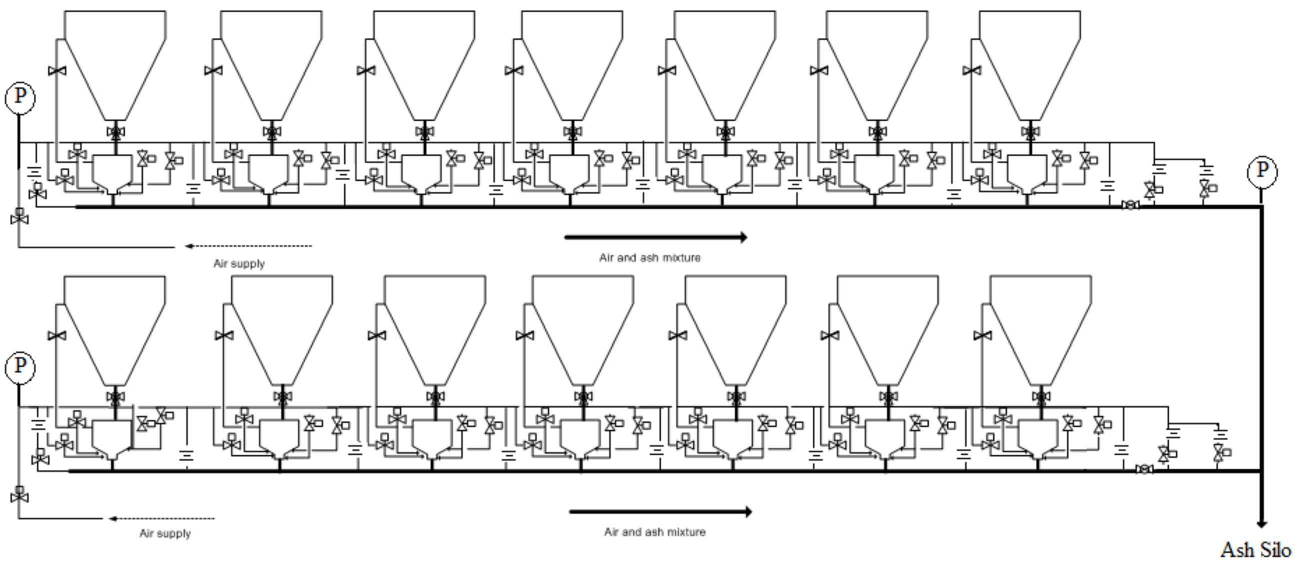


**Figure 3.3** Process flow diagram

### 3.2.3 Conveying pipes

The pressure vessels in each row are all interconnected by conveying pipes, 7 sections in series, with a total of 4 rows (28 vessels in total). All the pipes were of the same diameter of 265 mm in all the three Units. These were flanged connected pipes, made from mild steel with ceramic lined spool pieces for bends to ensure pipe wear is minimized (refer to Appendix B for more details on the pipe). The pipeline between the pressure vessels in each row also has an additional air supply line within the conveying pipe; this pipe-inside-the-pipe is designed to break up any consolidation of solids during start-up that could cause blockages.

Table 3.2 indicates the dimensions in terms of pipe diameters and lengths from the hoppers to the receiving silo per power station Unit. It can also be observed from Figure 3.1 that each Unit has two pipeline networks with each network independent from the other. As such, each Unit has two conveying pipelines to the silos. Refer to Table 3.2 for these conveying distances.

**Table 3.2** Conveying pipe diameter and distances from power plant to dedicated ash silos

| **Power plant Unit** | **Total horizontal** (m) | **Total vertical** (m) | **Total conveying distance** (m) | **Pipe inner bore** (mm) |
|---|---|---|---|---|
| Unit 6 Line 1 | 931 | 39 | 970 | 315 |
| Unit 6 Line 2 | 892 | 39 | 932 | 315 |
| Unit 5 Line 1 | 819 | 39 | 858 | 315 |
| Unit 5 Line 2 | 781 | 39 | 820 | 315 |
| Unit 4 Line 1 | 705 | 39 | 744 | 315 |
| Unit 4 Line 2 | 667 | 39 | 707 | 315 |
| Unit 3 Line 1 | 589 | 39 | 628 | 265 |
| Unit 3 Line 2 | 551 | 39 | 590 | 265 |
| Unit 2 Line 1 | 477 | 39 | 516 | 265 |
| Unit 2 Line 2 | 439 | 39 | 478 | 265 |
| Unit 1 Line 1 | 363 | 39 | 402 | 265 |
| Unit 1 Line 2 | 328 | 39 | 367 | 265 |

It can be observed from table 3.2 that each Unit is made up of two independent pipe sections, i.e., conveying pipe 1 and conveying pipe 2, simply referred to as line 1 and line 2. This is also visible from Figures 3.1 to 3.3.

### 3.2.4 Compressed air supply

Compressed air was supplied from a dedicated compressor for each Unit. These were Atlas Copco, Model ZH 15 000+ three stage centrifugal compressors (refer to Appendix A for more details on the compressed air system) with the maximum volumetric air flow specified as 203 Sm3/min. This compressed air was used in two areas, the boiler cleaning system (air pulsing system) and on the pneumatic conveying system. Unfortunately, there was no air flow meter solely dedicated to the conveying air and this is explained in chapter 5 in discussing the air flow meter data.

### 3.2.5 Silo filter and ash storage

Ash is conveyed into reception silos, and each Unit has its own dedicated silo. On top of the ash silo, a filter system is located for separating the clean air from the fly ash. This filter system also serves the purpose of keeping the silo at vacuum pressure. Details of the motor size and number of bags on the filter system are included in appendix D. This system is always in operation to ensure the silo is kept at vacuum pressure, at $-4$ kPaG.

Each silo has a capacity of 4000 tonnes. These are concrete silos with an internal vertical length of 29 m and an internal diameter of 15 m. The silo has two openings underneath feeding the ash conveyors situated directly below the silo for ash removal to the ash dump through a network of conveyor belts.

## 3.3 Research Limitations

The research was limited within the constraints of the power station and its production limitations, i.e., only the ash produced during the combustion process was used, only the air available from the compressors already installed, and similarly the instrumentation already installed was used (Section 3.5). This is explained in Sections 3.3.1 to 3.3.3.

### 3.3.1 Ash production

The design of each of the 800 MW power station Units required coal consumption at the rate of approximately 384 tons per hour, with an ash content of approximately 35% on average. This means that the total ash produced per Unit on full load is approximately 134 tons per hour. There are two types of ash produced, namely coarse ash and fly (fine) ash. Previous experimental investigations and general power production experience indicates that 90% of the total ash is fly ash, which is approximately 121 tons per hour. As such, the product mass flow rate is approximately 33.6 kg/s if the Unit is in full-load operation.

### 3.3.2 Air flow rate

The air compressor plant was designed to supply air to both the pneumatic ash conveying systems and the boiler pulsing installation. This plant was designed to supply air at a maximum pressure of 840 kPa gauge pressure and at a maximum volumetric flow rate of 203 Sm3/min per Unit. Each Unit was provided with its own compressor.

## 3.4 Fly Ash Properties

Knowledge of the properties of the type of ash is necessary as explained in Chapter 2, as this dictates the type of conveying system that can be used for conveying such material (Geldart, 1973). The two main properties that were measured in this research are the particle diameter and the bulk density.

### 3.4.1 Particle diameter

The average diameter of the fly ash was analyzed using a dry sieving process and the results thereof are discussed in Chapter 5. Figure 3.4 shows the various sieves and associated equipment used to deduce the average particle diameter.

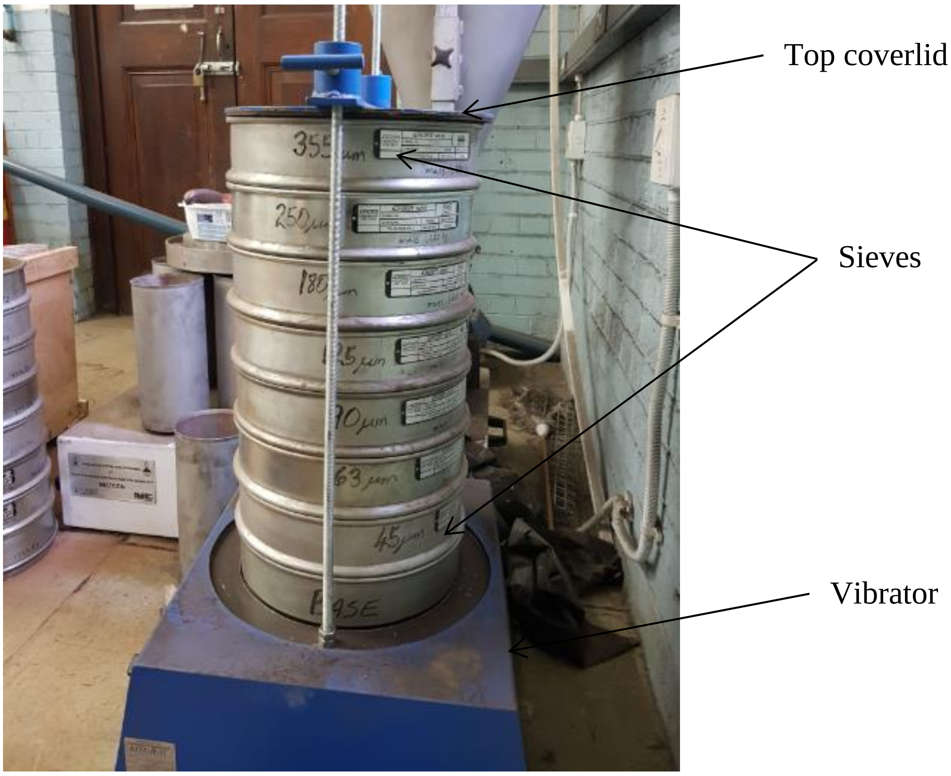


**Figure 3.4** Sieves used for analyzing the particle size distribution

**Table 3.3** Sieve size arrangement

| Sieve Number | Sieve size |
|---|---|
| 1 | 355 µm |
| 2 | 265 µm |
| 3 | 180 µm |
| 4 | 125 µm |
| 5 | 90 µm |
| 6 | 63 µm |
| 7 | 45 µm |
| 8 | Base |

All the sieves were manufactured using mild stainless steel in accordance to ISO3310.

After the fly ash was sized per sieve, it was then measured using the funnel and bucket as shown in Figure 3.5.

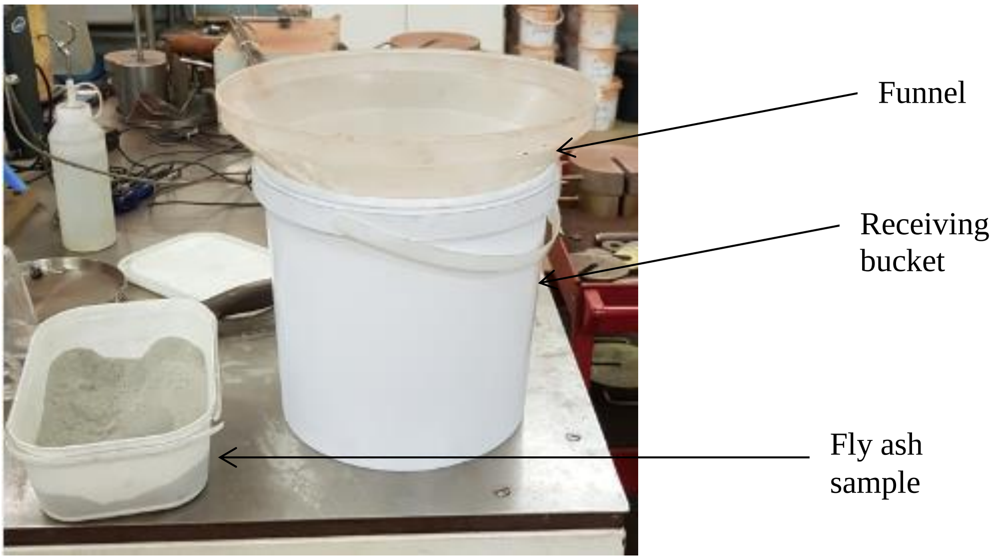


**Figure 3.5** Funnel and bucket

The mass inside the bucket was then taken for a mass meter reading using the scale as shown in Figure 3.6.


**Figure 3.6** Mass meter scale

### 3.4.2 Bulk density

Bulk density was measured using a stress consolidation facility known as the Jenike direct shear tester, and the equipment used is indicated in Figure 3.7. This method was preferred because the bulk density varies due to the voids and this method is ideal as the consolidation of stress allows for the reduction in voids (Mi. 1994).

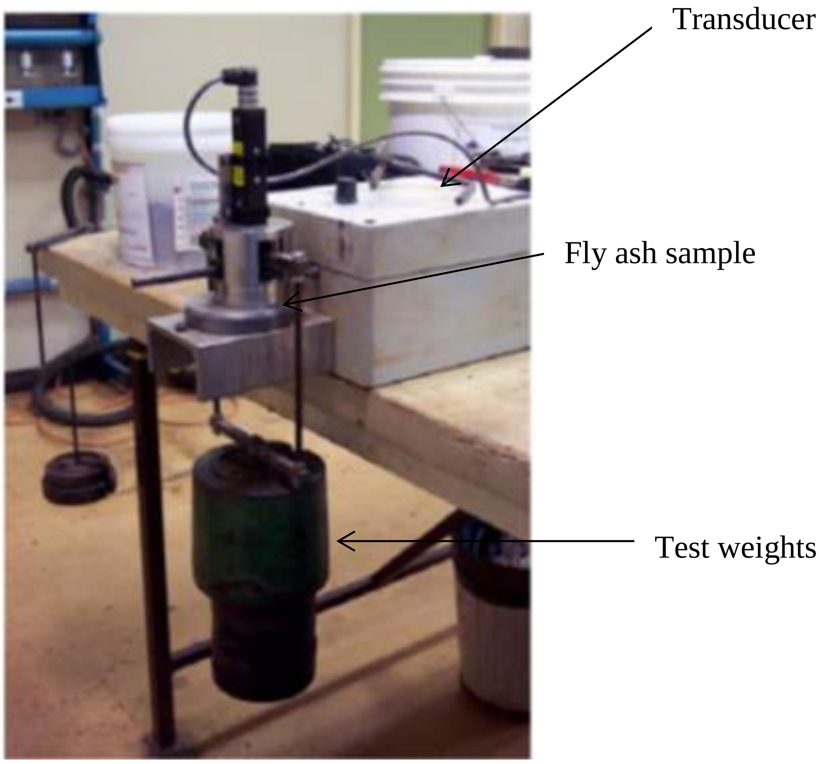


**Figure 3.7** Modified Jenike direct shear tester

The transducer is linked to a PC that captures the data, as shown in Figure 3.9.

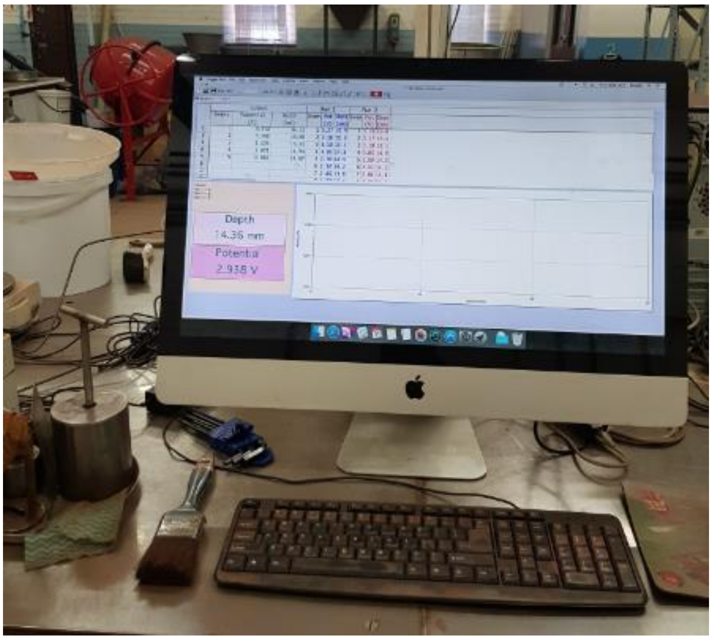


**Figure 3.8** Data capture system for the Jenike shear direct test

The consolidated bulk density is measured as follows (TUNRA Bulk Solids, Module 1, Small bulk density test, 3):

(i) Scoop the material into the cell as indicated in figure 3.7, and scrape off any excess material.

(ii) Place a lid over the solids such that the lid is flush against the cell and all the material is within the cell, taking care not to pack the material during this process.

(iii) Insert the twisting bar into the hole provided in the lid and apply nominally 20 twists (back and forth) over the amplitude allowed by the holder. Be careful not to apply any extra force with the twisting bar.

(iv) Record the compacted height reading.

(v) Repeat steps (i)-(iii) with a series of weights added in succession.

(vi) A data capture PC as indicated in figure 3.9 will create a plot of density as a function of consolidated stress is drawn.

(vii) Steps (i) – (v) are repeated until any additional weight does not result in significant change to the density, i.e., most of the voids have been displaced.

## 3.5 Instrumentation

The instrumentation used for this research comprised instruments already installed on the plant prior to the research. Calibration was not possible as the plant could not be taken down for calibration, as so the author relied on the calibration that is normally performed as part of maintenance on the plant. Unfortunately, certificates for this calibration could not be located when requested. The following instruments were used: pressure transmitters, mass meters, air flow meters and level indications. Figures 3.1 and 3.3 indicate location of pressure instruments as (P) and flow meter as (F).

### 3.5.1 Pressure transmitters

During each conveying cycle, conveying pressures and the pressure at the vessels are measured. As such the pressure in the system was measured at two locations: pressure between the vessels with a pressure transmitter installed at the first vessel, and the pressure as the ash enters the conveying lines (which is termed as the conveying pressure, refer to figure 3.1). The instrumentation used is similar in both applications. In this research, interest was only on the second pressure gauge as this was the conveying pressure whereas the first pressure reading is an indication of the blow tank's pressure. These pressure transmitters were Endress and Hauser PMP 71 instruments which had a range of 0 kPa to 10000 kPa. Refer to Appendix D for the data sheet of these instruments.

### 3.5.2 Air flow meter

Measurement of volumetric air flow was done using an Endress and Hauser thermal type air flow meter model number, t-mass 65 I. This instrument had a minimum and maximum measurement range of 1.63 Sm3/min to 886 Sm3/min.

As mentioned in section 3.3.2, this instrument measures the volumetric air flow rate that is servicing the boiler pulsing system as well as the pneumatic conveying system. As such, it was necessary to understand how much air flow is required for the boiler air pulsing, this is discussed in Chapter 5. The air flow meter is indicated as F1 in figure 3.1. Refer to appendix D for the data sheet of the flow meter.

### 3.5.3 Mass flow meter

Measurement of the fly ash mass per conveying cycle was not possible due to the unavailability of any instrumentation in the conveying system for measurement of fly ash. In this research, various methods were considered to arrive at a best approximation of this value. One possible method was by observing the amount of coal burnt, which can be used to estimate the amount of ash produced. However, this method is not necessarily accurate as the coal burnt may not include all the carbon content, and there is a significant amount of that ash captured as coarse clinkers. Even in the ash flow up until the hopper, there exist many areas where ash could leak into the atmosphere. Coal flow values were measured to obtain the best available approximation of how much ash can be expected to flow to the ash hoppers.

Each coal mill is fitted with a feeder that supplies coal into the furnace, and each of these gravimetric feeders also measures the amount of coal introduced into the furnace. These mass meters continuously measure coal intake into the boiler, with a range of 0-38 kg/s. Data sheets for these mass flow meters are included in Appendix D.

### 3.5.4 Hopper level measurement

Another method considered to quantify how much ash is conveyed during a conveying cycle was by observing the change in the level of ash inside each hopper. This was done by measuring the level of ash before and after a conveying cycle using a level instrument installed inside the hopper.

This instrument was in a percentage range of the amount of ash level inside the hopper. It had a range in meters, from 0 m to 6.5 m, and subsequently converted that value into a percentage, i.e., from 0% to 100% when the hopper was full. This instrument is a Rosemount guided wave transmitter instrument, model 530. Refer to appendix D for this data sheet.

This instrument was located inside the hopper and mounted on the side of the hopper, with a guided wave wire from the instrument to the bottom of the hopper, refer to Figure 3.10. These instruments were usually faulty and could not be relied upon as they were not suitable for ash at high temperatures. As such, results from these instruments were not considered in this research.

## 3.6 Data Acquisition

Information from the instruments (section 3.5) was stored in a central database within the power station, and permission to access to this data was obtained. The information remains confidential and is only used herein for research purpose.

The information is stored within a plant information system, and this system is accessible remotely through a network controlled locally to a specific site. This information was downloaded to a personal computer for further processing as discussed in Chapters 4 and 5.

# CHAPTER 4 OPERATING AND EXPERIMENTAL PROCEDURE

## 4.1 Introduction

The main parameters under investigation concerned the relationship that exists between the air flow rate, conveying pressure and the material mass flow rate of ash during a pneumatic conveying process. These are typical characteristics under investigation on improvement of a pneumatic conveying plant (Williams, 2008). During normal operation, ash is produced and transferred from the boiler via hoppers and pressure vessels to the ash silo. The time between the filling of the pressure vessels and conveying of ash until the conveying line is empty is termed as a conveying cycle. During each conveying cycle air flow rate, conveying pressure and solids flow rate were observed and these are analyzed in Chapter 5.

The plant was in full production mode and hence the normal operating philosophy of the power station for fly ash removal was followed. Section 4.2 explains the operating philosophy of the power station and the various power production regimes are indicated. Sections 4.3 and 4.4 detail how the coal and subsequent ash production rates were estimated. Section 4.5 details the necessary steps taken to acquire data specific for this research from the extensive data available during the production of power and how these data were arranged for this research. This is termed the experimental procedure which was an extension of the normal operating philosophy.

## 4.2 Operating Philosophy of the Power Station

Each power station Unit at full load produces just under 800 MW, and consumes coal at an average of approximately 380 tons per hour. This operation is based on a four out of five-mill operation, and each mill consumes on average 95 tons per hour of coal. During normal operation at full load all four mills are in service, and when necessary to reduce load, a mill is taken out of service for a specific demand. Table 4.1 shows the production requirements with a specific number of mills in service.

**Table 4.1** Power produced per mills in service

| **Power plant production** (MW) | **Number of mills in service** | **Approximate coal burn-rate** (t/h) |
|---|---|---|
| 800 | Four | 384 |
| 600 | Three | 285 |
| 400 | Two | 190 |

It is also not uncommon to find variation in mills and this is shown in chapter 5, where one Unit performs better than the next Unit in terms of power produced with the same number of mills in service. As such, Table 4.1 illustrates what is the expected average coal burn for a specific power production regime. The milling plant was also fitted with flow measurement devices such that during each time a mill is in service, the quantity of coal burnt per hour can be determined (Appendix D). As such during each production period a total of five coal flow readings are expected, with the last mill showing a zero value.

## 4.3 Coal quality

It was also important to ascertain the quality of the coal used during the combustion process. This is important in order to establish how much ash is expected to be produced. Samples were taken every 8 hours, meaning three samples taken daily and analysis conducted, however Table 4.2 only illustrates the ash content from 04 January 2019 to 08 January 2019 (with an average 35% ash content for the days reported).

**Table 4.2** Coal samples per date

| **Coal sample date** | **Ash Content (%)** | | | |
|---|---|---|---|---|
| | **Period 1** | **Period 2** | **Period 3** | **Daily average** |
| Fri, 04-Jan-19 | 37.3 | 34.7 | 34.7 | 35.6 |
| Sat, 05-Jan-19 | 36.2 | 33.2 | 36.7 | 35.4 |
| Sun, 06-Jan-19 | 36.7 | 39.7 | 37.7 | 38 |
| Mon, 07-Jan-19 | 33.7 | 33.2 | 34.6 | 33.8 |
| Tue, 08-Jan-19 | 33.1 | 34.3 | 33.3 | 33.6 |

## 4.4 Fly Ash Removal Philosophy

Once the amount of coal introduced into the power plant is known and with optimized milling plant, i.e., operation without oil support, the amount of fly ash produced can be quantified from the coal quality reports. This is detailed as part of Section 4.5 under Experimental Procedure.

Fly ash is discharged into hoppers from the boiler plant and these hoppers store the ash temporarily for discharge into the pneumatic conveying system. The following steps were followed once the ash is received into the ash hoppers for transfer to the ash silos - to be understood with Figure 4.1 and Table 4.3 for location of equipment on the plant **(in brackets)**:

1. Open the pressure vessels vent valves **(i).**
2. Open the inlet valves to allow ash to enter the vessels (blow tanks), this is the filling cycle **(ii).**
3. When three out of seven pressure vessels are full or time has expired of 120 seconds close all the inlet valves, this is the end of filling cycle **(iii).**
4. Close the vent valves **(i).**
5. Open the outlet dome valves **(iii).**
6. Open the air fluidizing line – starting with the fluidizing lines sequentially from the outlet vessel (vessel O) until the master vessel (vessel M) **(iv).**
7. Open the master air supply valve **(v).**
8. Material should flow in the pipe and this is visible on the pressure transmitters on the pressure vessels **(vi)** and line pressures equalizing **(viii).**
9. The air flow rate is also observed during this period by air flow transmitter **(vii).**
10. After some time, approximately 5 minutes, when the conveying pressure and vessels' pressure drop values are approximately 25-35 kPa, this signifies all the ash has been conveyed to the ash silo.
11. Stop the air supply valves **(iv)** and **(v)**.
12. Open the vent valves **(i).**
13. End of a conveying cycle.

Steps (1-13) were followed for each conveying cycle and when blockages were observed or there were inconsistencies in the readings, the data were discarded. The idea was to acquire steady state and reliable continuous conveying data and avoid transient periods (Jardine, 1986).

**Table 4.3** Description of equipment as shown in figure 4.1

| Equipment number | Equipment description | Equipment Symbol |
|---|---|---|
| (i) | Vent valves |  |
| (ii) | Inlet dome valves | 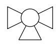 |
| (iii) | Outlet dome valves | 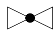 |
| (iv) | Fluidizing valves | 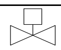 |
| (iv) | Orifice plates | 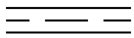 |
| (v) | Main air supply | 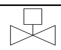 |
| (vi) | Tandem pressure vessels' pressure transmitter | 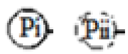 |
| (vii) | Air flow transmitter |  |
| (viii) | Conveying pressure transmitter |  |

Orifice plate details are shown in appendix E.

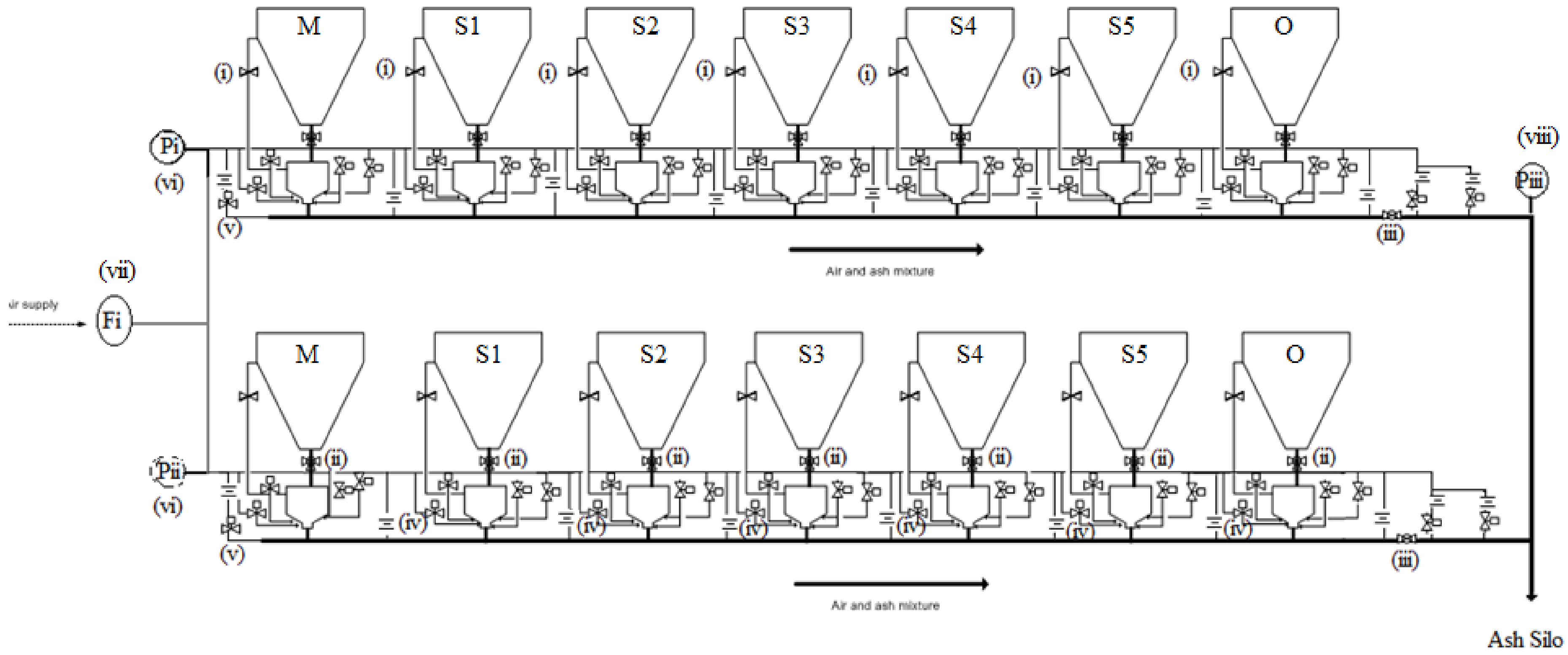


**Figure 4.1** Process flow diagram with description for half a Unit (similar for all Units)

*M – Master, S – Slaves, O – Outlet (Specific to each hopper and vessel, these are also numbered 1-7 from left to right also)*

## 4.5 Experimental Procedure

This section explains the additional steps followed to quantify data specific for this research. The following three steps were necessary, i.e., first, estimation of how much coal is consumed and in turn, how much ash is produced. The second step is to convey the ash and observe pneumatic conveying characteristics such as pressures and air flow rate. Lastly, integrate this information to be able to quantify for a single pneumatic conveying cycle, how much ash is transported, at what pressure and how much air is used. This is explained in detail in Sections 4.5.1-4.5.3.

### 4.5.1 Estimation of coal consumption and ash produced

As mentioned in Chapter 3, and also summarized in Table 4.1 and 4.2, knowledge of how much coal is burned in the power plant as well as the coal quality is necessary to estimate how much ash is produced. This method is not ideal and provided only an approximate estimate but was the only practical alternative in this case. Most researchers (Mills, 2006; Williams, 2008) use laboratory facilities such as single or double hopper-vessel configurations with installation of strain gauges for measurement of ash into a vessel. In this investigation there are 28 vessels for a single Unit and with a strain gauge per vessel support leg, at least 112 strain gauges would be necessary and even this may not be sufficient due to all the movements and vibrations around the area as strain gauges are very sensitive.)

In order to obtain reliable sets of data for ash production, it was necessary to avoid start-ups and shut-downs due to the erratic nature of the coal flow and use of oil support to sustain the furnace fires.

### 4.5.2 Pneumatic conveying characteristics during a conveying cycle

Ash is discharged as described in section 4.4 through the conveying line to the silo. During each cycle, the following pneumatic conveying characteristics were observed: pressure at the inlet to the conveying line and pressure at the pressure vessel, total air flow rate and time it takes for the ash to be emptied in the conveying line. It was also necessary to eliminate transient data points such as during plant start-up or shutting down. A cycle is completed in about 5 minutes (refer to section 5.5), and as such numerous cycle data points were recorded for a specific Unit operating range and at various points in time. This was done intentionally to ensure reliability and repeatability of experimental data although within the confines of the production environment. The air flow rate was also observed during these conveying cycles, comparing air flow rate during a conveying period and air flow rate when there was no conveying, viewed by a reduction in pressure drop; for more details refer to chapter 5, section 5.6.

### 4.5.5 Consolidated data for ash production, pressure drop and air flow rate for a conveying cycle

After the ash produced was estimated, and for a conveying cycle the pressure and air flow rate were known, these data were consolidated to ensure a full set of data for a particular conveying cycle. These then represented the system performance for that specific load, and this was performed at various loads to observe how air flow rate and pressure vary as the amount of ash is increased through increase in coal consumption. This was repeated for the three Units, also observing the effects when the conveying distance is increased, for example comparing Unit 1 with Unit 3. The findings are recorded in Chapter 5, as system performance and results.

# CHAPTER 5 SYSTEM PERFORMANCE AND RESULTS

## 5.1 Introduction

As detailed in the research objectives section 1.3, the main focus was to understand how much air is used during a conveying cycle and to use this information in conjunction with pressure and solids flow rate values to establish a model that predicts pneumatic conveying characteristics for this particular type of ash; with the latter part discussed in Chapter 6 and 7. This chapter is concerned with presentation of results and will initially focus on the type of ash that was under investigation and this is covered in Section 5.2. Section 5.3 indicates results for the pneumatic conveying characteristics, i.e., conveying pressure, air flow rate and solids mass flow rate results for each of the Units. Section 5.4 then presents this information in a consolidated and tabulated form for ease of comparison across the power generation Units.

## 5.2 Fly Ash Characteristics

A sample of fly ash was taken for analysis of average particle size and bulk density. This sample was compared with samples of ash obtained from the initial phases of the power station operation to ascertain whether there had been any variance in coal and ash properties (refer to Appendix F for PSD during commissioning). This was necessary to baseline the findings from the start of the generation of power. These results are discussed individually in sections 5.2.1 and 5.2.2 for bulk density results and particle size distribution, respectively.

### 5.2.1 Fly ash density

Using the modified Jenike shear test cell equipment as described in Chapter 3, bulk density was measured, and the following properties were observed that give an indication of the bulk density.

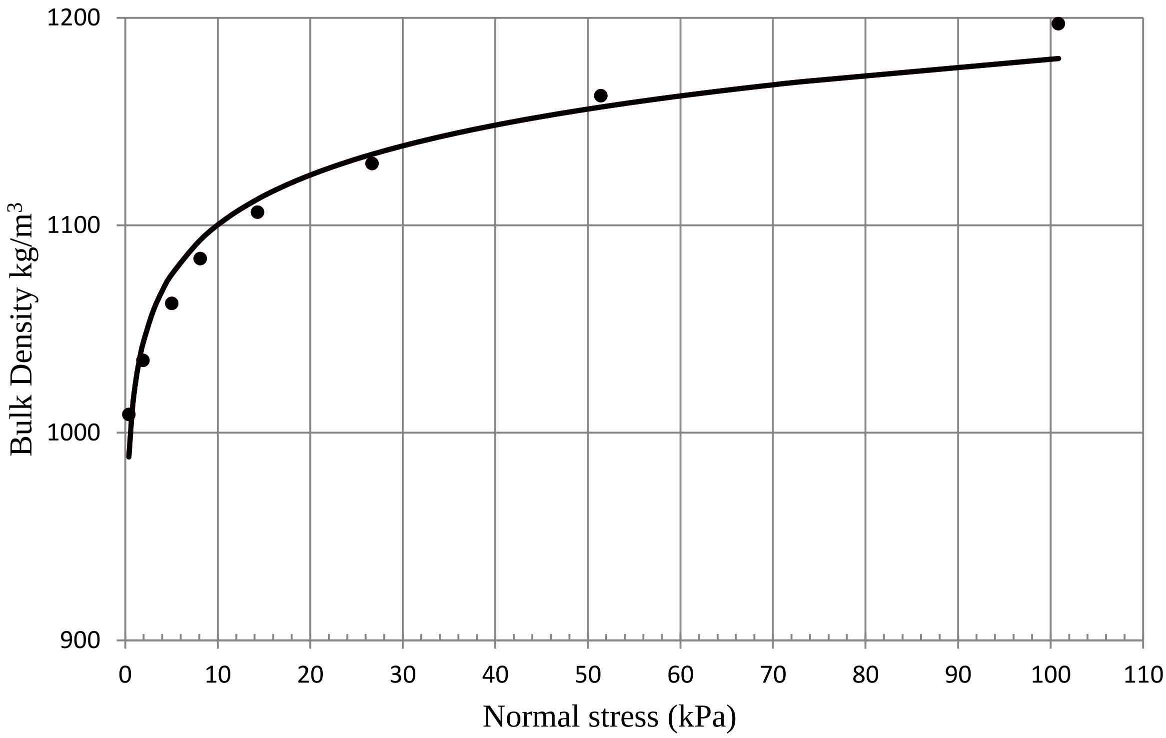


**Figure 5.1** Consolidated bulk density of fly ash

A similar test was performed during the design stage in 2010 using an ash sample from a nearby power station using coal from the same coal mine, and results of this test are indicated in Figure 5.2. What is worth noting is that there has not been any significant changes on the bulk density between the early stages of design in 2010 and what was tested in 2019.

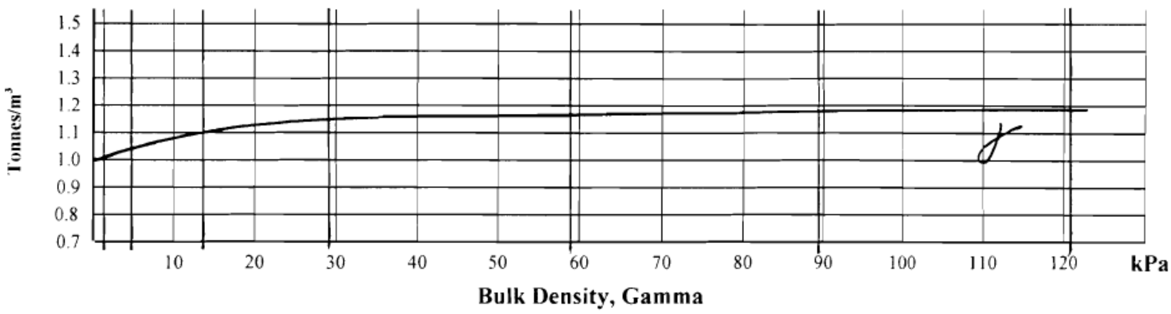


**Figure 5.2** Consolidated bulk density of fly ash, design stages test (Internal report, document number, 200-215389)

As can be observed by comparing Figures 5.1 and 5.2, the bulk densities for this particular type of ash is lower than 1200 kg/m3. According to Figure 5.1 based on the fitted curve, the value of 1180 kg/m3 for consolidated bulk density is observed.

### 5.2.2 Particle size distribution

As indicated in Chapter 3, a sieving method was used to estimate the average particle diameter of the fly ash. The finding was also compared to previous data available to obtain a view whether there has been variance in particle size during the various stages of the power station generation life. Figure 5.3 indicates the particle size distribution, samples were taken from each of the three power station Units and all had similar results.

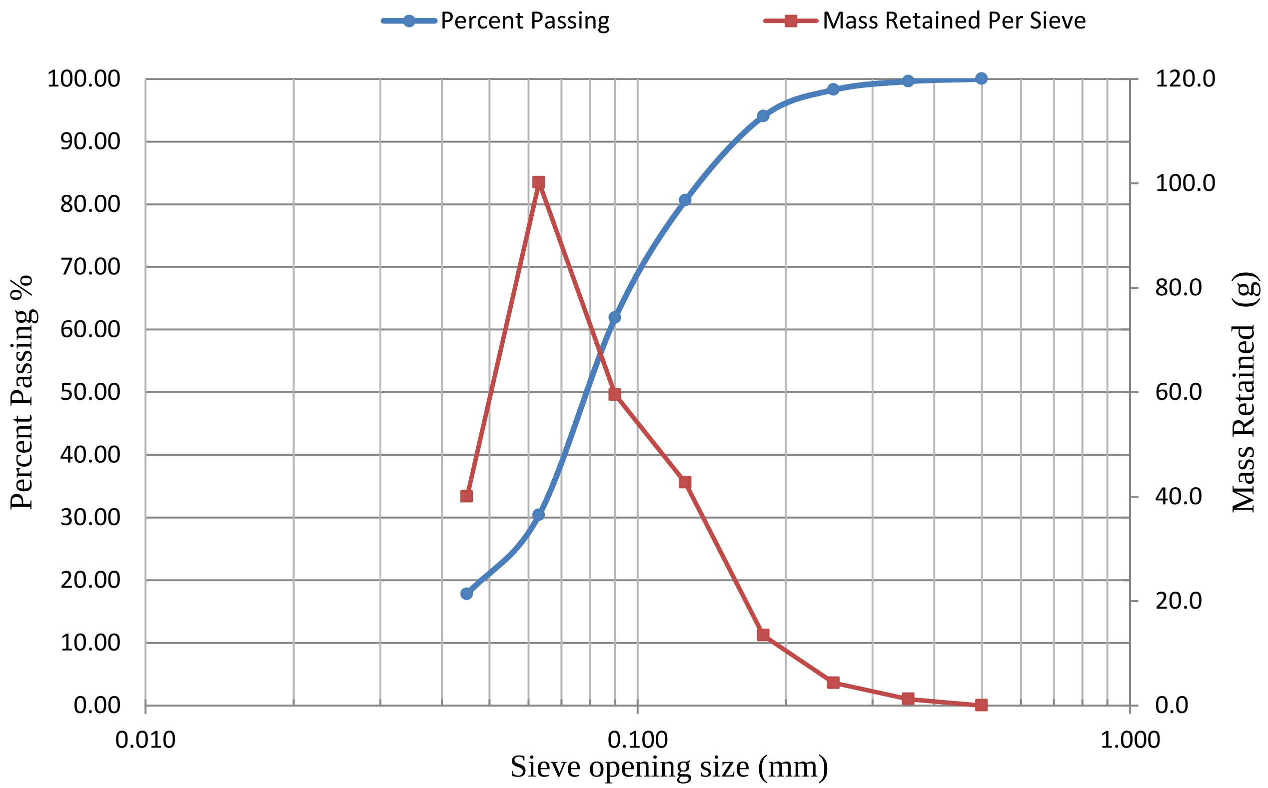


**Figure 5.3** Particle size distribution of fly ash, Unit 2

Figure 5.4 shows the particle size distribution curve for a similar burnt coal at the design stage (Bulk Solids Flow report, 2012).

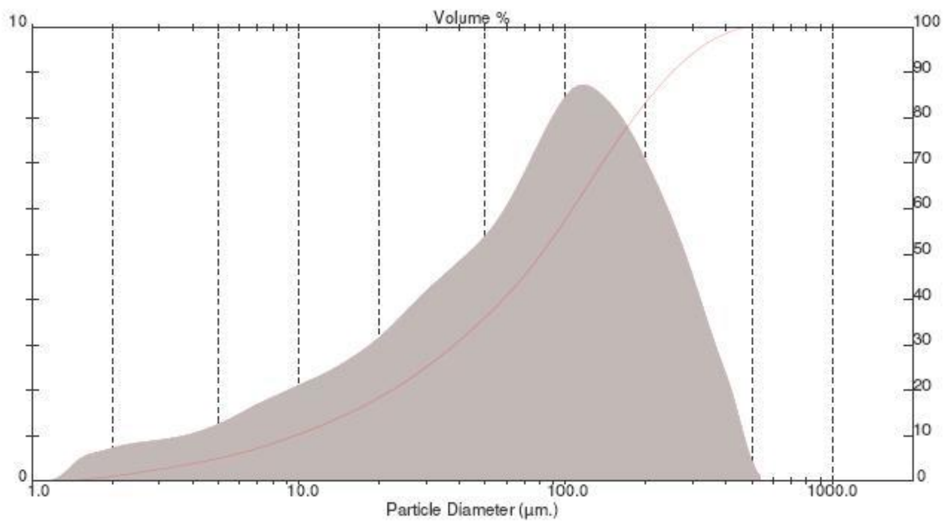


**Figure 5.4** Particle size distribution (Bulk Solids Flow report, 2012)

Figure 5.4 indicates a fly ash with an average 60 microns particle diameter and with particle density measurements as indicated in Figure 5.2. As such, ash properties have not significantly changed from initial stages of the design in 2010.

Figure 5.3 based on the sample obtained from Unit 2, which indicates ash with an average particle diameter of 63 microns. The fly ash properties of Units 1 and 3 were similar to those shown in figure 5.3 and this is the value considered in this research, i.e., $d_p = 63\mu m$. During the commissioning stages of the Units investigations were performed using different sieve sizes, for example the smallest sieves used were of less than $75\mu m$, and hence these cannot be compared accurately with Figure 5.3. However the values were useful to identify the variation in the fly ash although at higher sieve values. Results from these previous measurements are included in Appendix F.

## 5.3 Overview of the System Performance

Before presentation of results for pneumatic conveying characteristics it is necessary to explain the general performance of the system as this assists in understanding the variation in the overall results. During the testing phase of the research a number of performance anomalies were observed, and these anomalies need to be taken into account when presenting data. These anomalies are discussed below individually.

### 5.3.1 Instrumentation irregularities

It was observed during the investigation period that the instruments currently installed behaved differently from expectation in a way in which some of the data were discarded. Some of the reasons for these instruments to behave poorly emanated from possible lack of frequent calibration, and due to failures of valves such as non-return valves that allowed ash ingress into the clean air system. These deficiencies were attended to as and when observed, however the instruments would for that period have been providing incorrect readings.

The air flow meter readings were also problematic, particularly the flowmeter installed in Unit 3, as instances were observed where in a matter of seconds the reading dropped to less than 45 $Sm^3/min$ during a conveying cycle, which is highly improbable, and the instrument would pick up again, for example Unit 3 period 7, refer to appendix H. This was observed as an incorrect reading however the peak air flowrate was within expectation during those instances.

The hopper level instruments were very difficult to use as in most cases only 3 out of 28 hopper levels would be functional for a few minutes. This was attributed to the type of instrument used that was not suitable for fly ash at high temperatures, higher than the 130 degrees Celsius specified on the data sheet, refer to Appendix D. Records from the power station also indicate that these level instruments were usually faulty since commissioning, and brought into question doubts on whether these can be used at all. As such, hopper level readings were not considered for this research due to the unreliability of these instruments, and hence the method of estimation of ash from coal production was the preferred option.

### 5.3.2 System leaks and ash blockages

During the investigation period, the system was very prone to environmental leaks of ash; this was eventually addressed by additional teams on standby shifts to specifically attend to leaks as and when they occur. However leaks also contribute to reducing the amount of ash that was conveyed and if the leak was on the air line it led to loss of compressed air necessary for conveying.

Another important issue that was noted was blockages; these were noted by excessive increase in the conveying pressure values higher than $450\ \mathrm{kPa}$ without dropping over a number of minutes and this meant that there was a blockage in the system. These scenarios were also discarded from the results as only scenarios close to steady state were considered. The reason being that these blockages could be caused by a number of factors mainly foreign materials introduced into the system such as broken pieces of bags and cages.

### 5.3.3 Unit trips and planned maintenance

Recording of data was also interrupted when there were Unit trips. This led to instances when there was not enough ash in the hoppers, and downtime due to these trips and other outages varied from a day to a planned maintenance outage of three months or longer in certain periods. This is also indicated on the recorded data as some results skip days, weeks and months; as such the experimental data period had to be lengthy (between 2017 and 2019).

### 5.3.4 Inability to make plant modifications

As mentioned in Chapter 3, due to the operational nature of the experiment, it was not possible to do major plant modifications. As such, only available instruments were used and this limited the accuracy of the data as it relied in secondary information and assessment for the air flow and material mass flow rates without specific instruments for air flow and ash flow rate dedicated to pneumatic conveying.

This also meant that the data capturing process took much longer than typical pneumatic conveying experiments take with information readily available from installed instruments.

### 5.3.5 Plant deterioration

It was also notable that the state of the plant had deteriorated from the original state of the plant during commissioning. This was visible in certain valves taking longer to close compared to others, in some instances some valves would not open or would close unintentionally, among other such plant defects. As such, data had to be interrogated before inclusion to ensure all those defects were taken into consideration.

Due to the reasons noted in subsections 5.3.1 to 5.3.5, it was extremely important that steady state conditions were considered and utmost care was taken in interrogating data before inclusion of that data into the research, and although this was laborious it was necessary to ensure that the data presented is approximately what the system was experiencing and was not influenced by external factors. Even with the above care being taken, after data was processed, there was still evidence of these irregularities in the collected data.

### 5.3.6 Periods overview and selection of data

This section highlights the approach followed in acquiring data as there was a lot of data available, from as early as 2014. However as noted in subsection 5.3.5 some scrutiny was required to isolate the necessary data that best represents the system performance. Unit 2 is selected for illustration purposes, and for this Unit data was available from 2016 to 2019 as indicated in Figure 5.5. Figure 5.5 provides an overview of how Unit 2 performed in the period under discussion with the Megawatts produced superimposed over the pneumatic conveying variables. This was done in order to establish a relationship that exists between the various PCCs and power produced for this particular plant.

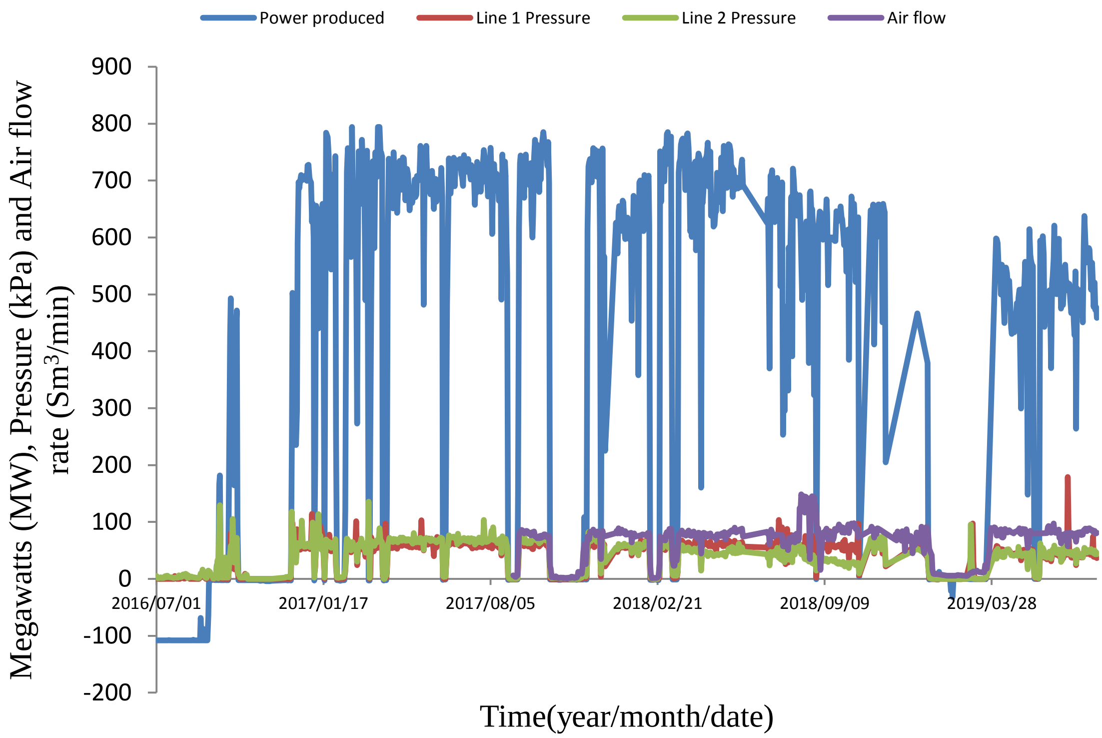


**Figure 5.5** Unit 2 data from 2016 to 2019

Figure 5.5 indicates periods of power production at high and low loads as well as shut down conditions. Megawatts below zero indicate a situation when the boiler is off and during that period some power is drawn from the system as opposed to supply of power into the grid. This figure then assists to classify periods of data which must be avoided and periods that can be used for the research; such periods would be made up of steady power production, steady conveying pressures and steady air flow rate data. The data was then classified in periods of time from 2017 to 2019, and these periods with their respective dates are listed in Table 5.1 for Unit 2. Data periods for Units 1 and 3 are indicated in Tables 5.2 and 5.3 respectively.

**Table 5.1** Periods overview for Unit 2

| **Unit 2 Periods** | **Dates per data period** |
|---|---|
| Period 1 | 08 September 2017 to 06 October 2017 |
| Period 2 | 30 November to 11 December 2017 |
| Period 3 | 24 Feb to 09 March 2018 |
| Period 4 | 21 March to 02 September 2018 |
| Period 5 | 2 September 2018 to 17 October 2018 |
| Period 6 | 2 April 2019 to 16 May 2019 |
| Period 7 | 27 May to 31 July 2019 |
| Period 8 | Not applicable |

**Table 5.2** Periods overview for Unit 1

| **Unit 1 Periods** | **Dates per data period** |
|---|---|
| Period 1 | 17 September 2017 to 29 September 2017 |
| Period 2 | 02 October 2017 to 29 October 2017 |
| Period 3 | 14 December 2017 to 16 March 2018 |
| Period 4 | 09 April 2018 to 07 May 2018 |
| Period 5 | 03 December 2018 to 15 Jan 2019 |
| Period 6 | 16 February 2019 to 29 March 2019 |
| Period 7 | 22 April 2019 to 02 June 2019 |
| Period 8 | 4 June 2019 to 31 July 2019 |

**Table 5.3** Periods overview for Unit 3

| **Unit 3 Periods** | **Dates per data period** |
|---|---|
| Period 1 | 01 May 2017 to 24 September 2017 |
| Period 2 | 21 October 2017 to 22 November 2017 |
| Period 3 | 31 December 2017 to 03 February 2018 |
| Period 4 | 03 March 2018 to 02 June 2018 |
| Period 5 | 02 July 2018 to 16 November 2018 |
| Period 6 | 20 December 2018 to 12 March 2019 |
| Period 7 | 01 April 2019 to June 2019 |
| Period 8 | 15 June to 23 July 2019 |

Figure 5.5 read in conjunction with Table 5.1 shows readings for specific periods. The values shown in Figure 5.5 are averaged values as the data is over a period of time and it is not possible to record raw data over a period such as a month or longer. As such, when a period is selected such as Period 1 in Table 5.3, from 01 May to 24 September 2017, this period is further broken down in days to obtain raw data for that period.

In sections 5.4 to 5.7 it is discussed how data is collected in raw form from specific periods of data as per Tables 5.1 to 5.3.

## 5.4 Coal Consumption and Ash Estimation

### 5.4.1 Coal consumption report

As indicated in Chapter 4, sections 4.2 and 4.3, ash production is heavily linked to how much power is produced as this is directly related to the amount of coal being consumed. In order to illustrate how raw data is obtained from a period, Unit 2 period 4 with data ranging from 21 March 2018 to 02 September 2018 is selected. Observation from Figure 5.5 shows steady state performance at 11 May, and a raw data period of 2 hours is selected.

Figure 5.6 illustrates such an example, with four out of five mills sending coal into the furnace for the selected data period on 11 May 2018 for 2 hours only. Table 5.4 also shows these values averaged over the 2-hour period under discussion.

**Table 5.4** Unit 2 coal consumption on 11 May 2018

| **Mill** | **Average coal consumption** (kg/s) |
|---|---|
| Mill 1 | 25.2 |
| Mill 2 | 30.6 |
| Mill 3 | 0 |
| Mill 4 | 29 |
| Mill 5 | 23.6 |
| Total | 108.4 (390 tonnes per hour) |

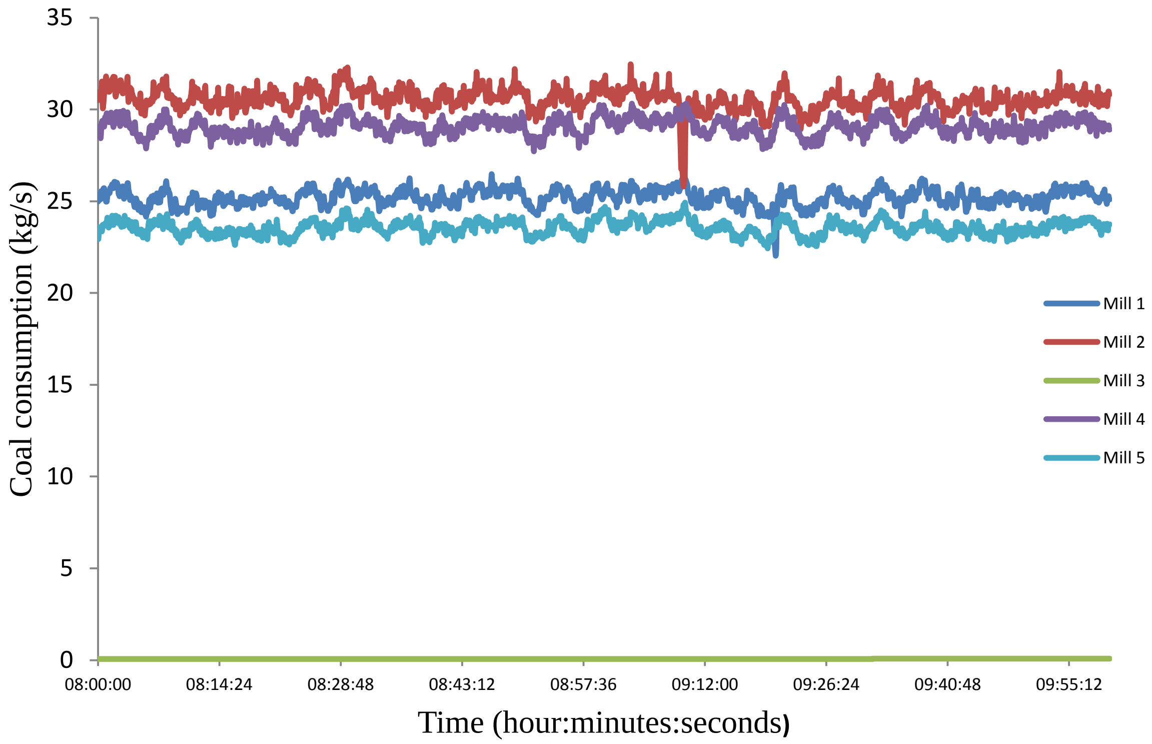


**Figure 5.6** Coal consumption over a 2 hour period for Unit 2

During the period under consideration in Figure 5.6, and Table 5.4, the load for Unit 2 was at 780 Megawatts.

This exercise was repeated for all the data recorded in raw values. In Unit 1 for illustration purposes, period 2 is selected from Table 5.2, and a specific date of 11 October 2017 is selected for raw data as indicated in Table 5.5 and figure 5.7.

**Table 5.5** Unit 1 coal consumption on 11 October 2017

| **Mill** | **Average coal consumption** (kg/s) |
|---|---|
| Mill 1 | 22 |
| Mill 2 | 22 |
| Mill 3 | 21.5 |
| Mill 4 | 22.1 |
| Mill 5 | 0 |
| Total | 87.6 (315 tonnes per hour) |

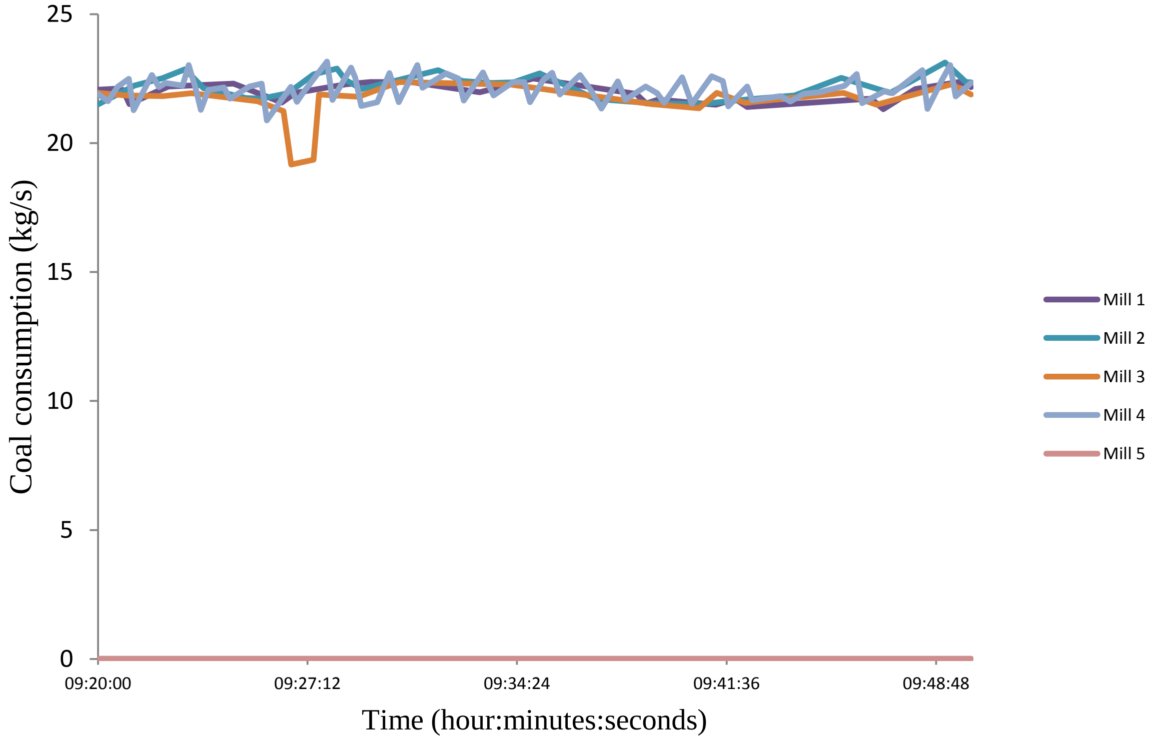


**Figure 5.7** Coal consumption over 2 hours for Unit 1 for 11 October 2017

Figure 5.7 and Table 5.5 relate to Unit 1 with a generation capacity of 650 megawatts. This Unit was not performing at maximum loads during the research period and therefore data was observed from as far back as 2017.

A similar approach was used as well with Unit 3, with period 8 used for illustration purposes. Raw data for 01 July 2019 are selected and this is recorded similarly in Table 5.6 and Figure 5.8.

**Table 5.6** Unit 3 coal consumption on 01 July 2019

| **Mill** | **Average coal consumption** (kg/s) |
|---|---|
| Mill 1 | 36.8 |
| Mill 2 | 33.2 |
| Mill 3 | 23.2 |
| Mill 4 | 0 |
| Mill 5 | 33.2 |
| Total | 126.6 (455 tonnes per hour) |

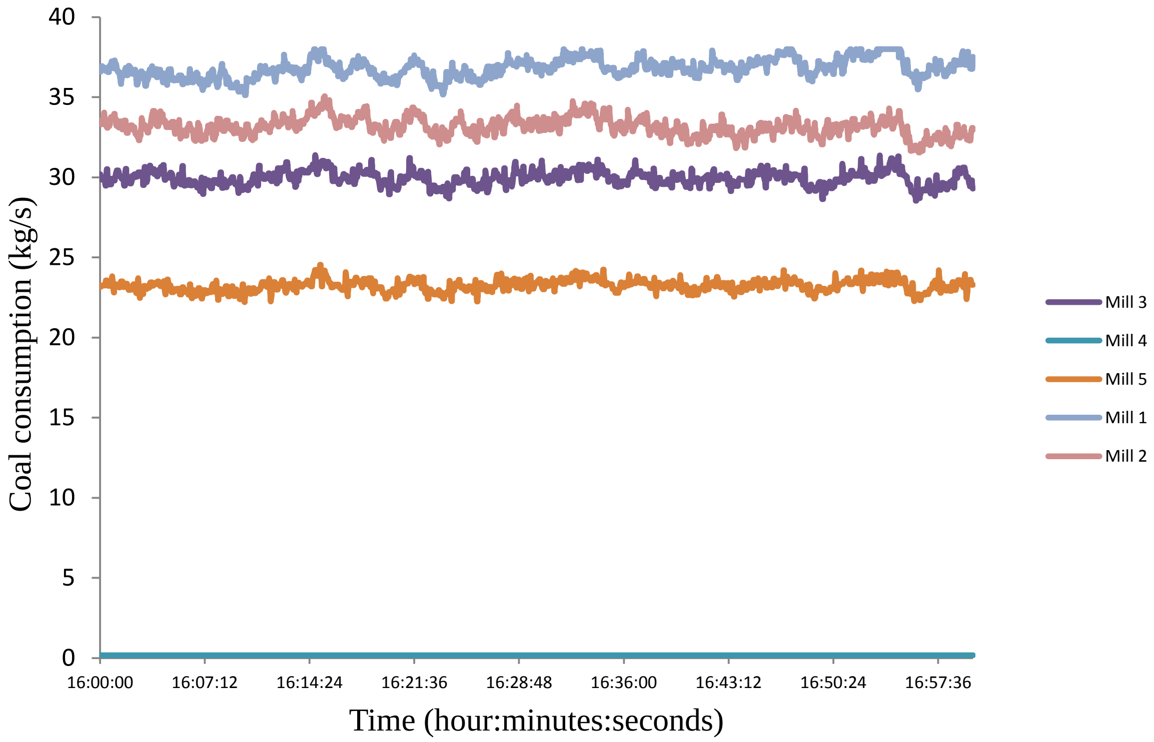


**Figure 5.8** Coal consumption for Unit 3 for 01 July 2019

Figure 5.8 and Table 5.6 relate to Unit 3 with a load of 783 megawatts production, on the 1st of July 2019 and as such, this Unit was performing much closer to full load of 794 megawatts.

### 5.4.1 Ash estimation

Tables 5.4 to 5.6 are used to establish the expected ash production on the particular dates under investigation, and these are done in conjunction with the ash quality reports. For illustration purposes, Table 5.4 is used with an average coal consumption of 108.4 kg/s. The coal quality report for this particular coal burned is as indicated in Table 5.7 below.

**Table 5.7** Coal quality report for 10-12 May 2018

| Date | Ash % | | |
|---|---|---|---|
| | Period 1 | Period 2 | Period 3 |
| 10-May-19 | 33.8 | 34 | 34.2 |
| 11-May-19 | 34 | 34 | 33.8 |
| 12-May-19 | 33.3 | 34.3 | 37 |

Based on this coal quality report, the average ash content was approximately 34 %, and based on experience that typically 90% of the total ash is fly ash, the calculation below can be applied to estimate the ash production for that period.

$$\text{Fly ash produced} = 108.4 \times 0.34 \times 0.9 = 33.8 \text{ kg/s}$$

Therefore approximately 119 tons per hour of fly ash was sent to the ash hoppers for conveying into the ash silos for Unit 2. The ash would then be split up into the four rows of seven hoppers each, with two rows of 7 hoppers each converging into a single conveying line, refer to Chapter 3, Figure 3.1. As such each Unit has two conveying lines.

Each individual conveying line would therefore transport approximately 59.5 tons of ash per hour to ensure continuous removal of ash at this particular power generation load. The above is repeated for each period in question for all the three generating Units, refer to Appendix I. See Section 5.7 for a consolidation of these data with pressure drop and air flow rates (discussed in the next two subsections).
It should be noted that there are two major assumptions made to obtain the fly ash values, namely ash content applicability and fly ash discharge into ash hoppers.

***Assumption on ash content***

The coal quality reports can only be useful if the coal that was measured with ash qualities such as reported in Table 5.7 was conveyed to the boiler for combustion at that time. Power plants are normally built with a stockpile and as such, coal may have been measured on a particular date to have specific ash qualities, however this does not necessarily mean that this was the coal that was burned on that day, due to coal stocking operations.

However this is not significant as the ash content varied between 34% to 36% and this difference is considered minor for this research. Whether a value of 34% or 35% is used has a small effect on the results.

***Assumption on fly ash discharge into ash hoppers***

The next assumption made is that all the fly ash (as per the 90% rule) is discharged into the fly ash hoppers for transport using pneumatic conveying. This assumes there is no leak in the boiler ducts between the ash hoppers and the furnace, and that there are no additional systems that extract ash in the boiler ducts, such as the flue gas de-ashing system that extracts any ash in the ducts between the furnace and the ash hoppers. This is done to prolong the life of the ducts against any ash lying on the ducts as over time the flue gas mixed with this ash easily erodes the boiler ducts.

However this assumption is sustained noting that the plant was designed to collect practically all the fly ash, and for this research all the three Units are assumed to behave similarly. The above assumption should be tested in future, with the use of a single hopper isolated with strain gauges to observe the amount of fly ash into a single hopper, unfortunately this was not possible during the research period.

After the amount of fly ash has been estimated, the conveying pressure and air flow rate can be calculated as the next part of the PCCs. These are covered in Sections 5.5 and 5.6 respectively.

## 5.5 Pressure Drop in the Conveying Lines

The pressure drop across the pressure vessels (blow tanks) was not considered for this research. This was in order to eliminate all the variations and pre-pressurization and pressure peaks at the start of the conveying and the acceleration pressure variations. Only the pressure measured at the start of the conveying lines was considered to yield the conveying pressure drop. The pressure drop along the conveying pipeline during a conveying cycle was observed from making use of the pressure transmitters installed on the conveying line; refer to Figure 4.1 and Table 4.3.

A similar process that was followed in section 5.4 to obtain raw data for the coal consumption is also followed in collecting pressure drop readings during conveying periods. Taking the period 6 for Unit 2 (refer to Table 5.1) with data ranging from 02 April 2019 to 16 May 2019, Figure 5.9 shows the average readings.

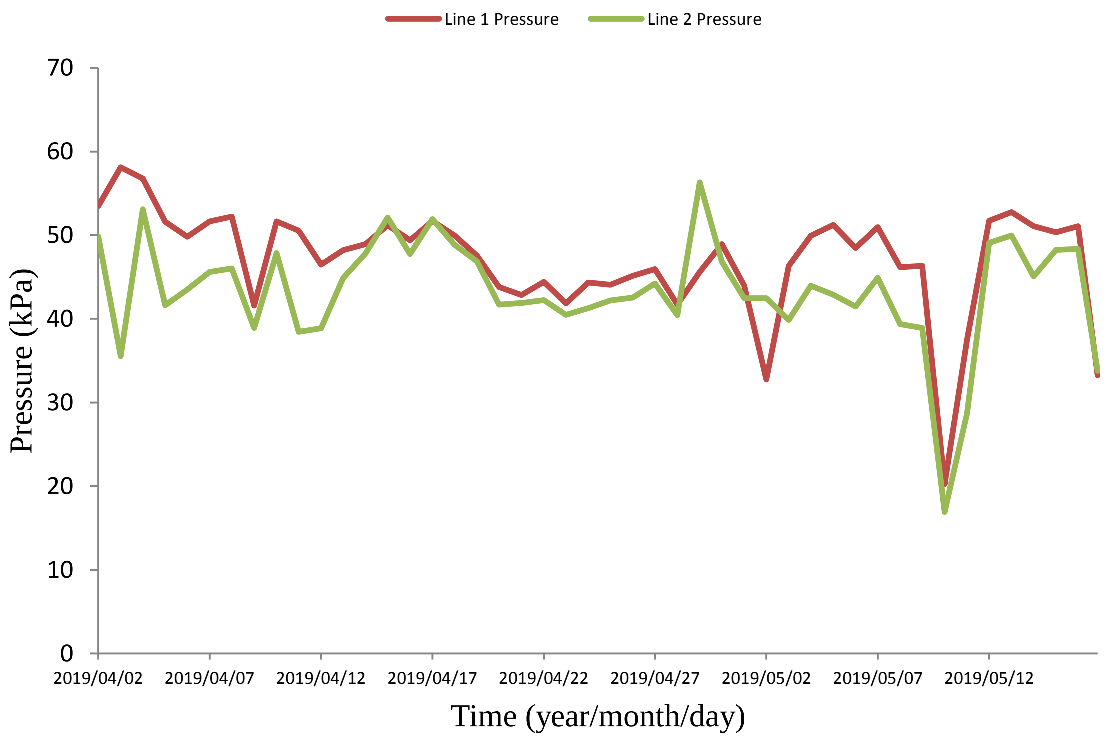


**Figure 5.9** Pressure drop as a function of time for Unit 2 from 2 April to 16 May 2019

From observing Figure 5.9, reasonably "steady state performance" is noted on 22 April 2019. This is then the period selected for a closer examination of the conveying pressure, and this is the performance as indicated in Figure 5.10 for a 20 minute period.

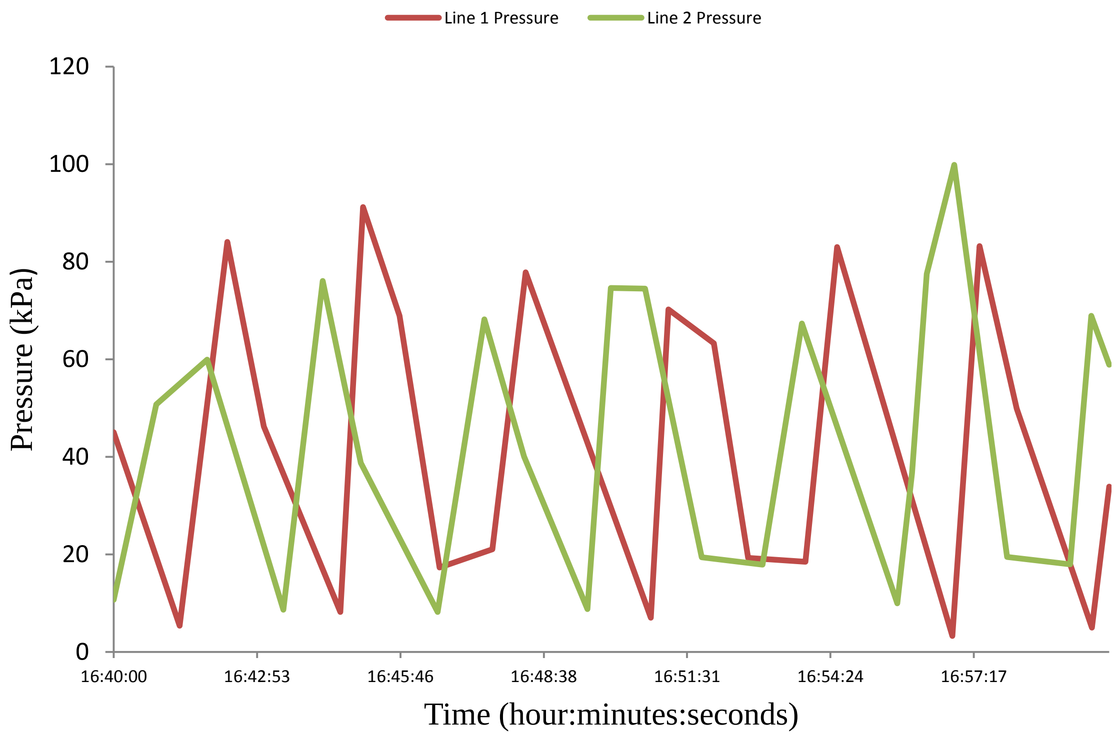


**Figure 5.10** Pressure drop as a function of time for Unit 2 on 22 April 2019

Figures for maximum conveying pressures for Unit 2 can be observed from Figure 5.10 for the selected reporting period. Reading from Figure 5.10, the two conveying lines (as indicated in Figure 3.1) had maximum conveying pressures of 91 kPa and 100 kPa respectively. Of particular note is the period when both conveying lines were not in service and this is visible in figure 5.10 when the two conveying lines had low pressures at the same time, at pressure readings of 18 kPa. This is discussed further in section 5.6.

The same approach as followed in observing conveying pressures for Unit 2 is followed for Unit 1 and Unit 3. Data period 2 for Unit 1 is used for illustration purposes, and results are as indicated in Figure 5.11 with raw data readings observed for 12 October 2017.

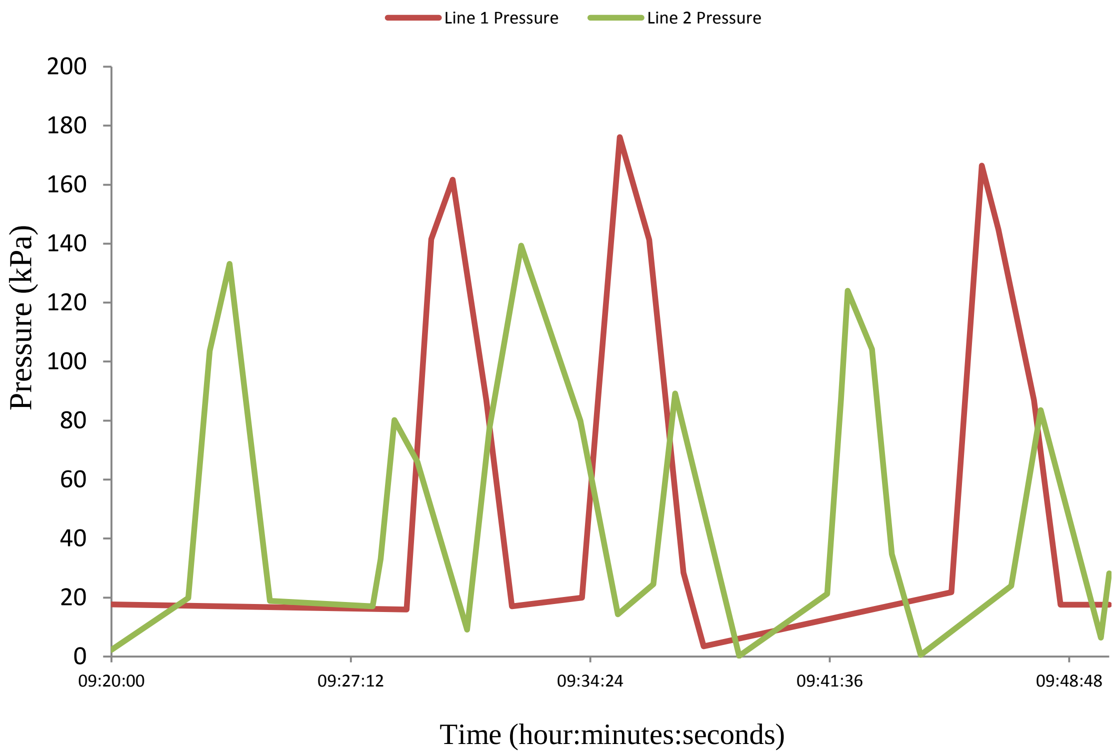


**Figure 5.11** Pressure drop as a function of time for Unit 1 raw data period 12 October 2017

Similarly with Unit 3, period 8 is selected for illustration purposes, and raw data values are as indicated in figure 5.12 for 01 July 2019. As with Unit 2, it is also worth noting the time at which both the conveying lines are at their lowest pressures, this is used for air flow determinations in section 5.6.

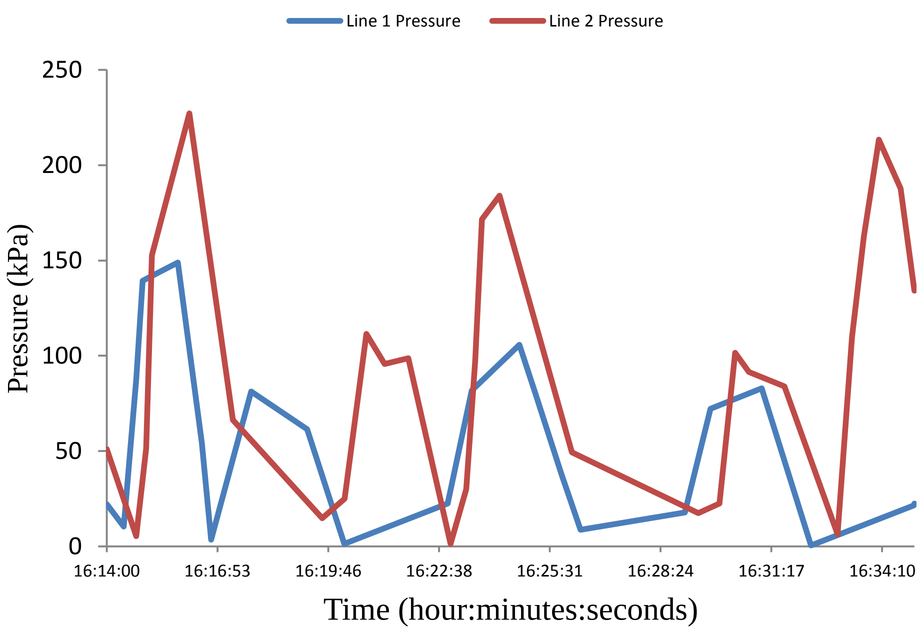


**Figure 5.12** Pressure drop as a function of time for Unit 3 raw data period 01 July 2019

Once the ash flow rate and conveying pressures have been determined, the last pneumatic conveying data necessary are the air flow rate values. Conveying pressure data for all other data periods are included in Appendix H.

## 5.6 Air Flow Rate Values

As indicated in Chapter 3, section 3.4.3, the air flow meter used during the investigation was measuring air flow simultaneously for two users, i.e., the pneumatic conveying system and the boiler cleaning system. It was therefore necessary to know how much air was used by the pneumatic conveying system alone, which was determined from an air mass balance given by the Equation below:

$$\mathrm{V_p = V_T - V_B} \qquad (5.1)$$

In equation 5.1, $\mathrm{V_p}$ is the pneumatic air flowrate, $\mathrm{V_T}$ is the total air flowrate and $\mathrm{V_B}$ is the boiler air flowrate in $\mathrm{m^3/min}$.

### 5.6.1 Boiler volumetric flow

The boiler cleaning process was designed to consume a maximum of 49 $\mathrm{Sm^3/min}$ (Internal report, Document number: 200-36048), and this value was also observed during the research period. This was observed by noting all the periods when the pneumatic system was not conveying, to obtain a value for the boiler cleaning air flow on its own. For illustration purposes, a period under investigation is selected for Unit 2, 08 September to 06 October 2017. During that period, air flow data was observed in shown in Figure 5.13.

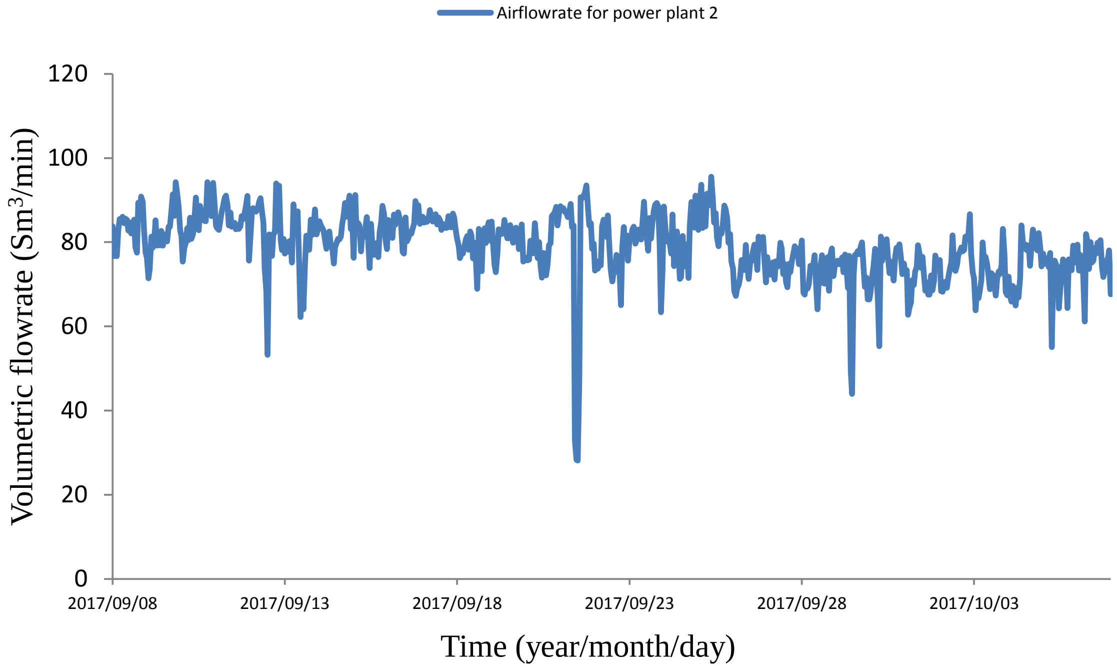


**Figure 5.13** Volumetric air flow as a function of time for Unit 2

The low point in figure 5.13 indicates a period when both conveying lines were inactive and only the cleaning system was consuming air; this is the point of interest. However, to ensure that this is indeed a point where both conveying lines were not conveying, it is necessary to superimpose the conveying pressures with air flow rate to indeed confirm this assumption: refer to Figure 5.14.

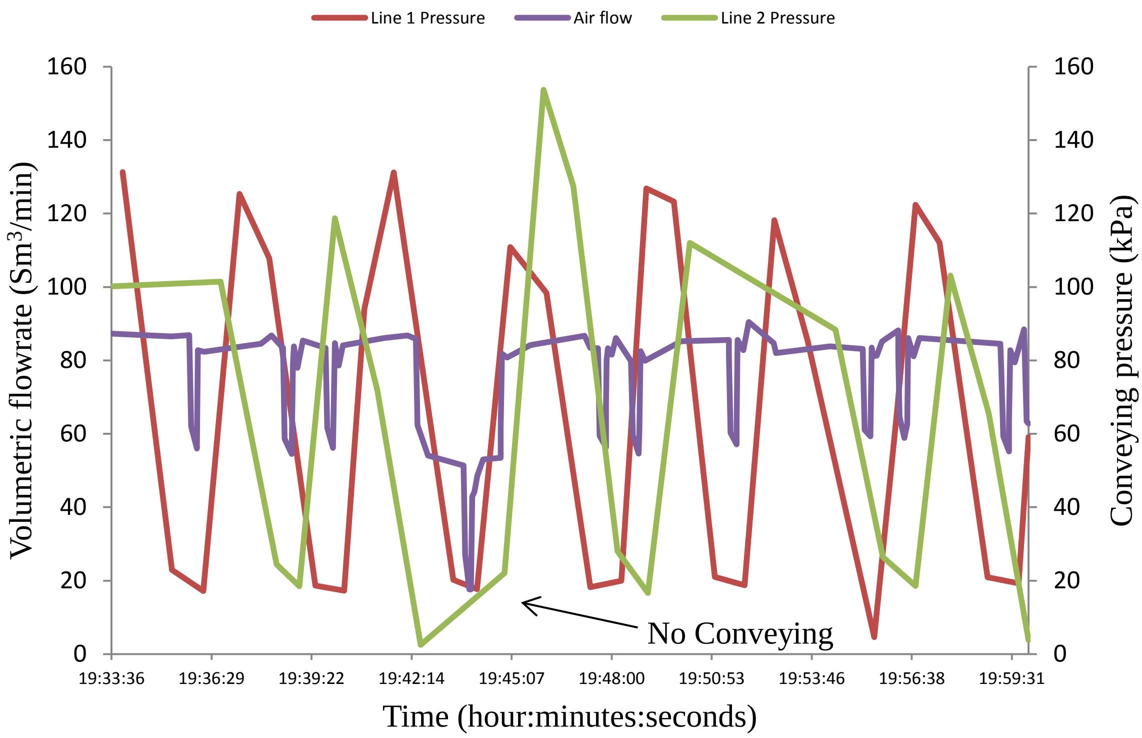


**Figure 5.14** Volumetric air flow as a function of time for Unit 2 with a no-conveying period indicated

The above process was also validated by observing instances when the air supply valves for the pneumatic conveying system were opened and closed. These valves for the period under discussion are as indicated in Figure 5.15.

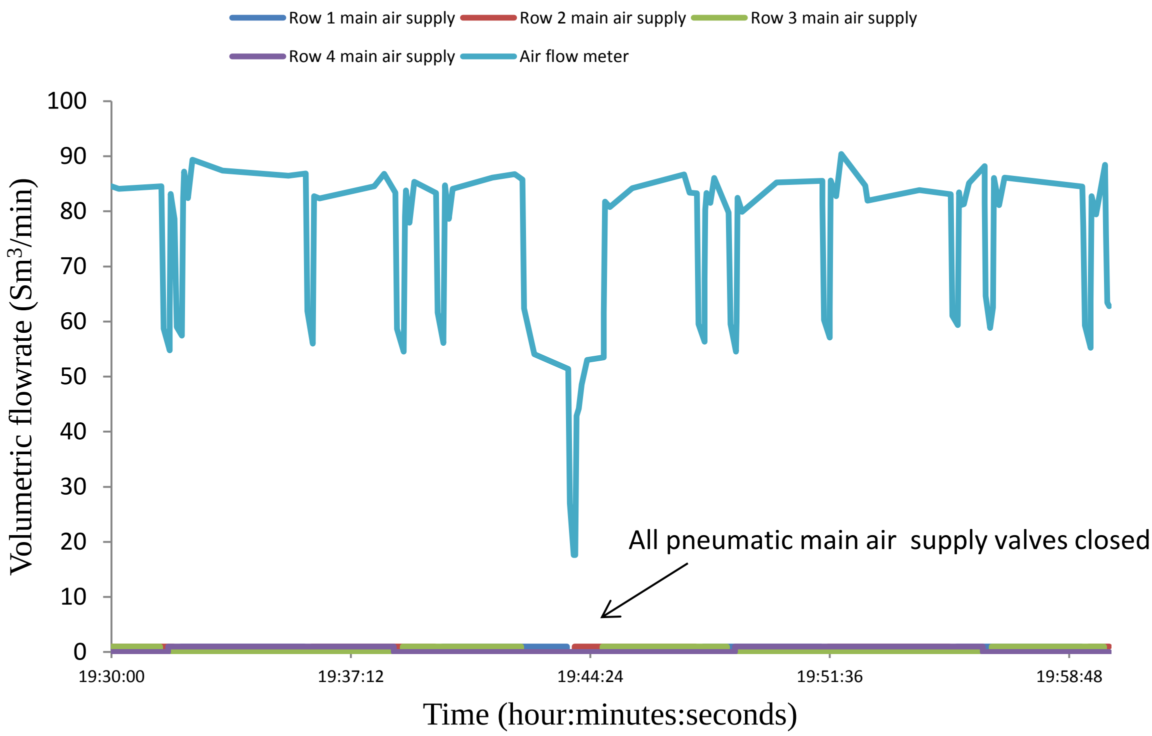


**Figure 5.15** Volumetric air flow as a function of time for Unit 2 with a no-conveying period indicated by closure of air valves

As such, a no-conveying period as indicated in Figure 5.14 and Figure 5.15 shows the amount of air used solely for the boiler cleaning process. In Figure 5.15 the boiler cleaning system consumes 17.6 standard cubic meters of air per minute. Equation 5.1 can then be applied at any other point during that period to estimate the amount of air used by the pneumatic conveying system. This is discussed in section 5.6.2 in detail.

### 5.6.2 Pneumatic conveying volumetric flow

Figure 5.15 indicates a value of 17.6 standard cubic meters of air per minute used for the cleaning system. The air usage can easily be deduced from figure 5.14 for scenarios when both conveying lines were in operation, and when either one of the conveying lines was in operation. Table 5.8 indicates these values of air flow rate for this period. The conveying values are averaged for both line 1 and line 2.

**Table 5.8** Air flow rate for Unit 2

| **System in operation** | **Volumetric flow rate ($Sm^3$/min)** |
|---|---|
| Boiler cleaning only | 17.6 |
| Line 1 conveying and boiler cleaning | 54 |
| Line 2 conveying and boiler cleaning | 56 |
| Both lines conveying and boiler cleaning | 86 |

Application of Equation 5.1, then leads to understanding of the air only used for pneumatic conveying, by subtracting the air used for boiler cleaning.

As such, for this period the air used for a single conveying line, such as line 2 from Equation 5.1,

$$\therefore V_p = V_T - V_B = 56 - 17.6 = 38.4 \text{ Sm}^3\text{/min}$$

A similar process is followed for line 1 and the total air used for conveying both lines at the same time, and these were 36.4 $Sm^3$/min and 68.4 $Sm^3$/min respectively.

The above process was repeated for all the periods under investigation for Units 1, 2 and 3. This information is included as Appendix J superimposed with the conveying pressures**.**

## 5.7 Consolidated Pneumatic Conveying Characteristics

This section consolidates the system performance and this is done by tabulating the results from each Unit. These results are tabulated to indicate the salient parameters such as the material mass flow rate, the air consumption and the conveying pressures. Unit 2 was used for illustration purposes as indicated in subsections 5.4 to 5.6 where the ash consumption, conveying pressure and air flow rate were analyzed. These are included in Table 5.9 for Unit 2, period 2. Similar sample tables were developed for Units 1 and 3, both Units with Period 1 data analyzed for the September 2017 period following the same methodology and these are included as Tables 5.10 and 5.11 for illustration.

**Table 5.9** Unit 2 data for period 2 on 5 December 2017

| **Material mass flow rates** (kg/s) | | **Conveying pressures** (kPa) | | **Volumetric air flow rate** ($Sm^3$/min) | |
|---|---|---|---|---|---|
| Mill10 coal flow rate | 36.8 | No conveying | 18 | Boiler cleaning only | 17.6 |
| Mill20 coal flow rate | 33.2 | | | | |
| Mill30 coal flow rate | 23.2 | Line 1 | 91 | Line 1 conveying | 36.4 |
| Mill40 coal flow rate | 0 | | | | |
| Mill50 coal flow rate | 33.2 | Line 2 | 100 | Line 2 conveying | 38.4 |
| Total coal consumption | 126.6 | | | | |
| Fly ash only | 38.8 | | | Both lines conveying | 68.4 |

**Table 5.10** Unit 1 data for period 1 on 24 September 2017

| **Material mass flow rates** (kg/s) | | **Conveying pressures** (kPa) | | **Air flow rate** ($Sm^3$/min) | |
|---|---|---|---|---|---|
| Mill10 coal flow rate | 25.6 | No conveying | 21 | Boiler cleaning only | 29 |
| Mill20 coal flow rate | 25.6 | | | | |
| Mill30 coal flow rate | 25.6 | Line 1 | 217 | Line 1 conveying | 56 |
| Mill40 coal flow rate | 25.6 | | | | |
| Mill50 coal flow rate | 0 | Line 2 | 184 | Line 2 conveying | 62 |
| Total coal consumption | 102.5 | | | | |
| Fly ash only | 32.3 | | | Both lines conveying | 111 |

**Table 5.11** Unit 3 data for period 1 on 11 September 2017

| **Material mass flow rates** (kg/s) | | **Conveying pressures** (kPa) | | **Volumetric air flow rate** ($Sm^3$/min) | |
|---|---|---|---|---|---|
| Mill10 coal flow rate | 26 | No conveying | 20 | Boiler cleaning only | 30 |
| Mill20 coal flow rate | 26 | | | | |
| Mill30 coal flow rate | 25 | Line 1 | 164 | Line 1 conveying | 61 |
| Mill40 coal flow rate | 0 | | | | |
| Mill50 coal flow rate | 26 | Line 2 | 181 | Line 2 conveying | 71 |
| Total coal consumption | 103 | | | | |
| Fly ash only | 32 | | | Both lines conveying | 130 |

Tables 5.9 to 5.11 contain data for selected periods for Units 1, 2 and 3. This exercise was completed for the full set of results as per periods indicated in Tables 5.1 to 5.3 for the three Units under consideration. These results are included in Table 5.12 for all the data recorded for Unit 1, and similar Tables are as indicated for Unit 2 and Unit 3, as Tables 5.13 and 5.14. The graphs pertaining to results shown in Tables 5.12 to 5.14 are included in appendix G for coal consumption data and appendix H for conveying pressure superimposed with the air flow rate data. The specific dates are as shown in appendix G and H for the reporting periods shown in Tables 5.12, 5.13 and 5.14 and as explained in section 5.4, to obtain raw data.

Values that were found to be outliers, as they vary significantly with other data sets are indicated in *italics*.

**Table 5.12** All values observed for Unit 1 for all the data periods under consideration

| **Pneumatic Conveying Data** | | **Period 1** | **Period 2** | **Period 3** | **Period 4** | **Period 5** | **Period 6** | **Period 7** | **Period 8** |
|---|---|---|---|---|---|---|---|---|---|
| Coal consumption mill 1 | (kg/s) | 25.6 | 21.9 | 20.2 | 20.9 | 0 | 23.4 | 21.4 | 19.5 |
| Coal consumption mill 2 | (kg/s) | 25.6 | 22.2 | 20.3 | 0 | 22.8 | 24.7 | 22.0 | 20.4 |
| Coal consumption mill 3 | (kg/s) | 25.6 | 21.6 | 20.4 | 20.7 | 23.8 | 27.6 | 24.5 | 21.8 |
| Coal consumption mill 4 | (kg/s) | 25.6 | 22.1 | 0 | 22.9 | 22.9 | 0 | 0 | 0 |
| Coal consumption mill 5 | (kg/s) | 0 | 0 | 20.3 | 22.9 | 21.5 | 26.8 | 26.4 | 25.8 |
| Fly ash mass flowrate (both lines) | (kg/s) | 32.3 | 27.7 | 25.6 | 27.5 | 28.6 | 32.7 | 29.8 | 27.6 |
| Conveying Pressure Line 1 (gauge) | (kPa) | 217 | 161 | 169 | 151 | 156 | 169 | *169* | *169* |
| Conveying Pressure Line 2 (gauge) | (kPa) | 184 | 140 | 138 | 133 | 124 | 150 | *150* | *150* |
| Air only pressure drop Line 1 (gauge) | (kPa) | 19 | 20 | 21 | 15.5 | 21.6 | 23.3 | 24.2 | 19.76 |
| Air only pressure drop Line 2 (gauge) | (kPa) | 18 | 16 | 19 | 21 | 23.4 | 18.7 | 19.4 | 16.2 |
| Volumetric air flowrate for line 1 | $Sm^3/min$ | 56 | 49 | 68.9 | 83 | 69 | 59 | *112.6* | 60 |
| Volumetric air flowrate for line 2 | $Sm^3/min$ | 62 | 64 | 83 | 67 | 53 | 55 | *104.6* | 53 |
| Boiler cleaning only air flowrate | $Sm^3/min$ | 29 | 27 | 22 | *48* | 21 | 34 | *14* | 26 |

**Table 5.13** All values observed for Unit 2 for all the data periods under consideration

| Pneumatic Conveying Data | | Period 1 | Period 2 | Period 3 | Period 4 | Period 5 | Period 6 | Period 7 |
|---|---|---|---|---|---|---|---|---|
| Coal consumption mill 1 | (kg/s) | 25.6 | 24.9 | 26.5 | 25.2 | 15.9 | 23.4 | 23.4 |
| Coal consumption mill 2 | (kg/s) | 25.6 | 25.9 | 27.5 | 30.5 | 20.9 | 0 | 27.2 |
| Coal consumption mill 3 | (kg/s) | 25.6 | 25.9 | 27.0 | *7.1* | 23.1 | 21.7 | 20.4 |
| Coal consumption mill 4 | (kg/s) | 25.6 | 0 | 0 | 29.1 | 0 | 20.7 | 0 |
| Coal consumption mill 5 | (kg/s) | 0 | 24.9 | 22.6 | 23.6 | 19.1 | 0 | 0 |
| Fly ash mass flowrate (both lines) | (kg/s) | 32.3 | 32 | 32.6 | 36.4 | 24.9 | 20.7 | 22.6 |
| Conveying Pressure Line 1 (gauge) | (kPa) | 131 | 165 | 113 | 166 | Invalid | 91 | *100* |
| Conveying Pressure Line 2 (gauge) | (kPa) | 153 | 141 | 141 | 111 | 141 | 99 | *100* |
| Air only pressure drop Line 1 (gauge) | (kPa) | 18.8 | 18.6 | 15.7 | 19.4 | Invalid | 19.3 | 17.9 |
| Air only pressure drop Line 2 (gauge) | (kPa) | 18.5 | 20.6 | 15.7 | 19.6 | 19.5 | 17.9 | 16.9 |
| Volumetric air flowrate for line 1 | $Sm^3/min$ | 35.4 | 36 | 32 | 38 | 40 | 39 | 33 |
| Volumetric air flowrate for line 2 | $Sm^3/min$ | 39.4 | 36 | 33 | 38.4 | 40 | 35 | 31 |
| Boiler cleaning only air flowrate | $Sm^3/min$ | 17.6 | 25 | 19 | 26 | 23 | 23 | 23 |

**Table 5.14** All values observed for Unit 3 for all the data periods under consideration

| Pneumatic Conveying Data | | Period 1 | Period 2 | Period 3 | Period 4 | Period 5 | Period 6 | Period 7 | Period 8 |
|---|---|---|---|---|---|---|---|---|---|
| Coal consumption mill 1 | (kg/s) | 26.0 | 26.2 | 20.8 | 29.9 | 25.2 | 18.9 | 29.9 | 36.8 |
| Coal consumption mill 2 | (kg/s) | 26.0 | 26.2 | 20.8 | 29.2 | 0 | 0 | 29.2 | 33.4 |
| Coal consumption mill 3 | (kg/s) | 25.0 | 26.2 | 20.8 | 0 | 25.2 | 22.9 | 0 | 30.0 |
| Coal consumption mill 4 | (kg/s) | 0 | 26.2 | 20.8 | 26.6 | 27.9 | 20.4 | 26.6 | 0 |
| Coal consumption mill 5 | (kg/s) | 26.0 | 0 | 0 | 25.1 | 0 | 0 | 25.1 | 36.8 |
| Fly ash mass flowrate (both lines) | (kg/s) | 32.5 | 32.9 | 26.2 | 35 | 24.6 | 19.6 | 35 | 43.2 |
| Conveying Pressure Line 1 (gauge) | (kPa) | 164 | 135 | 126 | 172 | 160 | *64* | 179 | *148* |
| Conveying Pressure Line 2 (gauge) | (kPa) | 181 | 156 | 145 | 100 | 129 | *78* | 223 | *227* |
| Air only pressure drop Line 1 (gauge) | (kPa) | 25 | 17.8 | 19.4 | 19.8 | 17.7 | 13.4 | 19.1 | 22.3 |
| Air only pressure drop Line 2 (gauge) | (kPa) | 21.8 | 14.9 | 22.8 | 16.0 | 20.7 | *11.1* | 21.8 | 17.3 |
| Volumetric air flowrate for line 1 | $Sm^3/min$ | 61 | 76 | 61 | 77 | 87 | *107* | 91 | 69 |
| Volumetric air flowrate for line 2 | $Sm^3/min$ | 71 | 78 | 86 | 75 | 87 | *98* | 91 | 65 |
| Boiler cleaning only air flowrate | $Sm^3/min$ | 20 | 37 | 28 | *44* | 42 | 29 | *29* | *46* |

# CHAPTER 6 ANALYSIS AND DISCUSSION OF PNEUMATIC CONVEYING CHARACTERISTICS

## 6.1 Introduction

Chapter 5 details the findings from this research in terms of raw unprocessed data, but it is necessary to analyze this data and list the salient findings of this research. This section of the report is dedicated to analysis of results and this is done as follows:

- Fly ash properties
- Analysis of air flow rate and solids loading ratio
- Discussion on the solids loading ratio and air flow rate
- Analysis and discussion of the conveying air velocity.

Pneumatic conveying characteristics such as solids friction factor and pressure drop values are discussed in Chapter 7, together with prediction techniques for solids pressure drop based on findings from the literature and this research.

## 6.2 Discussion of Fly Ash Properties

Using a sieving test and consolidated stress for bulk characterization as described in section 5.2, the particular characteristics for the fly ash under investigation were found with a bulk density of 1180 $kg/m^3$ and an average particle diameter of 63 µm. The particle diameter was also compared with results from commissioning periods as indicated in Appendix F. It is observed that the majority of the fly ash measured by weight as detailed in Appendix F were able to pass the 75 µm and less sieve sizes.

The bulk density was also compared with that of initial stages as indicated by bulk density in Figure 5.2. This was also found to be similar to the data observed during the experiment. Based on this information, it can be assumed that this type of ash can be transported in a dense phase system when considering Geldart's chart (Geldart, 1973) and also supported with findings from Williams (2008), depending of cause on the amount of air used in the conveying.

The question of which mode of dense phase conveying prevails, either fluidized bed or plug flow, can be considered based on the work of Deng and Bradley (2016). They concluded that materials with a mean diameter of less than 70 $\mu$m could generally be transported in fluidized dense phase conveying provided that the minimum conveying velocity is maintained (Deng and Bradley, 2016). With a larger particle size slug or plug flow could prevail. As such, it is inconclusive to suggest that the flow in the system would always remain fluidized, it can be expected that there may be instances where the ash would be conveyed in slug or plug flow. Based on the air flow rate data discussed in section 6.3, the system behaved similarly to a dilute phase system considering the air to solids ratio and noting the Mills (2016) findings with a requirement of a higher solids loading ratio for dense phase systems (above 20) which was not the case in most of this research.

To avoid this speculation, researchers prefer the installation of a sight glass as part of the conveying pipe system to be able to visually ascertain the type of conveying and mode of conveying (Wypych, 1989; Jones and Williams, 2003). Unfortunately this could not be done for this research as the conveying system was already installed and in full production.

## 6.3 Analysis of the Air Flow Rate

The design of a pneumatic conveying system centers on determining the required air flow rate. In Chapter 5, Section 5.6 shows the estimated volumetric air flow rate (Standard conditions, 0 °C and 101.3 kPa) for pneumatic conveying for each of the three Units at particular times (Tables 5.6 to 5.8). Volumetric air flow rate varies with changes in temperature and pressure of air and a more useful parameter in discussing conveying air flow rate is the air mass flow rate. As such it is necessary to covert the volumetric air flow rate into a mass air flow rate. To illustrate air mass flow rate computation, an arbitrary data point for Unit 2 such as period 4 is selected. The results for this example, as shown in Table 5.13, are presented as Table 6.1. Figure 6.1 also shows the volumetric air flow rate variation with conveying pressure for the selected data period for illustration purposes. As mentioned in section 5.4, each selected period is further scrutinized and for that date a smaller conveying period such as a few hours or minutes is selected, refer to figure 6.1.

**Table 6.1** Conveying pressure and volumetric air flow rate data for Unit 2 period 4 sample date 11 May 2018

| **System in operation** | **Average volumetric flow rate** ($Sm^3$/min) | **Average conveying pressures** (kPa) |
|---|---|---|
| Line 1 conveying | 38 | 145 |
| Line 2 conveying | 38.4 | 105 |
| Both lines conveying | 76.4 | - |
| Total air supply at Compressor plant | 97 | 740 kPa |

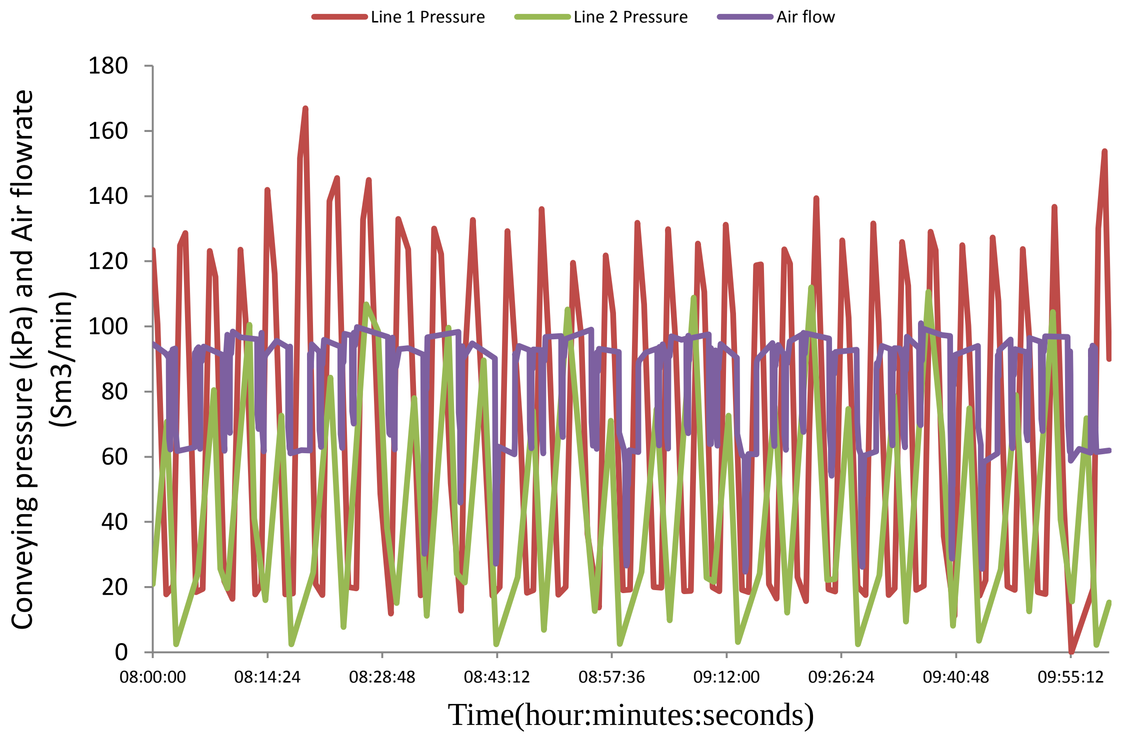


**Figure 6.1** Conveying pressure and volumetric air flow rate data for Unit 2 period 4 sample date 11 May 2018

From Table 6.1 and Figure 6.1, the total air flow rate is $\dot{V}_T = 97$ $Sm^3$/min, and from using ideal gas laws, a factor of conversion from volumetric to air mass flow rate of 0.02155 is used (refer to Appendix I for sample calculations). Therefore, the resulting total air mass flow rate is computed as, $\dot{m}_a = 2.09$ kg/s. The conversion factor of 0.02155 is based on the reference conditions for the design of the volumetric air flow meter (Internal document, design report, document number: 200-36048).

A similar calculation is followed to compute the pneumatic conveying only air flow rate,

$$\dot{m}_p = 0.0215 \times \dot{V}_p = 0.02155 \times 76.4 = 1.64 \text{ kg/s}$$

This is the total air flow rate for both the conveying lines, and if both lines are conveying at the same time with the same pressure and temperature, which is assumed to be the case, the conveying air flow rate per conveying line is simply half of this figure.

As such, a Table similar to 6.1 can be developed based on air mass flow rate such as indicated on Table 6.2.

**Table 6.2** Air mass flowrate data for power plant 2, period 4

| **System in operation** | **Average mass flow rate** (kg/s) |
|---|---|
| Line 1 conveying | 0.82 |
| Line 2 conveying | 0.82 |
| Both lines conveying | 1.64 |
| Total air supply at Compressor plant | 2.09 |

The complete set of analyzed results for conveying air mass flow rate for the three power station Units is included in section 6.4; Table 6.3 for Unit 1, Table 6.4 for Unit 2 and Table 6.4 for Unit 3 this forms part of the discussion about the solids loading ratio.

## 6.4 Review of the solids loading ratio (SLR)

After the air flow rate has been analyzed, the next set of data to be reviewed is the ash flow rate and this is done in order to determine the solids loading ratio (SLR). Section 6.4 is dedicated to the discussion of air flow rate together with solids loading ratio, as the air flow rate cannot be discussed on its own to have a conclusion whether a particular system consumes more air than necessary. This must always be in the context of the amount of fly ash that is being conveyed, and hence it is necessary to review the solids loading ratio as well. The dimensionless solids loading ratio μ (SLR) is used to define this relation, as given by Equation 2.2.

It is necessary to identify the ash flow rates for the conveying cycle periods indicated in Tables 6.3, 6.4 and 6.5 in order to quantify the SLR values for those conveying periods. Estimation of the fly ash mass flow rates is covered in Chapter 5, Section 5.4. Making use of Unit 2 as an example (Table 5.4), the fly ash mass flow rate for Unit 2, period 1 was estimated as 119 tons per hour (16.52 kg/s per line). On this particular conveying cycle, the air flow rate was 0.9 kg/s, See Table 6.4 (consolidated table for all air flow data). These values were substituted with fly ash mass flow rate into Equation 2.2,

$$\mu = \frac{m_s}{m_a} = \frac{16.1}{0.8} = 20.1$$

This calculation was performed for all the Units to find the SLR for selected periods under discussion, and Table 6.3 tabulates the findings for Unit 1. Units 2 and 3 are included in Tables 6.4 and 6.5 respectively. For ease of reference, kg/s units were used for both fly ash and air, instead of the usual tons per hour for fly ash. These ash mass flow rates are taken from Tables 5.12, 5.13 and 5.14 for Units 1, 2 and 3 respectively.

It should be noted that the air flow rate and solids mass flow rates indicated in Tables below are as per the plant configuration, representing half a Unit (one conveying pipeline), refer to Figure 3.1. As such, in terms of air mass flow rates and solids loading, both lines are observed to have similar air and ash flow rates.

**Table 6.3** Solids loading ratio for Unit 1

| **Period** | **Fly ash mass flow rate per conveying line** (kg/s) | **Conveying air mass flow rate per line** (kg/s) | **Solids loading ratio per line** (-) |
|---|---|---|---|
| 1 | 16.1 | 1.27 | 12.7 |
| 2 | 13.8 | 1.21 | 11.4 |
| 3 | 12.8 | 1.63 | 7.8 |
| 4 | 13.8 | 1.61 | 8.5 |
| 5 | 14.3 | 1.31 | 10.9 |

| Period | Fly ash mass flow rate per conveying line (kg/s) | Conveying air mass flow rate per line (kg/s) | Solids loading ratio per line (-) |
|---|---|---|---|
| 6 | 16.1 | 1.19 | 13.5 |
| 7 | 14.9 | 2.33 | 6.4 |
| 8 | 13.8 | 1.21 | 11.3 |

Values that were found to be outliers, as they vary significantly with other data sets are indicated in *italics*.

**Table 6.4** Solids loading ratio for Unit 2

| Period | Fly ash mass flow rate per conveying line (kg/s) | Conveying air mass flow rate per line (kg/s) | Solids loading ratio per line (-) |
|---|---|---|---|
| 1 | 16.1 | 0.80 | 20.1 |
| 2 | 16.0 | 0.77 | 20.7 |
| 3 | 16.3 | 0.70 | 23.4 |
| 4 | 18.2 | 0.82 | 22.1 |
| 5 | 12.4 | 0.86 | 14.5 |
| 6 | 10.4 | 0.80 | 13.0 |
| 7 | 11.3 | 0.69 | 16.4 |

**Table 6.5** Solids loading ratio for Unit 3

| Period | Fly ash mass flow rate per conveying line (kg/s) | Conveying air mass flow rate per line (kg/s) | Solids loading ratio per line (-) |
|---|---|---|---|
| 1 | 16.2 | 1.42 | 11.4 |
| 2 | 16.5 | 1.66 | 10.0 |
| 3 | 13.1 | 1.58 | 8.3 |
| 4 | 17.5 | 1.63 | 10.7 |
| 5 | 12.3 | 1.87 | 6.6 |
| 6 | 9.8 | 2.20 | 4.4 |
| 7 | 17.5 | 1.96 | 8.9 |
| 8 | 21.6 | 1.45 | 14.9 |

## 6.5 Discussion on Air Flow Rate and Solids Loading Ratio (SLR)

The data from Tables 6.3 to 6.5 has been superimposed to best illustrate the solids loading ratios for the three Units, as shown in Figure 6.2. In order to draw similar comparison, the SLR values were plotted against the ash flow rates. SLR 3 for example refers to solid loading ratio for Unit 3 and similar case for SLR 2 and SLR 1.

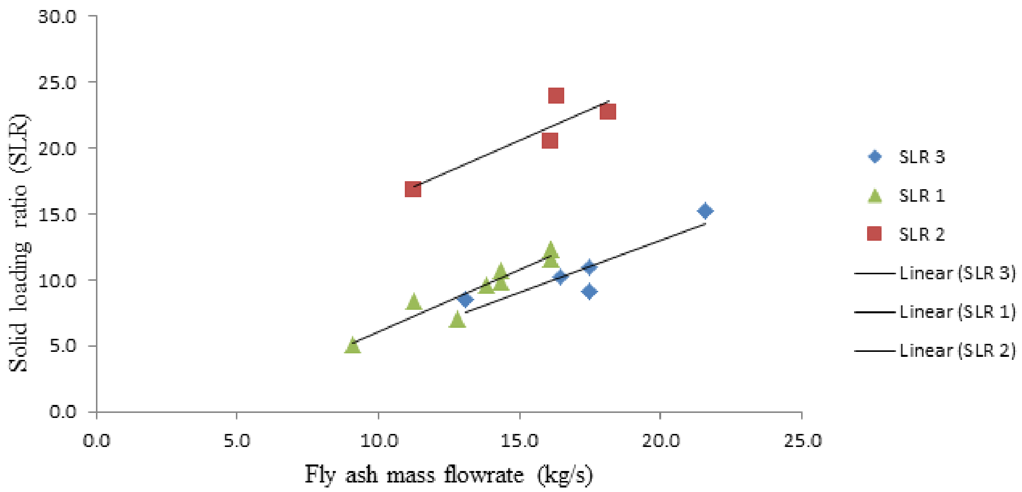


**Figure 6.2** Solids loading ratio for Units 1, 2 and 3 plotted against ash mass flowrate

The findings as recorded in Figure 6.2 provide an insight into how much air is being used by each particular Unit, and also helps to identify areas of improvements when the three Units are benchmarked against each other as well as comparison with literature expectations.

Figure 6.2 and Table 6.4 show that Unit 2, which is situated physically between Units 1 and 3 (refer to table 3.2), has higher solid loading ratio values than either of the two other Units. This indicates that this is the only Unit that is consuming air within expected values, and this is also confirmed by the higher solids loading ratio expected for dense phase conveying. As such, it appears that the air usage for Units 1 and 3 is higher than necessary for conveying, when baselined against Unit 2. Therefore there is room for improvement, in the short term at least; so that Unit 1 air consumption should not be more than that of Unit 2, and this can be done without any concern of blockage on the system based on results from Unit 2.

Mills and Agarwal (2001) define a dense phase system for fly ash as a system that should operate with higher solids loading ratio. In their analysis, they found solids loading ratio values of above 15-20 as typical values expected for dense phase, and any operation below that leads into a dilute phase system. Values for Unit 2 indicate close performance to a dense phase system according to this definition from Mills and Agarwal. Unit 1 and Unit 3 display performance that can be best described as borderline with certain periods close to dense phase but largely with a dilute phase performance. These Units (1 and 3) have solids loading ratio values of less than 10 in certain conveying periods and according to Mills and Agarwal these can be classified as performing in dilute phase mode.

As mentioned already, this is an inconclusive method as most researchers prefer to simply state the mode of conveying based on the suspension and non-suspension of the bulk solids, visible only through a sight glass on the conveying lines (Mallick, 2009). Researchers have observed dilute phase conveying based on visual inspections with solids loading ratios higher than 20, and as such the findings by Mills and Agarwal although a very good starting point, need to be verified by visual inspection (Bansal, 2012). The conveying velocity also assists in classifying the mode of conveying and this is discussed in the next section.

## 6.6 Analysis of the Conveying Air Velocity

The air velocity in pneumatic conveying is important in two ways, firstly the minimum transport velocity to carry the bulk solids and to keep these in motion. Second, it is also important in order to minimize the wear rate on the conveying pipes at high velocities due to the expansion of compressed air in the pipe line (Wypych, 1989). As such, designers of pneumatic conveying systems need to always be mindful of the air velocity expected in the system, and for dense phase systems these are usually low velocities at entry points of typically 3 m/s (Mills, 2016, Wypych, 1989). With a known conveying air mass flow rate, the inlet and discharge point air velocities can be calculated if the pressures and temperatures at those points are known (assuming no pipeline leakage) by using the ideal gas law.

Using Equation, 2.5 and selecting Unit 2 period 1 for illustration, the air inlet velocity into the conveying line can be computed from known values of pressure, temperature, and volumetric flow rate and pipe diameter. Refer to Table 5.6, with static pressure values for line 1 as 131 kPa and volumetric flow rate values of 36 $Sm^3$/min for both line 1 and 2. The temperature is that of the air-ash mixture, and this is taken at the design value of 160 degrees Celsius for fly ash temperature (Internal report, Design report: 200-215389). The barometric pressure is 89.6 kPa (Internal report, Design report: 200-36048). Calculating the air mass flow rate as discussed in section 6.5 and substituting the values from Table 6.5 into Equation 2.5,

$$v_{inlet} = \frac{4m_aRT}{P\pi D^2} = \frac{4\times0.80\times0.287\times(160+273)}{(131+89.6)\times3.142\times0.265^2} = 8.2 \text{ m/s}$$

The outlet velocity is calculated in the same manner, with changes only in the discharge conditions where the pressure and temperature is that at the entrance into the silo. The silo is fitted with an extraction fan that maintains the silo at vacuum pressure to avoid over-pressuring the silo and assist in flow of ash into the silo. This is controlled by a filter unit that maintains pressure at -4 kPa at the silo and a temperature at 80 degrees Celsius due to the warm ash at the discharge of the silo (Internal report, Design report: 200-215389). The outlet (exit) velocity is then calculated in like manner as,

$$v_{exit} = \frac{4m_aRT}{P\pi D^2} = \frac{4\times 0.80\times 0.287\times 353}{(89.6-4)\times 3.14\times 0.265^2} = 17.2 \text{ m/s}$$

The average velocity is calculated as the mean of the two velocities, and this is computed as,

$$v = \frac{v_{inlet}+v_{exit}}{2} = 12.71 \text{ m/s}$$

This process was followed for all selected periods for Unit 2, and the findings are as indicated in Table 6.6. Values for Units 1 and 3 are as indicated in Tables 6.7 and 6.8 respectively. Outlet conditions are the same for both conveying lines as the discharge is at the same location.

**Table 6.6** Conveying air velocity for Unit 2 for all periods

| **Period** | **Inlet velocity line 1** (kg/s) | **Inlet velocity line 2** (kg/s) | **Outlet velocity Line 1** (kg/s) | **Outlet velocity line 2** (kg/s) | **Average velocity line 1** (kg/s) | **Average velocity line 2** (kg/s) |
|---|---|---|---|---|---|---|
| Period 1 | 8.24 | 7.49 | 17.17 | 17.38 | 12.71 | 12.43 |
| Period 2 | 6.87 | 7.58 | 16.73 | 16.73 | 11.80 | 12.15 |
| Period 3 | 7.79 | 6.85 | 15.10 | 15.10 | 11.45 | 10.97 |
| Period 4 | 7.26 | 9.25 | 17.75 | 17.75 | 12.50 | 13.50 |
| Period 5 | Invalid | 8.42 | 18.58 | 18.58 | Invalid | 13.50 |
| Period 6 | 9.96 | 9.53 | 17.19 | 17.19 | 13.57 | 13.36 |
| Period 7 | 8.20 | 8.20 | 14.87 | 14.87 | 11.53 | 11.53 |

Invalid data point in Table 6.6 are due to unavailable pressure reading available for period 5 conveying pipe line 1, refer to Table 5.13.

**Table 6.7** Conveying air velocity Unit 1 for all periods

| **Period** | **Inlet velocity line 1** (kg/s) | **Inlet velocity line 2** (kg/s) | **Outlet velocity Line 1** (kg/s) | **Outlet velocity line 2** (kg/s) | **Average velocity line 1** (kg/s) | **Average velocity line 2** (kg/s) |
|---|---|---|---|---|---|---|
| Period 1 | 9.34 | 10.47 | 27.22 | 27.22 | 18.28 | 18.84 |
| Period 2 | 10.95 | 11.95 | 26.07 | 26.07 | 18.51 | 19.01 |
| Period 3 | 14.26 | 16.21 | 35.04 | 35.04 | 24.65 | 25.62 |
| Period 4 | 15.14 | 16.37 | 34.60 | 34.60 | 24.87 | 25.48 |
| Period 5 | 12.06 | 13.87 | 28.14 | 28.14 | 20.10 | 21.01 |
| Period 6 | 10.42 | 11.25 | 25.61 | 25.61 | 18.01 | 18.43 |
| Period 7 | *20.38* | *22.00* | *50.09* | *50.09* | *35.23* | *36.04* |
| Period 8 | 10.61 | 11.45 | 26.07 | 26.07 | 18.34 | 18.76 |

Velocities in *italics* represents outliers that are caused by the very high air flowrate for Unit 1 period 7 (refer to table 5.12).

**Table 6.8** Conveying air velocity for Unit 3 for all periods

| **Period** | **Inlet velocity line 1** (kg/s) | **Inlet velocity line 2** (kg/s) | **Outlet velocity Line 1** (kg/s) | **Outlet velocity line 2** (kg/s) | **Average velocity line 1** (kg/s) | **Average velocity line 2** (kg/s) |
|---|---|---|---|---|---|---|
| Period 1 | 8.99 | 8.42 | 30.66 | 30.66 | 19.83 | 19.54 |
| Period 2 | 11.84 | 10.83 | 35.78 | 35.78 | 23.81 | 23.30 |
| Period 3 | 11.78 | 10.82 | 34.15 | 34.15 | 22.96 | 22.49 |
| Period 4 | 10.03 | 13.86 | 35.31 | 35.31 | 22.67 | 24.58 |
| Period 5 | 12.04 | 13.75 | 40.42 | 40.42 | 26.23 | 27.09 |
| Period 6 | *23.08* | *21.15* | *47.62* | *47.62* | *35.35* | *34.39* |
| Period 7 | 11.70 | 10.05 | 42.28 | 42.28 | 26.99 | 26.17 |
| Period 8 | 9.79 | 7.34 | 31.28 | 31.28 | 20.53 | 19.31 |

Velocities in *italics* represents outliers that is caused by the lower conveying pressures for Unit 3, period 6 (refer to table 5.14). This can be assumed to be an incorrect set of data as it varies quite significantly with performance for the other periods in the research.

## 6.7 Discussion on Conveying Air Velocity

The pipe entry and pipe exit air velocities for Units 1, 2 and 3 are indicated by Tables 6.6 to 6.8. Figure 6.3 shows only the average velocities for pipeline 2 in each case, for improved visibility. A trend line curve was also fitted to assist in explaining the differences between the three Units.

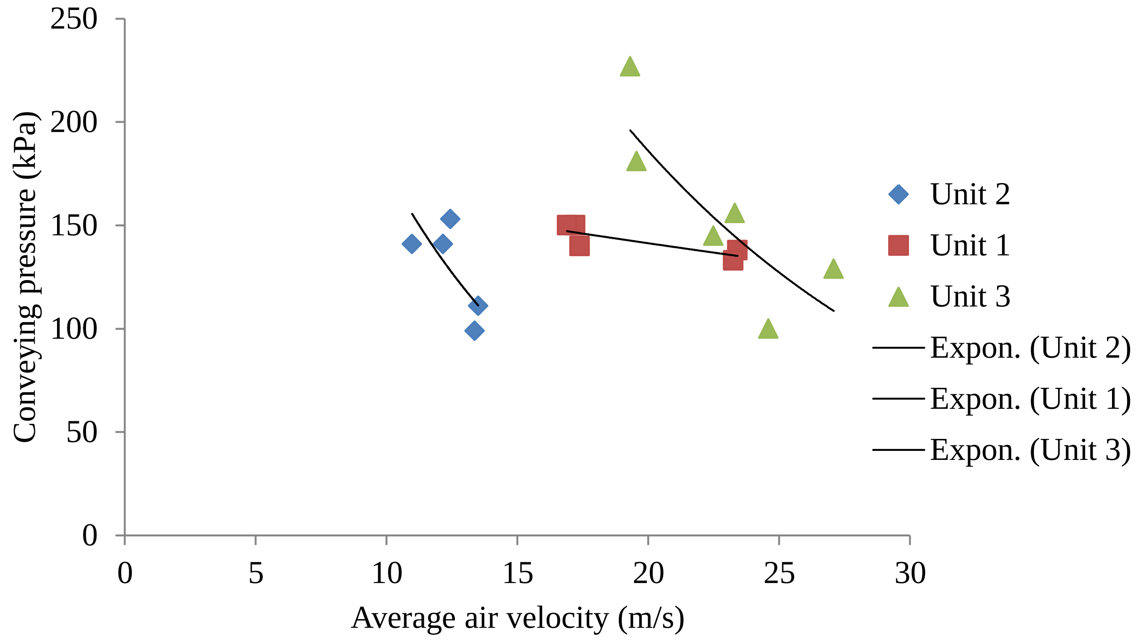


**Figure 6.3** Average air velocities for Units 1, 2 and 3 plotted against the conveying pressure

All the inlet air velocity values in Tables 6.6 to 6.8 are significantly higher than the expected values for dense phase conveying systems, with Mills (2016) suggesting values of 3-5 m/s. There exists room for further optimization of these units. Although Unit 2 demonstrated a better performance in terms of solids loading ratio, the air velocities are still much higher than expected with the lowest inlet velocity at approximately 7 m/s. Although it should also be stated that due to the location of the conveying pressure already in the pipe line, the velocities will also be expected to be higher than those expected by Mills (2016), as Mills entry point differs with the conveying pipe entry in this research. Jones and Williams (2003) suggest that as long as the average velocity is less than 15 m/s, flow can be assumed to be predominantly in the dense phase mode. Air velocity values for Units 1 and 3 show the need to reduce the air flow rate with Unit 3, the furthest Unit in this research (as shown in Figure 3.6), having the maximum average velocity of approximately 27 m/s.

The relationship between velocity ($v$) and wear rate ($E$) is expressed as $E \propto v^a$ wherein the power function $a = 2$ according to findings by Ratnayake (2007). However other authors such as Mbabazi, *et al.*, (2004) found this value to be in the order of 3 with variance between 2.42 and 3.64 based on various ash qualities. As such, based on the exponential relationship between velocity and pipe wear and considering the velocities as indicated in Tables 6.6, 6.7 and 6.8, it can be expected that there would be quite a significant wear on the pipes. The pipes were lined at all sensitive areas and no major wear leading to pipe leaks has yet been observed. There were spurious leaks but these were observed mostly on flange connections and can be assumed to be from faulty workmanship and not pipe wear as this would be expected mostly at the bends and no leaks at all were observed at the bends. As such, increasing the pipe diameter as the conveying distance increases is apparently not necessary if the conveying systems are lined or protected on their inside. Unfortunately wear measurements were not undertaken as part of this research but with Unit 1 being in operation for more than 5 years without any pipe replacement, it can be concluded that the pipe liner with tiling is effective in extending the pipe life.

# CHAPTER 7 DISCUSSION OF PRESSURE DROP AND SOLIDS FRICTION FACTOR MODELS

## 7.1 Introduction

In the Literature Review, a number of models are mentioned based on previous tests and in this chapter, some of these models as the Jones and Williams (2003) and the Behera *et al.* (2015) are considered for comparison. A new model is proposed based on the experimental data for these Units. Based on this model, the future performance of Unit 6, the furthest away from the fly ash silos, is estimated with primary focus on the horizontal pressure drop.

## 7.2 Pneumatic Conveying Characteristics Review

Predictive models are derived from experimental findings of the pneumatic conveying variables of pressure drop, air and ash mass flow rates, solids loading ratio and air velocity. Tables 7.1, 7.2 and 7.3 illustrate these values taken from Units 1, 2 and 3 respectively for all data periods as analyzed in Chapter 6. The pressures are as listed in Tables 5.12 to 5.14. In order to develop these predictive models, it is advisable to divide the total conveying pressure drop into its various components made up of the air-only pressure drop, the vertical pressure drop and the pressure drop at a bend, as explained by Equation 2.11. In this research report, due to the location of the conveying pressure transmitter (refer to Figure 4.3), the conveying pressure does not include the acceleration or pick-up pressure drop as the transmitter is placed after the location of the pick-up in the direction of ash conveying.

Equations 2.3, 2.6, 2.7 and 2.8 defined in Chapter 2, section 2.4 can be used to calculate the various components of the conveying pressure; however use of these equations also requires the knowledge of air density. Due to the changes in air density as the pressure and temperature changes, average values are preferred to inlet only conditions (Wypych, 1989).

In order to demonstrate how an average air density is calculated, Unit 1 period 1 and line 1 is selected, with prevailing pressure and temperatures conditions at the start of the conveying line defined by: $P = 217$ kPaG and $T = 160$ degrees Celsius (refer to Table 5.12). Using Equation 2.28 the air density can be computed as,

$$\rho_{inlet} = \frac{(217+89.6)}{0.287\times(160+273)} = 2.47\ \text{kg/m}^3$$

Atmospheric pressure in the plant is 89.6 kPa, and taking into account conditions at the discharge, the density is computed at an outlet pressure of $P = -4$ kPaG and $T = 80$ degrees Celsius.

$$\therefore \rho_{outlet} = \frac{(-4+89.6)}{0.287\times(80+273)} = 0.85\ \text{kg/m}^3$$

Computation of the mean conditions, as an average between the pipe inlet and outlet conditions as,

$$\therefore \rho_{mean} = \frac{2.47+0.85}{2} = 1.65\ \text{kg/m}^3.$$

All the mean densities are calculated in a similar manner, from known values of pressure and temperature for Unit 1, 2 and 3 using Tables 5.12 to 5.14 as shown in Tables 7.1 to 7.3. Other data necessary for computation of the friction factor models and estimation of the various pressure components are also included in Tables 7.1 to 7.3 as well for ease of reference.

**Table 7.1** Pneumatic conveying characteristics for Unit 1

| **Conveying line** | **Period** | **Solids mass flowrate** (kg/s) | **Air mass flowrate** (kg/s) | **Solids loading ratio** (-) | **Conveying pressure Gauge** (kPa) | **Average air density** ($\text{kg/m}^3$) | **Average air velocity** (m/s) |
|---|---|---|---|---|---|---|---|
| Line 1 | Period 1 | 16.13 | 1.27 | 12.7 | 217 | 1.65 | 18.28 |
| | Period 2 | 13.83 | 1.21 | 11.4 | 161 | 1.43 | 18.51 |
| | Period 3 | 12.80 | 1.63 | 7.8 | 169 | 1.46 | 24.65 |
| | Period 4 | 13.76 | 1.61 | 8.5 | 151 | 1.39 | 24.87 |
| | Period 5 | 14.32 | 1.31 | 10.9 | 156 | 1.41 | 20.10 |
| | Period 6 | 16.14 | 1.19 | 13.5 | 169 | 1.46 | 18.01 |
| | Period 7 | 14.87 | 2.33 | 6.4 | 169 | 1.46 | 35.23 |
| | Period 8 | 13.79 | 1.21 | 11.3 | 169 | 1.46 | 18.34 |

| Conveying line | Period | Solids mass flowrate (kg/s) | Air mass flowrate (kg/s) | Solids loading ratio (-) | Conveying pressure Gauge (kPa) | Average air density (kg/m$^3$) | Average air velocity (m/s) |
|---|---|---|---|---|---|---|---|
| Line 2 | Period 1 | 16.13 | 1.27 | 12.7 | 184 | 1.52 | 18.84 |
| | Period 2 | 13.83 | 1.21 | 11.4 | 140 | 1.34 | 19.01 |
| | Period 3 | 12.80 | 1.63 | 7.8 | 138 | 1.34 | 25.62 |
| | Period 4 | 13.76 | 1.61 | 8.5 | 133 | 1.32 | 25.48 |
| | Period 5 | 14.32 | 1.31 | 10.9 | 124 | 1.28 | 21.01 |
| | Period 6 | 16.14 | 1.19 | 13.5 | 150 | 1.39 | 18.43 |
| | Period 7 | 14.87 | 2.33 | 6.4 | 150 | 1.39 | 36.04 |
| | Period 8 | 13.79 | 1.21 | 11.3 | 150 | 1.39 | 18.76 |

**Table 7.2** Pneumatic conveying characteristics for Unit 2

| Conveying line | Period | Solids mass flowrate (kg/s) | Air mass flowrate (kg/s) | Solids loading ratio (-) | Conveying pressure Gauge (kPa) | Average air density (kg/m$^3$) | Average air velocity (m/s) |
|---|---|---|---|---|---|---|---|
| Line 1 | Period 1 | 16.13 | 0.80 | 20.1 | 131 | 1.31 | 10.11 |
| | Period 2 | 16.0 | 0.77 | 20.7 | 165 | 1.45 | 9.39 |
| | Period 3 | 16.32 | 0.70 | 23.4 | 113 | 1.24 | 8.98 |
| | Period 4 | 18.19 | 0.82 | 22.1 | 166 | 1.45 | 9.95 |
| | Period 5 | 12.45 | 0.86 | 14.5 | *Invalid* | *Invalid* | 11.20 |
| | Period 6 | 10.37 | 0.80 | 13.0 | 91 | 1.15 | 11.11 |
| | Period 7 | 11.3 | 0.69 | 16.4 | 100 | 1.19 | 9.01 |
| Line 2 | Period 1 | 16.13 | 0.80 | 20.1 | 153 | 1.40 | 9.87 |
| | Period 2 | 16.0 | 0.77 | 20.7 | 141 | 1.35 | 9.62 |
| | Period 3 | 16.32 | 0.70 | 23.4 | 141 | 1.35 | 8.68 |
| | Period 4 | 18.19 | 0.82 | 22.1 | 111 | 1.23 | 10.59 |
| | Period 5 | 12.45 | 0.86 | 14.5 | 141 | 1.35 | 10.69 |
| | Period 6 | 10.37 | 0.85 | 12.2 | 99 | 1.18 | 10.96 |
| | Period 7 | 11.3 | 0.69 | 16.4 | 100 | 1.19 | 9.01 |

**Table 7.3** Pneumatic conveying characteristics for Unit 3

| **Conveying line** | **Period** | **Solids mass flowrate** (kg/s) | **Air mass flowrate** (kg/s) | **Solids loading ratio** (-) | **Conveying pressure Gauge** (kPa) | **Average air density** ($kg/m^3$) | **Average air velocity** (m/s) |
|---|---|---|---|---|---|---|---|
| Line 1 | Period 1 | 16.2 | 1.42 | 11.4 | 164 | 1.44 | 17.30 |
| | Period 2 | 16.47 | 1.66 | 10.0 | 135 | 1.32 | 20.80 |
| | Period 3 | 13.1 | 1.58 | 8.3 | 126 | 1.28 | 20.07 |
| | Period 4 | 17.47 | 1.63 | 10.7 | 172 | 1.47 | 19.78 |
| | Period 5 | 12.32 | 1.87 | 6.6 | 160 | 1.42 | 22.89 |
| | Period 6 | 9.8 | 2.20 | 4.4 | 64 | 1.03 | 30.95 |
| | Period 7 | 17.47 | 1.96 | 8.9 | 179 | 1.50 | 23.53 |
| | Period 8 | 21.6 | 1.45 | 14.9 | 148 | 1.37 | 17.93 |
| Line 2 | Period 1 | 16.2 | 1.42 | 11.4 | 181 | 1.50 | 17.04 |
| | Period 2 | 16.47 | 1.66 | 10.0 | 156 | 1.40 | 20.34 |
| | Period 3 | 13.1 | 1.58 | 8.3 | 145 | 1.36 | 19.64 |
| | Period 4 | 17.47 | 1.63 | 10.7 | 100 | 1.18 | 21.51 |
| | Period 5 | 12.32 | 1.87 | 6.6 | 129 | 1.29 | 23.67 |
| | Period 6 | 9.8 | 2.20 | 4.4 | 78 | 1.09 | 30.10 |
| | Period 7 | 17.47 | 1.96 | 8.9 | 223 | 1.67 | 22.77 |
| | Period 8 | 21.6 | 1.45 | 14.9 | 227 | 1.69 | 16.80 |

Using values in Tables 7.1-7.3, a model can be developed to estimate the solids friction factor. Researchers (Williams, 2008) have often used data available from other researchers as well to develop their own models or verify other models based on PCC data from experiments performed by others. As such, these Tables are useful for research into fly-ash pneumatic conveying as a resource for proving or disproving specific models available in literature based on particular bulk solids characteristics.

Once the PCC data has been consolidated into Tables such as 7.1-7.3, the process followed in establishing a model is first to estimate the individual pressure drops due to air and solids. From such data, using a back-calculation method the solids friction factor is calculated. Once the friction factor is known then a model for estimating pressure drop can be developed for a particular type of bulk solids, fly ash in this research.

## 7.3 Solids Pressure Drop Estimation

### 7.3.1 Introduction

The back-calculation method for estimating the solids friction factor is based on separation of the total pressure drop into its various components such as pressure drop due to bend pressure drop and vertical pressure drop and lastly the air alone. After these have been computed and subtracted from the total conveying pressure, the solids-only horizontal pressure drop remains and with manipulation of Equation 2.3, the solids friction factor is then estimated (Jones and Williams, 2003; Behera et al., 2015). This is discussed in the sections below.

### 7.3.2 Bend pressure drop

The pressure drop is calculated using Equation 2.6 from making average velocity and density conditions as shown in Tables 7.1 to 7.3 for Unit 1, 2 and 3 respectively. Taking into account the number of bends and their radius as indicated in Appendix B conveying pipe details, with a total number of 7 bends, and using Table 2.1 with a bend factor of 0.5, the pressure drop as the flow comes into contact with a bend can be computed. To illustrate this calculation, Unit 3 line 1 period 1 is selected; from Table 7.1; average velocity, $v = 19.83\ \mathrm{m/s}$, average density, $\rho = 1.44\ \mathrm{kg/m^3}$, and solids loading ratio, $\mu = 11.4$

$$\therefore P_B = \frac{NB(1+\mu)\rho v^2}{2} = \frac{7\times 0.5(1+11.4)\times 1.44\times 19.83^2}{2} = 12.28\ \mathrm{kPa}$$

A similar process is followed to obtain the bend pressure drop for the remainder of the data for Unit 1, 2 and 3; results are as shown in Tables 7.4 to 7.6.

### 7.3.3 Vertical pressure drop

The vertical pressure drop is also computed using Equation 2.7 from average conditions; however this requires estimation of the velocity ratio between the solids and the air in the conveying stream. This velocity ratio is computed using Equation 2.9, which also requires the use of average conditions and a particle density.

The voids or porosity and particle density were not measured as part of this experiment, these were referenced values from previous research done (Design report, MP066-DR-001) where a particle density of $2200\ \text{kg/m}^3$ was found. This was verified by use of Equation 2.1 with a bulk density of 1180 as detailed in section 5.2.1, and this resulted in a void of 86%, typical for fly ash (Tu, et al., 2007). As such, with use of Table 7.3, with an average air density, $\rho = 1.44\ \text{kg/m}^3$, particle diameter, $d_p = 63 \times 10^{-3}\text{m}$, the velocity ratio is calculated as,

$$\frac{v_s}{v_a} = 1 - 0.0638 d_p^{0.3} \rho_s^{0.5} = 1 - 0.0638 \times (63 \times 10^{-6})^{0.3} \times 2200^{0.5} = 0.84$$

The above expression was used in experimentation of dilute phase systems (Rhodes, 2008) and in this research it was used for approximation purposes. The experimental findings by Mallick (2009) on the solids-to-air velocity ratio for fly ash in dense phase systems suggested that these values range between 0.9 and 0.92, and the above will be used as close approximation. As such, in this research a value of 0.9 will be used.

$$\therefore P_V = \mu \rho \text{g} L_v \left(\frac{v_s}{v_a}\right) = 11.4 \times 1.44 \times 9.81 \times 39.3 \times 0.9 = 5.7\ \text{kPa}$$

A similar process is followed to obtain the vertical pressure drop for the remainder of the data for Unit 1, 2 and 3; results are as shown in Tables 7.4 to 7.6.

### 7.3.4 Air-only pressure drop

The air-only pressure drop was determined by observing the conveying system pressure without any solids, at the end of a conveying cycle. In this process the pressure drop was observed and these values ranged from (16-62) kPa, refer to Chapter 5, Figures 5.10-5.12 and also refer to information in Appendix H. Although this method was applied with some level of confidence to estimate the air only pressure drop it was also necessary to verify these findings with theoretical values. Although Williams (2008) argues accuracy of the air only pressure drop should not really be of much concern as the air only component is very low compared to the total conveying, typically 10%, however as Pan (1992) also indicated this must not be ignored as it can have substantial impact on the overall results. Also due to instrument irregularities as noted in section (5.3.1), and with air only pressure drop models are widely available and there is confidence in their accuracy, this is the approach also adopted to estimate the final air only pressure drop.

The air-only pressure was also calculated using theoretical models as discussed in Chapter 2, section 2.5.1 where Equation 2.12 is used to predict the pressure drop due to air only. This computation requires knowledge of air density and velocity, and these are averaged values due to the expansion of air. To illustrate computation of the air-only pressure, Unit 1 period 1 line 1 is again selected with pipe inlet and outlet conditions without ash. As such, inlet temperature is air only, $T = 30℃$ and $P = 25$ kPa. Similarly, outlet conditions were determined without ash, with $T = 30℃$ and $P = -4$ kPa as the silo extraction fan continued to run to maintain the silo under vacuum. The average air density and velocities can be computed as:

$$\rho_{ave} = \frac{\bar{P}}{R\bar{T}} = \frac{(25+89.6/89.6-4)/2}{0.287\times303} = 1.15 \text{ kg/m}^3$$

$$v_{ave} = \frac{4m_a R\bar{T}}{\bar{P}\pi D^2} = \frac{4\times1.42\times0.287\times303}{100.1\times3.14\times0.265^2} = 22.83 \text{ m/s}$$

Using average values, the Reynolds number is then computed as,

$$Re = \frac{\rho V d}{\mu} = \frac{1.15\times22.83\times0.265}{1.86\times10^{-5}} = 374056$$

Air friction factor is computed using suggestions from Mills (2008),

$$\lambda_a = \frac{1.325}{\ln\left(\frac{5.74}{Re_a{}^{0.9}}\right)^2} = 0.014$$

The air- only pressure drop due to the horizontal length can then be computed by using the modified Equation 2.3 for air only as,

$$\therefore P_{aH} = \frac{(4\lambda_a)\rho_a v_a{}^2 L}{2D} = \frac{4\times0.014\times1.15\times22.83^2\times551}{2\times0.265} = 34.39 \text{ kPa}$$

Finally, the air-only pressure drop due to the bend is calculated, and the model proposed by Mills (2016) is used here for its simplicity with a bend $k$ factor of 8.4.

$$P_{aB} = k\frac{\rho V^2}{2} = 8.4 \times \frac{1.15 \times 22.83^2}{2} = 2.52$$

The effect of gravity as the air rises along the vertical sections is not considered (Pan, 1992). As such, the total air pressure drop is computed by adding the bend and horizontal section pressure drops.

$$P_A = P_{aH} + P_{aB} = 36.91 \text{ kPa}$$

The complete set of results is indicated in Table 7.4, 7.5 and 7.6 for Unit 1, 2 and 3 for all data points.

### 7.3.5 Solids-only pressure drop

Once the air-only pressure value has been estimated, a modified Equation 2.11 can be used to establish the solids-only pressure drop at the horizontal pipe section; this is re-written as Equation 7.1,

$$\Delta P_{Hs} = \Delta P_T - \Delta P_A - \Delta P_B - \Delta P_V \qquad (7.1)$$

In above Equation, $\Delta P_{Hs}$ is the solids-only horizontal pressure drop, $\Delta P_T$ is the total conveying pressure and $\Delta P_A$ is the air-only pressure drop as described in section 7.3.4. The solids conveying pressure drops for bend and vertical sections, $\Delta P_B$ and $\Delta P_V$ are as discussed in sections 7.3.2 and 7.3.3 respectively.

To illustrate use of Equation 7.1 to obtain solids-only horizontal pressure, Unit 3 period 1 line 1 will be used as in sections 7.3.2 and 7.3.3. This particular period had a conveying pressure of 164 kPa, refer to Table 7.3.

$$\therefore \Delta P_{Hs} = \Delta P_T - \Delta P_V - \Delta P_B - \Delta P_A = 164 - 5.7 - 12.28 - 36.91 = 109.1 \text{ kPa}$$

The above process was followed to calculate the horizontal solids-only pressure drop as indicated in section 7.3.2, 7.3.4 and 7.3.5 for all recorded data periods and these results are as indicated in the consolidated Tables 7.4 to 7.6 for Units 1, 2 and 3 respectively.

**Table 7.4** Pressure drops for Unit 1

| **Conveying line** | **Period** | **Conveying pressure drop** (kPa) | **Bend pressure drop** (kPa) | **Vertical pressure drop** (kPa) | **Air only pressure drop** (kPa) | **Solids only horizontal pressure drop** (kPa) |
|---|---|---|---|---|---|---|
| Line 1 | Period 1 | 217.00 | 11.51 | 7.30 | 18.90 | 179.28 |
| | Period 2 | 161.00 | 8.97 | 5.65 | 17.77 | 128.61 |
| | Period 3 | 169.00 | 11.66 | 3.97 | 30.51 | 122.86 |
| | Period 4 | 151.00 | 12.05 | 4.11 | 30.00 | 104.84 |
| | Period 5 | 156.00 | 10.01 | 5.34 | 20.49 | 120.16 |
| | Period 6 | 169.00 | 10.23 | 6.85 | 17.15 | 134.76 |
| | Period 7 | 169.00 | 19.87 | 3.23 | 58.92 | 86.98 |
| | Period 8 | 169.00 | 9.01 | 5.75 | 17.73 | 136.51 |
| Line 2 | Period 1 | 184.00 | 11.10 | 6.71 | 20.89 | 145.30 |
| | Period 2 | 140.00 | 8.80 | 5.31 | 19.59 | 106.30 |
| | Period 3 | 138.00 | 11.32 | 3.63 | 33.72 | 89.33 |
| | Period 4 | 133.00 | 11.86 | 3.90 | 33.01 | 84.23 |
| | Period 5 | 124.00 | 9.74 | 4.85 | 22.67 | 86.73 |
| | Period 6 | 150.00 | 10.04 | 6.49 | 18.89 | 114.58 |
| | Period 7 | 150.00 | 19.50 | 3.06 | 64.80 | 62.64 |
| | Period 8 | 150.00 | 8.85 | 5.45 | 19.52 | 116.19 |

**Table 7.5** Pressure drops for Unit 2

| **Conveying line** | **Period** | **Conveying pressure drop** (kPa) | **Bend pressure drop** (kPa) | **Vertical pressure drop** (kPa) | **Air only pressure drop** (kPa) | **Solids only horizontal pressure drop** (kPa) |
|---|---|---|---|---|---|---|
| Line 1 | Period 1 | 131.00 | 7.92 | 9.12 | 13.25 | 100.71 |
| | Period 2 | 165.00 | 7.63 | 10.37 | 12.25 | 134.75 |
| | Period 3 | 113.00 | 6.91 | 10.03 | 10.42 | 85.64 |
| | Period 4 | 166.00 | 9.19 | 11.15 | 13.60 | 132.07 |
| | Period 5 | Invalid instrument | N/A | N/A | N/A | N/A |
| | Period 6 | 91.00 | 5.20 | 5.20 | 13.19 | 67.41 |
| | Period 7 | 100.00 | 4.80 | 6.74 | 10.19 | 78.27 |
| Line 2 | Period 1 | 153.00 | 7.97 | 9.74 | 14.02 | 121.27 |
| | Period 2 | 141.00 | 7.56 | 9.68 | 13.16 | 110.60 |
| | Period 3 | 141.00 | 6.93 | 10.94 | 11.00 | 112.13 |
| | Period 4 | 111.00 | 9.08 | 9.45 | 14.76 | 77.71 |
| | Period 5 | 141.00 | 6.67 | 6.78 | 15.85 | 111.70 |
| | Period 6 | 99.00 | 4.88 | 5.01 | 13.36 | 75.75 |
| | Period 7 | 100.00 | 4.80 | 6.74 | 10.86 | 77.60 |

**Table 7.6** Pressure drops for Unit 3

| Conveying line | Period | Conveying pressure drop (kPa) | Bend pressure drop (kPa) | Vertical pressure drop (kPa) | Air only pressure drop (kPa) | Solids only horizontal pressure drop (kPa) |
|---|---|---|---|---|---|---|
| Line 1 | Period 1 | 164.0 | 12.28 | 0.84 | 36.91 | 109.1 |
| | Period 2 | 135.0 | 14.33 | 0.84 | 50.00 | 66.1 |
| | Period 3 | 126.0 | 11.00 | 0.84 | 45.68 | 65.6 |
| | Period 4 | 172.0 | 15.44 | 0.84 | 48.50 | 102.5 |
| | Period 5 | 160.0 | 12.97 | 0.84 | 62.55 | 81.2 |
| | *Period 6* | *64.0* | *12.30* | *0.84* | *85.77* | *-35.7* |
| | Period 7 | 179.0 | 18.94 | 0.84 | 67.62 | 87.7 |
| | Period 8 | 148.0 | 16.11 | 0.84 | 38.56 | 86.1 |
| Line 2 | Period 1 | 181.0 | 12.50 | 0.84 | 39.64 | 122.8 |
| | Period 2 | 156.0 | 14.60 | 0.84 | 53.73 | 82.8 |
| | Period 3 | 145.0 | 11.17 | 0.84 | 48.12 | 81.7 |
| | Period 4 | 100.0 | 14.57 | 0.84 | 52.26 | 28.7 |
| | Period 5 | 129.0 | 12.61 | 0.84 | 65.94 | 47.4 |
| | *Period 6* | *78.0* | *12.27* | *0.84* | *92.05* | *-28.1* |
| | Period 7 | 223.0 | 19.90 | 0.84 | 71.37 | 126.5 |
| | Period 8 | 227.0 | 17.55 | 0.84 | 41.68 | 159.0 |

## 7.4 Solids Friction Factor Estimation

### 7.4.1 Solids friction factor from experimental results

The solids-only horizontal pressure drop allows for a method for estimation of the solids friction factor, and this is done using Equation 2.3 for the horizontal section. This is known as the back calculation method, and making the solids friction factor the subject as indicated in Equation 7.2.

$$\lambda_s = \frac{2P_{Hs}D}{\mu\rho_a {v_a}^2 L} \quad (7.2)$$

To illustrate the use of Equation 7.2, Unit 3 is selected, picking a random data point such as period 1, line 1. To use this data point with Equation 7.2, Tables 3.2, 7.3 and 7.6 are used to obtain the following solids friction factor (refer to Table 7.7):

$$\lambda_s = \frac{2\Delta P_{Hs} D}{\mu \rho_a {v_a}^2 L} = \frac{2\times109.1\times1000\times0.265}{11.4\times1.44\times19.83^2\times551} = 0.016$$

**Table 7.7** Conveying data for Unit 3, period 1, line 1 used to obtain solids friction factor

| Conveying parameter | Symbol | Value | Reference |
|---|---|---|---|
| Solids only pressure (horizontal) | $\Delta P_s$ | 109.1 kPa | Table 7.6 |
| Pipe diameter | $D$ | 265 mm | Table 3.2 |
| Solids loading ratio | $\mu$ | 11.4 | Table 7.3 |
| Average air density | $\rho_a$ | 1.44 $\text{kgm}^{-3}$ | Table 7.3 |
| Average air velocity | $v_a$ | 19.83 m/s | Table 7.3 |
| Horizontal conveying length | $L$ | 551 m | Table 3.2 |

The same process was followed to obtain the solids friction factors for the rest of the data, and a full set of results is given in Table 7.8.

**Table 7.8** Solids friction factor for horizontal pipe sections based on experimental conveying pressure for Unit 1, 2 and 3

| Conveying line | Period | Unit 1 solids friction factor (−) | Unit 2 solids friction factor (−) | Unit 3 solids friction factor (−) |
|---|---|---|---|---|
| Line 1 | Period 1 | 0.041 | 0.019 | 0.016 |
| | Period 2 | 0.037 | 0.025 | 0.009 |
| | Period 3 | 0.028 | 0.019 | 0.011 |
| | Period 4 | 0.022 | 0.021 | 0.012 |
| | Period 5 | 0.030 | Invalid | 0.012 |
| | *Period 6* | 0.033 | 0.021 | *0.006* |
| | Period 7 | 0.012 | 0.026 | 0.009 |
| | Period 8 | 0.039 | N/A | 0.010 |

| **Conveying line** | **Period** | **Unit 1 solids friction factor (−)** | **Unit 2 solids friction factor (−)** | **Unit 3 solids friction factor (−)** |
|---|---|---|---|---|
| Line 2 | Period 1 | 0.030 | 0.021 | 0.017 |
| | Period 2 | 0.028 | 0.020 | 0.010 |
| | Period 3 | 0.018 | 0.022 | 0.013 |
| | Period 4 | 0.016 | 0.012 | *0.003* |
| | Period 5 | 0.020 | 0.023 | *0.007* |
| | Period 6 | 0.023 | 0.002 | 0.004 |
| | *Period 7* | *0.007* | 0.024 | 0.011 |
| | Period 8 | 0.026 | N/A | 0.015 |

Table 7.8 shows the solids friction factor values determined from experimental values. It is necessary to compare these values with solids friction factors based on expectations from models proposed in the literature. Although there are a number of such models, only two models were selected for comparison of solids friction factors with experimental findings, namely the Weber model as modified by Jones and Williams (2003) for fluidized materials and a power law method as used by Behera, *et al* (2015). These models will be discussed as the 'Jones and Williams model' and the 'power law model' for identification in this report. These models were used for fly ash in dense phase systems and were derived using the power laws, in this report they are just differentiated using their authors.

### 7.4.2 Jones and Williams (2003)

To illustrate the use of this model, Unit 2, period 1, line 1 is selected. Table 7.2 shows average velocity and solids loading ratio of $v_a = 12.81\ \mathrm{m/s}$ and $\mu = m^* = 20.1$. The average (or mean) Froude number is calculated using average velocity, shown as:

$$F_r = \frac{v_a}{\sqrt{\mathrm{gD}}} = \frac{12.81}{\sqrt{9.81 \times 0.265}} = 7.94$$

Using Table 7.2, the solids friction factor can be computed using the Jones and Williams model as shown in Equation 7.3,

$$\lambda_s = \frac{83}{m^{*0.9}\mathrm{Fr}^2} \tag{7.3}$$

$$\therefore \lambda_s = \frac{83}{20.1^{0.9} \times 7.94^2} = 0.088$$

It is also necessary to review the difference between the prediction of this model and the experimental finding. The difference in percentage from the Jones and Williams model is calculated as $(\text{model} - \text{experimental})/(\text{model}) \times 100$

$$\therefore \%\Delta = \frac{0.088 - 0.019}{0.088} \times 100 = 78\%$$

The above process is repeated for all the average Froude numbers and solids friction factors for Units 1, 2 and 3 as indicated in Table 7.9. The differences from the experimental findings to the Jones and Williams findings are also indicated in Table 7.9.

**Table 7.9** Solids friction factors using the Jones and Williams (2003) model for Units 1, 2 and 3

| | | **Unit 1** | | | **Unit 2** | | | **Unit 3** | | |
|---|---|---|---|---|---|---|---|---|---|---|
| **Conveying line** | **Period** | **Froude Number** (-) | **Solids Friction (J&W)** (-) | %Δ | **Froude Number** (-) | **Solids Friction (J&W)** (-) | %Δ | **Froude Number** (-) | **Solids Friction (J&W)** (-) | %Δ |
| Line 1 | Period 1 | 11.3 | 0.065 | 38 | 7.94 | 0.088 | 78 | 12.3 | 0.061 | 74 |
| | Period 2 | 11.5 | 0.071 | 48 | 7.32 | 0.102 | 75 | 14.8 | 0.048 | 82 |
| | Period 3 | 15.3 | 0.056 | 50 | 7.10 | 0.097 | 80 | 14.2 | 0.061 | 82 |
| | Period 4 | 15.4 | 0.051 | 56 | 7.75 | 0.085 | 76 | 14.1 | 0.050 | 76 |
| | Period 5 | 12.5 | 0.062 | 51 | 6.95 | 0.155 | Invalid | 16.3 | 0.057 | 79 |
| | Period 6 | 11.2 | 0.064 | 48 | 8.42 | 0.116 | 82 | 21.9 | 0.045 | 113 |
| | Period 7 | 21.9 | 0.033 | 65 | 7.15 | 0.131 | 80 | 16.7 | 0.041 | 79 |
| | Period 8 | 11.4 | 0.072 | 46 | N/A | N/A | N/A | 12.7 | 0.045 | 79 |
| Line 2 | Period 1 | 11.7 | 0.062 | 51 | 7.71 | 0.094 | 78.09 | 12.1 | 0.063 | 73 |
| | Period 2 | 11.8 | 0.067 | 59 | 7.54 | 0.096 | 78 | 14.5 | 0.050 | 81 |
| | Period 3 | 15.9 | 0.052 | 64 | 6.81 | 0.105 | 79 | 13.9 | 0.064 | 80 |
| | Period 4 | 15.8 | 0.048 | 67 | 8.37 | 0.073 | 79 | 15.2 | 0.042 | 92 |
| | Period 5 | 13.0 | 0.057 | 65 | 8.38 | 0.107 | 83 | 16.8 | 0.054 | 87 |
| | Period 6 | 11.4 | 0.061 | 58 | 8.29 | 0.127 | 78 | 21.3 | 0.048 | 109 |
| | Period 7 | 22.4 | 0.031 | 77 | 7.15 | 0.131 | 99 | 16.2 | 0.044 | 75 |
| | Period 8 | 11.6 | 0.069 | 56 | N/A | N/A | N/A | 12.0 | 0.051 | 70 |
| **Average (%Δ)** | | | | 56 | | | 79 | | | 80 |

The findings in Table 7.9 are included graphically to show the variance from the Jones and Williams model (J&W) to experimental findings for both lines 1 and 2 for Unit 1, 2 and 3. These figures plotting the solids friction factor as a function of Froude number have been included in figures 7.1 to 7.3.

### 7.4.3 Friction factor model as proposed by Behera *et al* (2015)

The solids friction factor model proposed by Behera et al. (2015) is discussed in Chapter 2 and Equation 2.17 is rewritten here as Equation (7.4).

$$\lambda_s = \frac{364.4}{\mathrm{m}^{*1.29}\mathrm{Fr}^{2.36}} \tag{7.4}$$

This model was also obtained from conveying tests using fly ash and the insight gained in developing this model allowed the author to improve this model as explained in section 7.4.4. To illustrate computation of solids friction factor using Equation 7.4; Unit 2 conveying line 1, period 1 is selected, similar to the data ($m^* = 20.1, Fr = 7.94$) selected for use of the Jones and Williams model in 7.4.2.

$$\lambda_s = \frac{364.4}{m^{*1.29}Fr^{2.36}} = \frac{364.4}{20.1^{1.29}7.94^{2.36}} = 0.057$$

The percentage difference was calculated as: $(\mathrm{model} - \mathrm{experimental})/(\mathrm{model}) \times 100$

$$\therefore \%\Delta = \frac{0.057 - 0.019}{0.057} \times 100 = 67\%$$

As such, even observation only with Unit 2 findings for conveying pipe line 1, it can be observed that the model by Behera *et al* represents a better relationship to the actual experimental conditions (67% difference) when compared with the Jones and Williams model (78% difference). This is also visible when observing the gap that exists between the Behera *et al* model results and the experimental results in Figures 7.1 to 7.3. Of the two models, the Behera *et al* model is less conservative compared to the Jones and Williams model for the specific bulk solids data and facilities as in this research. The results for the complete data sets for Units 1, 2 and 3 are as indicated in Table 7.10 with the percentages differences to the experimental results also indicated.

**Table 7.10** Calculated solids friction factors using the Behera model for Units 1, 2 and 3

| | | Unit 1 | | Unit 2 | | Unit 3 | |
|---|---|---|---|---|---|---|---|
| **Conveying line** | **Period** | **Solids Friction (Behera *et al*) (-)** | %Δ | **Solids Friction (Behera *et al*) (-)** | %Δ | **Solids Friction (Behera *et al*) (-)** | %Δ |
| Line 1 | Period 1 | 0.044 | 8 | 0.057 | 67 | 0.042 | 62 |
| | Period 2 | 0.050 | 26 | 0.067 | 62 | 0.033 | 74 |
| | Period 3 | 0.041 | 32 | 0.061 | 69 | 0.045 | 75 |
| | Period 4 | 0.036 | 38 | 0.053 | 61 | 0.033 | 64 |
| | Period 5 | 0.043 | 30 | *Invalid* | - | 0.044 | 73 |
| | Period 6 | 0.043 | 22 | 0.087 | 75 | 0.036 | 116 |
| | Period 7 | 0.023 | 50 | 0.095 | 73 | 0.028 | 69 |
| | Period 8 | 0.051 | 24 | N/A | N/A | 0.028 | 65 |
| Line 2 | Period 1 | 0.041 | 26 | 0.061 | 66 | 0.044 | 62 |
| | Period 2 | 0.047 | 41 | 0.062 | 68 | 0.034 | 72 |
| | Period 3 | 0.037 | 51 | 0.068 | 67 | 0.047 | 73 |
| | Period 4 | 0.034 | 53 | 0.044 | 72 | 0.028 | 88 |
| | Period 5 | 0.039 | 49 | 0.077 | 70 | 0.041 | 83 |
| | Period 6 | 0.040 | 36 | 0.090 | 76 | 0.039 | 111 |
| | Period 7 | 0.022 | 66 | 0.095 | 75 | 0.030 | 63 |
| | Period 8 | 0.048 | 38 | N/A | N/A | 0.032 | 52 |
| **Average (%Δ)** | | | 37 | | 69 | | 72 |

Integrated graphs plotting the solids friction factor as a function of solids loading ratio are shown in figures 7.1 to 7.3. These figures represent findings for Units 1, 2 and 3 for both line 1 and line 2 respectively.

### 7.4.4 New model based on the experimental findings using a power function

As discussed in Chapter 2, section 2.5.2, one is able to propose a new friction factor model by use of the power law of Equation 2.16 by using specific data obtained from these experiments. This Equation is rewritten here as 7.5, with $(\rho_s/\rho_a)$ assumed to be a unity (1) as the value of its power function is approximately zero ($c = 0.01$) (Williams, 2008).

$$\lambda_s = C(m^*)^a(Fr_a)^b \qquad (7.5)$$

Equation 7.5 is solved using a 3x3 matrix to solve for power functions *a*, *b* and *C* using the data from the experiments: solids loading ratio (Tables, 7.1; 7.2 and 7.3), solids friction factors (Table 7.8) and Froude numbers (Table 7.9 (see Appendix K). In order to complete Equation 7.5, it is necessary to select three experimental periods of data. To illustrate use of Equation 7.5, Unit 1 conveying line 1 data is selected, with periods 1, 5 and 7 selected from Table 7.9. These periods were selected as their solids friction factor range (0.012 to 0.041) included values from all other periods and as such it is expected that the solution found would cover all the periods for Unit 1.

**Table 7.11** Unit 1 data for line 1 period 1, 5 and 7 selected for power law factors determination

| **Conveying parameter** | **Symbol** | **Value** (-) | **Reference Table** |
|---|---|---|---|
| Solids friction factor (period 1) | $\lambda_s$ | 0.041 | Table 7.8 |
| Solids friction factor (period 5) | $\lambda_s$ | 0.030 | Table 7.8 |
| Solids friction factor (period 7) | $\lambda_s$ | 0.012 | Table 7.8 |
| Solids loading ratio (period 1) | $\mu = m^*$ | 12.7 | Table 7.1 |
| Solids loading ratio (period 5) | $\mu = m^*$ | 10.9 | Table 7.1 |
| Solids loading ratio (period 7) | $\mu = m^*$ | 6.4 | Table 7.1 |
| Average Froude numbers (period 1) | $Fr_a$ | 11.3 | Table 7.9 |
| Average Froude numbers (period 5) | $Fr_a$ | 12.5 | Table 7.9 |
| Average Froude numbers (period 7) | $Fr_a$ | 21.9 | Table 7.9 |

Substituting the conveying parameters in Table 7.10 into Equation 7.5, three equations are developed that can be solved for the unknowns. Using Microsoft Excel to solve for the three unknowns in a 3x3 matrix, the unknowns were solved as $C = 1985$, $a = 1.40$, $b = 3.07$. The new model based on the experimental results for Unit 1 is described by Equation 7.6 (Refer to Appendix K on how Excel was used to solve for this 3x3 matrix).

$$\lambda_s = \frac{1985}{m^{*1.40} Fr^{3.07}} \qquad (7.6)$$

The above process was also conducted for Unit 2 and Unit 3, with Equations 7.7 and 7.8 developed from using data for Unit 2 and Unit 3; refer to Appendix K for Excel computation of these equations and the data periods selected.

$$\lambda_s = \frac{214}{m^{*1.08} Fr^{3.02}} \tag{7.7}$$

$$\lambda_s = \frac{22}{m^{*0.91} Fr^{2.08}} \tag{7.8}$$

Equations 7.6, 7.7 and 7.8 represent best approximations to experimental data for the solids friction factor for Units 1, 2 and 3; it is also necessary to check how these differ from the actual individual solids friction factors. The difference or variance of these models to actual data is included in Table 7.11. The percentage difference is computed in the same manner as discussed in 7.4.2.

These results have been integrated in Figures 7.1 to 7.3 with findings obtained using proposed models by Jones and Williams (2003) and Behera et al (2015).

**Table 7.12** Variance of the solids friction factor using new models to experimental findings for Unit 1, 2 and 3

| | | **Unit 1** | | | **Unit 2** | | | **Unit 3** | | |
|---|---|---|---|---|---|---|---|---|---|---|
| **Conveying line** | **Period** | **Solids Friction (Experimental) (-)** | **Solids Friction [New model Equation 7.6] (-)** | %Δ | **Solids Friction (Experimental) (-)** | **Solids Friction [New model Equation 7.7] (-)** | %Δ | **Solids Friction (Experimental) (-)** | **Solids Friction [New model Equation 7.8] (-)** | %Δ |
| Line 1 | Period 1 | 0.041 | 0.033 | 24 | 0.019 | 0.016 | 20 | 0.016 | 0.013 | 24 |
| | Period 2 | 0.037 | 0.037 | 1 | 0.025 | 0.020 | 28 | 0.009 | 0.010 | 16 |
| | Period 3 | 0.028 | 0.026 | 8 | 0.019 | 0.019 | 0 | 0.011 | 0.013 | 13 |
| | Period 4 | 0.022 | 0.022 | 0 | 0.021 | 0.015 | 33 | 0.012 | 0.011 | 16 |
| | Period 5 | 0.030 | 0.030 | 0 | *Invalid* | 0.034 | N/A | 0.012 | 0.012 | 0 |
| | Period 6 | 0.033 | 0.032 | 5 | 0.021 | 0.021 | 0 | 0.006 | 0.009 | 36 |
| | Period 7 | 0.012 | 0.012 | 0 | 0.026 | 0.027 | 4 | 0.009 | 0.009 | 0 |
| | Period 8 | 0.039 | 0.038 | 2 | - | - | - | 0.010 | 0.010 | 0 |
| Line 2 | Period 1 | 0.030 | 0.030 | 1 | 0.021 | 0.017 | 18 | 0.017 | 0.014 | 24 |
| | Period 2 | 0.028 | 0.034 | 19 | 0.020 | 0.018 | 11 | 0.010 | 0.011 | 8 |
| | Period 3 | 0.018 | 0.023 | 20 | 0.022 | 0.022 | 2 | 0.013 | 0.014 | 5 |
| | Period 4 | 0.016 | 0.021 | 22 | 0.012 | 0.012 | 0 | 0.003 | 0.009 | 62 |
| | Period 5 | 0.020 | 0.027 | 26 | 0.023 | 0.019 | 21 | 0.007 | 0.011 | 40 |
| | Period 6 | 0.026 | 0.030 | 13 | 0.022 | 0.022 | 4 | 0.004 | 0.010 | 55 |
| | Period 7 | 0.007 | 0.011 | 32 | 0.024 | 0.027 | 12 | 0.011 | 0.009 | 20 |
| | Period 8 | 0.030 | 0.036 | 16 | - | - | - | 0.015 | 0.011 | 40 |
| **Average (%Δ)** | | | | 12 | | | 12 | | | 22 |

## 7.5 Integrated Results for Solids Friction Factor

Results for solids friction factors from the models as discussed in sections 7.4.1 to 7.4.4 have been integrated graphically into Figures 7.1, 7.2 and 7.3 for Units 1, 2 and 3 respectively, with experimental results also.

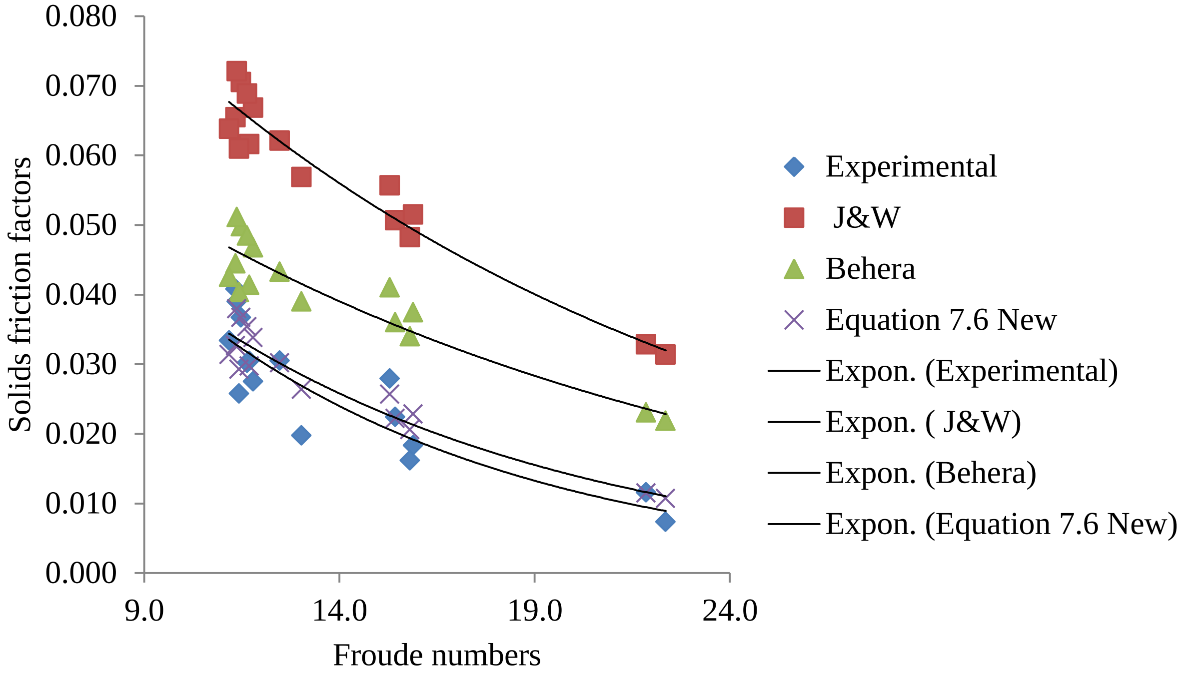


**Figure 7.1** Integrated results for solids friction factors for Unit 1 plotted against the Froude numbers

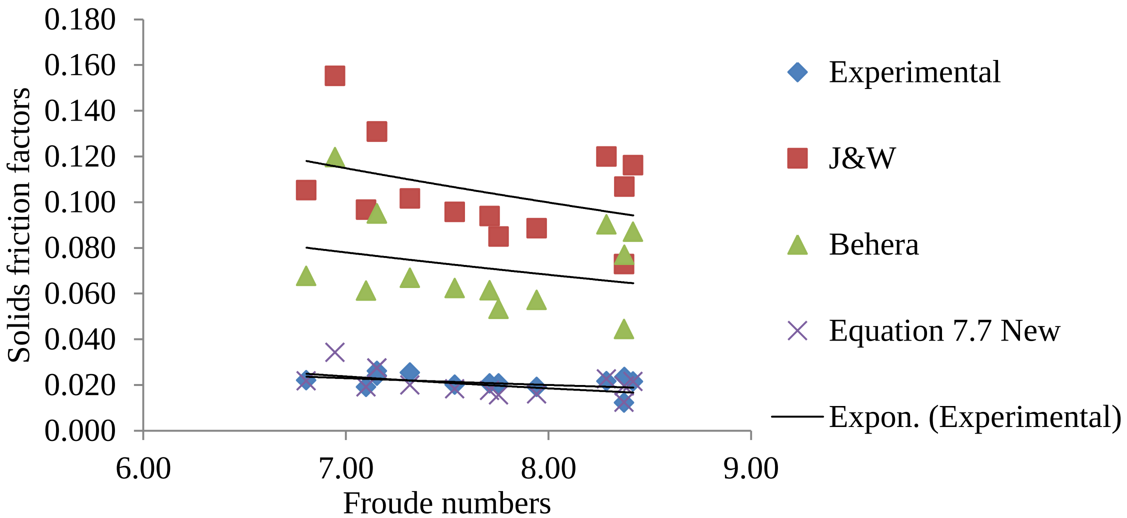


**Figure 7.2** Integrated results for solids friction factors for Unit 2 plotted against the Froude numbers

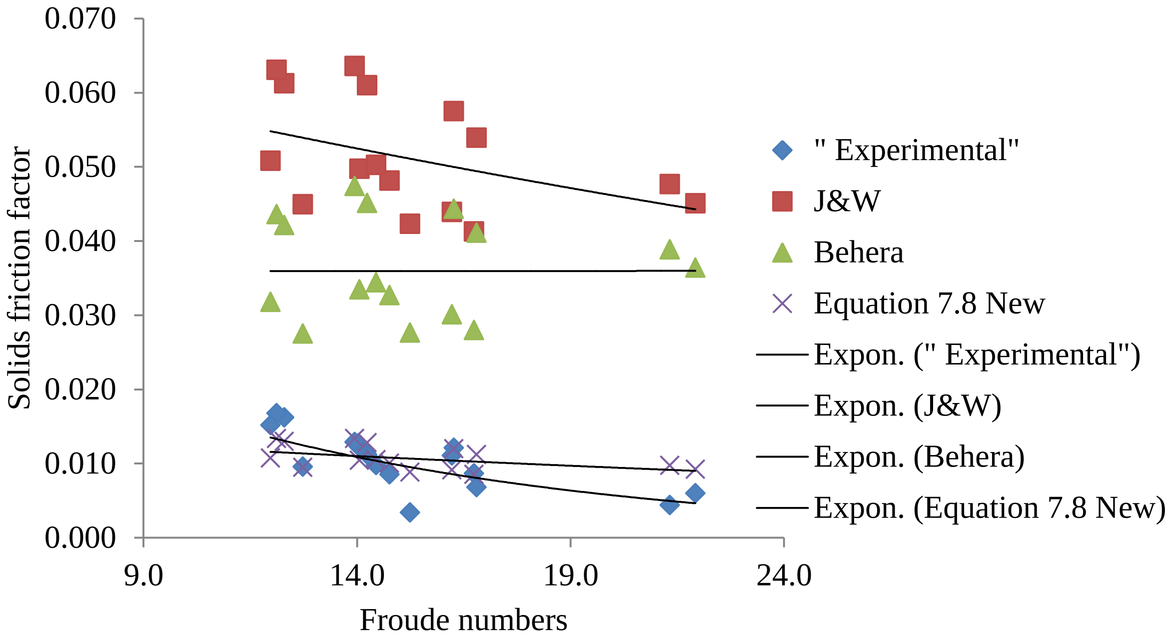


**Figure 7.3** Integrated results for solids friction factors for Unit 3 plotted against the Froude numbers

Figures 7.1 to 7.3 indicate that the Equations proposed in section 7.4.4 proved to have a better prediction of the solids friction factor to experimental results when compared to the Behera *et al* and the Jones and Williams model. This was to be expected as these models were derived directly from experimental results. It was also necessary to integrate the results in tables 7.8, 7.9, 7.10 and 7.12 for solids friction factors in order to have one proposed model that best represents results for all three Units with the lowest error in prediction. Figure 7.4 indicates the integrated solids friction factors obtained from the experimental results.

Table 7.13 indicates results for how these proposed models predict results for solids friction factors for Unit 1, 2 and 3. The models vary when predicting solids friction factors for Units 1, 2 and 3 with Equation 7.6 the best equation with the lowest average error of 43% across all units. The next proposed model with better prediction was Equation 7.8 with a 48% error across the Units. The Behera et al model, Jones and Williams and model proposed by Equation 7.7 provided errors in estimating the solids friction factors in the order of 60%, 72% and 126% respectively.

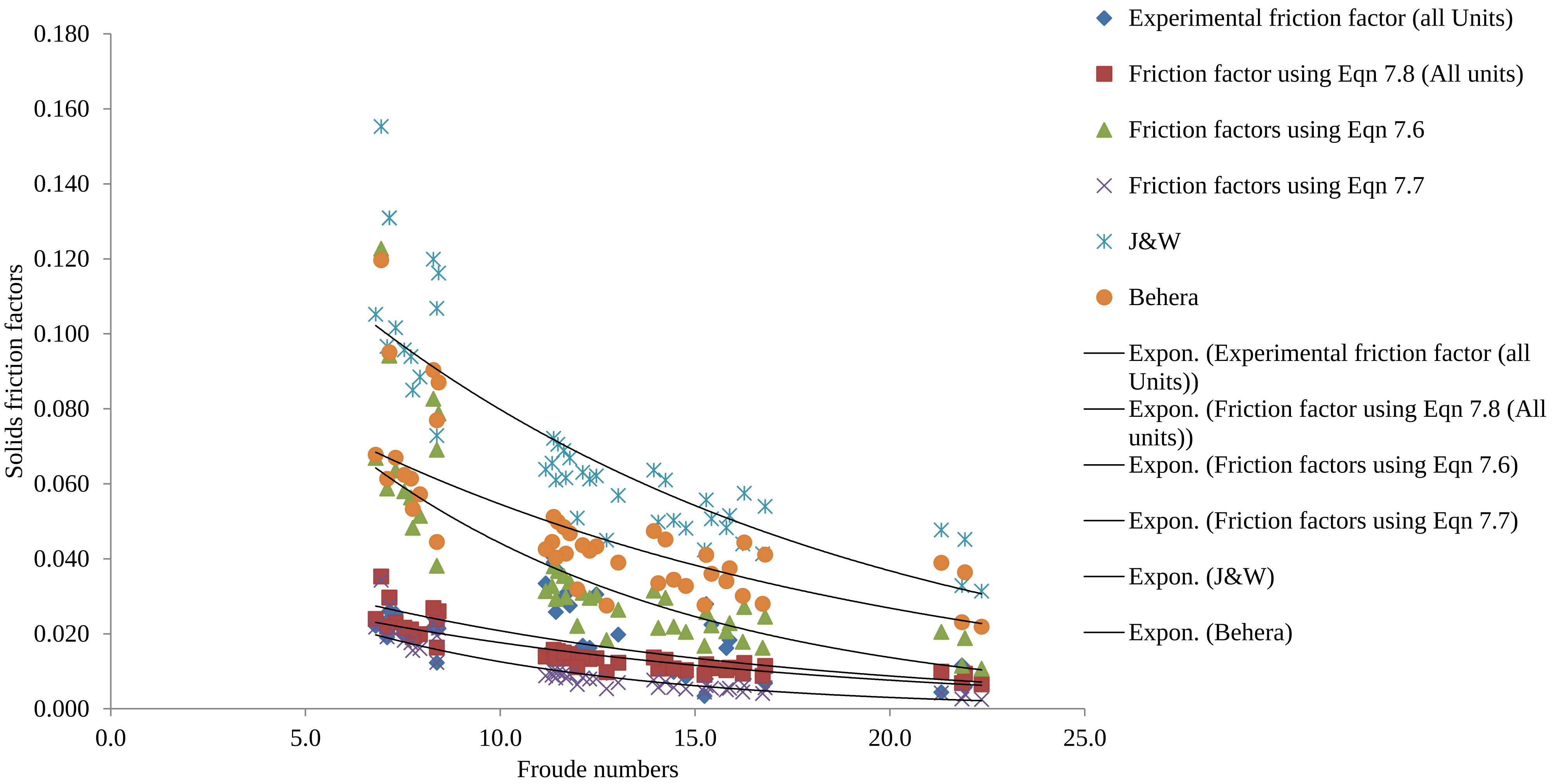


**Figure 7.4** Integrated results for solids friction factors using proposed models for Units 1, 2 and 3 with the experimental results

**Table 7.13** Consolidated results for predicted solids friction factors for Units 1, 2 and 3 using the Jones and Williams (2003), Behera et al (2016) and Equations 7.6, 7.7 and 7.8 with average errors also indicated

| **Line** | **Conveying pipe** | **Experimental** | **Jones and Williams (2003)** | %Δ | **Behera *et al* (2015)** | %Δ | **Solids friction factor using Equation 7.6** | %Δ | **Solids friction factor using Equation 7.7** | %Δ | **Solids friction factor using Equation 7.8** | %Δ |
|---|---|---|---|---|---|---|---|---|---|---|---|---|
| Unit 1 | Line1 | 0.041 | 0.065 | 38 | 0.044 | 8 | 0.033 | 25 | 0.009 | 354 | 0.014 | 185 |
| | | 0.037 | 0.071 | 48 | 0.050 | 26 | 0.037 | 0 | 0.010 | 277 | 0.015 | 139 |
| | | 0.028 | 0.056 | 50 | 0.041 | 32 | 0.026 | 9 | 0.006 | 355 | 0.012 | 135 |
| | | 0.022 | 0.051 | 56 | 0.036 | 38 | 0.022 | 1 | 0.005 | 311 | 0.011 | 107 |
| | | 0.030 | 0.062 | 51 | 0.043 | 30 | 0.030 | 1 | 0.008 | 284 | 0.013 | 127 |
| | | 0.033 | 0.064 | 48 | 0.043 | 22 | 0.031 | 6 | 0.009 | 280 | 0.014 | 140 |
| | | 0.012 | 0.033 | 65 | 0.023 | 50 | 0.011 | 1 | 0.003 | 343 | 0.007 | 70 |
| | | 0.039 | 0.072 | 46 | 0.051 | 24 | 0.038 | 3 | 0.010 | 288 | 0.016 | 148 |
| | Line 2 | 0.030 | 0.062 | 51 | 0.041 | 26 | 0.030 | 2 | 0.008 | 272 | 0.013 | 127 |
| | | 0.028 | 0.067 | 59 | 0.047 | 41 | 0.034 | 19 | 0.009 | 206 | 0.015 | 89 |
| | | 0.018 | 0.052 | 64 | 0.037 | 51 | 0.023 | 20 | 0.005 | 235 | 0.011 | 67 |
| | | 0.016 | 0.048 | 67 | 0.034 | 53 | 0.021 | 22 | 0.005 | 219 | 0.010 | 57 |
| | | 0.020 | 0.057 | 65 | 0.039 | 49 | 0.026 | 25 | 0.007 | 184 | 0.012 | 61 |
| | | 0.026 | 0.061 | 58 | 0.040 | 36 | 0.029 | 12 | 0.008 | 214 | 0.013 | 94 |
| | | 0.007 | 0.031 | 77 | 0.022 | 66 | 0.011 | 31 | 0.002 | 201 | 0.006 | 13 |
| | | 0.030 | 0.069 | 56 | 0.048 | 38 | 0.035 | 15 | 0.009 | 221 | 0.015 | 101 |
| Unit 2 | Line1 | 0.019 | 0.088 | 78 | 0.057 | 67 | 0.051 | 63 | 0.016 | 19 | 0.020 | 4 |
| | | 0.025 | 0.102 | 75 | 0.067 | 62 | 0.064 | 60 | 0.020 | 27 | 0.023 | 10 |
| | | 0.019 | 0.097 | 80 | 0.061 | 69 | 0.059 | 68 | 0.019 | 1 | 0.022 | 13 |
| | | 0.021 | 0.085 | 76 | 0.053 | 61 | 0.048 | 57 | 0.016 | 32 | 0.019 | 8 |
| | | 0.021 | 0.116 | 82 | 0.087 | 75 | 0.079 | 73 | 0.021 | 0 | 0.026 | 18 |
| | | 0.026 | 0.131 | 80 | 0.095 | 73 | 0.094 | 72 | 0.027 | 5 | 0.030 | 12 |

| Line | Conveying pipe | Experimental | Jones and Williams (2003) | %Δ | Behera *et al* (2015) | %Δ | Solids friction factor using Equation 7.6 | %Δ | Solids friction factor using Equation 7.7 | %Δ | Solids friction factor using Equation 7.8 | %Δ |
|---|---|---|---|---|---|---|---|---|---|---|---|---|
| Unit 2 | Line 2 | 0.021 | 0.094 | 78 | 0.061 | 66 | 0.056 | 63 | 0.018 | 17 | 0.021 | 3 |
| | | 0.020 | 0.096 | 79 | 0.062 | 68 | 0.058 | 65 | 0.018 | 10 | 0.022 | 7 |
| | | 0.022 | 0.105 | 79 | 0.068 | 67 | 0.067 | 67 | 0.022 | 2 | 0.024 | 8 |
| | | 0.012 | 0.073 | 83 | 0.044 | 72 | 0.038 | 68 | 0.012 | 1 | 0.016 | 25 |
| | | 0.023 | 0.107 | 78 | 0.077 | 70 | 0.069 | 66 | 0.019 | 20 | 0.024 | 2 |
| | | 0.022 | 0.120 | 82 | 0.090 | 76 | 0.083 | 74 | 0.023 | 4 | 0.027 | 19 |
| | | 0.024 | 0.131 | 82 | 0.095 | 75 | 0.094 | 75 | 0.027 | 13 | 0.030 | 19 |
| Unit 3 | Line1 | 0.016 | 0.061 | 74 | 0.042 | 62 | 0.030 | 45 | 0.008 | 106 | 0.013 | 22 |
| | | 0.009 | 0.048 | 82 | 0.033 | 74 | 0.020 | 58 | 0.005 | 62 | 0.010 | 17 |
| | | 0.011 | 0.061 | 82 | 0.045 | 75 | 0.030 | 62 | 0.007 | 57 | 0.013 | 14 |
| | | 0.012 | 0.050 | 76 | 0.033 | 64 | 0.022 | 43 | 0.006 | 116 | 0.011 | 14 |
| | | 0.012 | 0.057 | 79 | 0.044 | 73 | 0.027 | 55 | 0.006 | 97 | 0.012 | 1 |
| | | 0.006 | 0.045 | 87 | 0.036 | 84 | 0.019 | 68 | 0.004 | 56 | 0.009 | 36 |
| | | 0.009 | 0.041 | 79 | 0.028 | 69 | 0.016 | 47 | 0.004 | 113 | 0.009 | 1 |
| | | 0.010 | 0.045 | 79 | 0.028 | 65 | 0.018 | 48 | 0.005 | 80 | 0.010 | 2 |
| | Line 2 | 0.017 | 0.063 | 73 | 0.044 | 62 | 0.031 | 46 | 0.008 | 104 | 0.014 | 23 |
| | | 0.010 | 0.050 | 81 | 0.034 | 72 | 0.022 | 55 | 0.006 | 74 | 0.011 | 9 |
| | | 0.013 | 0.064 | 80 | 0.047 | 73 | 0.031 | 59 | 0.008 | 69 | 0.014 | 6 |
| | | 0.003 | 0.042 | 92 | 0.028 | 88 | 0.017 | 80 | 0.004 | 24 | 0.009 | 63 |
| | | 0.007 | 0.054 | 87 | 0.041 | 83 | 0.025 | 72 | 0.006 | 22 | 0.011 | 40 |
| | | 0.004 | 0.048 | 91 | 0.039 | 89 | 0.020 | 79 | 0.004 | 6 | 0.010 | 56 |
| | | 0.011 | 0.044 | 75 | 0.030 | 63 | 0.018 | 38 | 0.004 | 149 | 0.009 | 19 |
| | | 0.015 | 0.051 | 70 | 0.032 | 52 | 0.022 | 31 | 0.006 | 137 | 0.011 | 37 |
| **Average deviations from experimental (%Δ)** | | | | 72 | | 60 | | 43 | | 126 | | 48 |

## 7.6 Pressure Drop Prediction for the Furthest Unit

The proposed models discussed in section 7.4.1 to 7.4.4 are used here to predict the conveying pressure drop for the furthest Unit, which is still under construction. Based on results as shown in Figure 7.4 and Table 7.13, it is expected that Equations 7.6 and 7.8 will provide better approximations for the conveying pressure drop, however it was necessary to compute these pressure using all models for comparison.

Unit 6 is the furthest away from the delivery point and it can be expected to be a system with a higher conveying pressure and higher exit velocities due to the greater conveying length. Although only the horizontal pressure drop is considered in the following calculations, this is sufficiently indicative noting that the horizontal length (931m) is much greater than the vertical distance (39.3) m, refer to Table 3.2.

It is necessary to make few assumptions in order to calculate the other unknown pneumatic conveying characteristics based on performance of Units 1, 2 and 3.

The first assumption to be made is to estimate the solids loading ratio, as proposed by Mills in his pneumatic design flow chart (Mills, 2016). By observing the best performing Unit in terms of solids loading ratio and air consumption, Unit 2; it can be assumed that this type of ash can be conveyed in a dense phase system with a solids loading ratio of 20. With this assumption of the solids loading ratio and a maximum ash flow rate per line that can be expected to be 18.2 kg/s based on full load ash production, the air mass flow rate can be calculated as,

$$m_a = \frac{m_s}{\mu} = \frac{18.2}{20} = 0.91 \text{ kg/s}$$

The inlet and discharge temperature and pressure conditions are based on the conditions for Units 3, 2 and 1 noting that the air mass flow rate is for a single conveying line. The inlet pressure varies, however this be approximated to compute the inlet air density. The average density and velocities were calculated using Equations 2.4 and 2.5. Assuming a conveying pressure of 300 kPa to calculate density and an ash/air mixture at 160 degrees Celsius, based on findings for Units 1, 2 and 3; the air density at the inlet is computed as,

$\rho_i = \frac{P}{RT} = \frac{300+89.6}{0.287 \times 433} = 3.13 \text{ kg/m}^3$

Similarly, the inlet velocity is calculated as,

$v_i = \frac{4 m_a RT}{P \pi D^2} = \frac{4 \times 0.91 \times 0.287 \times 433}{389.6 \times 3.14 \times 0.315^2} = 3.68 \text{ m/s}$

The outlet velocity is calculated in a similar fashion, with changes to outlet conditions where the silo temperature is at 80 degrees Celsius due to the hot ash and vacuum pressure of $-4$ kPa is maintained as in other Units.

$\therefore v_o = \frac{4 m_a RT}{P \pi D^2} = \frac{4 \times 0.91 \times 0.287 \times 353}{85.6 \times 3.14 \times 0.315^2} = 13.83 \text{m/s}$

Similarly, the outlet density, $\rho_o = \frac{P}{RT} = \frac{85.6}{0.287 \times 353} = 0.85 \text{ kg/m}^3$

As suggested by Wypych (1989) the average velocity is used for computation of the Froude number and therefore:

$v_a = \frac{v_o + v_i}{2} = 8.77 \text{ m/s}$ , and $\rho_a = \frac{\rho_o + \rho_i}{2} = 2 \text{ kg/m}^3$

$\therefore Fr_a = \frac{v_a}{\sqrt{\text{gD}}} = \frac{8.77}{\sqrt{9.81 \times 0.315}} = 5$

The above values allow for computation of the solids friction factor and the solids pressure drop across the horizontal length excluding the air component. This is performed using the models discussed in section 7.4.1 to 7.4.4 as,

Jones and Williams, $\lambda_s = \frac{83}{20^{0.9} 5^2} = 0.224$

Behera *et al* power law, $\lambda_s = \frac{364.4}{20^{1.29} 5^{2.36}} = 0.171$

Experimental model defined by Equation 7.6, $\lambda_\text{s} = \frac{1985}{\text{m}^{*1.40} \text{Fr}^{3.07}} = \frac{1985}{20^{1.40} 5^{3.07}} = 0.214$

Experimental model defined by Equation 7.7, $\lambda_s = \frac{214}{m^{*1.08} Fr^{3.02}} = \frac{214}{20^{1.08} 5^{3.02}} = 0.065$

Experimental model defined by Equation 7.8, $\lambda_s = \frac{22}{m^{*0.91} Fr^{2.08}} = \frac{22}{20^{0.91} 5^{2.08}} = 0.051$

The pressure drop is calculated as,

$$P_{Hs(J\&W)} = \lambda_s \frac{\mu \rho_a {v_a}^2 L}{2D} = 0.224 \times \frac{20 \times 2 \times 8.77^2 \times 892}{2 \times 0.315} = 976 \text{ kPa}$$

$$P_{Hs(Behera)} = \lambda_s \frac{\mu \rho_a {v_a}^2 L}{2D} = 0.171 \times \frac{20 \times 2 \times 8.77^2 \times 892}{2 \times 0.315} = 684 \text{ kPa}$$

$$P_{Hs(Eqn\ 7.6)} = \lambda_s \frac{\mu \rho_a {v_a}^2 L}{2D} = 0.214 \times \frac{20 \times 2 \times 8.77^2 \times 892}{2 \times 0.315} = 932 \text{ kPa}$$

$$P_{Hs(Eqn\ 7.7)} = \lambda_s \frac{\mu \rho_a {v_a}^2 L}{2D} = 0.065 \times \frac{20 \times 2 \times 8.77^2 \times 892}{2 \times 0.315} = 283 \text{ kPa}$$

$$P_{Hs(Eqn\ 7.8)} = \lambda_s \frac{\mu \rho_a {v_a}^2 L}{2D} = 0.051 \times \frac{20 \times 2 \times 8.77^2 \times 892}{2 \times 0.315} = 221 \text{ kPa}$$

The same process was followed for line 2, with a longer conveying distance of 931 m, and the full set of results is as shown in Table 7.14. Both pipes had the same diameter (Table 3.2).

**Table 7.14** Predicted pneumatic conveying performance for Unit 6

| Conveying characteristic | Line 1 | | Line 2 | |
|---|---|---|---|---|
| | Value | Units | Value | Units |
| Conveying distance | 892 | m | 931 | m |
| Solids mass flow rate | 18.2 | kg/s | 18.2 | kg/s |
| Air mass flow rate | 0.91 | kg/s | 0.91 | kg/s |
| Solids loading ratio | 20 | (−) | 20 | (−) |
| Average velocity | 8.77 | m/s | 8.77 | m/s |
| Froude number | 5 | (−) | 5 | (−) |
| Solids friction factor (Jones and Williams) | 0.224 | (−) | 0.224 | (−) |
| Solids friction factor (Behera power law) | 0.171 | (−) | 0.171 | (−) |
| Solids friction factor (Experimental model, Equation 7.6) | 0.215 | (−) | 0.215 | (−) |
| Solids friction factor (Experimental model, Equation 7.7) | 0.297 | (−) | 0.297 | (−) |
| Solids friction factor (Experimental model, Equation 7.8) | 0.051 | (−) | 0.051 | (−) |
| Horizontal solids pressure drop (Jones and Williams) | 974 | kPa | 1018 | kPa |
| Horizontal solids pressure drop (Behera power law) | 746 | kPa | 779 | kPa |
| Horizontal solids pressure drop (Experimental model, Equation 7.6) | 932 | kPa | 975 | kPa |
| Horizontal solids pressure drop (Experimental model, Equation 7.7) | 283 | kPa | 297 | kPa |
| Horizontal solids pressure drop (Experimental model, Equation 7.8) | 221 | kPa | 230 | kPa |

## 7.7 Discussion on Friction Factor and Pressure Drop Estimation

Noting table 7.14, and with focus on conveying pipe line 1 for this discussion. The above results show that the Jones and Williams and the Behera *et al* models are very conservative when predicting conveying pressure drop for Unit 6, with predictions of 974 kPa and 746 kPa respectively. These values are very high when compared with actual conveying pressure data for Units 1, 2 and 3. It was also expected that models represented by Equation 7.6 will provide results that are within expectations, however observing findings for Unit 6 it is also clear that Equation 7.6 over predicts the solids friction factor and subsequently the conveying pressure at 932 kPa. Only Equations 7.7 and 7.8 with predicted horizontal conveying pressures of 283 kPa and 221 kPa respectively were within expectations for Unit 6 based on performance of the Units in operation. As such, based on this information and also taking note of Tables 7.13 and Figure 7.4, model proposed by Equation 7.8 is observed to be the best model for predicting pressure drop across all Units although with an expected error in prediction.

As such, using experimental findings to improve on the solids friction factor models already available provides for better estimation of the solids friction factor. This again emphasizes the need to perform experiments in large industrial applications of pneumatic conveying of solids and from that data improve on the current proposed models as these available models although a good starting point, the errors in predicted pressure is significant to ignore. This is because some of these models were developed using scale up conditions, and had provided better error margins when scaled up in their particular environment with results of less than 15% error margin to experimental results. However, when these models are applied to different conveying characteristics they show significant error margins, as shown in this research.

The models discussed in sections 7.4.1 to 7.4.4 were all based on the solids loading ratio and the Froude numbers. As such, it is also worth noting that a slight change in the Froude number and the solids loading ratio during actual conveying has a significant impact on the solids friction factor. The Froude number is a function of the convening air velocity and therefore it is necessary to maintain the air flowrate during conveying as this air flowrate will have a direct impact on the solids friction factor and conveying pressure. Similarly the solids loading ratio is also a function of the air flowrate based on Equation 2.2. It is for this purpose that researchers are also considering other models such as the volumetric loading ratio based model that computes solids friction factors in separate forms for dilute and dense phase within a single conveying cycle (Setia *et al*., 2016).

The predicted performance for Unit 6 will need to be confirmed with actual system performance after the system has been fully constructed and commissioned. However based on these findings it can be expected that total conveying pressure drop values will not exceed 280 kPa during normal conveying. The other components such as pressure drop due to the air, vertical elevations and flow around a bend relationship with the bulk solids during conveying have been approximated to 23% of the total conveying, averaged from Units 1, 2 and 3. This is provided all other pneumatic conveying characteristics are similar to the assumptions made for these calculations.

# CHAPTER 8 CONCLUSION AND RECOMMENDATIONS

## 8.1 Conclusion

The characterization of the fly ash that was considered during this research indicated that this ash can be conveyed in dense phase mode. However, when comparing the actual air flowrates and subsequent solids loading ratio, it was also indicative of the need to further optimize performance of the system, this was particularly the case for Units 1 and 3. Although the increased air flowrate also has some benefits in terms of reducing the conveying pressure drop (Equation 7.2) it also increases the wear rate on the system.

In this investigation, Unit 2 had the least air usage, with typical flow rates of 1.86 kg/s when conveying at full load, with solids loading ratio values averaging 19 (both conveying lines). Although these can be assumed to be dense phase conditions, there is scope for improvement to ensure continuous performance at values higher than 20. However Unit 1 indicated results that were not expected, with higher air flow rates than expected at 2.8 kg/s during full load conditions; these were much higher when also compared to Unit 2. These also resulted to lower than expected solids loading ratios averaging 10. This indicates areas of improvement that exist within the current installation by reducing the amount of air into the system. Unit 3 was the furthest Unit of the three Units under investigation and was performing similarly to Unit 1, with average air flow rate of 2.8 kg/s and solids loading ratio of 10. Based on the results from Unit 2, improvements can be rolled out with some level of confidence that predominant dense phase conveying can be expected for Units 1 and 3.

Based on the experimental findings, previously-reported models were compared with findings from the research. Typical models for dense phase systems transporting fly ash were considered, such as the Jones and Williams (2003) model and a similar model proposed by Behera *et al*., (2015). These models overestimated results for solids friction factor and pressure drop when compared with experimental results. Using the power law method as applied by Behera *et al* new models were presented to estimate solids friction factors, represented by Equations 7.6, 7.7 and 7.8. These new models also had overestimates when applied across all the Units, with Equation 7.8 proving to be the best solids friction factor model, although with average errors of 48%. The other models all resulted in higher error margins when compared to experimental results across all the Units. These errors were also magnified when the models were applied to estimate the conveying pressure drop for the last Unit.

The research also confirmed that the current installed compressors will be able to meet the demand for all the Units. Whilst the air consumption is very high, particularly for Unit 1 and 3, these values are still within the capacity of the installed compressors, indicating that the current compressors have been oversized. The advantages of reducing these air flowrate figures was also noted, in terms of reducing the system air velocities that results in reduced maintenance and operational cost reduction. It is therefore necessary that the pneumatic conveying system is optimized.

It is also worthwhile to also highlight the uncertainties that were noted in this research, as included in Appendix J. These were computed in line with guidelines by Taylor (1997). The error in obtaining the experimental conveying pressure and air flowrate was approximately 12% and 9% respectively, due to the methods used to obtain data. These errors were propagated to other pneumatic conveying characteristics, and errors in the order of 50% to 60% of the results obtained were observed in estimation of the solids friction factor and conveying pressures. As such, it is necessary to minimize the extent of these errors when the conditions are favorable and the experiment is performed.

## 8.2 Recommendations for Future Work

Although it is hoped that the results obtained will assist engineers and researchers with a better understanding of actual fly ash conveying systems and how they are performing, there were concerns and questions raised during the investigation that were not answered. These were outside the scope of this project and are mentioned here as areas of improvement and tasks that require further development. These have been divided into two categories; operational changes required to improve the plant and additional research into other friction factor models that should be considered in such a commercial pneumatic conveying system.

### 8.2.1 Future work that will enhance the current plant's operational performance

1. Investigation into blockage conditions for fly ash conveying could be undertaken in principle by reducing the air flow rate continuously until a blockage condition is observed. Minimum transport conditions for this fly ash could then be developed with minimum air flow rate and air velocity computations. This was not possible during this research as the plant was in commercial operation.

2. The air flow rates for Units 1 and 3 are higher than normal for dense phase systems, and Unit 1 can be improved drastically by reducing the orifice sizes to ensure reduction in air flow rate. As a first approximation for orifice sizes, the Unit 2 orifice plate design values can be used for Unit 1.

3. The solids loading ratios for all the Units considered were not as high as expected for dense phase systems, as such as part of recommendation (1), all the Units should be tested for blockage conditions to establish the true minimum air flow rates. This will assist to improve the solids loading ratio to true dense phase conveying mode.

4. Installation of transparent conveying pipe sections would ensure visualization of the conveying mode to conclude whether flow is dense phase or dilute phase. These transparent pipe sections or sight glasses should be installed preferably at three locations: at the start of the conveying pipe, at the middle, and at the end of the conveying pipe.

5. Ideally, a dedicated period should be set aside for pneumatic conveying tests to be performed. Such tests should not be hindered by production demands for that period. Equipment restoration would be required such as instrument calibration, piping checks for wear and all valves to be restored before testing can commence. The installation of dedicated air flow measurement devices for pneumatic conveying is particularly important, with an air flow meter for each conveying bank. At least half a Unit should be installed with solids mass flowrates detections instrument such as strain gauges to measure the actual amount of fly ash introduced into the ash hoppers.

### 8.2.2 Future work that will also enhance understanding of dense phase systems

6. Results obtained in section 8.2.1 will provide performance data at ideal experimental conditions without the limitations imposed due to operational requirements and these will need to be analyzed further to verify the experimental findings in this research.

7. Other models used for development of solids friction factors and pressure drop should be pursued as these may yield results closer to experimental findings. This research was focused on models that made use of the Froude number and solids loading ratio as key input parameters with both the Jones and Williams (2003) and Behera *et al*, 2015 models based on this principle. As such other methods that take into account the real form of solids during conveying displaying both dense and dilute-like behavior during conveying, especially on fluidized dense phase conveying. One such model to be investigated in more detail using a fully commercial pneumatic conveying system is the volumetric loading ratio and a velocity ratio form to develop solids friction factors. This approach has been widely researched by (Setia *et al*, 2015) and could form the basis for further research.

# REFERENCES


Anantharaman, A., Cahyadi, A., Hadinoto, K., Chew JW. (2016) *Impact of particle diameter, density, and sphericity on minimum pick up velocity of binary mixture in gas-solids pneumatic conveying*, Powder Technology, 297, 311-319.

Bettman, R. (1987), *Long Distance Pneumatic Conveying*, University of Witwatersrand, Johannesburg, South Africa.

Behera, N., Agarwal, VK. Jones, MG. (2015), *A Model of Solids Friction Factor For Fluidised Dense Pneumatic Conveying*, Powder Technology, 284, 403-410.

Bansal, A. (2012), *An Investigation into Straight Pipe Pressure Drop and Flow-Mode Transition Criteria for Fluidized Dense Phase Pneumatic Conveying System*, Thapar University, Patiala, India.

Chan, CY. (2001), *Pneumatic Conveying of Slush Ice Through Horizontal Plastic Pipes (Thesis)*, University of Witwatersrand, Johannesburg, South Africa.

Deng, T and Bradley, MSA. (2016) *Determination of a particle size distribution criterion for predicting dense phase pneumatic conveying behaviour of granular and powder materials*, Powder Technology, 304, 32-40.

Geldart, D. (1973) *Types of gas fluidization*, Powder Technology, 7, 285-292.

Gu, ZH. And McLean, AG. (1991), *Consolidation-related bulk density and permeability models for bulk solids,* Powder Technology, 72, 39-44

Guya, S.R. (2018), *Calibration of Discrete Finate Element Modelling Parameters for Bulk Materials Handling Applications*, University of Witwatersrand, Johannesburg, South Africa.

Jardine, R.K. (1987), *An Investigation Into The System Characteristics of a Steady State, Tandem Vessel Pneumatic Conveying System When Transporting Fly Ash for the Use in Backfilling of Coal Mines (Thesis),* University of Witwatersrand, Johannesburg, South Africa.

Jones, MG and Williams, KC. (2003) *Solids Friction Factors for Fluidized Dense Phase Pneumatic Conveying,* Particulate Science and Technology, 21, 45-56.

Kalman, H., Satran, A., Meir, D., Rabinovich, E. (2005) *Pick Up (Critical) Velocity for Particles*, Powder Technology, 160. 103-113.

Li, H., Liu, G., Cao, Y. (2014) *Content and Distribution of Trace Elements and Polycyclic Aromatic Hydrocarbons in Fly Ash from a Coal-Fired CHP Plant*, Aerosol and Air Quality Research, 14. 1179-1188.

Mallick, SS. (2009), *Modelling of Fluidized Dense Phase Pneumatic Conveying of Powders,* University of Wollongong, Australia.

Mbabazi, J.G., Sheer, T.J., Shandu, R. (2004), *A model to predict erosion on mild steel surfaces impacted by boiler fly ash particles,* Wear, 257, 612-624.

Mi, B. (1994), *Low Velocity Penumatic Transportation of Bulk Solids,* University of Wollongong, Australia.

Mills, D. (2016) Pneumatic Conveying Design Guide, 3rd Edition, Elsevier.

Mills, D. and Agarwal, VK. (2015) *Conveying Air Velocity Requirements for Pneumatic Conveying Systems* CHoPS - 8th International Conference for Conveying and Handling of Particulate Solids, Tel Aviv, Israel.

Mills, D. and Agarwal, VK. (2001), Pneumatic Conveying Systems, Trans Tech Publications.

Ratnayake, C. (2005), *Pneumatic Transport Systems, (PhD Thesis),* The Norwegian University of Science and Technology, Norway.

Setia, G. and Mallick, SS. (2015) *Modelling fluidized dense-phase pneumatic conveying of fly ash*, Powder Technology, 270, 39-45.

Setia, G. Mallick, SS. Pan, R. Wypych P. (2017) *An experimental investigation into modelling solids friction factor for fluidized dense-phase pneumatic transport of powders*, Particuology, 30, 83-91.

Sharma, K. Mallick SS. Mittal, A. and Wypych, P. (2019), *Modelling Solids Friction for Fluidized Dense-Phase Pneumatic Conveying,* Particulate Science and Technology.

Sheer, T.J. (1991) *Pneumatic Conveying of Ice Particles through Mine-Shaft Pipelines*, (PhD Thesis), University of Witwatersrand, Johannesburg, South Africa.

Snowsill ,W.L. , in Instrumentation Reference Book (Fourth Edition), 2010

Taylor, RJ. (1997). *An Introduction into Error Analysis, The Study Of Uncertainties in Physical Measurements*, Second Edition, University Science Books.

Tu, W. Zand, B. Ajlouni, MA. Butalia, TS. Wolfe, WE. (2007) *The Cosolidation Characteristics of Impounded Class F Fly Ash – A Case History*, Ohio State University, Columbus, United States of America.

Weber, M. (1981) *Principles Of Hydraulic and Pneumatic Conveying In Pipes*, Bulk Solids Handling, 1, 57-63.

Williams, KC. (2008) *Dense Phase Pneumatic Conveying of Powders: Design Aspects and Phenomena*, (PhD Thesis), University of Newcastle, Australia.

Wypych, P. (1989), *Pneumatic Conveying of Bulk Solids (PhD Thesis)*, University of Wollongong, Australia.

Van Deventer, P. (2011) *Efficiency of Pneumatic Ash Systems*, Research and Innovation Department, Technology Strategy and Planning, RES/RR/10/32537.

Von Blittersdorff M., Klatt C., (2017), Chapter 13 - *The Grind—Particles and, The Craft and Science of Coffee*, Academic Press, Pages 311-328. (https://0-www-sciencedirect-com.innopac.wits.ac.za/topics/agricultural-and-biological-sciences/sieving)

**Internal Design Reports: Confidential**

- Internal Document, Design Report, Document number: 200-36048
- Internal Document, Design Report, Document number: 200-215389
- Internal Document, Design Report, Document number: 200-36048

# APPENDICES

The appendices are listed as below chapters:

# APPENDIX A COMPRESSED AIR SUPPLY SYSTEM

A compressor house contains the common compressors supplying process air to various users on the station. There are three (3) process (conveying) air compressors in each compressor house, plus two (2) redundant compressors each with the following specifications:

## A1 Compressors

| | |
|---|---|
| Make | : Atlas Copco |
| Model | : ZH 15 000+ |
| Type | : Centrifugal |
| Stages | : Three (3) |
| Installed motor | : 1 385 kW |
| Coupling power | : 1 259.8 kW |
| Suction conditions | : 90 kPa, 30 degrees C, 50% RH, 32 degrees C cooling water inlet |
| Discharge conditions | : 840 kPaG, 130.9 degrees C |
| Air delivery | : 203.4 Sm3/min. |
| Air quality | : Oil free, ISO 8573-1 Class 0 |
| Specific power | : 304.8 J/l |
| Specific energy | : 308.6 kJ/kg |

## A2 Air receivers

| | |
|---|---|
| Capacity | : 20.8 m3 – installed |
| Pressure | : 750 kPaG – normal operating. |
| | : 1 000 kPaG – design. |
| Compressor handover time | : 30 sec. |
| Operating pressure | : 500 kPa – min |
| | : 700 kPa – max. |

# APPENDIX B CONVEYING PIPE DETAILS

**Table B.1** Conveying pipe detail

| **Pipe detail** | **Specification** |
|---|---|
| Design code | ASME B31.3 |
| Material specification | API-5L-X42 |
| Pipe thickness | 8 mm |
| Pipe outside diameter | 273 mm |
| Male-Female gasket size | 2 mm |
| Design pressure | 8 Bar |
| Corrosion/Erosion allowance | 3 mm |
| Number of bends | 7 |
| Design temperature | 100 degrees Celsius |
| Ceramic tile | 10 mm thick 92% alumina |
| 90 degrees bend radius | 1265 mm |
| 30 degrees bend radius | 950 mm |
| 60 degrees bend | 1500 mm |

# APPENDIX C PRESSURE VESSEL DETAILS

Each pressure vessel had the following specification (shell only),

**Table C.1** Pressure vessel detail

| **Vessel detail** | **Specification** |
|---|---|
| Design code | PD5500 Cat2 2009 |
| Material specification (Shell) | EN10028-2-P264GH |
| Wall thickness | 10 mm |
| Design pressure | 8 Bar |
| Corrosion/Erosion allowance | 1 mm |
| Design temperature | 200 Degrees Celcius |
| Volume | 2.27 $m^3$ |
| Quantity | 28 vessels per Unit (84 in total) |

# APPENDIX D DATA SHEETS

**Table D.1** Pressure transmitter data sheet

| **Item** | **Specification** |
|---|---|
| Maker | Endress+Hauser |
| Model | PMP 71 |
| Range | 0-1000 kPa |
| Product temperature | 130 degrees Celsius |
| IP rating | 65 |

**Table D.2** Flowmeter transmitter data sheet

| **Item** | **Specification** |
|---|---|
| Maker | Endress+Hauser |
| Model | t-mass 65I (Thermal Mass Flowmeter) |
| Range | 1.63-886 $Nm^3$/min |
| Reference temperature | 0 degrees Celsius |
| IP rating | 67 |

**Table D.3** Hopper level transmitter

| **Item** | **Specification** |
|---|---|
| Maker | Rosemount |
| Model | 5303 (Guided wave radar) |
| Range | 0-100 % |
| Product temperature | 130 degrees Celsius |
| IP rating | 65 |

**Table D.4** Mill mass meter data sheet

| **Item** | **Specification** |
|---|---|
| Maker | MICRO-TECH |
| Model | MICRO-TECH 2000 INTEGRATOR |
| Range | 0-38 kg/s |
| IP rating | 65 |

**Table D.5** Silo filter details

| **Vessel detail** | **Specification** |
|---|---|
| Extraction Fan | |
| Motor size | 22 kW |
| Bag filter | |
| No. of bags and cages | 200 |

**Table D.6** Data sheet for silo filter system

| **Item** | **Specification** |
|---|---|
| Maker | MICRO-TECH |
| Model | MICRO-TECH 2000 INTEGRATOR |
| Range | 0-38 kg/s |
| IP rating | 65 |

# APPENDIX E ORIFICE PLATE DETAILS AND LOCATION

**Table E.1** List of orifice plates for Unit 1

| **Blow Tanks** | **Air Supply Type** | **Row 1** | | **Row 2** | | **Row 3** | | **Row 4** | |
|---|---|---|---|---|---|---|---|---|---|
| | | Hole Size Ø [mm] | Number of Holes | Hole Size Ø [mm] | Number of Holes | Hole Size Ø [mm] | Number of Holes | Hole Size Ø [mm] | Number of Holes |
| Master | Fluidising | 3 | 12 | 3 | 12 | 3 | 12 | 3 | 7 |
| Master | Pipe in a pipe | 4 | 1 | 4 | 1 | 4 | 1 | 4 | 1 |
| Master | Main Supply | 3 | 7 | 3 | 7 | 3 | 7 | 3 | 7 |
| Slave 1 | Fluidising | 3 | 7 | 3 | 7 | 3 | 7 | 3 | 7 |
| Slave 1 | Pipe in a pipe | 4 | 1 | 4 | 1 | 4 | 1 | 4 | 1 |
| Slave 2 | Fluidising | 3 | 7 | 3 | 7 | 3 | 7 | 3 | 7 |
| Slave 2 | Pipe in a pipe | 4 | 1 | 4 | 1 | 4 | 1 | 4 | 1 |
| Slave 3 | Fluidising | 3 | 7 | 3 | 7 | 3 | 7 | 3 | 7 |
| Slave 3 | Pipe in a pipe | 4 | 1 | 4 | 1 | 4 | 1 | 4 | 1 |
| Slave 4 | Fluidising | 3 | 7 | 3 | 7 | 3 | 7 | 3 | 7 |
| Slave 4 | Pipe in a pipe | 4 | 1 | 4 | 1 | 4 | 1 | 4 | 1 |
| Slave 5 | Fluidising | 3 | 7 | 3 | 7 | 3 | 7 | 3 | 7 |
| Slave 5 | Pipe in a pipe | 4 | 1 | 4 | 1 | 4 | 1 | 4 | 1 |

| Blow Tanks | Air Supply Type | Row 1 | | Row 2 | | Row 3 | | Row 4 | |
|---|---|---|---|---|---|---|---|---|---|
| | | Hole Size Ø [mm] | Number of Holes | Hole Size Ø [mm] | Number of Holes | | | Hole Size Ø [mm] | Number of Holes |
| Outlet | Fluidising | 3 | 7 | 3 | 7 | 3 | 7 | 3 | 7 |
| Outlet | Additional Air | 6 | 5 | 6 | 5 | 6 | 5 | 6 | 5 |
| Outlet | Bypass BP004 | 4 | 3 | 4 | 3 | 4 | 3 | 4 | 3 |
| Outlet | Bypass BP003 | 4 | 3 | 4 | 3 | 4 | 3 | 4 | 3 |

**Table E.2** List of orifice plates for Unit 2

| Blow Tanks | Air Supply Type | Row 1 | | Row 2 | | Row 3 | | Row 4 | |
|---|---|---|---|---|---|---|---|---|---|
| | | Hole Size Ø [mm] | Number of Holes | Hole Size Ø [mm] | Number of Holes | Hole Size Ø [mm] | Number of Holes | Hole Size Ø [mm] | Number of Holes |
| Master | Fluidising | 3 | 12 | 3 | 12 | 3 | 7 | 3 | 7 |
| Master | Pipe in a pipe | 4 | 1 | 4 | 1 | 4 | 1 | 4 | 1 |
| Master | Main Supply | 3 | 7 | 3 | 7 | 3 | 7 | 3 | 7 |
| Slave 1 | Fluidising | 3 | 7 | 3 | 7 | 3 | 7 | 3 | 7 |
| Slave 1 | Pipe in a pipe | 4 | 1 | 4 | 1 | 4 | 1 | 4 | 1 |
| Slave 2 | Fluidising | 3 | 7 | 3 | 7 | 3 | 7 | 3 | 7 |
| Slave 2 | Pipe in a pipe | 4 | 1 | 4 | 1 | 4 | 1 | 4 | 1 |
| Slave 3 | Fluidising | 5 | 2 | 6 | 5 | 6 | 5 | 6 | 5 |

| Blow Tanks | Air Supply Type | Row 1 | | Row 2 | | Row 3 | | Row 4 | |
|---|---|---|---|---|---|---|---|---|---|
| | | Hole Size Ø [mm] | Number of Holes | Hole Size Ø [mm] | Number of Holes | Hole Size Ø [mm] | Number of Holes | Hole Size Ø [mm] | Number of Holes |
| Slave 3 | Pipe in a pipe | 4 | 1 | 4 | 1 | 4 | 1 | 4 | 1 |
| Slave 4 | Fluidising | 3 | 7 | 3 | 7 | 3 | 7 | 3 | 7 |
| Slave 4 | Pipe in a pipe | 4 | 1 | 4 | 1 | 4 | 1 | 4 | 1 |
| Slave 5 | Fluidising | 3 | 7 | 3 | 7 | 3 | 7 | 3 | 7 |
| Slave 5 | Pipe in a pipe | 4 | 1 | 4 | 1 | 4 | 1 | 4 | 1 |
| Outlet | Fluidising | 3 | 7 | 3 | 7 | 3 | 7 | 3 | 7 |
| Outlet | Additional Air | 6 | 5 | 6 | 5 | 6 | 5 | 6 | 5 |
| Outlet | Bypass BP004 | 4 | 3 | 4 | 3 | 4 | 3 | 4 | 3 |
| Outlet | Bypass BP003 | 4 | 3 | 4 | 3 | 4 | 3 | 4 | 3 |

**Table E.3** Orifice plate list for Unit 3

| Blow Tanks | Air Supply Type | Row 1 | | Row 2 | | Row 3 | | Row 4 | |
|---|---|---|---|---|---|---|---|---|---|
| | | Hole Size Ø [mm] | Number of Holes | Hole Size Ø [mm] | Number of Holes | Hole Size Ø [mm] | Number of Holes | Hole Size Ø [mm] | Number of Holes |
| Master | Fluidising | 3 | 12 | 3 | 12 | 3 | 12 | 3 | 12 |
| Master | Pipe in a pipe | 4 | 1 | 4 | 1 | 4 | 1 | 4 | 1 |
| Master | Main Supply | 3 | 7 | 3 | 15 | 3 | 7 | 3 | 7 |
| Slave 1 | Fluidising | 3 | 7 | 3 | 7 | 3 | 7 | 3 | 7 |
| Slave 1 | Pipe in a pipe | 4 | 1 | 4 | 1 | 4 | 1 | 4 | 1 |
| Slave 2 | Fluidising | 3 | 7 | 3 | 7 | 3 | 7 | 3 | 7 |
| Slave 2 | Pipe in a pipe | 4 | 1 | 4 | 1 | 4 | 1 | 4 | 1 |
| Slave 3 | Fluidising | 3 | 7 | 3 | 7 | 3 | 7 | 3 | 7 |
| Slave 3 | Pipe in a pipe | 4 | 1 | 4 | 1 | 4 | 1 | 4 | 1 |
| Slave 4 | Fluidising | 3 | 7 | 3 | 7 | 3 | 7 | 3 | 7 |
| Slave 4 | Pipe in a pipe | 4 | 1 | 4 | 1 | 4 | 1 | 4 | 1 |
| Slave 5 | Fluidising | 3 | 7 | 3 | 7 | 3 | 7 | 3 | 7 |
| Slave 5 | Pipe in a pipe | 4 | 1 | 4 | 1 | 4 | 1 | 4 | 1 |
| Outlet | Fluidising | 6 | 4 | 6 | 4 | 6 | 4 | 6 | 4 |
| Outlet | Additional Air | 6 | 5 | 6 | 5 | 6 | 5 | 6 | 5 |
| Outlet | Bypass BP004 | 4 | 3 | 4 | 3 | 4 | 3 | 4 | 3 |
| Outlet | Bypass BP003 | 4 | 3 | 4 | 3 | 4 | 3 | 4 | 3 |

# APPENDIX F PSD DURING COMMISSIONING

Particle size distribution (PSD) observed during commissioning stages for each of the three Units is also indicated. This was done to observe variance from the initial commission until the period under the research period. Each PSD data is tabulated with an indication of how much ash particles passed the 75 micron sieves, and these are also shown in figures as well. The information is presented as follows:

- Unit 1 PSD commissioning data
- Unit 2 PSD commissioning data
- Unit 3 PSD commissioning data

## F1 Unit 1 PSD commissioning data

**Table F.1** Unit 1 PSD data findings on 22/03/2016

| **Sieve sizes** | **Mass (g)** | **%** |
|---|---|---|
| 300 | 3 | 4.1 |
| 150 | 7 | 9.6 |
| 106 | 11 | 15.1 |
| 75 | 11 | 15.1 |
| -75 | 41 | 56.2 |
| Total | 73 | 100.0 |

The total amount of particles that pass the 75 microns and less particle sieve size is 71%. This was obtained by adding the 75 and -75 sieves, by observing the amount of material that passes and divide by the total such as (41+11)/(73) for Unit 1.

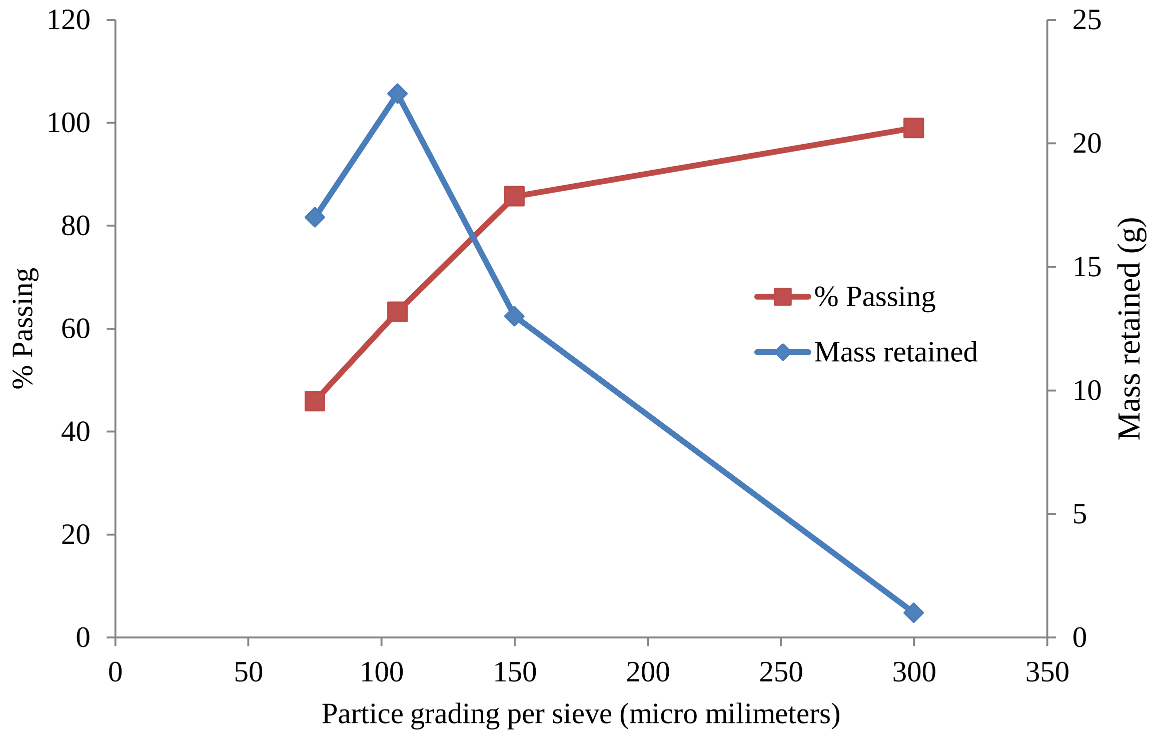


**Figure F.1** Unit 1 Commissioning data period March 2016

## F2 Unit 2 PSD commissioning data

**Table F.2 Unit 2 PSD data findings on 21/03/2017**

| Sieve sizes | Mass (g) | Percentage passing |
|---|---|---|
| 300 | 0 | 0.0 |
| 150 | 5 | 6.9 |
| 106 | 9 | 12.5 |
| 75 | 12 | 16.7 |
| -75 | 46 | 63.9 |
| Total | 72 | 100.0 |

In the period above, more than 80% of solids pass the 75 sieve sizes.

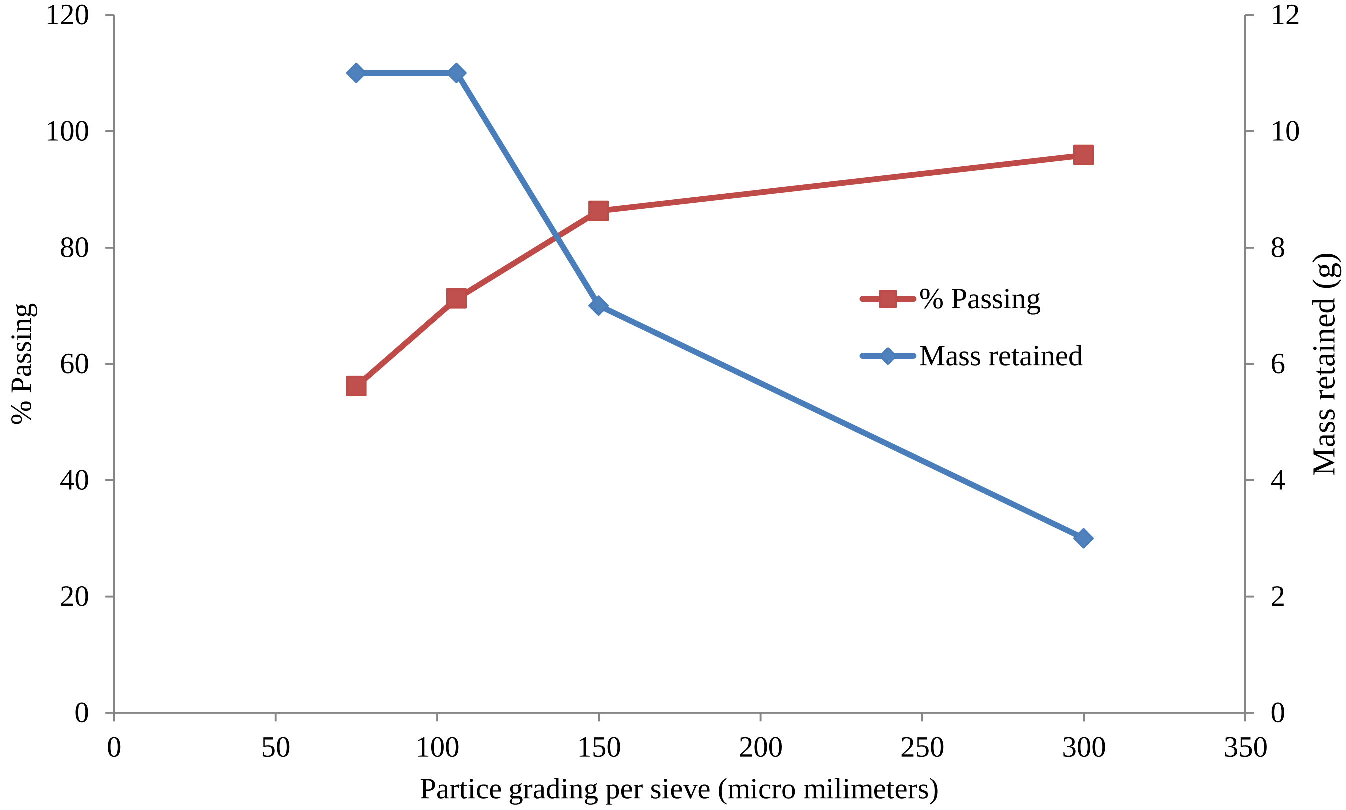


**Figure F.2** Unit 2 Commissioning PSD data findings on 21/03/2017

**Table F.3** Unit 2 PSD data on 31/01/2017

| **Sieve sizes (microns)** | **Mass (g)** | **%** |
|---|---|---|
| 300 | 0 | 0.0 |
| 150 | 6 | 8.2 |
| 106 | 14 | 19.2 |
| 75 | 14 | 19.2 |
| -75 | 39 | 53.4 |
| Total | 73 | 100.0 |

As per the above Table, bulk solids that pass the 75 and less sieve sizes are 72% of the total solids that were sampled.

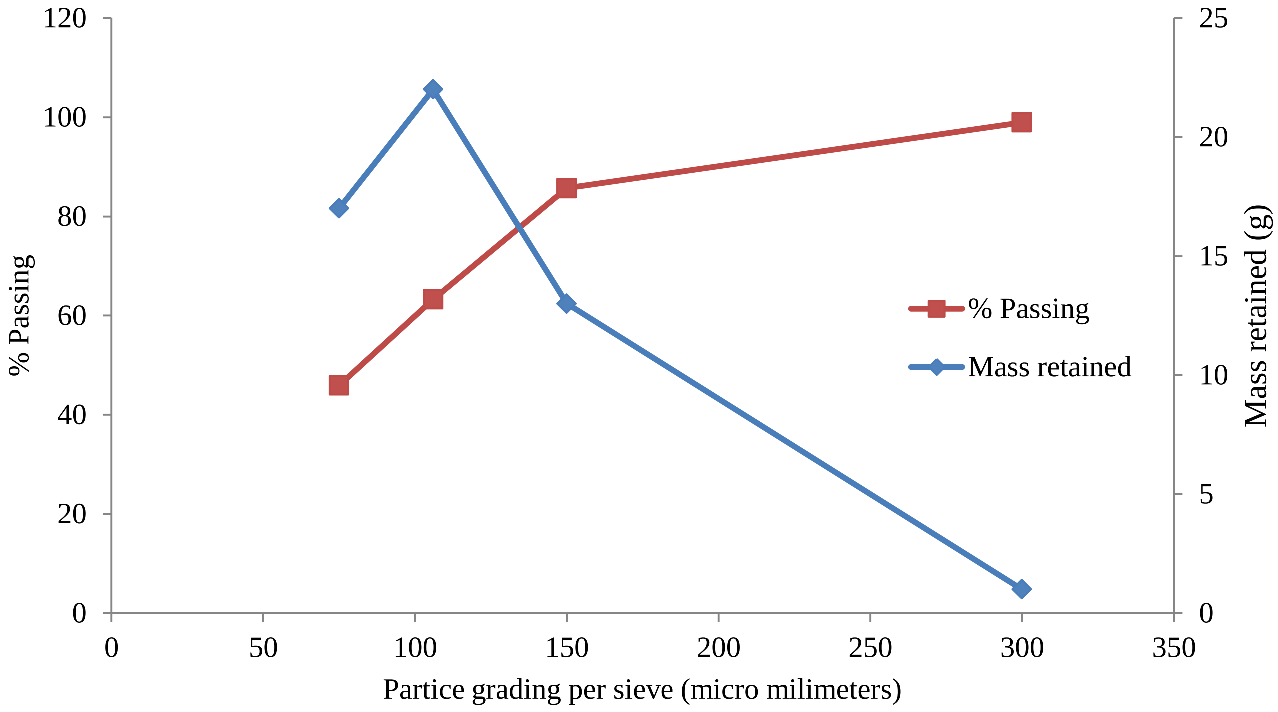


**Figure F.3** Unit 2 Commissioning PSD data on 31/01/2017

## F3 Unit 3 PSD commissioning data

**Table F.4** Unit 3 Commissioning PSD on 13/07/2017

| Size Grading (microns) | Mass (g) | % |
|---|---|---|
| 300 | 0 | 0.0 |
| 150 | 14 | 12.0 |
| 106 | 18 | 15.4 |
| 75 | 17 | 14.5 |
| -75 | 68 | 58.1 |
| Total | 117 | 100.0 |

As can be observed, 72.3% of the solids taken for sampling passed the 75 sieve sizes.

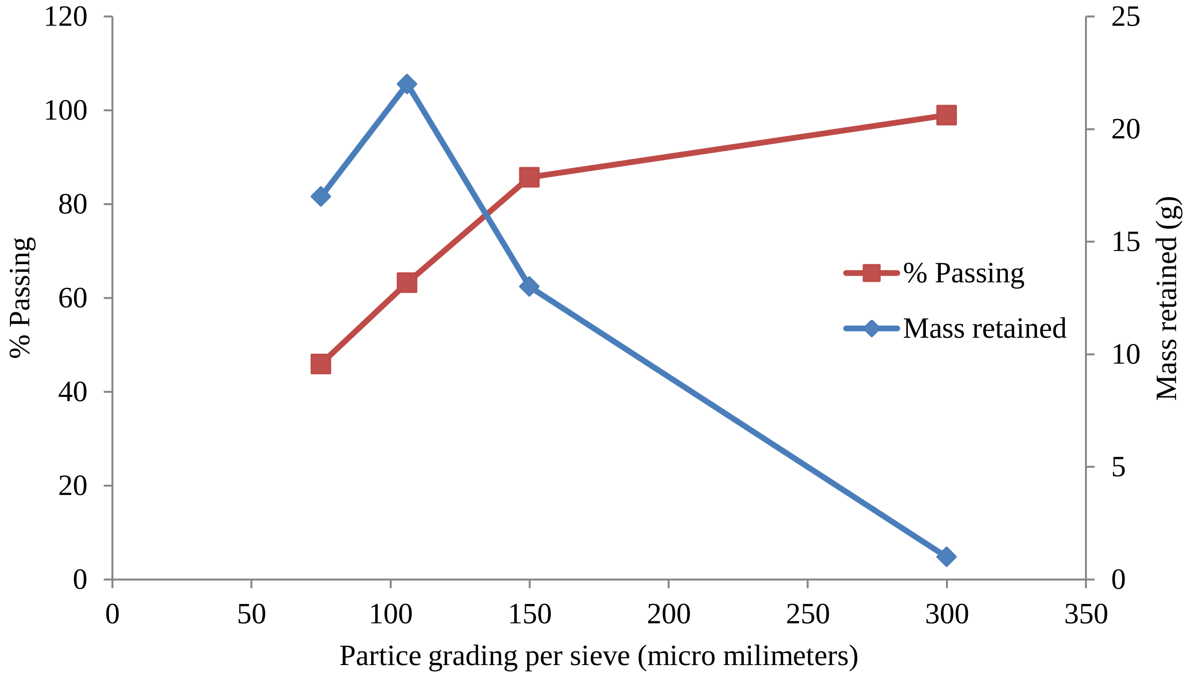


**Figure F.4** Unit 3 Commissioning PSD on 13/07/2017

**Table F.5** Unit 3 commissioning PSD data on 25/07/2017

| **Size Grading (microns)** | **Mass (g)** | **%** |
|---|---|---|
| 300 | 1 | 1.0 |
| 150 | 13 | 13.3 |
| 106 | 22 | 22.4 |
| 75 | 17 | 17.3 |
| -75 | 45 | 45.9 |
| Total | 98 | 100.0 |

It can be observed that 63% of the solids sampled passed the 75 sieve sizes.

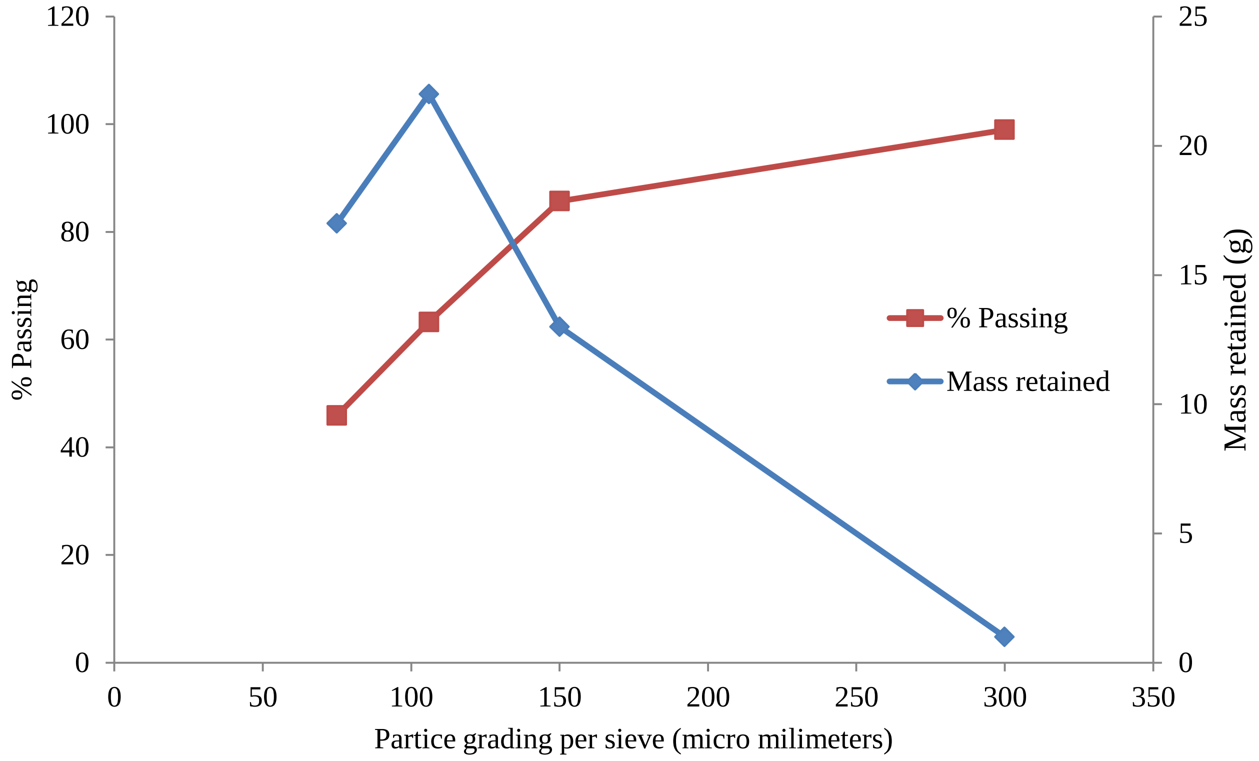


**Figure F.5** Unit 3 commissioning PSD data on 25/07/2017

# APPENDIX G COAL CONSUMPTION AND ASH ESTIMATION

Coal consumption and ash estimating readings for the periods as defined in chapter 5, Table 5.2 (Unit 1), Table 5.1 (Unit 2) and Table 5.3 (Unit 3) are included in this section. The raw data for each period's sampled date only are indicated. Figure 13 and following shows coal consumption data for the mills in service on the reporting period. As mentioned in 5.6, only raw data as used in the research is included herein with specific periods as mentioned in the description of each figure.

## G1 Unit 1 Coal Consumption Data

Period 1: 24 September 2017 [Graph not available]

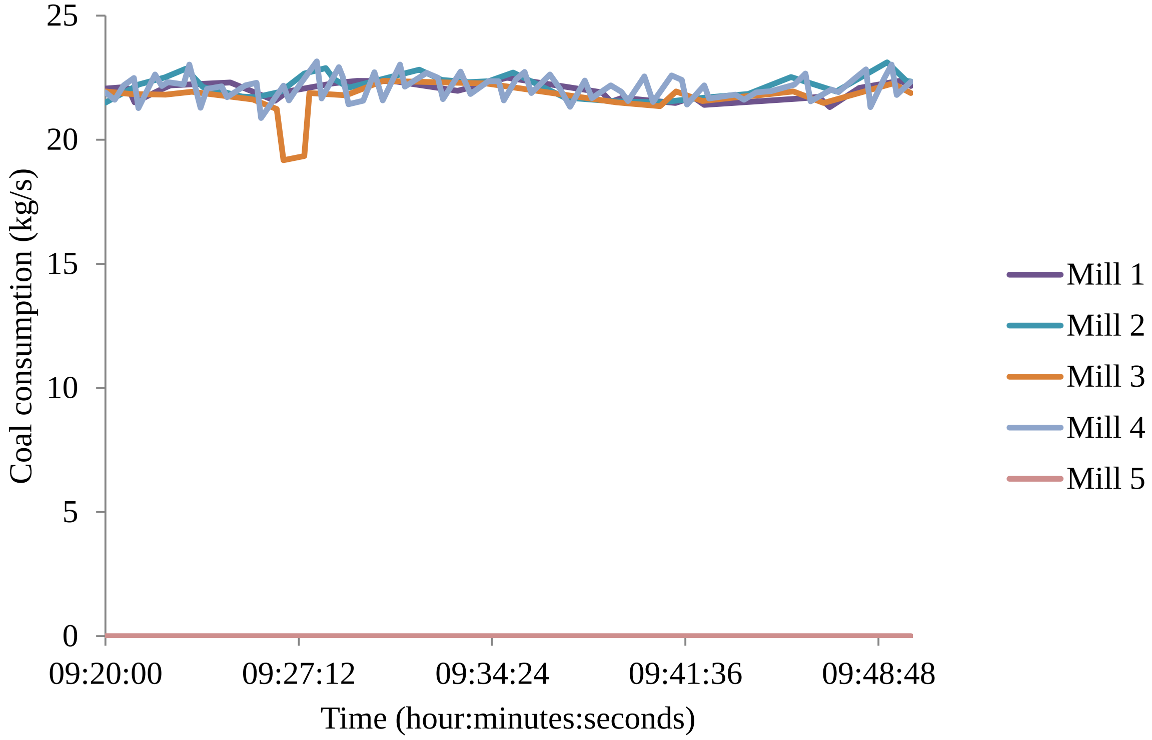


**Figure G.1** Unit 1 coal consumption data for Period 2 sample date 12 October 2017

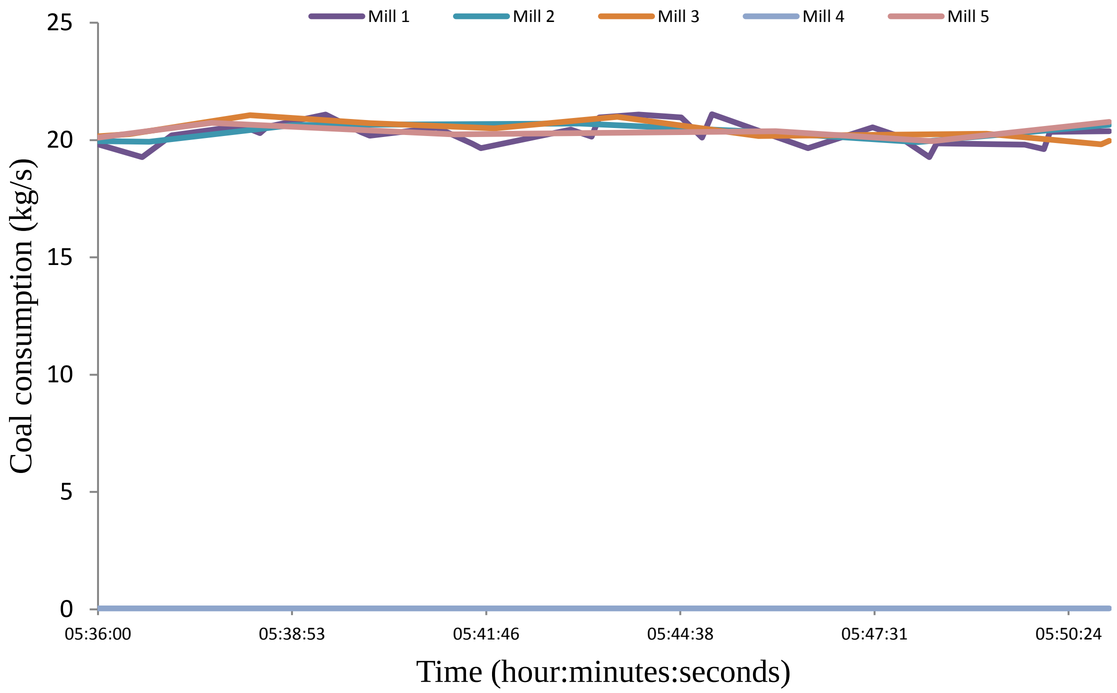


**Figure G.2** Unit 1 coal consumption data for period 3 sample date 01/18/2018

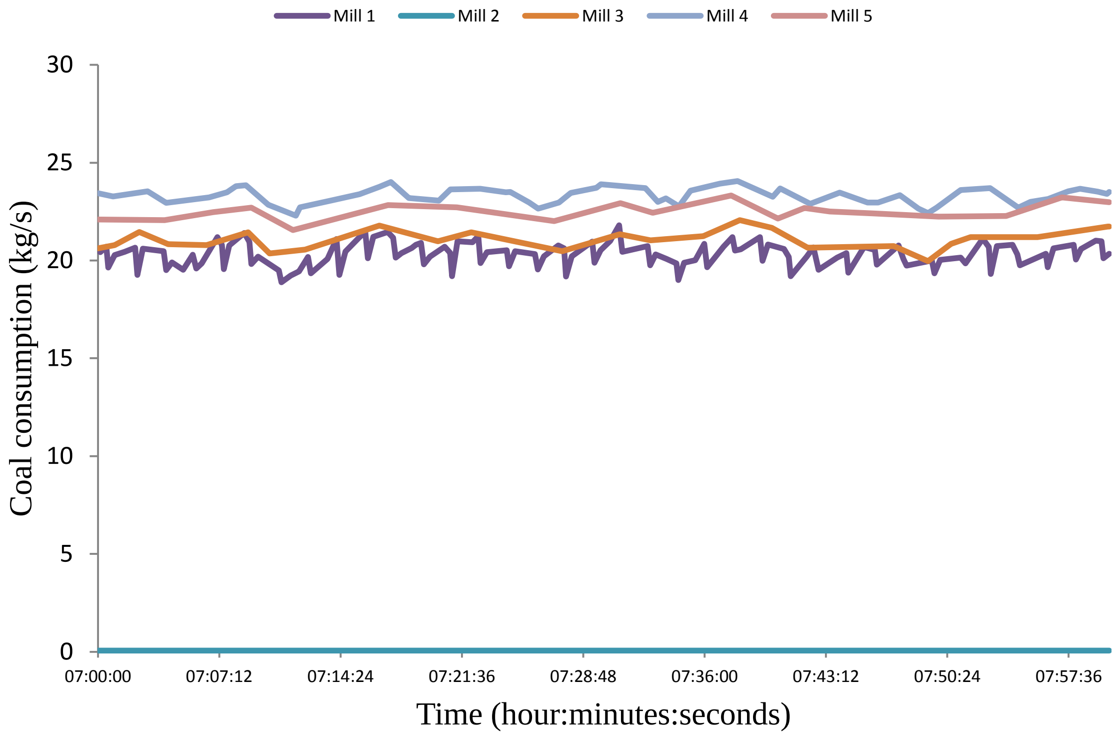


**Figure G.3** Unit 1 coal consumption data for period 4 sample date 05/02/2018

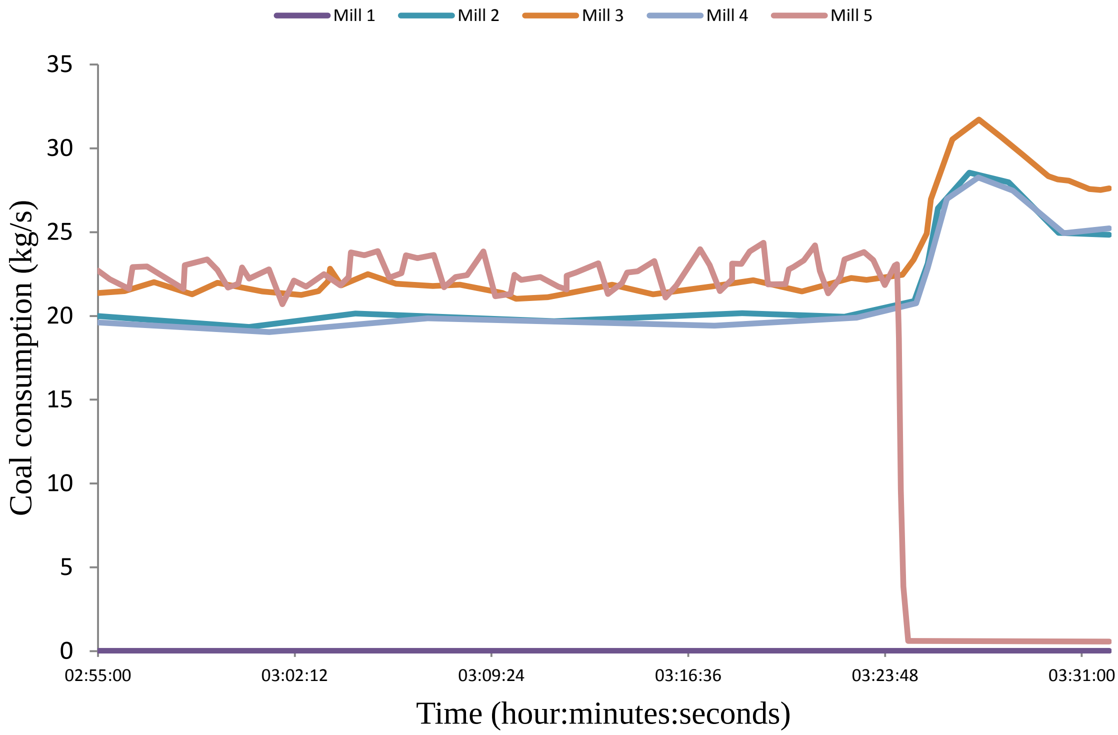


**Figure G.4** Unit 1 coal consumption data for period 5 sample date 12/13/2018

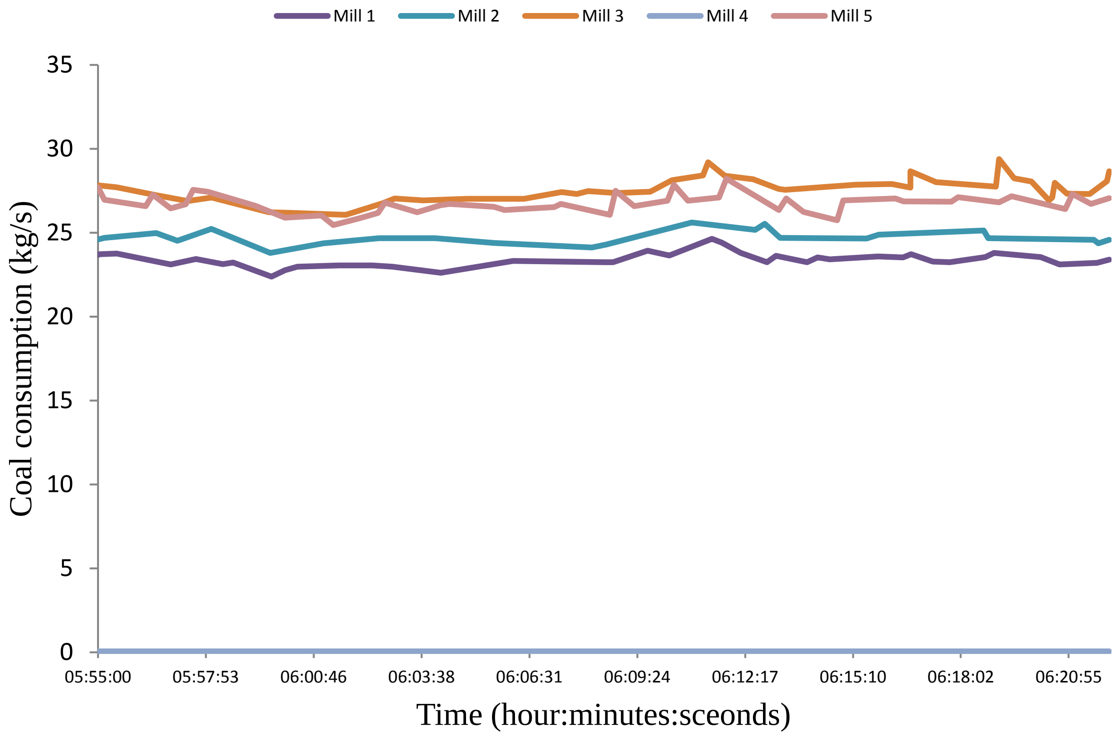


**Figure G.5** Unit 1 coal consumption data for period 6 sample date 03/22/2019

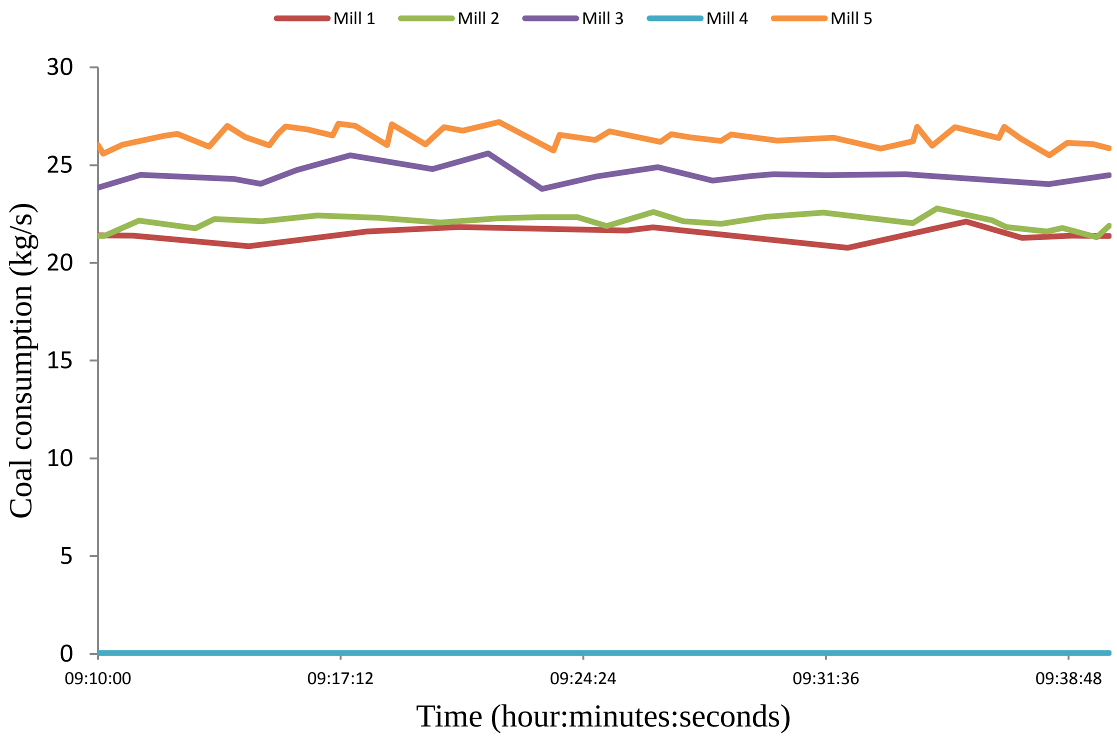


**Figure G.6** Unit 1 coal consumption data for Period 7 sample date 05/08/2019

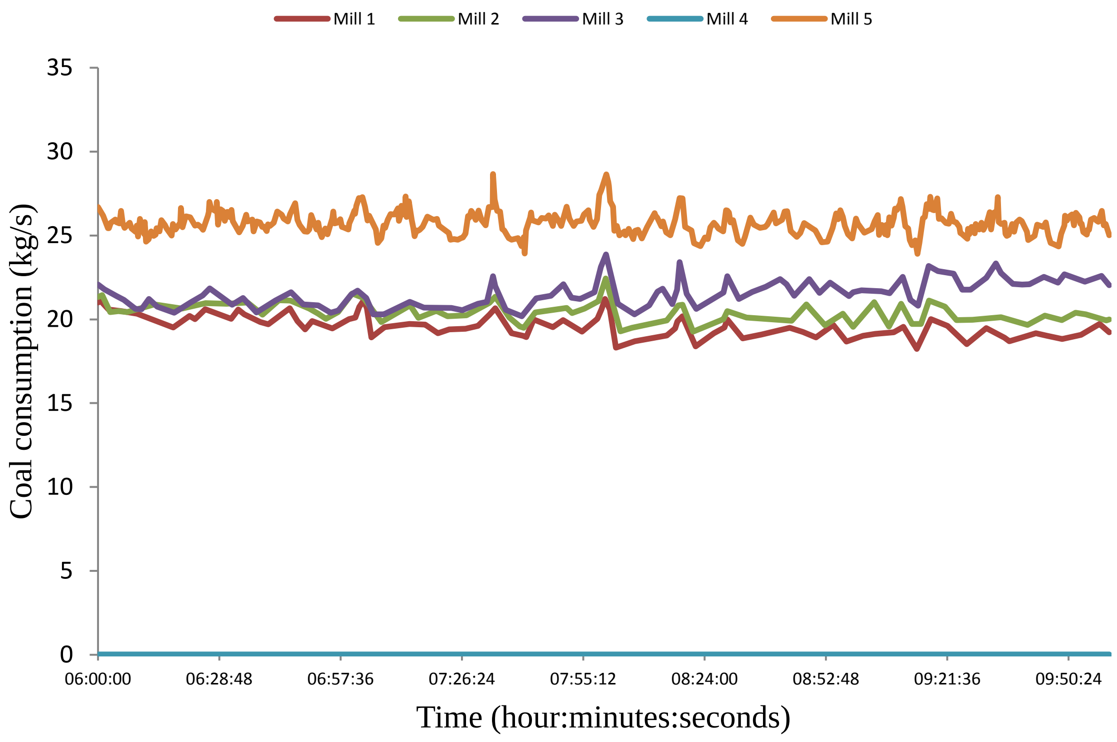


**Figure G.7** Unit 1 coal consumption data for period 8 sample date 07/21/2019

## G2 Unit 2 Coal Consumption Data

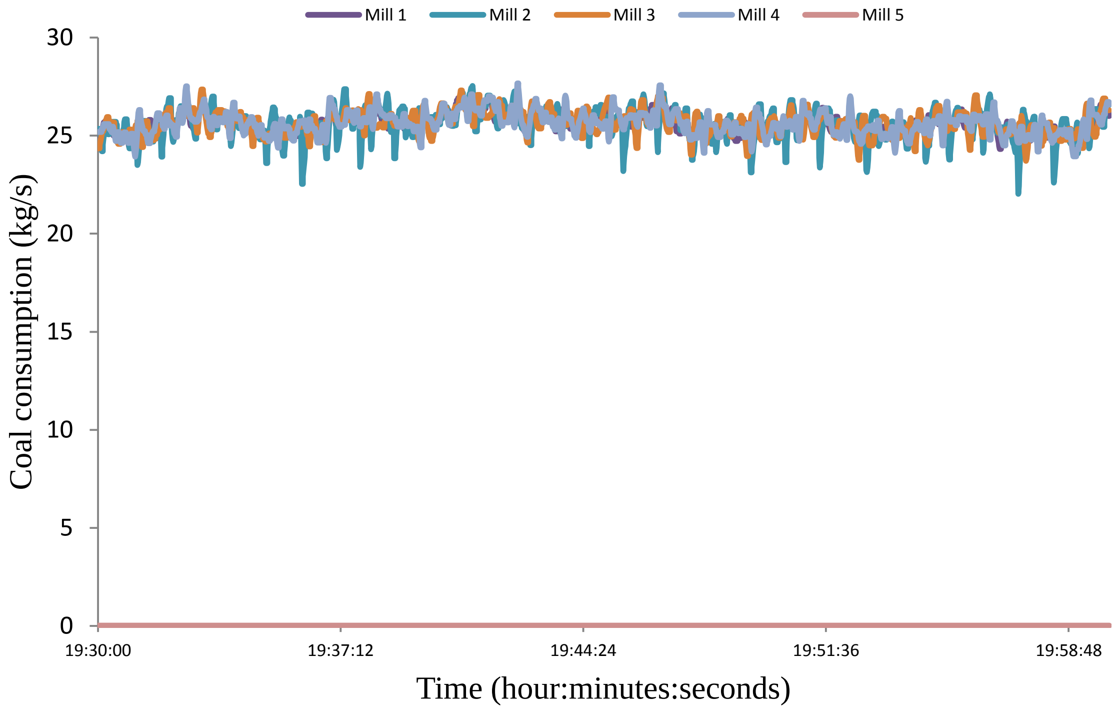


**Figure G.8** Unit 2 coal consumption for period 1, data for 26/09/2017

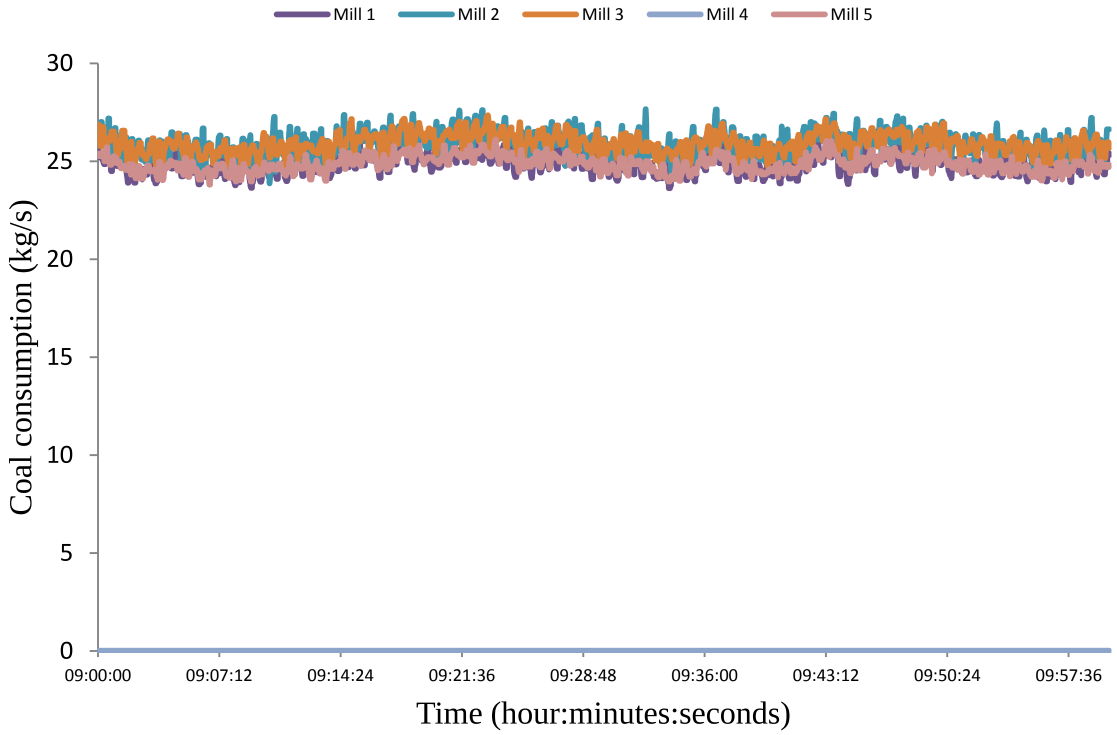


**Figure G.9** Unit 2 coal consumption data for Period 2 sample date for 12/05/2017

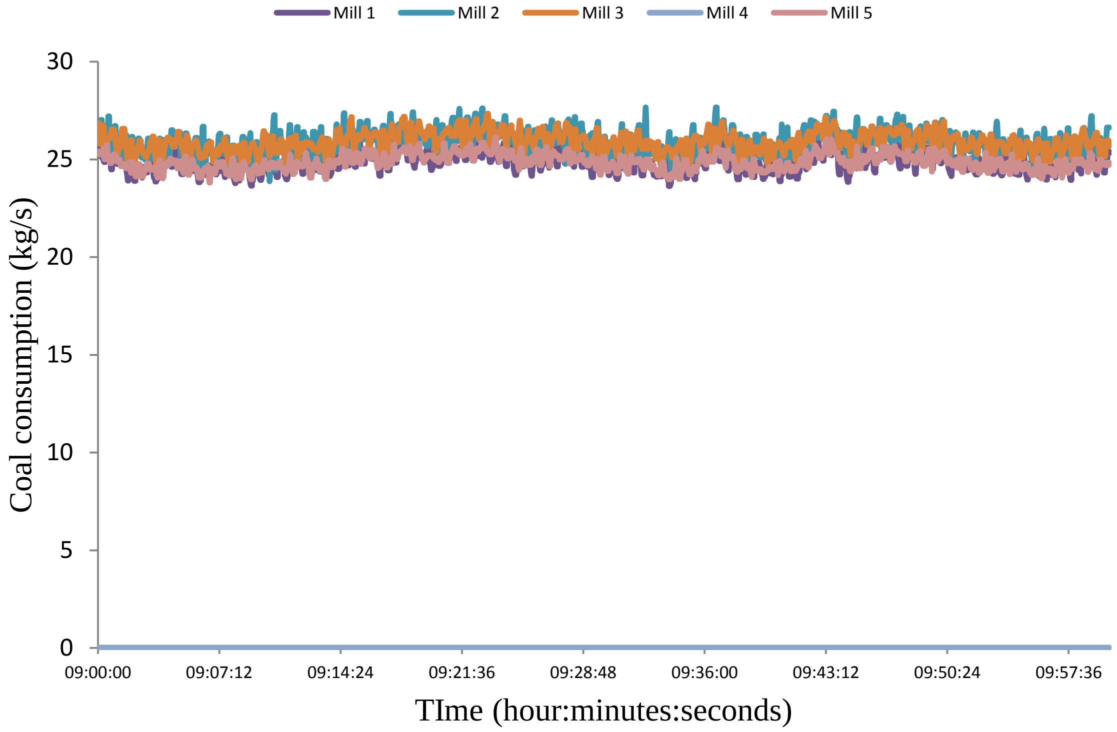


**Figure G.10** Unit 2 coal consumption data for Period 3 sample date 02/27/2018

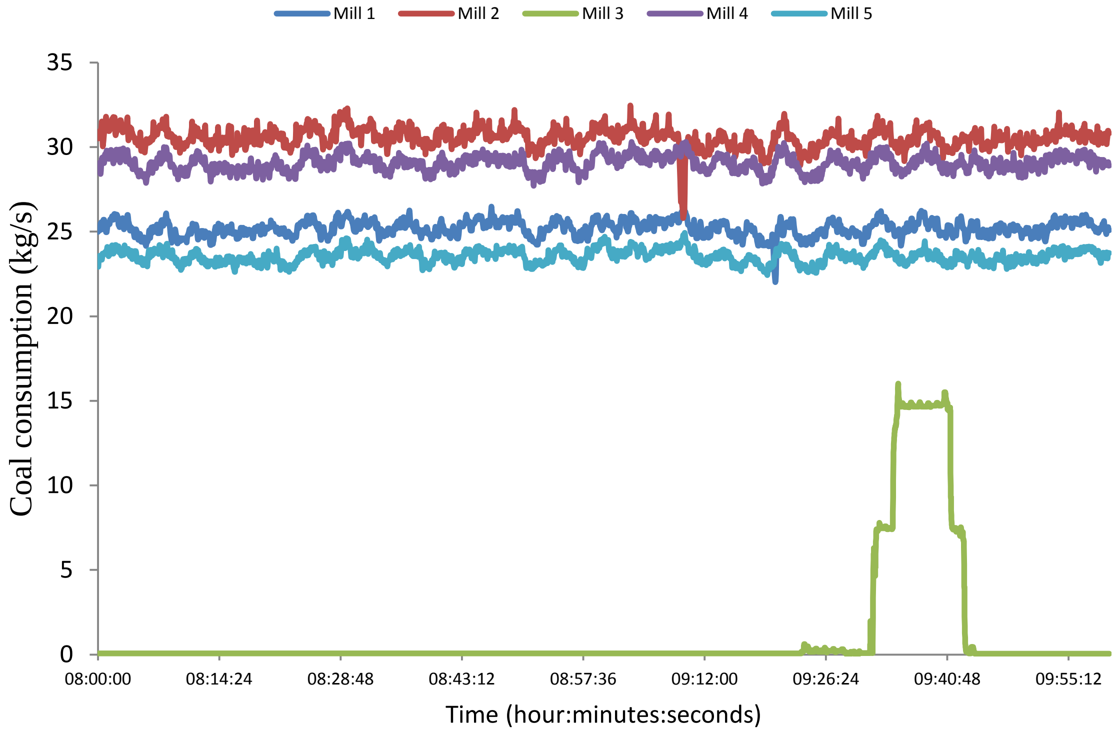


**Figure G.11** Unit 2 coal consumption data for Period 4 sample date 05/11/2018

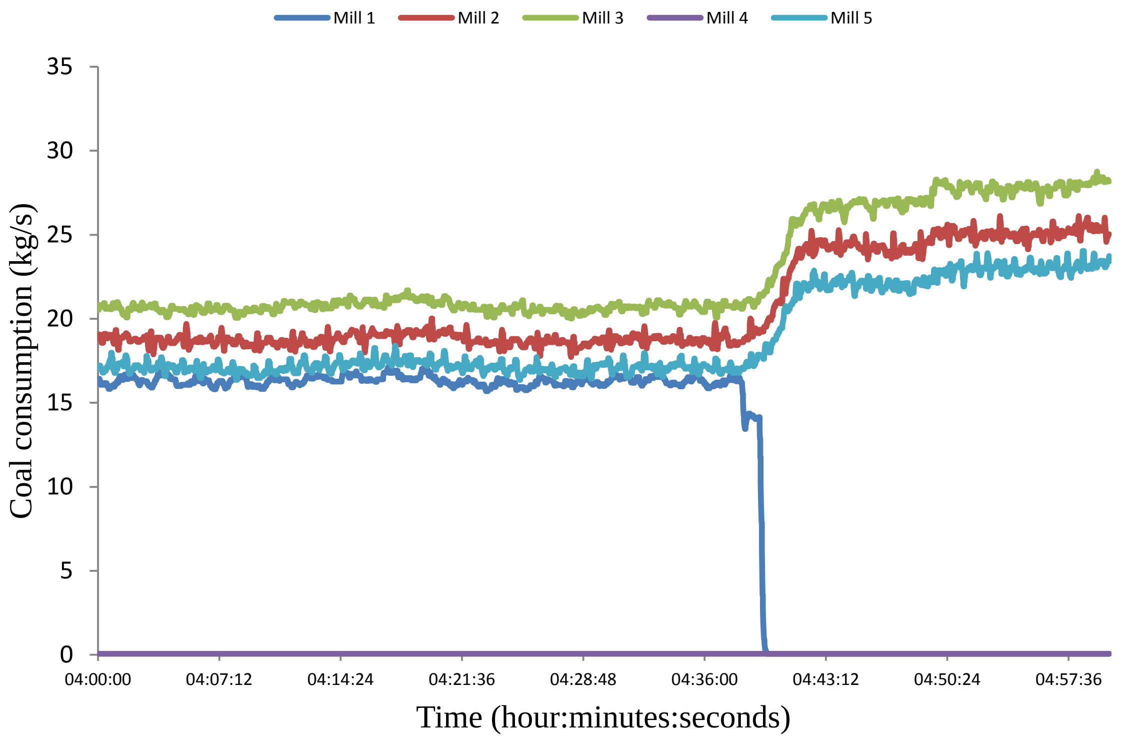


**Figure G.12** Unit 2 coal consumption data for Period 5 sample date 10/17/2018

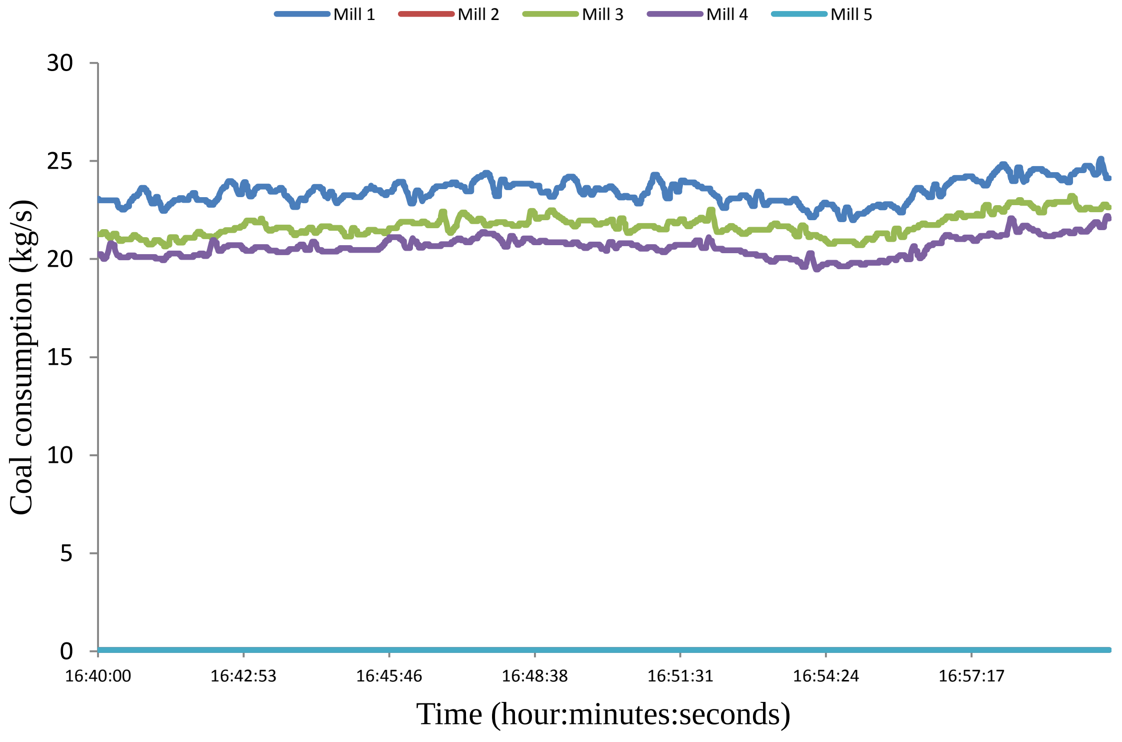


**Figure G.13** Unit 2 coal consumption data for Period 6 sample date 04/22/2019

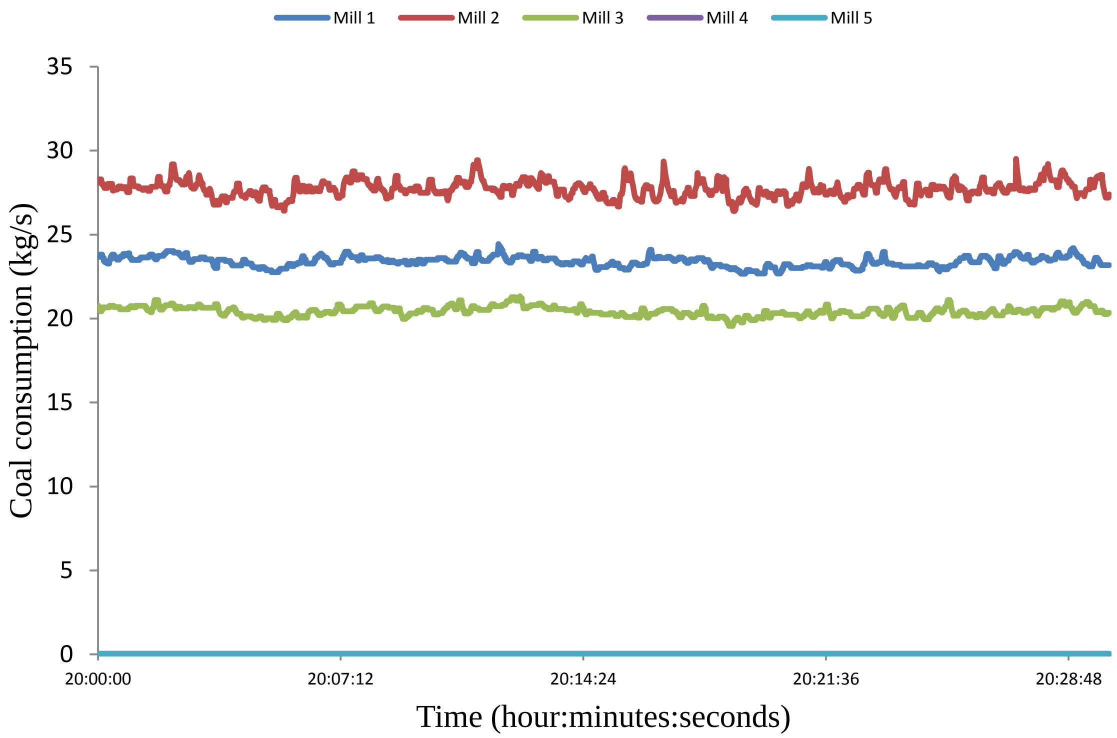


**Figure G.14** Unit 2 coal consumption data for Period 7 sample date 07/12/2019

## G3 Unit 3 Coal Consumption Data

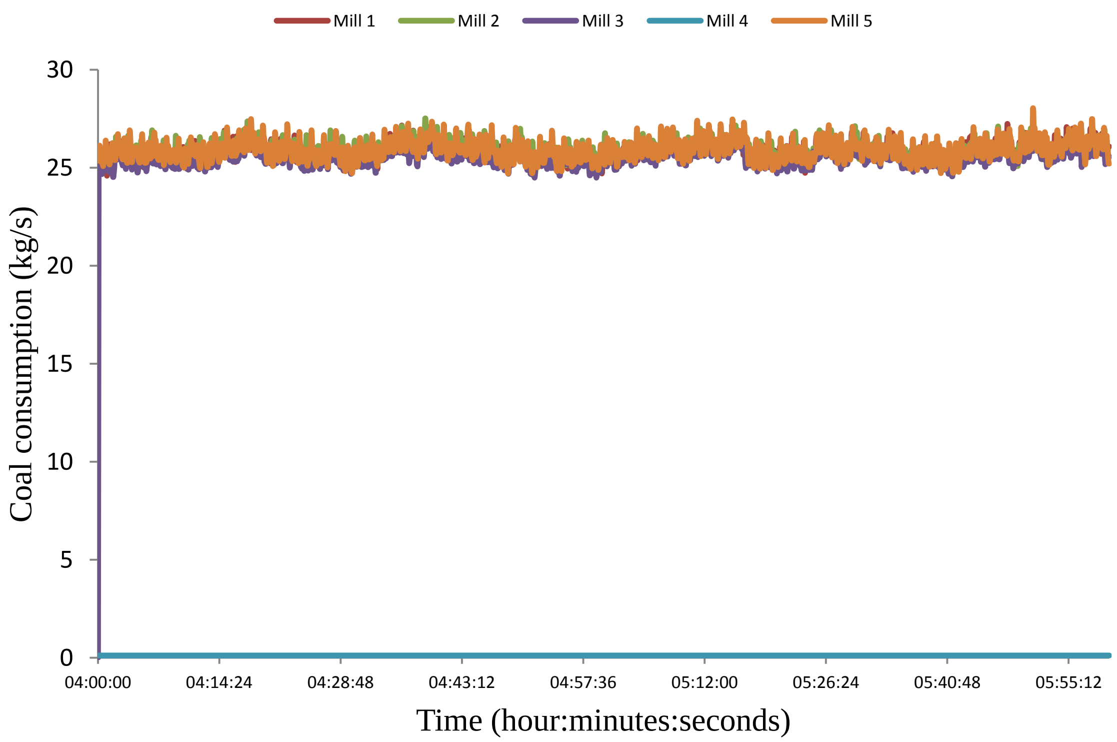


**Figure G.15** Unit 3 Coal consumption data for Period 1 sample date 09/11/2017

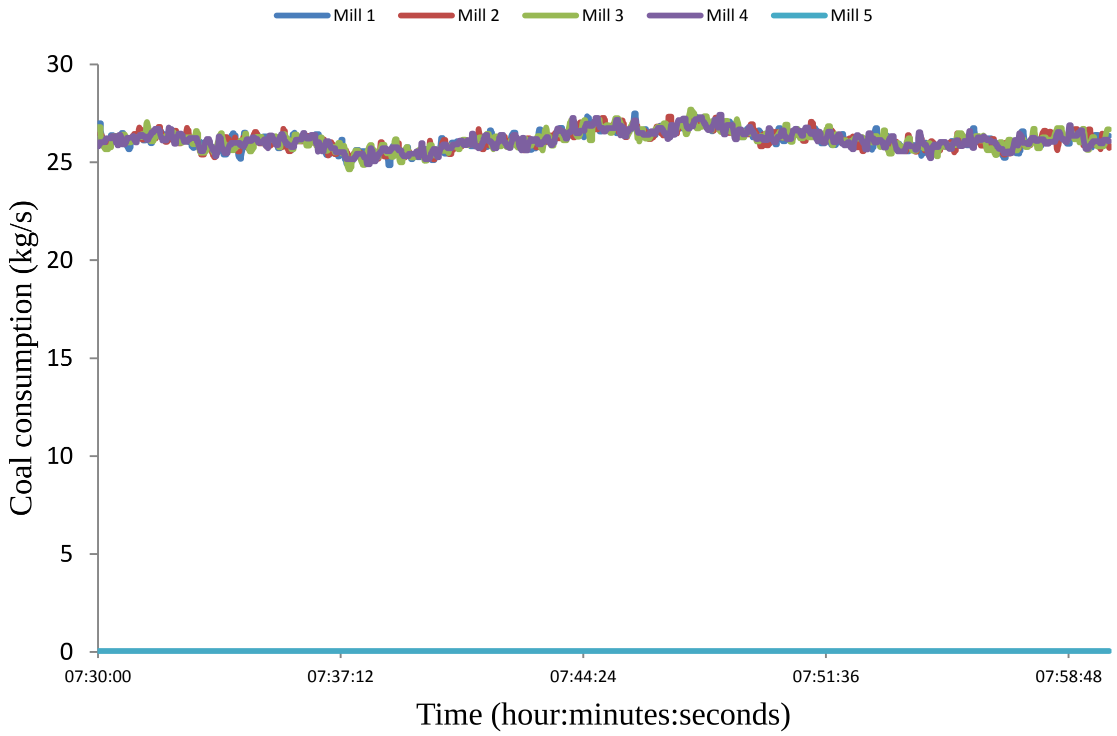


**Figure G.16** Unit 3 coal consumption data for Period 2 sample date 10/29/2017

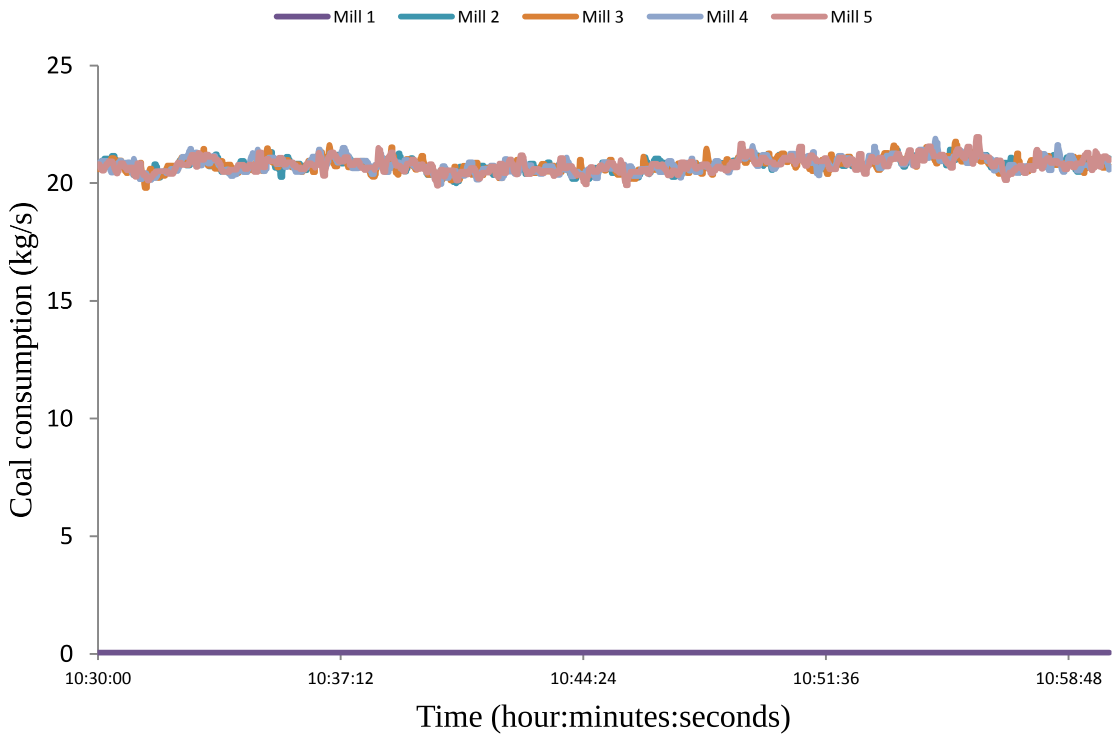


**Figure G.17** Unit 3 coal consumption data for Period 3 sample date 01/01/2018


**Figure G.18** Unit 3 coal consumption data for Period 4 sample date 03/20/2018

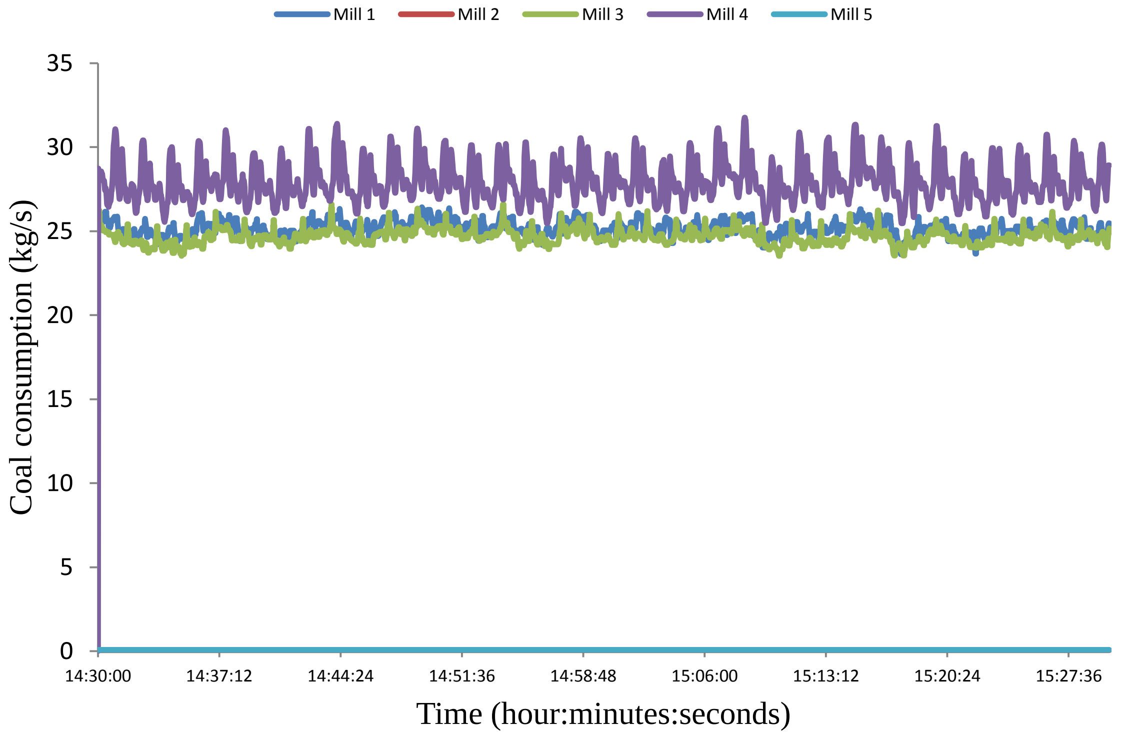


**Figure G.19** Unit 3 coal consumption data for Period 5 sample date 07/13/2018

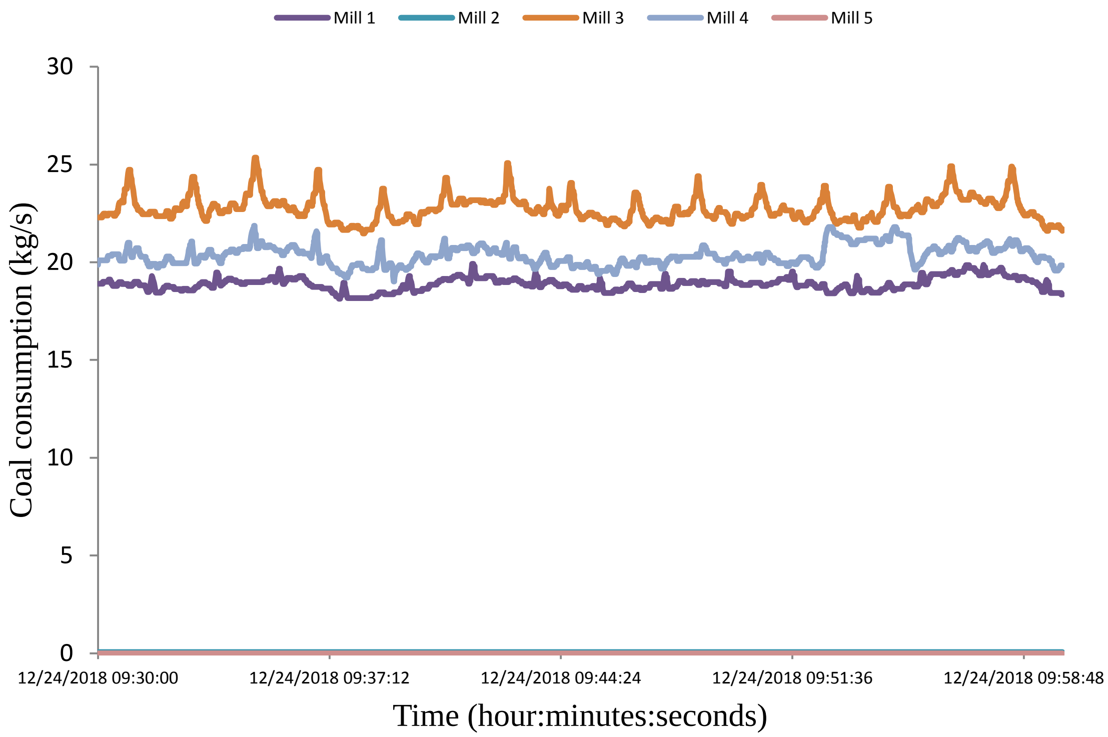


**Figure G.20** Unit 3 coal consumption data for Period 6 sample date 12/24/2018

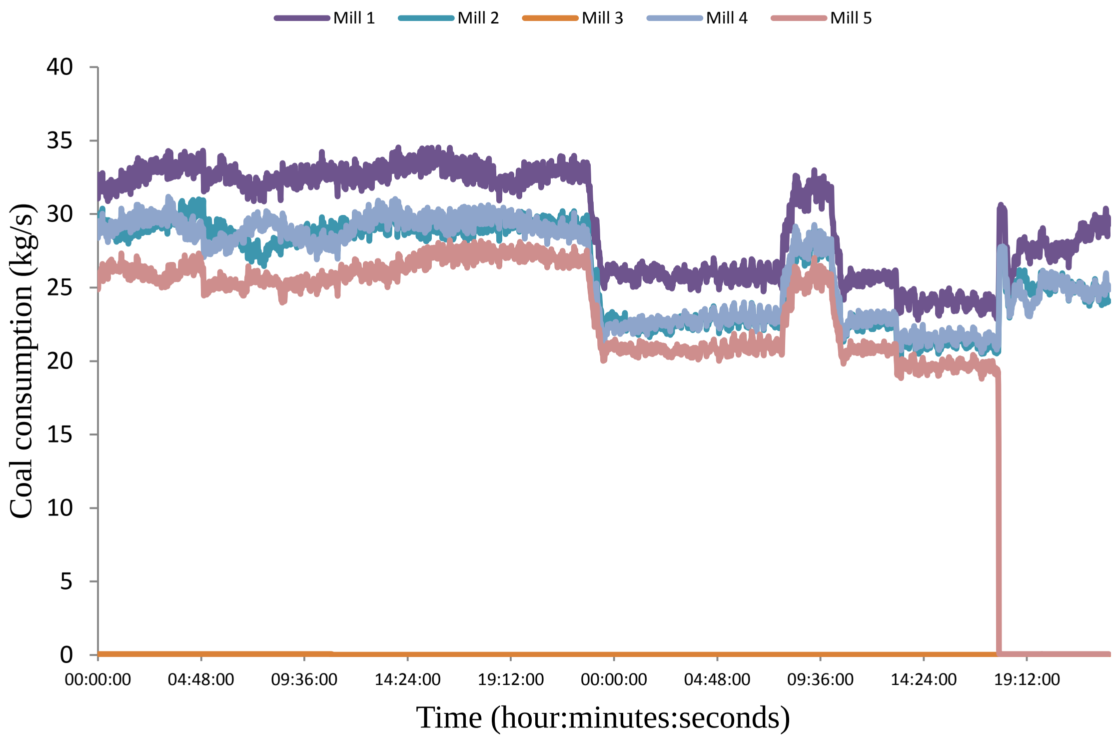


**Figure G.21** Unit 3 coal consumption data for Period 7 sample date 05/04/2019

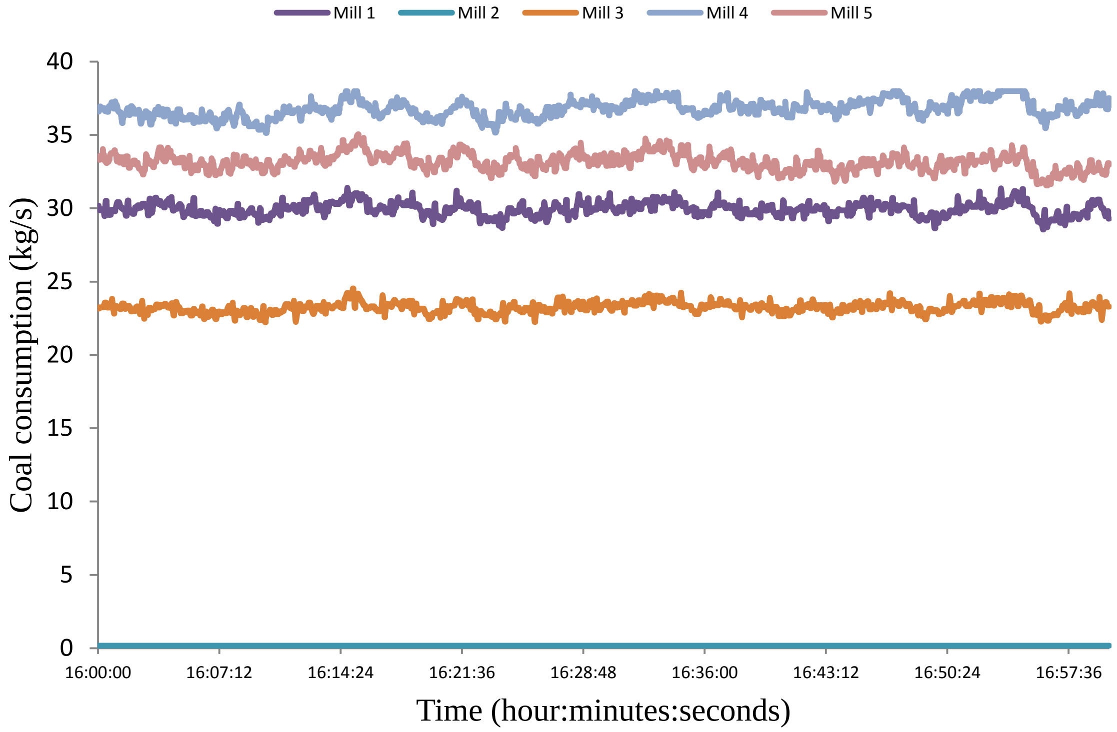


**Figure G.22** Unit 3 coal consumption data for Period 8 sample date 07/01/2019

# APPENDIX H CONVEYING PRESSURE AND AIR FLOW RATE

Conveying pressure readings for the periods as defined in Table 5.2 (Unit 1), Table 5.1 (Unit 2) and Table 5.3 (Unit 3) are included in this section.

## H1 Unit 1 Conveying Pressure and Air Flow rate Data

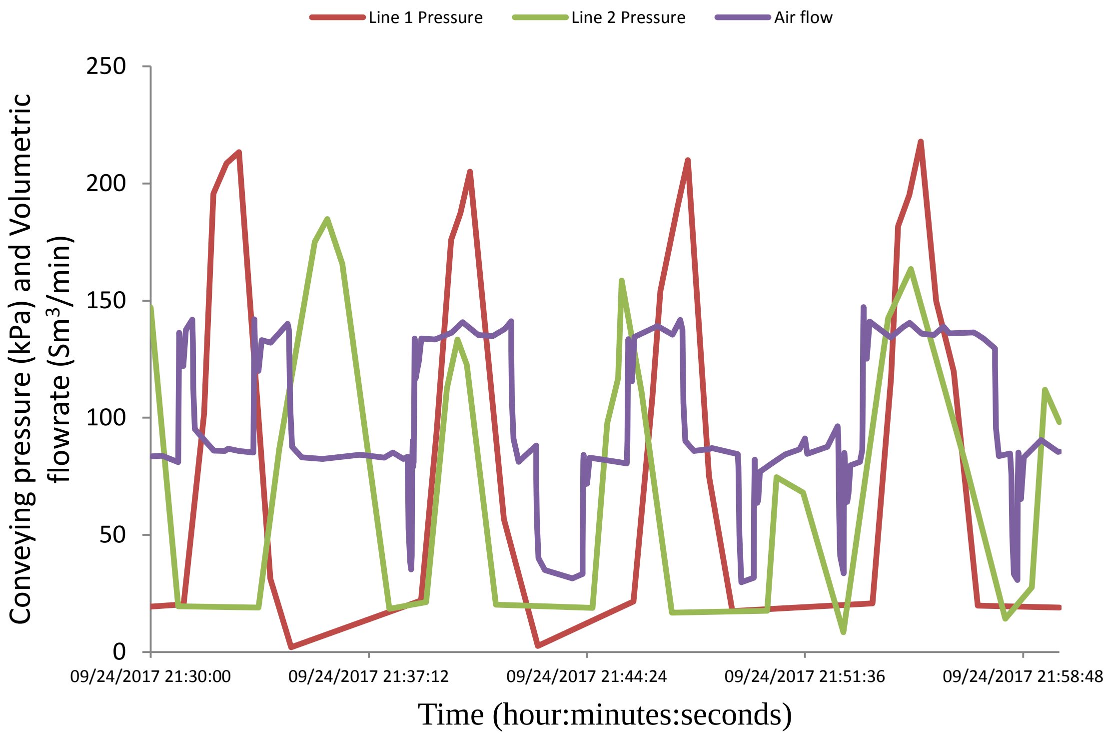


**Figure H.1** Unit 1 conveying pressure and air flowrate for Period 1 sample date 09/24/2017

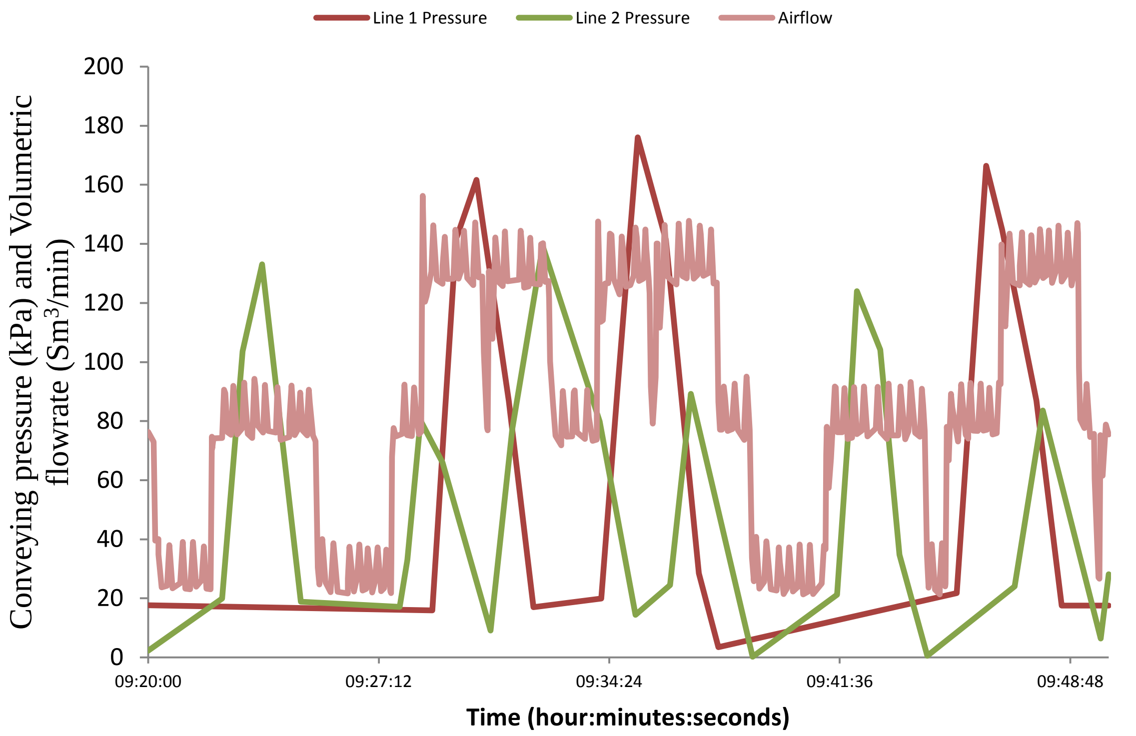


**Figure H.2** Unit 1 conveying pressure and air flow for Period 2 sample date 10/12/2017

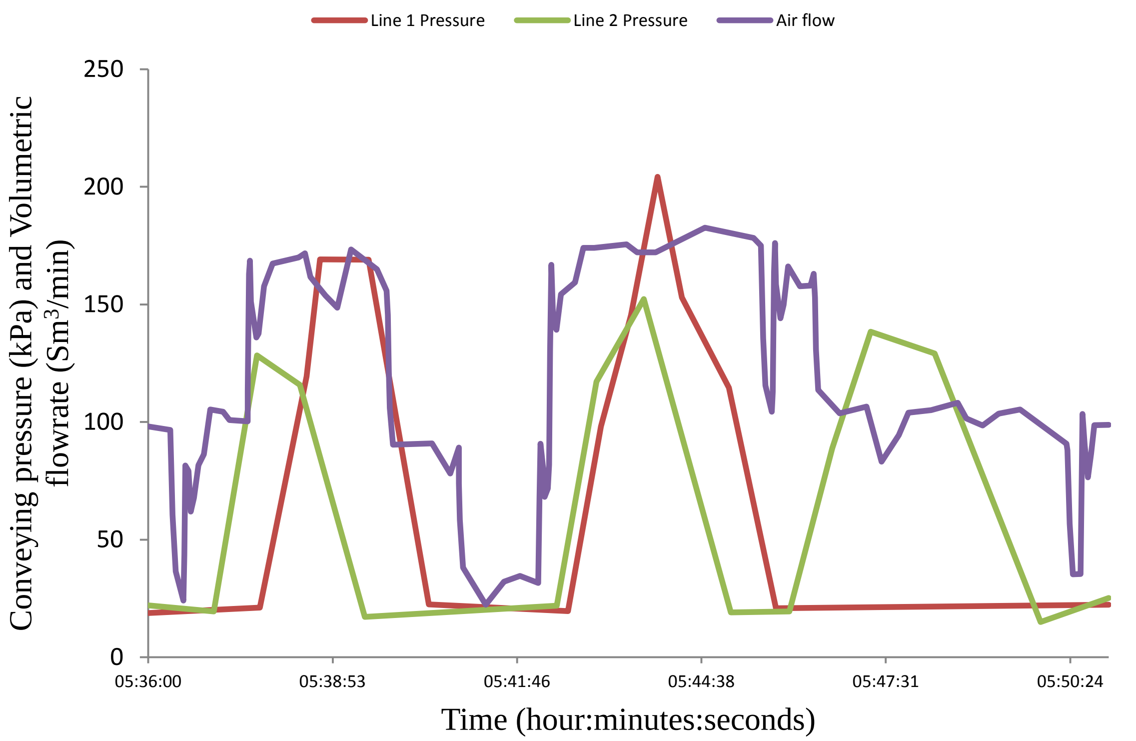


**Figure H.3** Unit 1 conveying pressure and air flow rate for Period 3 sample date 01/18/2018

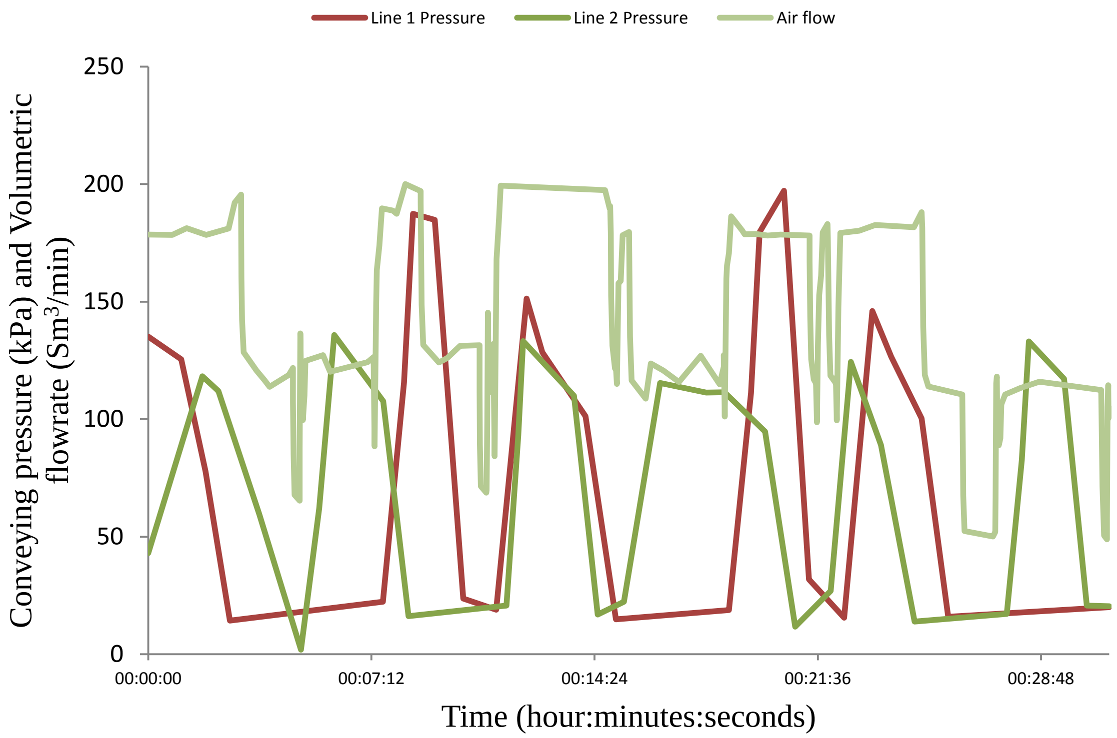


**Figure H.4** Unit 1 conveying pressure and air flowrate for Period 4 sample date 05/02/2018

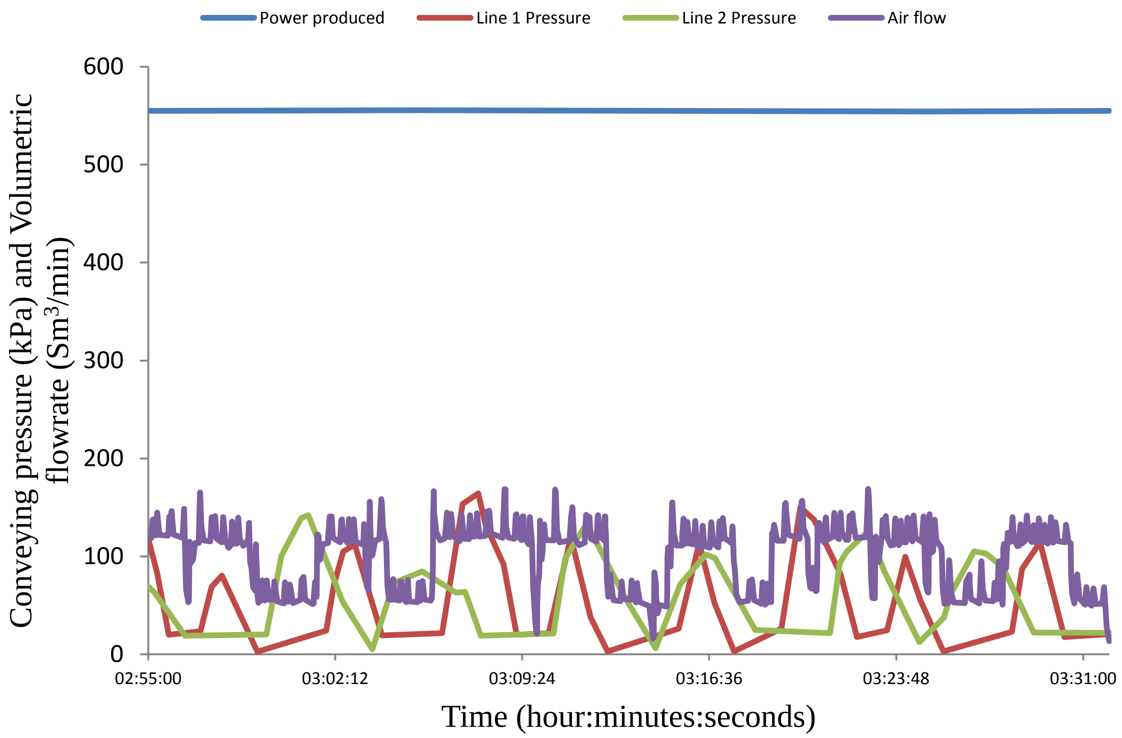


**Figure H.5** Unit 1 conveying pressure and air flowrate for Period 5 sample date 12/13/2018

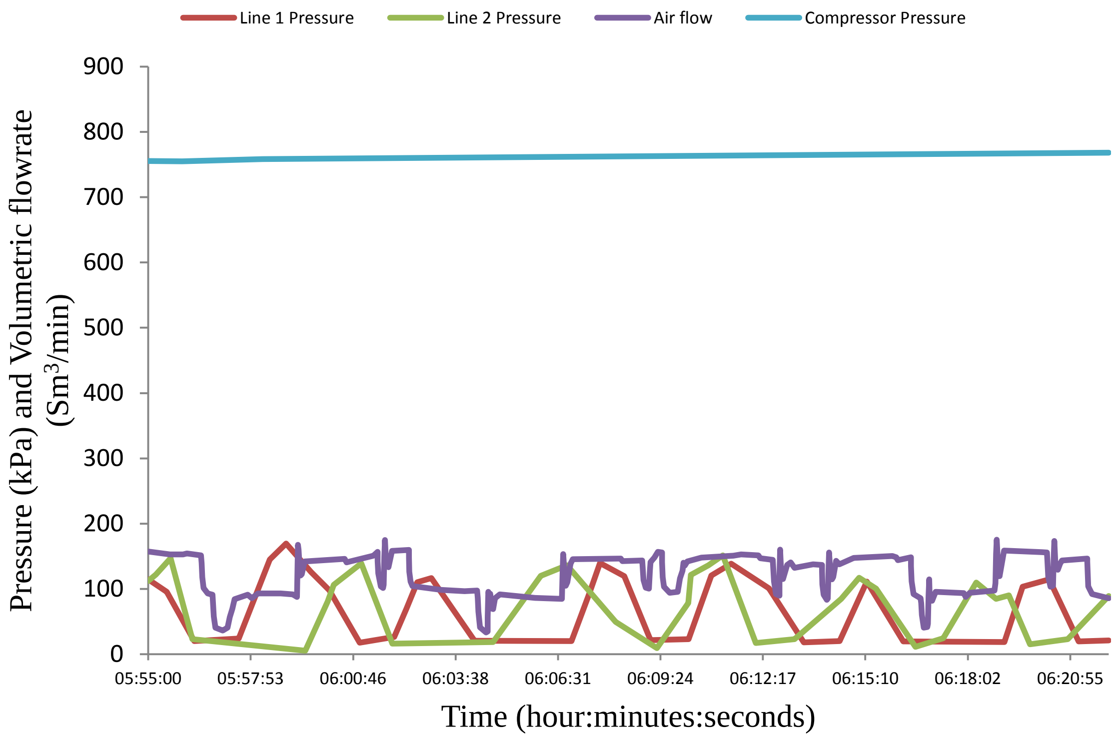


**Figure H.6** Unit 1 conveying pressure and air flowrate data for Period 6 sample date 03/22/2019

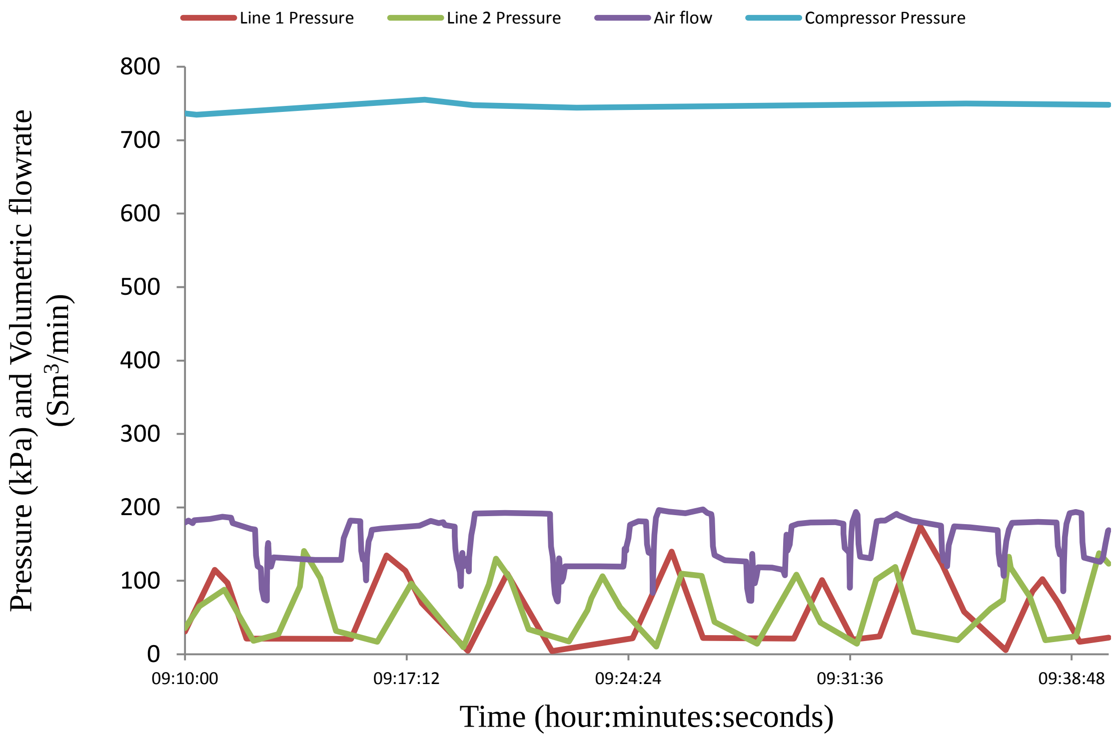


**Figure H.7** Unit 1 conveying pressure and air flow rate for Period 7 sample date 05/08/2019

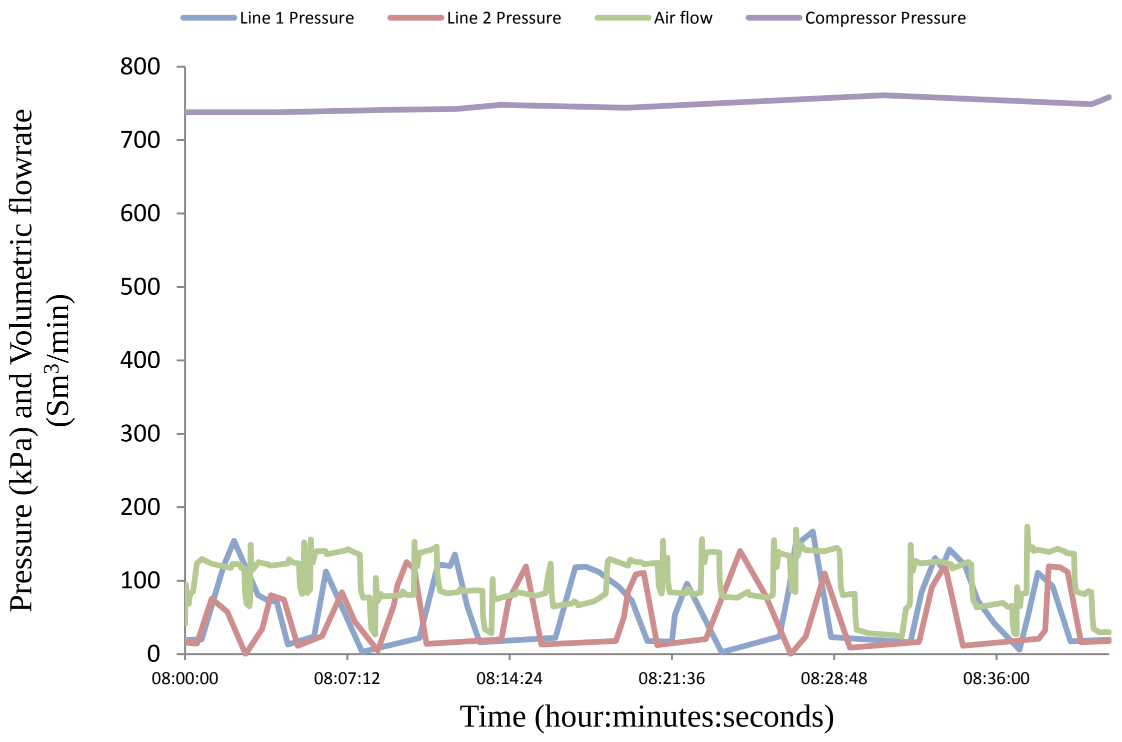


**Figure H.8** Unit 1 conveying pressure and air flow rate for Period 8 sample date 07/21/2019

## H2 Unit 2 Conveying Pressure and Air Flow rate Data

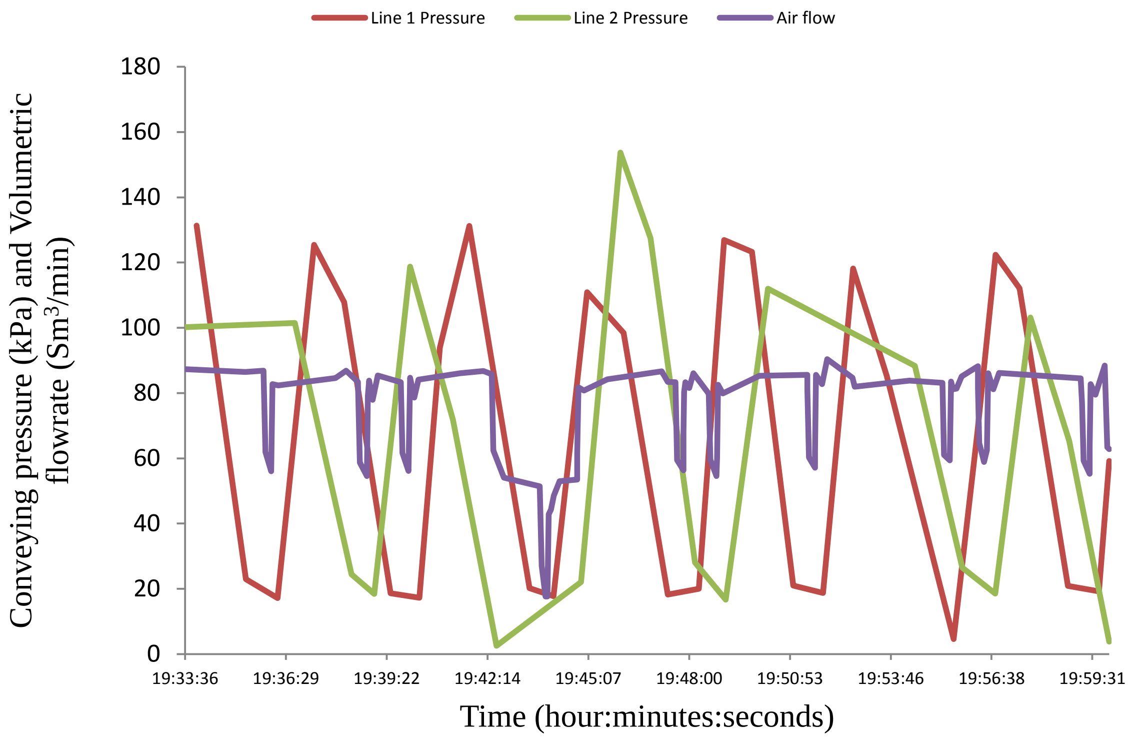


**Figure H.9** Unit 2 conveying pressure and air flow rate for Period 1 sample date 26/09/2017

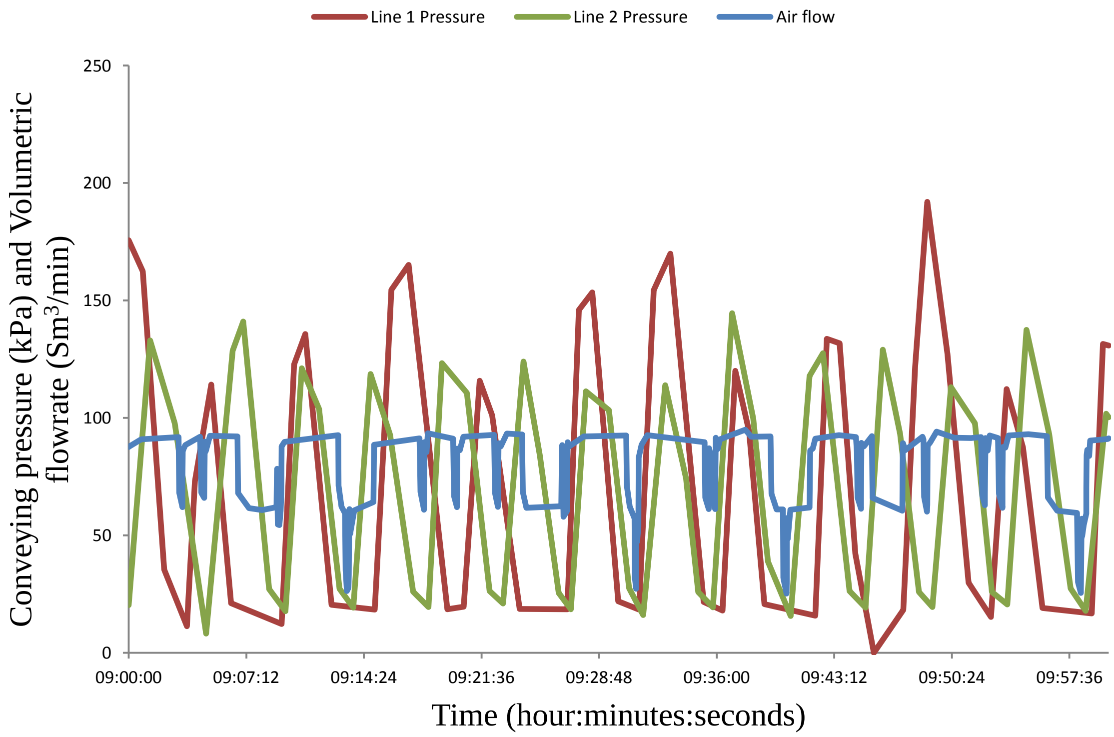


**Figure H.10** Unit 2 conveying pressure and air flow rate for Period 2 sample date 12/05/2017

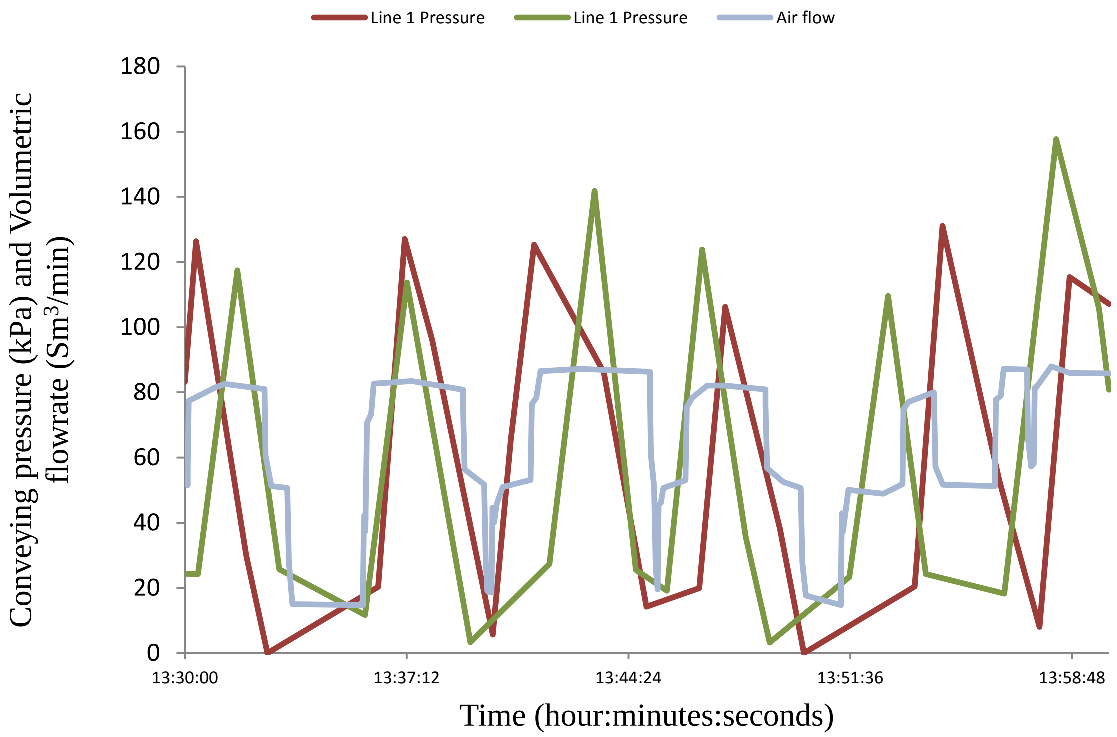


**Figure H.11** Unit 2 conveying pressure and air flowrate for Period 3 sample date 02/27/2018

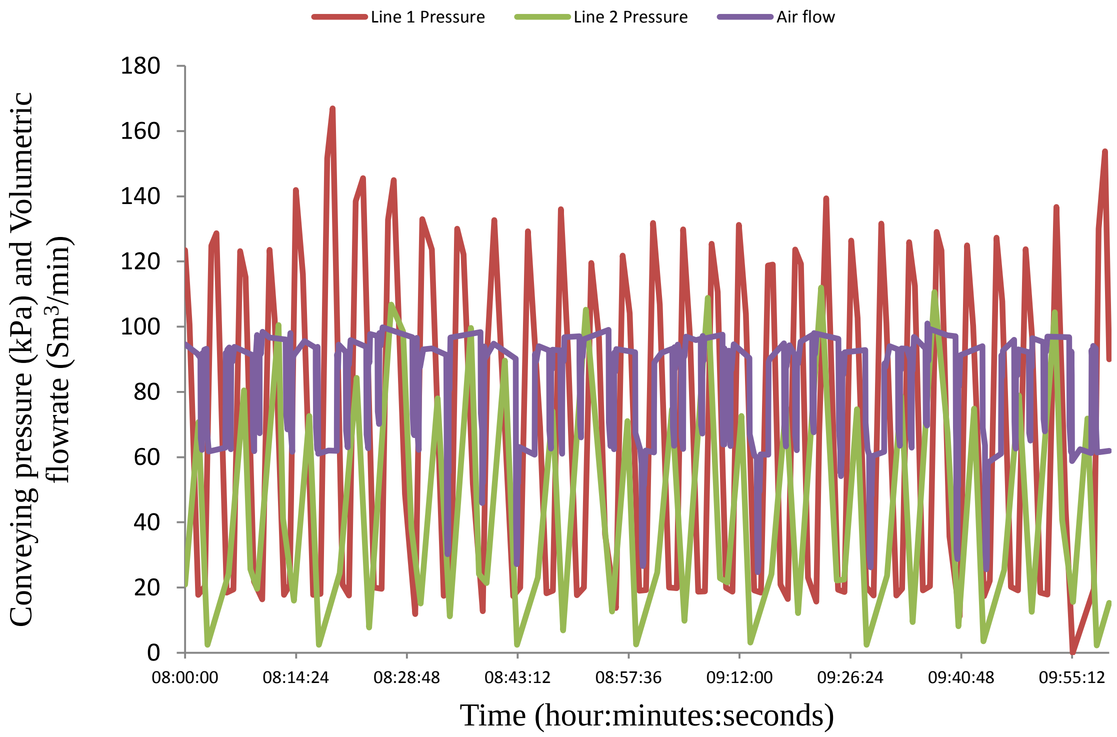


**Figure H.12** Unit 2 conveying pressure and air flow rate for Period 4 sample date 05/11/2018

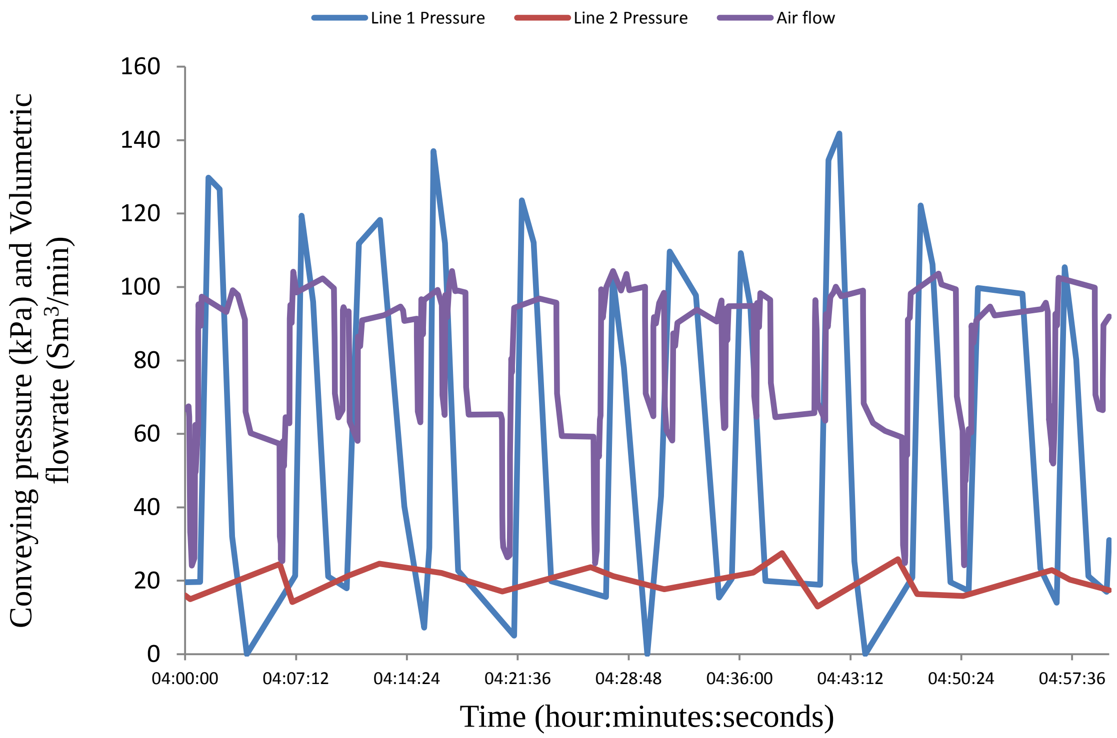


**Figure H.13** Unit 2 conveying pressure and air flow rate for Period 5 sample date 10/17/2018

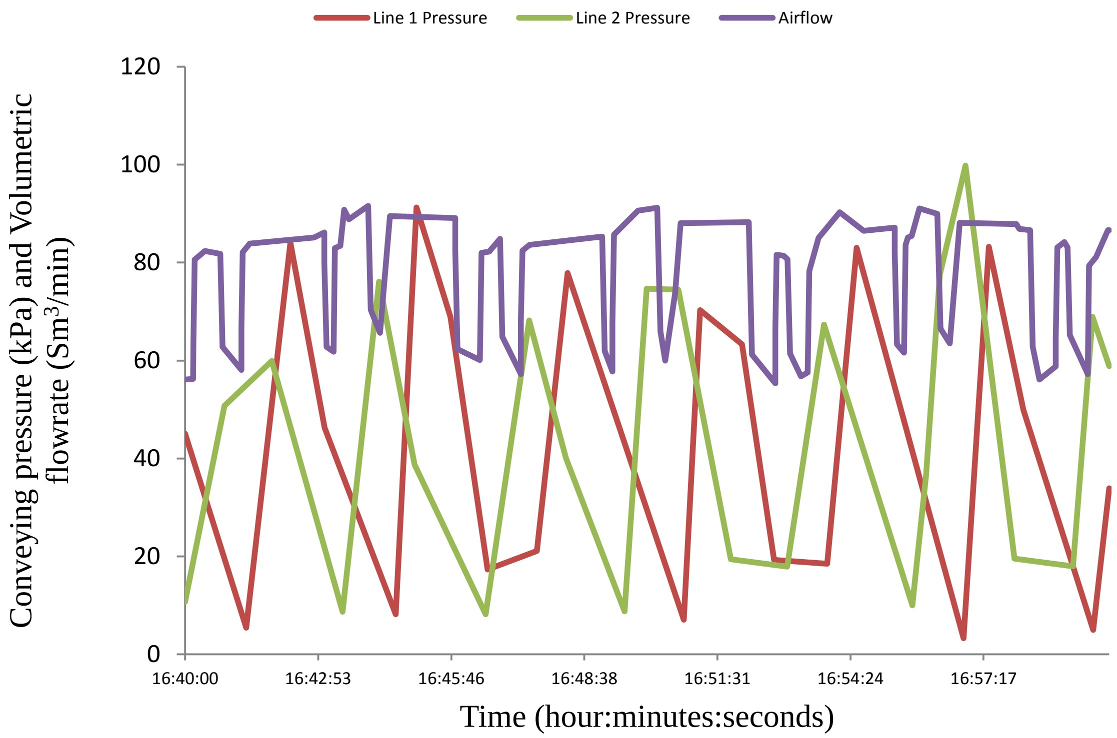


**Figure H.14** Unit 2 conveying pressure and air flow rate for Period 6 sample date 04/22/2019

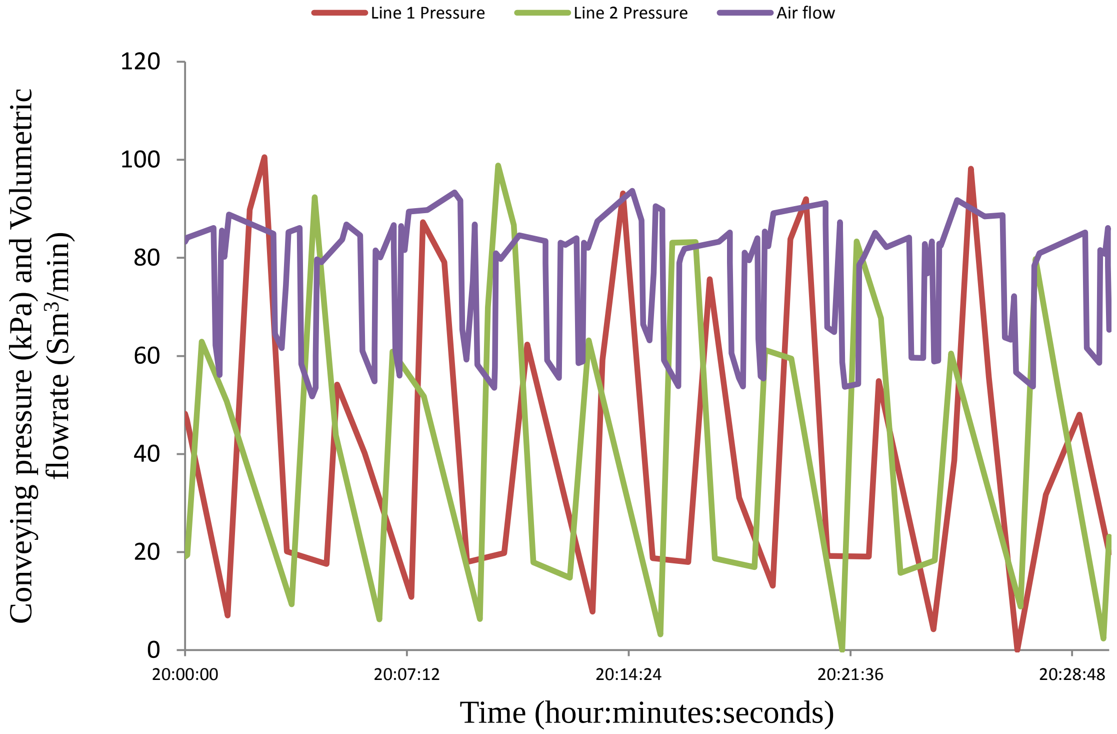


**Figure H.15** Unit 2 conveying pressure and air flow rate for Period 7 sample date 07/12/2019

## H3 Unit 3 Conveying Pressure and Air Flow rate Data

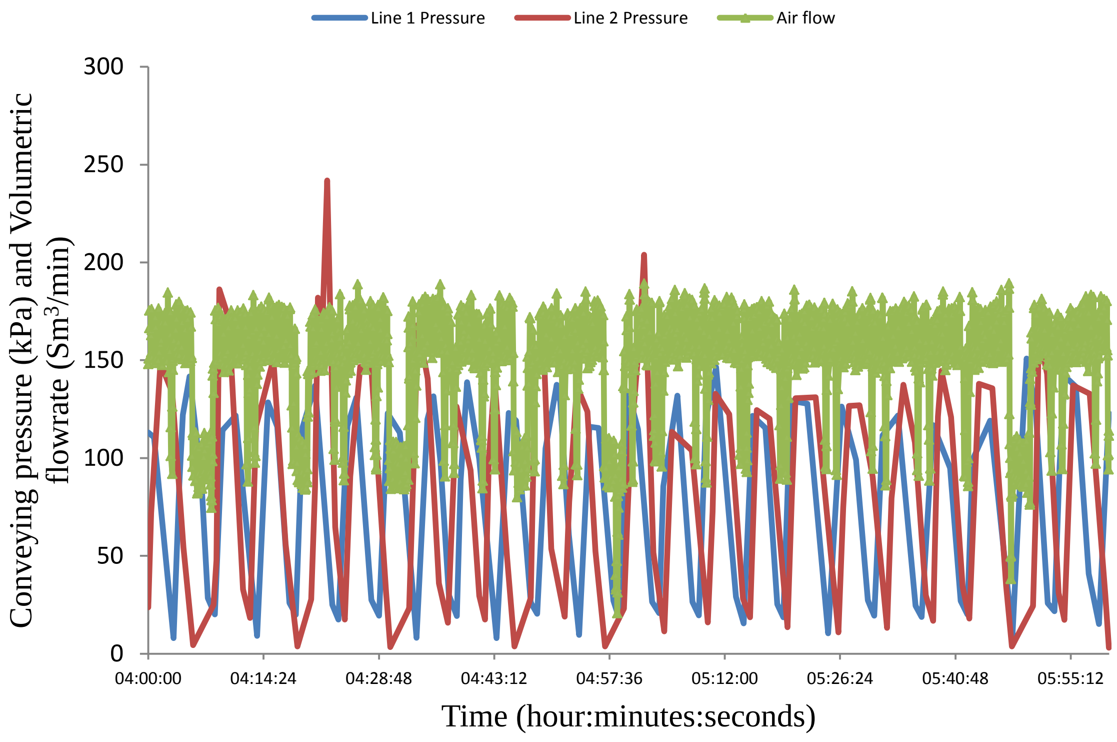


**Figure H.16** Unit 3 conveying pressure and air flow rate for Period 1 sample date 09/11/2017

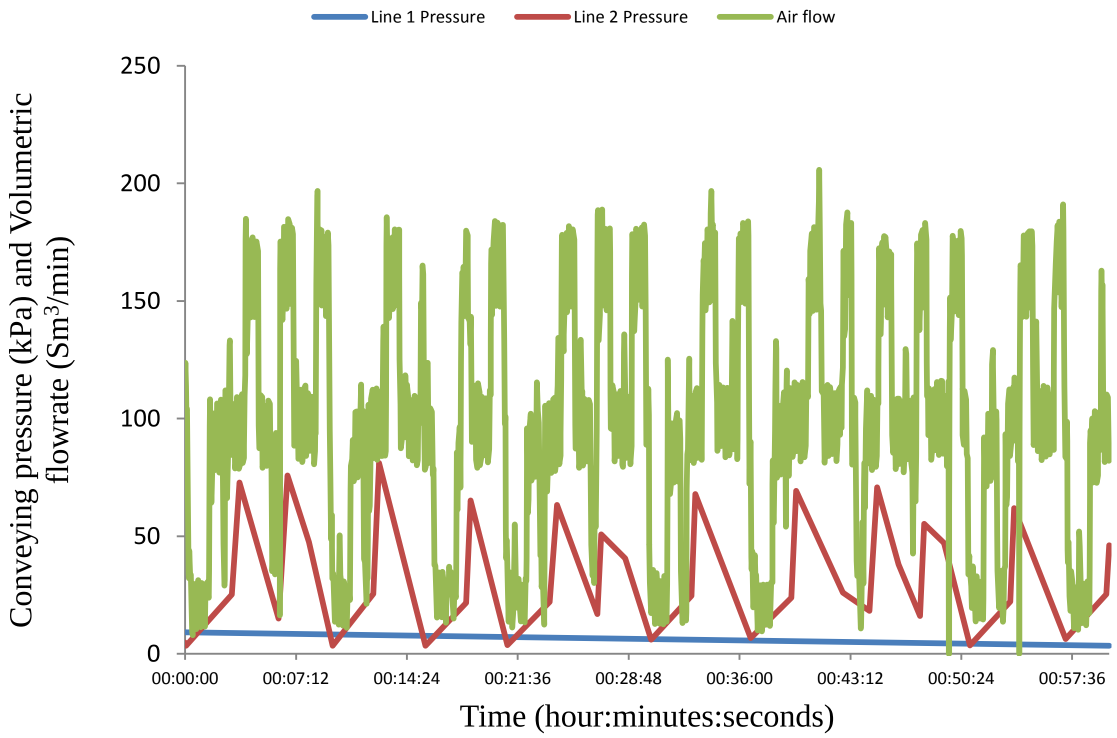


**Figure H.17** Unit 3 conveying pressure and air flow rate for Period 2 sample date 10/30/2017

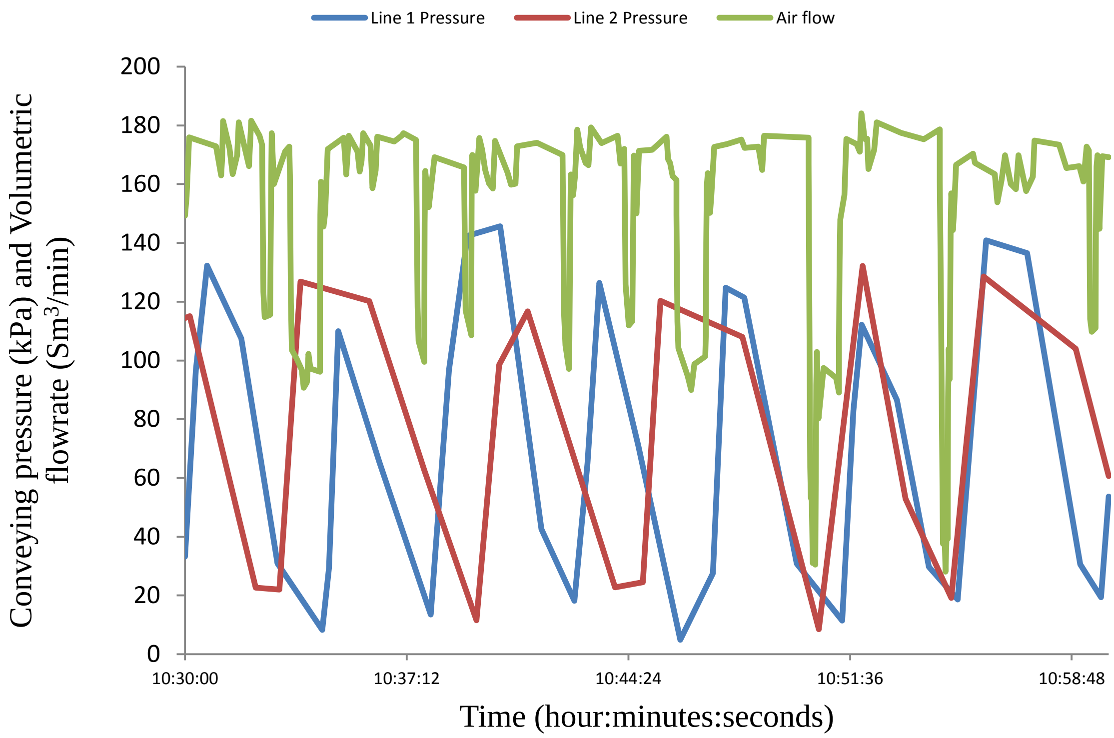


**Figure H.18** Unit 3 conveying pressure and air flow rate for Period 3 sample date 01/01/2018

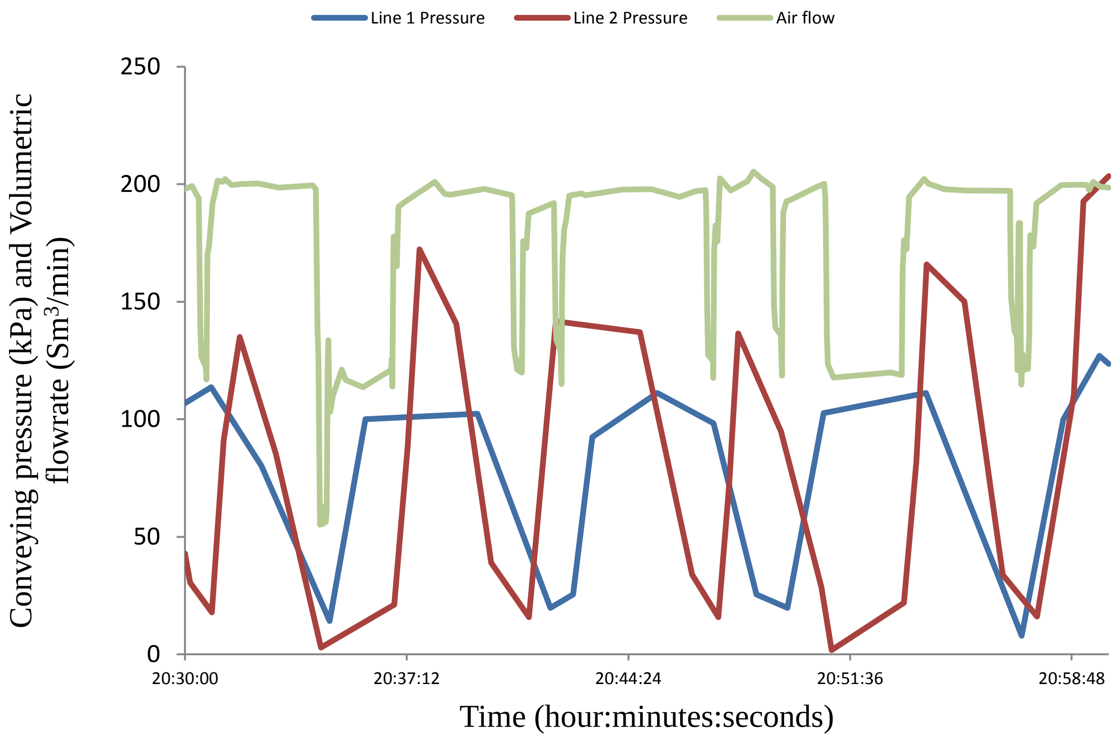


**Figure H.19** Unit 3 conveying pressure and air flow rate for Period 4 sample date 03/20/2018

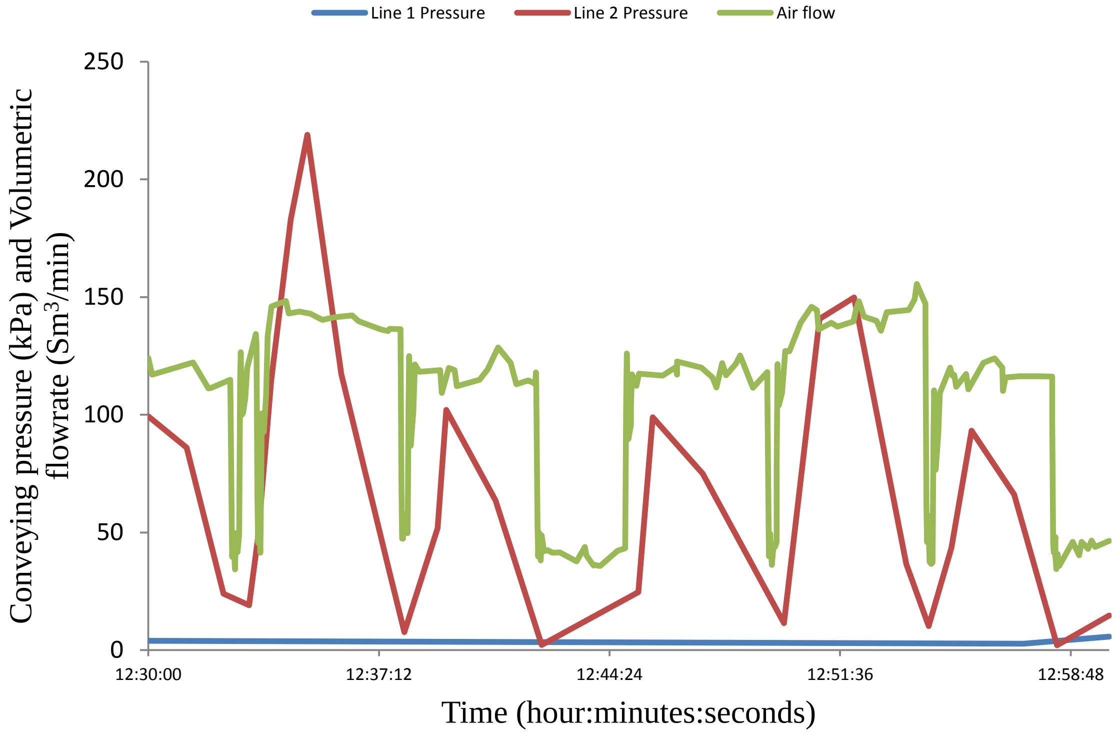


**Figure H.20** Unit 3 conveying pressure and air flow rate for Period 5 sample date 08/29/2018

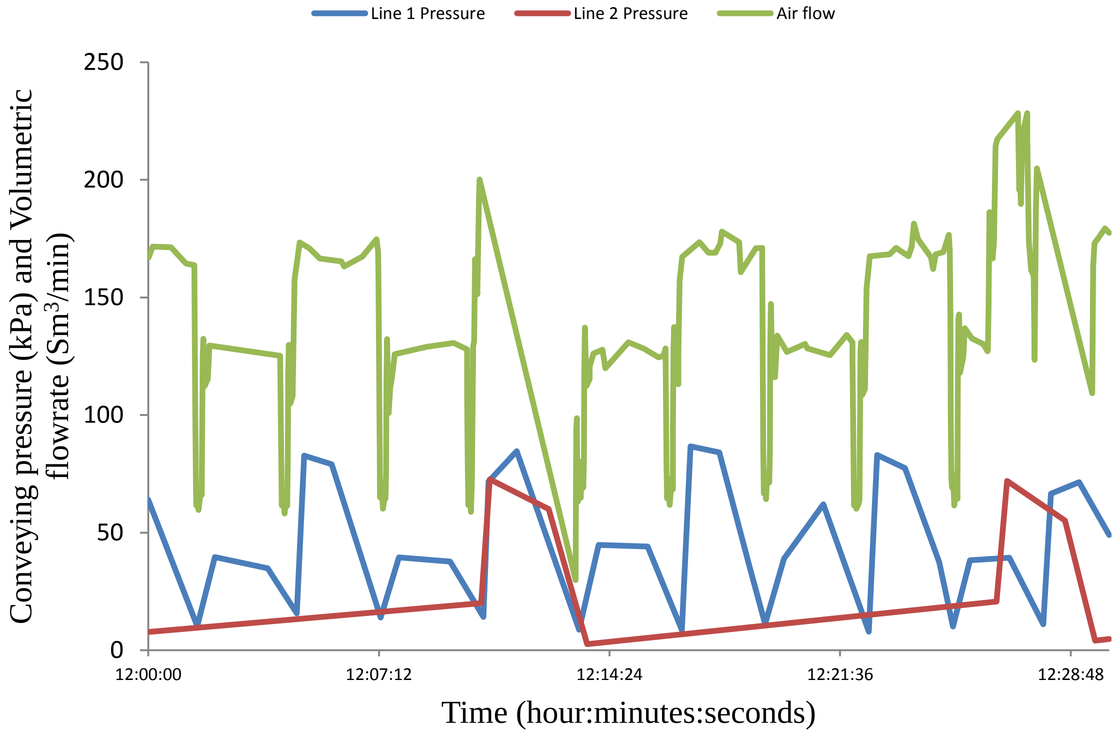


**Figure H.21** Unit 3 conveying pressure and air flow rate for Period 6 sample date 12/24/2018

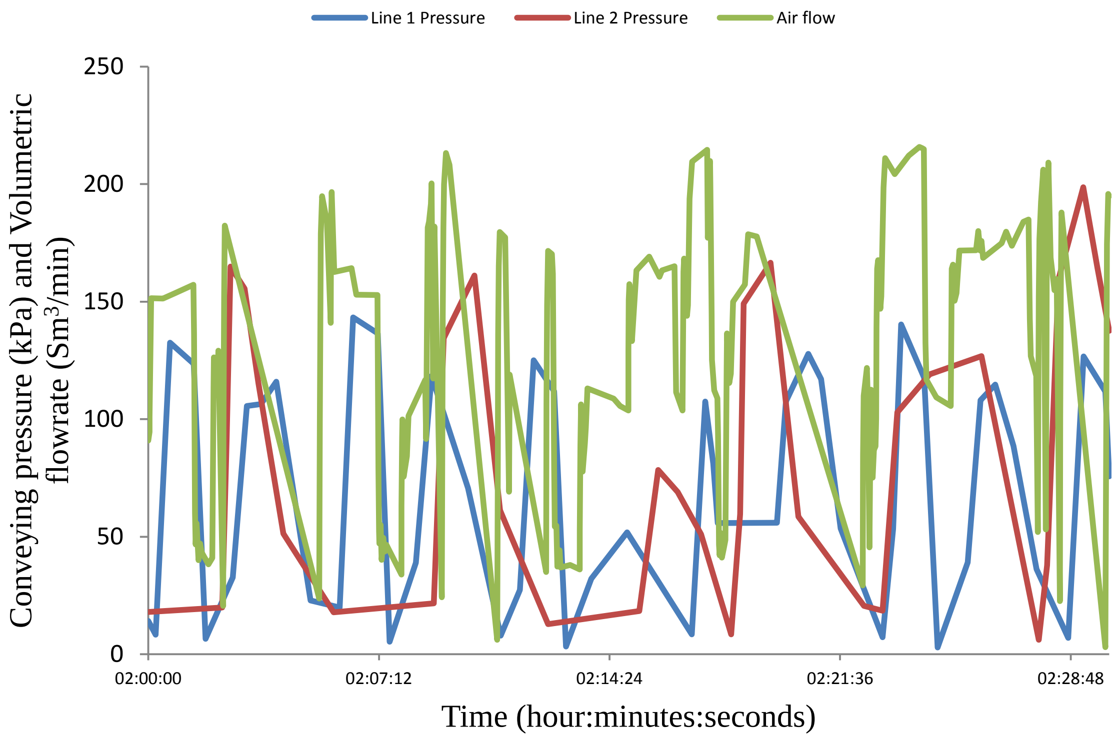


**Figure H.22** Unit 3 conveying pressure and air flow rate for Period 7 sample date 05/03/2019

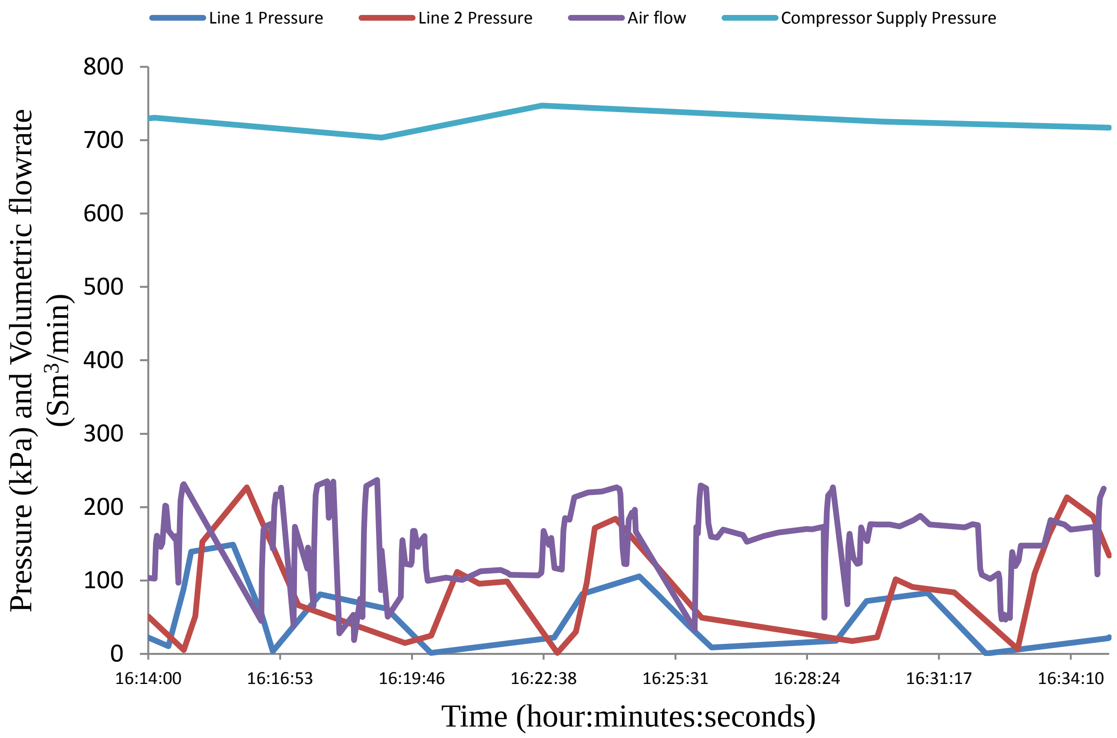


**Figure H.23** Unit 3 conveying pressure and air flow rate for Period 8 sample date 07/01/201

# APPENDIX I SAMPLE CALCULATIONS

Selecting a typical set of pneumatic conveying results as included in chapter 5 for sample calculations, Unit 1 is selected, conveying pipe 2 and data set for period 6. Table 5.12 and Figure H.6 indicate the raw data findings for this conveying period. These raw data specific to Unit 3, period 6 has been included in Table I1 period for sample calculations purposes.

**Table I.1** Unit 1 period 6 measured data

| Pneumatic Conveying Data | | Period 6 |
|---|---|---|
| Coal consumption mill 1 | (kg/s) | 23.4 |
| Coal consumption mill 2 | (kg/s) | 24.7 |
| Coal consumption mill 3 | (kg/s) | 27.6 |
| Coal consumption mill 4 | (kg/s) | 0 |
| Coal consumption mill 5 | (kg/s) | 26.8 |
| Fly ash mass flowrate (both lines) | (kg/s) | 32.7 |
| Conveying Pressure Line 1 (gauge) | (kPa) | 169 |
| Conveying Pressure Line 2 (gauge) | (kPa) | 150 |
| Air only pressure drop Line 1 (gauge) | (kPa) | 23.3 |
| Air only pressure drop Line 2 (gauge) | (kPa) | 18.7 |
| Volumetric air flowrate for line 1 | $Sm^3/min$ | 59 |
| Volumetric air flowrate for line 2 | $Sm^3/min$ | 52 |
| Boiler cleaning only air flowrate | $Sm^3/min$ | 34 |

## I1 Air Mass Flow Rate Calculations

The air mass flowrate is obtained from the volumetric flow rate, whilst noting the standard reference conditions for the flow meter as indicated.

Standard Temperature = 273 Kelvin (0 degrees Celsius)
Standard Pressure = 101.3 kPa

The total volumetric air flowrate for conveying pipe line 2 can be read from H.6 as 89 $\mathrm{Sm}^3/\mathrm{min}$. The boiler cleaning air flow rate can also be read as 34 $\mathrm{Sm}^3/\mathrm{min}$. The conveying air flowrate for pneumatic conveying only can then be computed as,

$$V_P = V_T - V_B = 89 - 34 = 55\ \mathrm{Sm}^3/\mathrm{min}$$

Using ideal gas laws, the ratio between the prevailing condition and standard condition a conversion constant is computed as $\frac{P}{RT\times 60} = \frac{101.3}{0.287\times 272\times 60} = 0.0215$.

The above constant is then used to convert the volumetric mass flowrate to air mass flowrate, based on the standard conditions as defined.

$$\therefore \dot{m}_a = 0.0215\dot{V}_p = 0.0215 \times 55 = 1.19\ \mathrm{kg/s}$$

## I2 Air Velocity Calculations

Air inlet velocity can be computed from known values of pressure, temperature, and volumetric flow rate and pipe diameter. Refer to Tables I1, with static pressure values for line 1 as 150 kPa, conveying line diameter is as per Table 3.1. The ash temperature at maximum is 160 degrees Celsius and reduces temperature to 80 degrees at the outlet,

$$\therefore v_{inlet} = \frac{4m_a RT}{P\pi D^2} = \frac{4\times 1.19\times 0.287\times 433}{(150+89.6)\times 3.14\times 0.265^2} = 11.25\ \mathrm{m/s}$$

The outlet velocity is calculated in the same manner, with pressure at the silo at -4 kPa and temperature at 80 degrees Celsius, discharge conditions. The outlet (exit) velocity is then calculated as,

$$v_{exit} = \frac{4m_a RT}{P\pi D^2} = \frac{4\times1.19\times0.287\times353}{(89.6-4)\times3.14\times0.265^2} = 25.6 \text{ m/s}$$

The average velocity is calculated as the mean of the two velocities, and this is computed as,

$$\bar{v} = \frac{v_{inlet}+v_{exit}}{2} = 18.4\ m/s$$

Average density is also computed,

$$\overline{\rho_a} = \frac{\frac{P_i}{RT_i}+\frac{P_0}{RT_0}}{2} = \frac{\frac{(150+89.6)}{0.287\times(160+273)}+\frac{(89.6-4)}{0.287\times(80+273)}}{2} = 1.39$$

## I3 Pressure drop due to bend and vertical sections

### Bend pressure

$$P_B = \frac{NB(1+\mu)\rho v^2}{2} = \frac{7\times0.5(1+13.5)\times1.39\times18.4^2}{2} = 11.97 \text{ kPa}$$

### Vertical pressure

$$\frac{v_s}{v_a} = 1 - 0.0638 d_p^{0.3}\rho_s^{0.5} = 1 - 0.0638\times(63\times10^{-6})^{0.3}\times2200^{0.5} = 0.9$$

$$\therefore P_V = \mu\rho g L_v\left(\frac{v_s}{v_a}\right) = 13.5\times1.39\times9.81\times39.3\times0.9 = 6.51 \text{ kPa}$$

# I4 Air Only Pressure Drop

As discussed in chapter 2, 2.4.1, air only pressure models have been widely researched, and the total air only pressure drop due to horizontal length and bend.

**Horizontal air only pressure drop**

The Reynolds number, air friction factor and air only horizontal pressure drop is computed using average air velocity and density using air only conditions.

$$\rho_{ave} = \frac{\bar{P}}{R\bar{T}} = \frac{\left((18.7+89.6)+(89.6-4)\right)/2}{0.287\times303} = 1.11 \text{ kg/m}^3$$

Air only average velocity is calculated from air only conditions, similar to density;

$$\bar{v} = \frac{\frac{4\times1.19\times0.287\times303}{(89.6+18.7)\times3.14\times0.265^2}+\frac{4\times1.19\times0.287\times303}{(89.6-4)\times3.14\times0.265^2}}{2} = 19.98\ m/s$$

$$\therefore Re = \frac{\rho V d}{\mu} = \frac{1.19\times19.98\times0.265}{1.8\times10^{-5}} = 350039$$

Air friction factor is computed as,

$$\lambda_a = \frac{1.325}{\ln\left(\frac{5.74}{Re_a{}^{0.9}}\right)^2} = 0.014$$

The horizontal air pressure drop alone is then calculated as,

$$P_H = \frac{(4\lambda_a)\rho_a v_a{}^2 L}{2D} = \frac{4\times0.014\times1.11\times19.98^2\times362.8}{2\times0.265} = 17.3 \text{ kPa}$$

**Pressure drop at the bend for air only**

$$P_b = k\frac{\rho V^2}{2} = 8.4\times\frac{1.11\times19.98^2}{2} = 1.9 \text{ kPa}$$

As such, the total air only pressure drop is $P_a = P_H + P_b = 19.2$ kPa

## I5 Solids only horizontal pressure

$$\Delta P_{Hs} = \Delta P_T - \Delta P_A - \Delta P_B - \Delta P_V = 150 - 11.97 - 6.51 - 19.2 = 112.3 \text{ kPa}$$

## I6 Coefficient Of Friction Calculation

The experimental solids friction factor is computed using,

$$\lambda_s = \frac{2P_{Hs}D}{\mu \rho_a {v_a}^2 L} = \frac{2\times112.3\times1000\times0.265}{13.5\times1.39\times18.4^2\times362.8} = 0.026$$

The theoretical coefficient of friction is calculated using the Jones and Williams and Behera proposed models. These models are all related to the Froude number and the solids loading ratio of 13.5 for period 6 as indicated in Table 7.1

**Froude number**

$$Fr = \frac{V}{\sqrt{gD}} = \frac{18.4}{\sqrt{9.81\times0.25}} = 11.4$$

**Jones and Williams model**

$$\lambda_s = \frac{83}{m^{*0.9} Fr^2} = \frac{83}{13.5^{0.9}\times11.4^2} = 0.061$$

**Behera model**

$$\lambda_s = \frac{364.4}{m^{*1.29} Fr^{2.62}} = \frac{364.4}{13.5^{1.29}\times11.4^{2.36}} = 0.040$$

**Differences between experimental and theoretical models**

$$\%\Delta = (\text{model} - \text{experimental})/(\text{model}) \times 100$$

Difference to Jones and Williams' proposed model:

$$\therefore \%\Delta_{JW} = \frac{0.061 - 0.026}{0.061} \times 100 = 57\%$$

Difference to Behera proposed model:

$$\therefore \%\Delta_{JW} = \frac{0.040 - 0.026}{0.040} \times 100 = 36\%$$

# APPENDIX J UNCERTAINTY ANALYSIS

The uncertainty analysis was performed in two ways, uncertainty in the measured values and propagation of uncertainty due to the calculations involving values with uncertainties. These were performed in line with guidelines recommended by Taylor (1997).

## J1 Measured value uncertainties

Whilst the instruments measured error was performed during initial calibration and these are recorded in the data sheets, the error in the data collected during the research is what is considered in this section. The following three values were recorded; volumetric air flowrate, conveying pressure and coal consumption. Sample data point 1, line 1 for Unit 3 is used for this purpose.

***Volumetric air flowrate measured value error***

The total peak air flowrate is shown, refer to figure H.16 for total.

| | |
|---|---|
| Maximum peak air flow | 181.9 |
| Minimum peak air flow | 163.1 |
| Average peak air flow | 172.5 |
| Error in measurement | 16.5 |

$$\therefore \frac{\Delta V_T}{\overline{V_T}} = \frac{16.5}{172.5}$$

$$= 9.6\%$$

The boiler only air flowrate is shown, refer to figure H.16 for total.

| | |
|---|---|
| Maximum boiler air flow | 38.2 |
| Minimum boiler air flow | 20.6 |
| Average boiler air flow | 29.4 |
| Error in measurement | 8.8 |

$$\therefore \frac{\Delta V_B}{\overline{V_B}} = \frac{8.8}{29.4}$$

$$= 29.9\%$$

***Conveying pressure measured value error***

Referring to figure H.16, it can be observed that the various conveying cycles indicate different maximum conveying pressure and similar with minimum.

| | |
|---|---|
| Maximum upper conveying pressure | 150.9 |
| Minimum upper conveying pressure | 116.0 |
| Average upper conveying pressure | 133.5 |
| Error in measurement | 17 |

$$\therefore \frac{\Delta P}{\bar{P}} = \frac{17}{133.5}$$

$$= 12.7\%$$

The above represents the error in the total conveying pressure.

***Coal consumption measured value error***

Making use of one of the mills in operation, such as Mill 1 refer to G.15.

| | |
|---|---|
| Maximum coal combustion | 27.2 |
| Minimum coal combustion | 24.6 |
| Average coal combustion | 25.9 |
| Error in measurement | 1.3 |

$$\therefore \frac{\Delta \dot{m}}{\bar{\dot{m}}} = \frac{1.3}{25.9}$$

$$= 5\%$$

The solids mass flow rate is directly related to the coal consumption at $5\%$.

## J2 Propagation of Uncertainty

***Volumetric flow pneumatic conveying***

$V_P = V_T - V_B$

$\therefore \frac{\Delta V_P}{V_P} = \sqrt{\frac{{\Delta V_T}^2 - {\Delta V_B}^2}{(V_T - V_B)^2}} = \sqrt{\frac{16.5^2 - 8.8^2}{(172.5 - 29.4)^2}}$

$= 9.8\%$

***Air mass flowrate***

$\dot{m}_a = 0.0215\dot{V}_s$

As such, based on the assumption of a constant, 0.0215; the air mass flowrate will have the same error as the volumetric flow rate data of 9.8%.

***Average air density***

$\rho = \frac{P}{RT}$

The air density Equation contains the function $(1/RT)$, and as these were not measured during the research these were a constant for inlet conditions; and will also be a constant for outlet conditions. As such, the air inlet and outlet density error will be the same as the error predicted in the measured pressure values of 12.7%. As such, only average densities error can be computed from densities values as discussed in 7.2.

$\bar{\rho}_a = \frac{\rho_{inlet} + \rho_{outlet}}{2}$

$\therefore \frac{\Delta \bar{\rho}_a}{\bar{\rho}_a} = \sqrt{\frac{{\Delta \bar{\rho}_i}^2 + {\Delta \bar{\rho}_o}^2}{(\rho_i + \rho_o)^2}}$

$= \sqrt{\frac{(0.127 \times 2.47)^2 + (0.127 \times 0.85)^2}{(2.47 + 0.85)^2}}$

$= 9.9\%$`

***Conveying air velocity***

$$v_a = \frac{4m_a RT}{P\pi D^2}$$

The only variables was the air mass flowrate and the pressure data, applicable for both inlet and outlet conditions. As such, the error can be computed as;

$$\therefore \frac{\Delta v_a}{v_a} = \sqrt{\left(\frac{\Delta m_a}{m_a}\right)^2 + \left(-\frac{\Delta P}{P}\right)^2}$$

$$= \sqrt{\left(\frac{0.098\times 1.42}{1.42}\right)^2 + \left(\frac{17}{133.5}\right)^2}$$

$$= 29.2\%$$

The error in the average velocity is then computed similar to the average density as,

$$\therefore \frac{\Delta \bar{v}_a}{\bar{v}_a} = \sqrt{\frac{\Delta {v_i}^2 + \Delta {v_o}^2}{(v_i + v_o)^2}}$$

$$= \sqrt{\frac{(0.292\times 8.99)^2 + (0.292\times 30.6)^2}{(8.99+30.6)^2}}$$

$$= 23.5\%`$$

***Reynolds number***

$$Re = \frac{\rho V d}{\mu}$$

In the Reynolds number the function $\left(\frac{d}{\mu}\right)$ is a constant in this research, as such the error analysis is computed as,

$$\therefore \frac{\Delta Re}{Re} = \sqrt{\left(\frac{\Delta \bar{\rho}_a}{\bar{\rho}_a}\right)^2 + \left(\frac{\Delta \bar{v}_a}{\bar{v}_a}\right)^2}$$

$$= \sqrt{0.099^2 + 0.235^2}$$

$$= 25.5\%$$

***Solids loading ratio***

$$\mu = \frac{m_s}{m_a}$$

$$\therefore \frac{\Delta\mu}{\mu} = \sqrt{\left(\frac{\Delta m_s}{m_s}\right)^2 + \left(-\frac{\Delta m_a}{m_a}\right)^2}$$

$$= \sqrt{0.05^2 + 0.098^2}$$

$$= 11.0\%$$

***Froude number***

$$F_r = \frac{v_a}{\sqrt{\mathrm{gD}}}$$

In the Froude number computation, ($\sqrt{\mathrm{gD}}$) is a constant and as such, the Froude number will have the same error as the velocity used, of $23.5\%$.

***Bend pressure***

$$P_B = \frac{NB(1+\mu)\rho v^2}{2}$$

The bend pressure has the component $\big(NB(1+\mu)\big)$as a constant, therefore the error is computed as,

$$\therefore \frac{\Delta P_B}{P_B} = \sqrt{\left(\frac{\Delta\bar{\rho}_a}{\bar{\rho}_a}\right)^2 + \left(\frac{\Delta 2\bar{v}_a}{\bar{v}_a}\right)^2}$$

$$= \sqrt{0.099^2 + (2 \times 0.235)^2}$$

$$= 48\%$$

***Vertical pressure***

$$P_V = \mu\rho \mathrm{g} L_v \left(\frac{v_s}{v_a}\right)$$

The vertical pressure drop has the component $(\mu g L_v)$ as a constant and the velocity ratio is defined as $\frac{v_s}{v_a} = 1 - 0.0638 d_p^{0.3} \rho_s^{0.5}$, is always a constant in this research.

the error is computed as,

$$\therefore \frac{\Delta P_V}{P_V} = \sqrt{\left(\frac{\Delta \bar{\rho}_a}{\bar{\rho}_a}\right)^2}$$

$$= 9.9\%$$

This is similar to the density error as the other components are constants.

***Air only horizontal pressure***

$$P_{aH} = \frac{(4\lambda_a)\rho_a {v_a}^2 L}{2D}$$

$$\therefore \frac{\Delta P_{aH}}{P_H} = \sqrt{\left(\frac{\Delta \bar{\rho}_a}{\bar{\rho}_a}\right)^2 + \left(\frac{\Delta 2\bar{v}_a}{\bar{v}_a}\right)^2}$$

$$= 48\%$$

This is similar to the bend pressure error.

***Horizontal solids pressure***

$$P_{Hs} = P_T - P_V - P_B - P_A$$

The horizontal solids pressure is then computed as,

$$\therefore \frac{\Delta P_{Hs}}{P_{Hs}} = \sqrt{\frac{{\Delta P_T}^2 - {\Delta P_V}^2 - {\Delta P_B}^2 - {\Delta P_A}^2}{(P_T - P_V - P_B - P_A)^2}}$$

$$= \sqrt{\frac{(0.127\times164)^2 - (0.099\times5.7)^2 - (0.48\times12.28)^2 - (0.48\times36.91)^2}{(164 - 5.7 - 12.28 - 36.91)^2}}$$

$$= 8.4\%$$

***Experimental solids friction factor***

$$\lambda_s = \frac{2P_{Hs}D}{\mu \rho_a {v_a}^2 L}$$

The experimental solids friction factor was computed with $\left(\frac{D}{\mu L}\right)$ is a constant,

$$\therefore \frac{\Delta\lambda_s}{\lambda_s} = \sqrt{\left(\frac{\Delta P_{HS}}{P_{Hs}}\right)^2 + \left(-\frac{\Delta\mu}{\mu}\right)^2 + \left(-\frac{2\Delta\bar{v}_a}{\bar{v}_a}\right)^2}$$

$$= \sqrt{\left(\frac{\Delta P_{HS}}{P_{Hs}}\right)^2 + \left(-\frac{\Delta\mu}{\mu}\right)^2 + \left(-\frac{2\Delta\bar{v}_a}{\bar{v}_a}\right)^2}$$

$$= \sqrt{(0.084)^2 + (-0.11)^2 + (-2 \times 0.292)^2}$$

$$= 60\%$$

***Calculated solids friction factor***

$$\lambda_s = \frac{83}{m^{*0.9}Fr^2}, \lambda_s = \frac{364.4}{m^{*1.29}Fr^{2.36}}$$

The calculated solids friction factor from the models can be calculated noting that ($m^* = \mu$),

$$\therefore \frac{\Delta\lambda_s}{\lambda_s} = \sqrt{\left(-\frac{1.29\Delta\mu}{\mu}\right)^2 + \left(-\frac{2.36\Delta F_r}{F_r}\right)^2}$$

$$= \sqrt{(-1.29 \times 0.11)^2 + (-2.36 \times 0.235)^2}$$

$$= 57.2\%`$$

# APPENDIX K SOLVING SIMULTANEOUS EQUATIONS TO OBTAIN SOLIDS FRICTION FACTOR

## K1 Unit 1 application for developing new model

The following steps were taken to solve for the 3 unknowns in EXCEL,

(i) The first step is selection of experimental data for solids friction, solids loading ratio and Froude number and solving their log functions

| | | $\log \lambda_s$ | $\log \mu$ | $\log F_{ri}$ |
|---|---|---|---|---|
| Eq1 | Period 1 | -1.6500517 | 0.931091431 | 1.18822064 |
| Eq2 | Period 7 | -1.9376588 | 0.804339294 | 1.33950831 |
| Eq3 | Period 5 | -1.5159524 | 1.038365698 | 1.09578332 |

(ii) These were then rearranged into a 3X3 Matrices vector for to solve for the unknowns

| | $\log C + a \log \mu + b \log F_{ri} = \log \lambda_s$ | | | | |
|---|---|---|---|---|---|
| | x1 | $\log \mu$ | $\log F_{ri}$ | Unknown | $\log \lambda_s$ |
| Eq.1 | 1 | 0.931091 | 1.188221 | LogC | -1.65 |
| Eq.2 | 1 | 0.804339 | 1.339508 | a | -1.94 |
| Eq.3 | 1 | 1.038366 | 1.095783 | b | -1.52 |

(iii) Using an EXCEL function for inverting and multiplying matrices known as minverse and mmult, the unknowns were then solved as

| | | | |
|---|---|---|---|
| LogC | 3.30 | C | **1984.684** |
| a | **-1.40** | | |
| b | **-3.07** | | |
| | | | |

$\therefore \lambda_s = C(m^*)^a (Fr_a)^b$

$$= \frac{1985}{m^{*1.40} Fr^{3.07}} \qquad \text{(K1)}$$

Above prove process performed for Unit 2 and Unit 3 data as shown in K2 and K3 sections.

## K2 Unit 2 application for developing new model

(i) Data points selected representative of the overall results

| | | $\log \lambda_s$ | $\log \mu$ | $\log F_{ri}$ |
|---|---|---|---|---|
| Eq1 | Period4L2 | -1.911916896 | 1.34534806 | 0.922890232 |
| Eq2 | Period3L1 | -1.720723832 | 1.36837202 | 0.851234241 |
| E13 | Period6L1 | -1.669447037 | 1.11506423 | 0.925257322 |

(ii) The data rearranged into a 3X3 matrices

$\log C + a \log \mu + b \log F_{ri} = \log \lambda_s$

| | x1 | $\log \mu$ | $\log F_{ri}$ | Unknown | $\log \lambda_s$ |
|---|---|---|---|---|---|
| Eq.1 | 1 | 1.34534806 | 0.922890232 | LogC | -1.911916896 |
| Eq.2 | 1 | 1.368372022 | 0.851234241 | a | -1.720723832 |
| Eq.3 | 1 | 1.115064229 | 0.925257322 | b | -1.669447037 |

(iii) Matrices solved to obtain

| | | | |
|---|---|---|---|
| LogC | 2.330223447 | C | **213.9062** |
| a | **-1.083923918** | | |
| b | **-3.016485934** | | |
| | | | |

$\therefore \lambda_s = C(m^*)^a (Fr_a)^b$

$$= \frac{214}{m^{*1.08} Fr^{3.02}} \quad (K2)$$

## K3 Unit 2 application for developing new model

(i) Data points selected representative of the overall results

| | | $\log \lambda_s$ | $\log \mu$ | $\log F_{ri}$ |
|---|---|---|---|---|
| Eq1 | Period8 | -2.019084469 | 1.17391959 | 1.104992605 |
| Eq2 | Period5 | -1.917340722 | 0.81869618 | 1.211350362 |
| E13 | Period7 | -2.063352254 | 0.95088353 | 1.223748372 |

(ii) The data rearranged into a 3X3 matrices

| | $\log C + a \log \mu + b \log F_{ri} = \log \lambda_s$ | | | | |
|---|---|---|---|---|---|
| | x1 | $\log \mu$ | $\log F_{ri}$ | Unknown | $\log \lambda_s$ |
| Eq.1 | 1 | 1.17392 | 1.104993 | LogC | -2.019084469 |
| Eq.2 | 1 | 0.818696 | 1.21135 | a | -1.917340722 |
| Eq.3 | 1 | 0.950884 | 1.223748 | b | -2.063352254 |

(iii) Matrices solved to obtain

| | | | |
|---|---|---|---|
| LogC | 1.347727682 | C | 22.27038 |
| a | -0.909423445 | | |
| b | -2.08075796 | | |

$$\therefore \lambda_s = C(m^*)^a (Fr_a)^b$$

$$= \frac{22}{m^{*0.91} Fr^{2.08}} \quad \text{(K3)}$$